NUREG/CR-5188
MEA-2325

Fracture Toughness Characterization of Nuclear Piping Steels

Prepared by A. L. Hiser

Materials Engineering Associates, Inc.

Prepared for
U.S. Nuclear Regulatory Commission

AVAILABILITY NOTICE

Availability of Reference Materials Cited in NRC Publications

Most documents cited in NRC publications will be available from one of the following sources:

1. The NRC Public Document Room, 2120 L Street, NW, Lower Level, Washington, DC 20555

2. The Superintendent of Documents, U.S. Government Printing Office, P.O. Box 37082, Washington, DC 20013-7082

3. The National Technical Information Service, Springfield, VA 22161

Although the listing that follows represents the majority of documents cited in NRC publications, it is not intended to be exhaustive.

Referenced documents available for inspection and copying for a fee from the NRC Public Document Room include NRC correspondence and internal NRC memoranda; NRC Office of Inspection and Enforcement bulletins, circulars, information notices, inspection and investigation notices; Licensee Event Reports; vendor reports and correspondence; Commission papers; and applicant and licensee documents and correspondence.

The following documents in the NUREG series are available for purchase from the GPO Sales Program: formal NRC staff and contractor reports, NRC-sponsored conference proceedings, and NRC booklets and brochures. Also available are Regulatory Guides, NRC regulations in the *Code of Federal Regulations*, and *Nuclear Regulatory Commission Issuances*.

Documents available from the National Technical Information Service include NUREG series reports and technical reports prepared by other federal agencies and reports prepared by the Atomic Energy Commission, forerunner agency to the Nuclear Regulatory Commission.

Documents available from public and special technical libraries include all open literature items, such as books, journal and periodical articles, and transactions. *Federal Register* notices, federal and state legislation, and congressional reports can usually be obtained from these libraries.

Documents such as theses, dissertations, foreign reports and translations, and non-NRC conference proceedings are available for purchase from the organization sponsoring the publication cited.

Single copies of NRC draft reports are available free, to the extent of supply, upon written request to the Office of Information Resources Management, Distribution Section, U.S. Nuclear Regulatory Commission, Washington, DC 20555.

Copies of industry codes and standards used in a substantive manner in the NRC regulatory process are maintained at the NRC Library, 7920 Norfolk Avenue, Bethesda, Maryland, and are available there for reference use by the public. Codes and standards are usually copyrighted and may be purchased from the originating organization or, if they are American National Standards, from the American National Standards Institute, 1430 Broadway, New York, NY 10018.

DISCLAIMER NOTICE

NUREG/CR-5188
MEA-2325
RF, R5

Fracture Toughness Characterization of Nuclear Piping Steels

Manuscript Completed: October 1989
Date Published: November 1989

Prepared by
A. L. Hiser

Materials Engineering Associates, Inc.
9700-B Martin Luther King, Jr. Highway
Lanham, MD 20706-1837

Prepared for
Division of Engineering
Office of Nuclear Regulatory Research
U.S. Nuclear Regulatory Commission
Washington, DC 20555
NRC FIN B8900

ABSTRACT

To assess the integrity of piping systems in nuclear power plants, materials' property information such as fracture toughness and stress-strain data are required. This report summarizes findings from testing of heats of piping steel representing a cross-section of those included in nuclear plants. Included are ferritic steels, austenitic stainless steels and one heat of an Inconel alloy.

Besides the characterization of piping steels, additional studies examined the effect on J-R curves of flattening specimen blanks, and assessed specimen size effects and through-thickness variability on stress-strain curves.

CONTENTS

LIST OF FIGURES

LIST OF FIGURES

LIST OF FIGURES

LIST OF FIGURES

LIST OF FIGURES

LIST OF FIGURES

LIST OF TABLES

LIST OF TABLES

FOREWORD

The work reported here was performed at Materials Engineering Associates (MEA) under the program, Structural Integrity of Water Reactor Pressure Boundary Components, F. J. Loss, Program Manager. The program is sponsored by the Office of Nuclear Regulatory Research of the U. S. Nuclear Regulatory Commission (NRC). The technical monitor for the NRC is Alfred Taboada.

Prior reports under the current contract are listed below:

1. J. R. Hawthorne, "Significance of Nickel and Copper to Radiation Sensitivity and Postirradiation Heat Treatment Recovery of Reactor Vessel Steels," USNRC Report NUREG/CR-2948, Nov. 1982.

2. "Structural Integrity of Water Reactor Pressure Boundary Components, Annual Report for 1982," F. J. Loss, Ed., USNRC Report NUREG/CR-3228, Vol. 1, Apr. 1983.

3. J. R. Hawthorne, "Exploratory Assessment of Postirradiation Heat Treatment Variables in Notch Ductility Recovery of A 533-B Steel," USNRC Report NUREG/CR-3229, Apr. 1983.

4. W. H. Cullen, K. Torronen, and M. Kemppainen, "Effects of Temperature on Fatigue Crack Growth of A 508-2 Steel in LWR Environment," USNRC Report NUREG/CR-3230, Apr. 1983.

5. "Proceedings of the International Atomic Energy Agency Specialists' Meeting on Subcritical Crack Growth," Vols. 1 and 2, W. H. Cullen, Ed., USNRC Conference Proceeding NUREG/CP-0044, May 1983.

6. W. H. Cullen, "Fatigue Crack Growth Rates of A 508-2 Steel in Pressurized, High-Temperature Water," USNRC Report NUREG/CR-3294, June 1983.

7. J. R. Hawthorne, B. H. Menke, and A. L. Hiser, "Light Water Reactor Pressure Vessel Surveillance Dosimetry Improvement Program: Notch Ductility and Fracture Toughness Degradation of A 302-B and A 533-B Reference Plates from PSF Simulated Surveillance and Through-Wall Irradiation Capsules," USNRC Report NUREG/CR-3295, Vol. 1, Apr. 1984.

8. J. R. Hawthorne and B. H. Menke, "Light Water Reactor Pressure Vessel Surveillance Dosimetry Improvement Program: Postirradiation Notch Ductility and Tensile Strength Determinations for PSF Simulated Surveillance and Through-Wall Specimen Capsules," USNRC Report NUREG/CR-3295, Vol. 2, Apr. 1984.

9. A. L. Hiser and F. J. Loss, "Alternative Procedures for J-R Curve Determination," USNRC Report NUREG/CR-3402, July 1983.

10. A. L. Hiser, F. J. Loss, and B. H. Menke, "J-R Curve Characterization of Irradiated Low Upper Shelf Welds," USNRC Report NUREG/CR-3506, Apr. 1984.

11. W. H. Cullen, R. E. Taylor, K. Torronen, and M. Kemppainen, "The Temperature Dependence of Fatigue Crack Growth Rates of A 351 CF8A Cast Stainless Steel in LWR Environment," USNRC Report NUREG/CR-3546, Apr. 1984.

12. "Structural Integrity of Light Water Reactor Pressure Boundary Components -- Four-Year Plan 1984-1988," F. J. Loss, Ed., USNRC Report NUREG/CR-3788, Sep. 1984.

13. W. H. Cullen and A. L. Hiser, "Behavior of Subcritical and Slow-Stable Crack Growth Following a Postirradiation Thermal Anneal Cycle," USNRC Report NUREG/CR-3833, Aug. 1984.

14. "Structural Integrity of Water Reactor Pressure Boundary Components: Annual Report for 1983," F. J. Loss, Ed., USNRC Report NUREG/CR-3228, Vol. 2, Sept. 1984.

15. W. H. Cullen, "Fatigue Crack Growth Rates of Low-Carbon and Stainless Piping Steels in PWR Environment," USNRC Report NUREG/CR-3945, Feb. 1985.

16. W. H. Cullen, M. Kemppainen, H. Hanninen, and K. Torronen, "The Effects of Sulfur Chemistry and Flow Rate on Fatigue Crack Growth Rates in LWR Environments," USNRC Report NUREG/CR-4121, Feb. 1985.

17. "Structural Integrity of Water Reactor Pressure Boundary Components: Annual Report for 1984," F. J. Loss, Ed., USNRC Report NUREG/CR-3228, Vol. 3, June 1985.

18. A. L. Hiser, "Correlation of C_v and K_{Ic}/K_{Jc} Transition Temperature Increases Due to Irradiation," USNRC Report NUREG/CR-4395, Nov. 1985.

19. W. H. Cullen, G. Gabetta, and H. Hanninen, "A Review of the Models and Mechanisms For Environmentally-Assisted Crack Growth of Pressure Vessel and Piping Steels in PWR Environments," USNRC Report NUREG/CR-4422, Dec. 1985.

20. "Proceedings of the Second International Atomic Energy Agency Specialists' Meeting on Subcritical Crack Growth," W. H. Cullen, Ed., USNRC Conference Proceeding NUREG/CP-0067, Vols. 1 and 2, Apr. 1986.

21. J. R. Hawthorne, "Exploratory Studies of Element Interactions and Composition Dependencies in Radiation Sensitivity Development," USNRC Report NUREG/CR-4437, Nov. 1985.

22. R. B. Stonesifer and E. F. Rybicki, "Development of Models for Warm Prestressing," USNRC Report NUREG/CR-4491, Jan. 1987.

23. E. F. Rybicki and R. B. Stonesifer, "Computational Model for Residual Stresses in a Clad Plate and Clad Fracture Specimens," USNRC Report NUREG/CR-4635, Oct. 1986.

24. D. E. McCabe, "Plan for Experimental Characterization of Vessel Steel After Irradiation," USNRC Report NUREG/CR-4636, Oct. 1986.

25. E. F. Rybicki, J. R. Shadley, and A. S. Sandhu, "Experimental Evaluation of Residual Stresses in a Weld Clad Plate and Clad Test Specimens," USNRC Report NUREG/CR-4646, Oct. 1986.

26. "Structural Integrity of Water Reactor Pressure Boundary Components: Annual Report for 1985," F. J. Loss, Ed., USNRC Report NUREG/CR-3228, Vol. 4, June 1986.

27. G. Gabetta and W. H. Cullen, "Application of a Two-Mechanism Model for Environmentally-Assisted Crack Growth," USNRC Report NUREG/CR-4723, Oct. 1986.

28. W. H. Cullen, "Fatigue Crack Growth Rates in Pressure Vessel and Piping Steels in LWR Environments," USNRC Report NUREG/CR-4724, Mar. 1987.

29. W. H. Cullen and M. R. Jolles, "Fatigue Crack Growth of Part-Through Cracks in Pressure Vessel and Piping Steels: Air Environment Results, USNRC Report NUREG/CR-4828, Oct. 1988.

30. D. E. McCabe, "Evaluation of Surface Cracks Embedded in Reactor Vessel Cladding Unirradiated Bend Specimens," USNRC Report NUREG/CR-4841, May 1987.

31. H. Hanninen, M. Vulli, and W. H. Cullen, "Surface Spectroscopy of Pressure Vessel Steel Fatigue Fracture Surface Films Formed in PWR Environments," USNRC Report NUREG/CR-4863, July 1987.

32. A. L. Hiser and G. M. Callahan, "A User's Guide to the NRC's Piping Fracture Mechanics Data Base (PIFRAC)," USNRC Report NUREG/CR-4894, May 1987.

33. "Proceedings of the Second CSNI Workshop on Ductile Fracture Test Methods (Paris, France, April 17-19, 1985)," F. J. Loss, Ed., USNRC Conference Proceeding NUREG/CP-0064, Aug. 1988.

34. W. H. Cullen and D. Broek, "The Effects of Variable Amplitude Loading on A 533-B Steel in High-Temperature Air and Reactor Water Environments," USNRC Report NUREG/CR-4929, Apr. 1989.

35. "Structural Integrity of Water Reactor Pressure Boundary Components: Annual Report for 1986," F. J. Loss, Ed., USNRC Report NUREG/CR-3228, Vol. 5, July 1987.

36. F. Ebrahimi et al., "Development of a Mechanistic Understanding of Radiation Embrittlement in Reactor Pressure Vessel Steels: Final Report," USNRC Report NUREG/CR-5063, Jan. 1988.

37. J. B. Terrell, "Fatigue Life Characterization of Smooth and Notched Piping Steel Specimens in 288°C Air Environments," USNRC Report NUREG/CR-5013, May 1988.

38. A. L. Hiser, "Tensile and J-R Curve Characterization of Thermally Aged Cast Stainless Steels," USNRC Report NUREG/CR-5024, Sept. 1988.

39. J. B. Terrell, "Fatigue Strength of Smooth and Notched Specimens of ASME SA 106-B Steel in PWR Environments," USNRC Report NUREG/CR-5136, Sept. 1988.

40. D. E. McCabe, "Fracture Evaluation of Surface Cracks Embedded in Reactor Vessel Cladding: Material Property Evaluations," USNRC Report NUREG/CR-5207, Sept. 1988.

41. J. R. Hawthorne and A. L. Hiser, "Experimental Assessments of Gundremmingen RPV Archive Material for Fluence Rate Effects Studies," USNRC Report NUREG/CR-5201, Oct. 1988.

42. J. B. Terrell, "Fatigue Strength of ASME SA 106-B Welded Steel Pipes in 288°C Air Environments," USNRC Report NUREG/CR 5195, Dec. 1988.

43. A. L. Hiser, "Post-Irradiation Fracture Toughness Characterization of Four Lab-Melt Plates," USNRC Report NUREG/CR-5216 Rev. 1, Jun. 1989.

44. R. B. Stonesifer, E. F. Rybicki and D. E. McCabe, "Warm Prestress Modeling: Comparison of Models and Experimental Results," USNRC Report NUREG/CR-5208, Apr. 1989.

45. A. L. Hiser and J. B. Terrell, "Size Effects on J-R Curves for A 302-B Plate," USNRC Report NUREG/CR-5265, Jan. 1989.

46. D. E. McCabe, "Fracture Evaluation of Surface Cracks Embedded in Reactor Vessel Cladding," USNRC Report NUREG/CR-5326, Mar. 1989.

47. J. R. Hawthorne, "An Exploratory Study of Element Interactions and Composition Dependencies in Radiation Sensitivity Development: Final Report," USNRC Report NUREG/CR-5357, Apr. 1989.

48. J. R. Hawthorne, "Steel Impurity Element Effects on Post-Irradiation Properties Recovery by Annealing: Final Report," USNRC Report NUREG/CR-5388, Aug. 1989.

49. H. H. Hanninen and W. H. Cullen, "Slow Strain Rate Testing of a Cyclically Stabilized A 516 Gr. 70 Piping Steel in PWR Environments," USNRC Report NUREG/CR-5327, Nov. 1989.

50. J. R. Hawthorne and A. L. Hiser, "Irradiation-Anneal-Reirradiation (IAR) Studies of Prototypic Reactor Vessel Weldments," USNRC Report NUREG/CR-5469, Nov. 1989.

ACKNOWLEDGMENT

This work was sponsored by the Division of Engineering, with A. Taboada and M. Vagins serving as the technical monitors during various portions of this work.

The assistance of Battelle's Columbus Division (G. Wilkowski and G. Kramer) in procuring some of the materials summarized in this report is appreciated.

The assistance of many people at MEA helped to give this study a successful conclusion. Of particular assistance were B. Menke, E. D'Ambrosio, T. Ramey, G. Carlson and E. Martinez.

1. INTRODUCTION

As one aspect of assessing the overall safety of nuclear power plants, the integrity of both the primary and secondary piping systems must be considered. Such integrity assessments require data such as tensile strength and fracture toughness for the materials under consideration, in particular to determine whether or not a flaw will propagate through the thickness of the pipe under specified loading scenarios, and additionally, whether or not a through-thickness flaw will be stable or will result in a large break.

For a particular evaluation, data for the specific pipe under consideration would provide the most accurate assessment. However, fracture toughness data, in particular, are generally not available on a heat-by-heat basis, and generally only a few Charpy-V (C_v) impact energy values are available. Therefore, generic results for the different materials used in piping applications do provide one means for performing such a safety evaluation.

In recognition of the need for fracture toughness data from typical piping materials, a task to develop a computerized data base containing such information was initiated. As a part of this task, heats of nuclear grade piping materials have been procured and characterized. This report covers characterization results (including fracture toughness, C_v and tensile data) for ferritic steels and wrought austenitic-stainless steels, as well as results for one heat of a nickel-based alloy. Similar results for cast austenitic stainless steels, in particular for several thermally-aged conditions, are given in Ref. 1. All of these materials are listed in Table 1-1.

All of the results given in this report and Ref. 1, along with other data, are available through the USNRC's Piping Fracture Mechanics Data Base (PIFRAC), the computerized data base mentioned above. PIFRAC is described in Ref. 2 and 3.

Some of the materials covered under this report have been included in Phase II of the NRC's Degraded Piping Program at Battelle's Columbus Division. Details can be found in Ref. 4.

Table 1-1 Piping Materials Characterized By This Program

Material	Identification Code	Pipe Diameter (mm)	Pipe Schedule	Wall Thickness (mm)
Ferritic Steels				
A 106-B	ZP14	152	XXS	21.9
A 106-B	ZP15	152	120	14.3
A 106-B	ZP2	152	80	11.0
A 106-B	ZP13	152	40	7.1
A 106-C	ZP21	813	---	82.6
A 516 Gr. 70	B	940	---	82.5
Weld (A516 Gr 70)	W	940	---	82.5
Wrought Stainless Steels				
SA 182 (Type 304)	ZP6	508	100	31.0
SA 376 (Type 304)	ZP17	152	120	14.3
SA 376 (Type 304)	ZP1	168	80	11.0
SA 376 (Type 304)	ZP12	152	40	7.1
Cast Stainless Steels[a]				
SA 451-C(P)F8	P1[b]	890	---	63.5
SA 351-CF8	C1	600	---	57.2
SA 351-CF8A	ZP18	813	---	57.0
SA 351-CF3	I[b]	---[c]	---[c]	----[c]
SA 451-C(P)F3	P2[b]	930	---	73.0
SA 351-CF8	68[b]	---[d]	---[d]	----[d]
SA 351-CF3	69[b]	---[d]	---[d]	----[d]
SA 351-CF8M	70[b]	---[d]	---[d]	----[d]
Nickel-Based Alloy				
Inconel 600	ZP16	152	80	11.0

[a] Described in Ref. 1.
[b] Data for thermally-aged conditions are also available.
[c] Static cast pump impeller.
[d] Cast as 76-mm thick slabs.

2. TEST AND DATA ANALYSIS PROCEDURES

2.1 Charpy-V Tests

The Charpy-V tests were made using the Type A specimen given in ASTM Standard E 23 (Fig. 2-1). In some cases, the specimen thickness (B) had to be reduced somewhat, due to pipe curvature and thickness. The test procedures used were as outlined in the ASTM standard.

To simplify analysis of the test data, the energy results were curvefit to a hyperbolic tangent (tanh) equation, as given by

$$C_V = A + B \tanh\left[\frac{T-T_o}{C}\right] \qquad (2\text{-}1)$$

In this case, the upper shelf is given as A+B, and the temperature at an arbitrary C_V level "E" is given by

$$T_E = T_o + C \tanh^{-1}\left[\frac{E-A}{B}\right] \qquad (2\text{-}2)$$

2.2 Tensile Tests

The tensile tests were made using round specimens with threaded-ends, generally subsize to the standard specimen design in ASTM Standard E 8. The design used for each heat is described in the section giving the results for that heat. Testing was in accordance with ASTM Standards E 8 and E 21. The loading rate (on the elastic portion of the stress-strain curve) was generally ~ 500 MPa/min (72.5 ksi/min). Strain was evaluated from an axial transducer mounted across the center of the gage section. Load and transducer displacement were typically stored on floppy disk for post-test processing of the test data. Engineering stress (σ_E) and strain (ϵ_E) were calculated from the initial gage diameter and length, respectively, as given by:

$$\sigma_E = \frac{P}{A_o} \qquad (2\text{-}3)$$

$$\epsilon_E = \frac{\Delta L}{L_o} \qquad (2\text{-}4)$$

where P is the applied load, A_o is the gage section area given by πr_o^2 (where r_o is the initial gage section radius), ΔL is the extensometer displacement and L_o is the initial extensometer gage length.

Because of necking, true stress-strain values are calculated from measured load and extensometer displacement up to maximum load only; the final gage diameter and radius of curvature (of the necked region) are used to obtain values of true stress-strain at fracture. Up to maximum load, true strain (ϵ_T) is calculated from:

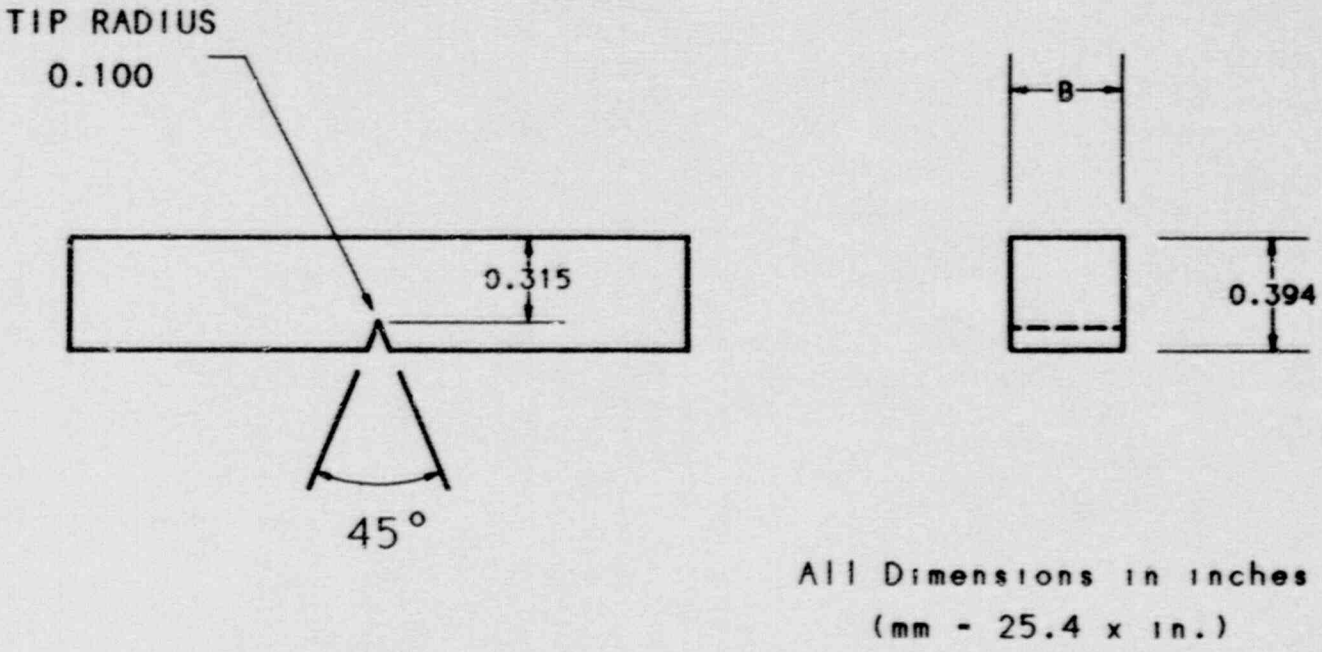

Fig. 2-1 The Charpy V-notch specimen design used was the Type A specimen from ASTM E 23, with thickness "B" of 10 mm (0.394 in.). In some cases, pipe geometry (wall thickness or diameter) caused reduced thickness specimens to be used.

$$\epsilon_T = \text{LOG}_e\ (\epsilon_E + 1) \qquad (2\text{-}5)$$

whereas true stress (σ_T) is calculated from:

$$\sigma_T = \sigma_E\ (\epsilon_E + 1) \qquad (2\text{-}6)$$

based on assumptions of constant volume (i.e., incompressibility) and a homogeneous distribution of strain along the gage length (Ref. 5).

The true strain at fracture (ϵ_{Tf}) is calculated from:

$$\epsilon_{Tf} = \text{LOG}_e\ (A_o/A_f) \qquad (2\text{-}7)$$

where A_f, the final (measured) gage area, is given by πr_f^2. Dimension r_f is the measured final gage section radius.

The true stress at fracture (σ_{Tf}) is calculated using a Bridgman correction (Ref. 6):

$$\sigma_{Tf} = P_f\ /\ [A_f\ (1 + 2\ R/r_f)\ \text{LOG}_e(1 + r_f/2R)] \qquad (2\text{-}8)$$

where P_f is the load at fracture and R is the measured radius of curvature of the necked region. This correction, from a mathematical analysis, adjusts the average axial stress to account for the introduction of transverse stresses.

For use in structural analysis, the true stress strain curve is usually approximated using a Ramberg-Osgood equation, as given by:

$$\frac{\epsilon_T}{\epsilon_o} = \left(\frac{\sigma_T}{\sigma_o}\right) + \alpha \left(\frac{\sigma_T}{\sigma_o}\right)^n \qquad (2\text{-}9)$$

where σ_o and ϵ_o represent the true yield strength and the yield strain, respectively. The parameters α and n are adjusted to optimize the fit to the measured data.

2.3 Fracture Toughness Tests

The fracture toughness tests used compact tension (CT) specimens of various sizes (ranging from 0.4T-CT up to 4T-CT) and thicknesses (from 6 mm to 51 mm). In general these specimens are proportional (i.e., the specimen thickness, B, is one-half of the specimen width, W), although in some cases the pipe configuration forced the use of

reduced thicknesses. The various specimens used are described in the sections on each heat.

Since these materials generally exhibit upper shelf behavior at the temperatures of interest from ambient to 343°C (650°F), J-integral resistance, or J-R curves are the appropriate fracture toughness evaluations. In some cases, cleavage fracture or pop-ins occurred during testing.

2.3.1 Displacement Measurements

Displacements were measured along the specimen load-line in all cases. Typically these measurements were in the standard location between the loading pin-holes, termed V_{LL}, although in other cases a location external to the loading pin-holes, termed V_{LL}', was used (Fig. 2-2). The unloading compliance method was used to monitor crack growth, with the standard Hudak-Saxena equation (Ref. 7) used to relate compliance measurements to crack length.

2.3.2 Specimen Preparation

After machining, fatigue precracks were introduced into the specimens via cycling at load levels within the linear elastic range. The target final (surface) crack-length to specimen width (a/W) ratio was 0.5. To facilitate crack initiation from the machined notches, the specimens were compressed to a load level not more than that required to give a stress intensity of 26 MPa$\sqrt{m}$ (~ 23 ksi$\sqrt{in.}$), for a tensile load of the same magnitude. At the final stage of precracking, K_{Max} was ~ 22 MPa$\sqrt{m}$ (~ 20 ksi$\sqrt{in.}$) or somewhat lower in cases where that level would have exceeded the elastic limit. Although some specimens were tested in a plane-sided condition, most of the specimens were side grooved after precracking.

Side grooved specimens were side grooved by 20% of the total specimen thickness (B), 10% per side, using a C_v notch cutter (45° induced angle and 0.25 mm, 0.01 in., root radius). The resultant net specimen thickness (B_N) was then equal to 0.8 B. In general, side grooving is used to promote uniform (straight) crack growth during testing and to give lower bound J-R curve levels. The straight crack growth improves the performance of the unloading compliance method used for estimating crack growth during testing, and indicates a closer tendency towards generalized plane strain across the crack front.

2.3.3 Test Procedures

The procedures used for these tests are in accordance with ASTM Standards E 813 and E 1152. Specifically, the unloading compliance method was used to evaluate crack length during each test. The appropriate compliance expressions for the loadline measurement positions were used (Ref. 7).

All tests were performed on a servohydraulic test frame, with the load capacity of the test frame and the load cell optimized for each specimen size. A forced-air recirculating environmental chamber (with

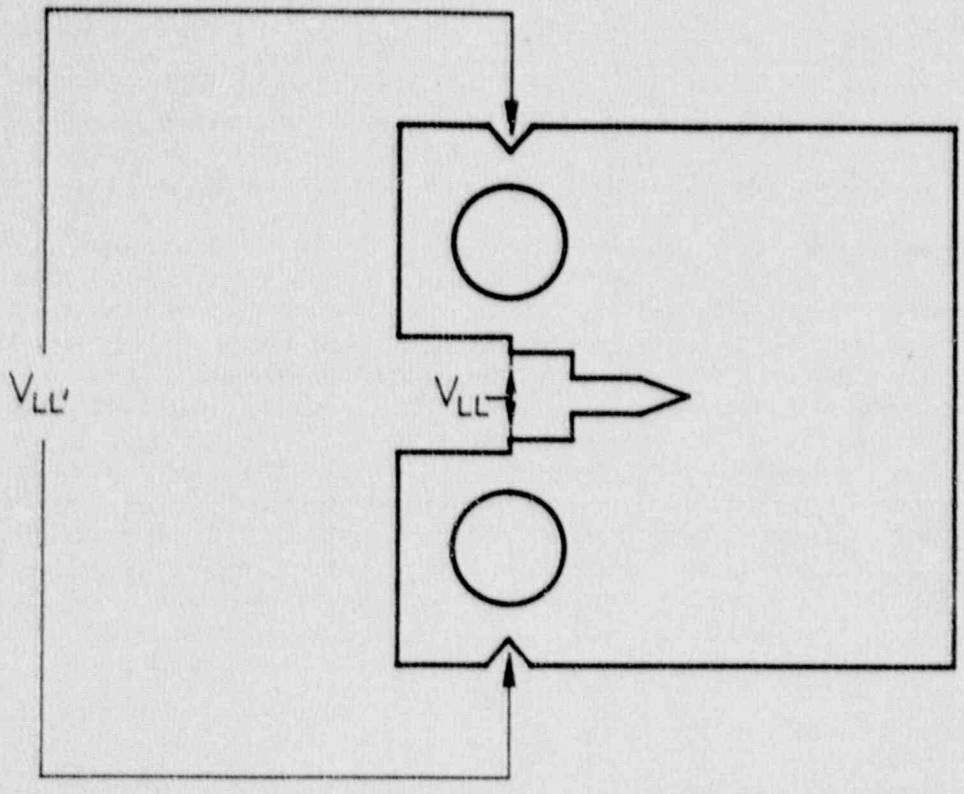

Fig. 2-2 The compact tension (CT) specimens used measurements of load-line displacement at the standard location (V_{LL}) or at a location external to the loading pin holes ($V_{LL'}$).

resistance heaters) was used to achieve the desired test temperatures. A thermocouple was mounted in each specimen to check temperatures throughout each test. Temperature was generally maintained at ± 3°C (5°F) of the desired test temperature throughout each test.

An analog trace of load vs. load-line displacement was made for each test. Load and displacement data were digitized using digital voltmeters and stored on floppy disks using a desktop computer. This system simplified post-test analysis and correction of the test data.

After each test, the specimen was heated using an acetylene torch to promote oxidation of the exposed fracture surface, i.e., to heat tint the surface. For ferritic specimens, once the specimen had returned to near ambient temperature, the specimen was chilled to near liquid nitrogen temperature and then fractured, exposing the fracture surface. For non-ferritic materials, the specimen was fatigue-cycled to failure, using a maximum load no more than 80% of the final test load. The specimen initial (precrack) and final (test) crack lengths were measured directly from the fracture surface using an optical measurement system. This system consists of an X-Y micrometer slide assembly and a magnifying eyepiece. The crack lengths were evaluated using the 9/8 averaging technique, in which the two near surface measurements are averaged together, with the resultant value averaged with the other seven measurements.

2.3.4 Data Analysis Procedures

As mentioned previously, the unloading compliance method has been used to determine crack length during the testing of each specimen. The Hudak-Saxena calibration equation (Ref. 7) is used to relate the measurements of compliance on the specimen load line to crack length. Both rotation (Ref. 8) and modulus corrections are made to the compliance data, as specified in ASTM standard E 1152-87.

J integral values have been determined using the deformation theory (J_D) and modified (J_M) forms. In this report, J_M is used to illustrate the toughness trends, although J_D results are also given in PIFRAC (Ref. 2), and some comparisons of the various J formulations are given in this report.

Ernst used a deformation theory of plasticity interpretation of J to develop a crack growth corrected form of the J integral, termed here J_D (Ref. 9). J_D is given by

$$J_{D\ i+1} = \left[J_{D\ i} + \left(\frac{\eta}{b}\right) \frac{A_{i,\ i+1}}{B_N} \right] \left[1 - \left(\frac{\gamma}{b}\right)_i \left(a_{i+1} - a_i\right) \right] \qquad (2\text{-}10)$$

$\eta = 2 + 0.522\ b/W$ for compacts

$\gamma = 1 + 0.76\ b/W$ for compacts

Deformation theory J, i.e., J_D, is the formulation of the J integral specified for use in ASTM Standards E 813 and E 1152. The validity criteria associated with J_D have restricted J_D-R curves to the point that they are virtually useless for application to structural stability determinations, primarily due to the limits on crack extension. Evaluation of J_D-R curves for different sizes of CT specimens have demonstrated a specimen size dependence as well (Refs. 10, 11 and 12).

One characteristic of J_D which was quickly found was a tendency towards a size-effect, whereby smaller specimens would give lower J-R curve levels than larger specimens, with negative J-R curve slopes resulting in many cases. To address these concerns, Ernst introduced a modified form of J, termed J_M (Ref. 11). Some of the attributes of J_M cited by Ernst include a better description of the process of deformation and crack growth, specimen-size independence, and a large relaxation of the restrictions on the amount of crack extension and/or initial remaining ligament needed to produce valid data. The specimen size independent characteristic of J_M was initially demonstrated in Ref. 11 for an A 508 Class 2A steel using data from 0.5T- to 10T-CT specimens. Confirmation of this can also be found in Refs. 10 and 12.

J_M is given by (Ref. 11)

$$J_M = J_D - \int_{a_o}^{a} \left. \frac{\partial \left(J_D - G \right)}{\partial a} \right|_{\delta_{pl}} da \qquad (2\text{-}11)$$

where

J_D = deformation theory J

G = Griffith linear elastic energy release rate

$= K_I^2 \, (1-\nu^2)/E$

a_o, a = the initial and current crack lengths, respectively

J_D-G = J_{pl}, the plastic portion of the deformation theory J

δ_{pl} = the plastic portion of the displacement

ν = Poisson's ratio

and $K_I = P \, f\left(\frac{a}{w}\right) \, (WBB_N)^{-1/2}$

where P is the hold load at a partial unloading, $f\left(\frac{a}{w}\right)$ is given in ASTM Standard E 399, and W, B, and B_N are the specimen width, thickness, and net thickness, respectively.

Reference 11 also provides an incremental form of Eq. 2-11:

$$J_{M\,i+1} = J_{D\,i+1} + \Delta J_{i+1} \qquad (2\text{-}12)$$

where

$$\Delta J_{i-1} = \Delta J_i + \left(\frac{\gamma}{b} J_{pl}\right)_i \left(a_{i+1} - a_i\right) \qquad (2\text{-}13)$$

The J_D and J_M equations described above represent "total area" forms of each whereby the area under the load-total displacement curve is used along with a single η term to evaluate J. Recent work indicates that the η term used tends to underestimate the elastic η, η_{el}, for the compact specimens. Therefore, a more appropriate way to evaluate J_D and J_M is to sum the elastic and plastic portions of each:

$$J = J_{el} + J_{pl} \qquad (2\text{-}14)$$

In this case,

$$J_{el} = K^2 \left(1 - \nu^2\right)/E \qquad (2\text{-}15)$$

with K from ASTM E 399, ν is Poisson's ratio (0.3) and E is Young's modulus. The plastic part of the J integral is then evaluated by substituting A_{pl} (the area under the load-plastic displacement curve) for A in Eq. 2-10 for evaluation of J_D. This same J_{pl} is used in Eq. 2-13 for the evaluation of J_M. The forms of J_D and J_M which result from this separation of the elastic and plastic J are denoted by a subscript of "*", i.e., J_{D*} and J_{M*} for clarity sake.

The J integral does have a certain validity criteria associated with it, generally to ensure that a region of "J dominance" exists. The primary criteria for "J dominance" include:

$$\omega = \frac{b}{J}\frac{dJ}{da} \gg 1 \qquad (2\text{-}16)$$

$$\Delta a < (0.06 \text{ or } 0.1\, b_o) \qquad (2\text{-}17)$$

$$J < \min (b,B)\, \sigma_f / 15,\ 20,\ \text{or } 25) \qquad (2\text{-}18)$$

The ω criteria (Eq. 2-16) is from Hutchison and Paris (Ref. 13), with a critical ω value of 5 normally suggested. The Δa limit of 0.06 was suggested by Shih (Ref. 14) whereas ASTM E 1152 uses a limit of 0.1. The J limits can be found variously in ASTM E 813-81 and E 1152, with E 813-81 specifying the factor of 25 for J_{Ic} validity and 15 for data used to determine J_{Ic}, whereas ASTM E 1152 specifies 20 as an upper limit on J evaluation.

A typical J-R curve is illustrated in Fig. 2-3. The J-R curve format is in accordance with that of ASTM E 813-81. The line emanating from the origin, called the blunting line, is given by $J = 2\sigma_f \Delta a$, where σ_f is the flow strength (the average of the 0.2% offset yield strength and the ultimate strength). The exclusion lines are constructed parallel to the blunting line, but offset by 0.15 mm (0.006 in.) and 1.5 mm (0.006 in.).

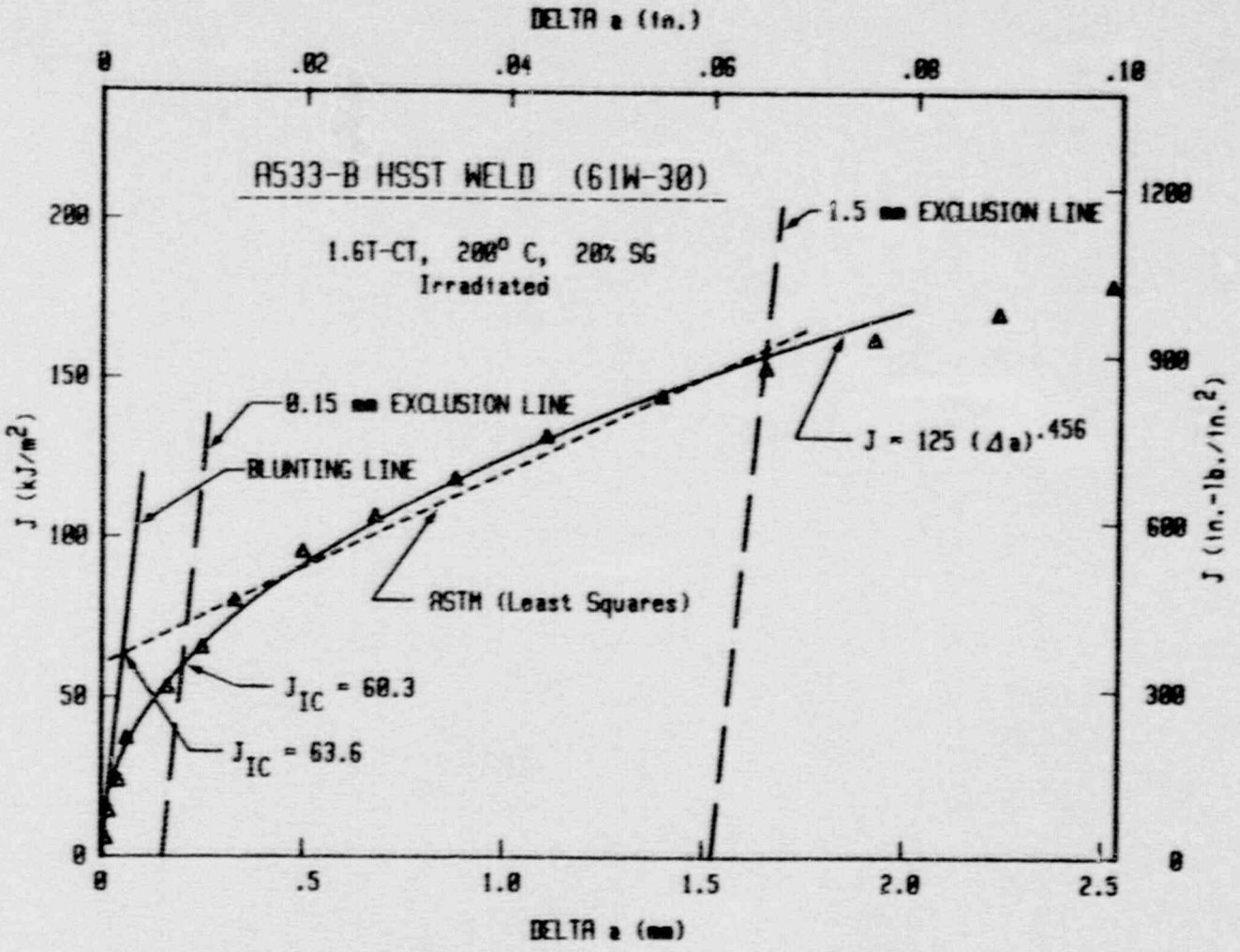

Fig. 2-3 The J-R curve format used with these data is in general conformance with that of ASTM standard E 813-81, with a 2 σ_f blunting line. Values of J_{Ic} are determined as in ASTM E 813, and using a power law curve-fit intersection with the 0.15 mm offset exclusion line.

By ASTM E 813-81 procedures, a straight line is fit to the test data between the 0.15 and 1.5 mm exclusion lines. This line is extrapolated back to the blunting line; the intersection is termed J_Q. J_{Ic} equals J_Q if various validity criteria are satisfied.

In the power-law evaluation of the J-R curve data, an equation of the form $J = C\,\Delta a^n$ is fit to the data between the exclusion lines. Power law J_{Ic} values are defined as the intersection of the power-law curve with a line parallel to the blunting line but offset by 0.2 mm (according to ASTM E 813-87), or as the intersection of the power-law with the 0.15-mm exclusion line. Previous experience has shown that the latter definition of J_{Ic} tends to give values nearly equivalent to those from ASTM E 813-81 for low alloy RPV steels.

Another parameter used to characterize the tearing resistance of structural materials is the tearing modulus, T_M, as given by

$$T_M = \frac{E}{\sigma_f^2} \frac{dJ}{da} \qquad (2\text{-}19)$$

where dJ/da is the slope of the J-R curve. Since the J-R curve generally conforms to a power-law, with $0 < n < 1$, the value of T_M changes (decreases) with increasing crack growth. For comparison purposes, average values of T_M, termed T_{avg} typically are used. The "ASTM" T_{avg} value (as defined here) uses the slope of the linear-fit as dJ/da; the "P.L." or power law T_{avg} value is determined from a fit of the power law to a straight line, defining dJ/da as an average slope evaluated in a closed-form manner (see Appendix H of Ref. 10).

2.4 Orientation Nomenclature

The orientation nomenclature specified in ASTM Standard E 616 ("Standard Terminology Relating to Fracture Testing") is used throughout this report.

In a pipe or tube, the three primary directions are longitudinal (L), circumferential (C) and radial (R). As illustrated in Fig. 2-4, orientation for crack growth specimens (i.e., C_v and fracture toughness) is denoted with a two-letter identifier. The first letter represents the direction normal to the crack plane, and the second letter represents the expected direction of crack growth. For the pipe or tube geometry, the four pertinent orientations are L-C, C-L L-R and C-R; R-L and R-C represent delamination-type of orientations which are not critical. Of the four pertinent orientations, L-R and C-R represent part-through flaws growing through-thickness, whereas L-C and C-L represent part-through flaws propagating length-wise, or through-flaws growing towards a large break. Principally for thinner pipes, the L-R and C-R orientations are impossible to sample using standard laboratory test specimen designs.

For uniaxial tension test specimens, an analogous single-letter nomenclature is used, with the single letter representing the

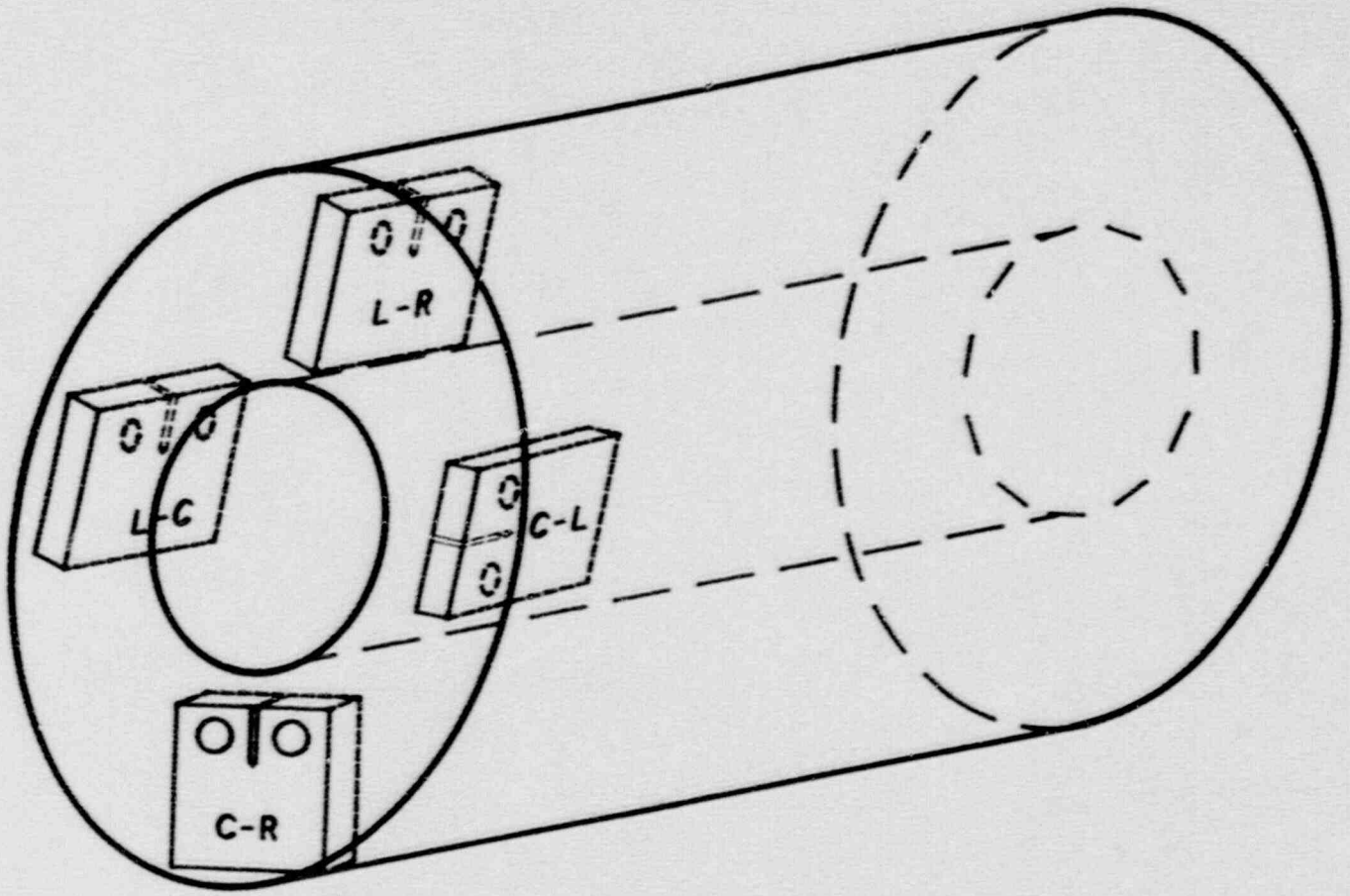

Fig. 2-4 The specimen orientation nomenclature follows the procedures of ASTM standard E 616, as illustrated for crack growth specimens. Tensile specimens are represented with a single letter indicating the axis of the specimen.

direction coincident with loading. Therefore, "C" orientation tensile data are pertinent to fracture toughness data in the C-L and C-R orientations.

3. FERRITIC STEELS

The ferritic steels tested include single heats of A 106 Grade C and A 516 Grade 70, a weld of A 516 Grade 70 to A 516 Grade 70, and several heats of A 106 Grade B. Chemical compositions for these heats are given in Table 3-1.

3.1 A 106 Grade C

3.1.1 Material Description

The heat of A106 Grade C was procured as an 813-mm (32-in.) diameter by 83-mm (3.25-in.) thick pipe. Environmentally-assisted fatigue crack growth rate data for this heat are also available (Ref. 15).

3.1.2 Charpy-V Data

Standard C_v specimens were tested from the C-R and L-R orientations of this heat, at temperatures ranging from ambient to 200°C. Specimens were located at the inside diameter, the mid-thickness and the outside diameter. These data are summarized in Table 3-2 and illustrated in Fig. 3-1. As illustrated, the L-R orientation exhibits higher energy levels than does the C-R orientation by 76% on average. Both orientations demonstrate considerable through-thickness variability. However, this is not consistent between the two orientations as the inside diameter has the highest energy levels for the L-R orientation and generally the lowest energy levels for the C-R orientation.

3.1.3 Tensile Data

The strength properties for this heat were determined using threaded-end specimens, with a gage diameter of 6.4 mm (0.252 in.) and a gage length of 25.4 mm (10 in.) used for elongation measurements.

The strength data are summarized in Table 3-3, and illustrated in Fig. 3-2. Both orientations demonstrate similar strength levels, athough the circumferential orientation does exhibit slightly higher strength. For both orientations, ductility is lower at 232°C (450°F) than at the other test temperatures, although the strength levels are virtually invariant with temperature.

3.1.4 Fracture Toughness Data

All four principal crack-plane orientations were sampled for fracture toughness testing. For the L-R and C-R orientations, 1T-CT specimens were used (Fig. 3-3), with standard load-line measurements of displacement. For the L-C and C-L orientations, 2T-CT specimens were used (Fig. 3-4). All specimens were side grooved by 20%, except for the L-C orientation test at 20°C.

Results for the fracture toughness tests are summarized in Table 3-4. All of these tests resulted in fully ductile behavior, with full J-R curves.

Table 3-1 Chemical Composition (Wt. %) of the Ferritic Piping Steels

Heat ID	Specification	Chemical Composition (Wt. %)							
		C	Mn	P	S	Si	Ni	Cr	Mo
A106	A 106 Gr.C	0.25	0.86	0.016	0.017	0.22	0.25	0.10	0.033
ZP15	A 106 Gr.B	0.18	0.72	0.02	0.013	ND[a]	ND[a]	ND[a]	ND[a]
ZP13	A 106 Gr.B	0.17	0.83	0.028	0.026	0.290	ND[a]	ND[a]	ND[a]
ZP14	A 106 Gr.B	0.24	1.01	0.022	0.019	ND[a]	ND[a]	ND[a]	ND[a]
B	A 516 Gr.70[b]	0.26	1.06	0.009	0.012	0.220	0.093	0.60	0.022
W	Weld (A 516 Gr.70)[c]	0.11	1.66	0.011	0.008	0.38	0.077	0.073	0.45

[a] Not determined.

[b] Also, 0.130 Cu, 0.003 V, 0.028 Al, 0.007 W, 0.010 Sn.

[c] Also, 0.14 Cu, 0.004 Sn, 0.009 Al, 0.007 V, 0.003 Cb, 0.006 Zr, 0.005 Co, 0.0004 B.

Table 3-2 Charpy-V Data for A 106 Grade C Steel (ZP21)

Orientation	Location	Test Temperature (°C)	Charpy-V Energy	
			Average (J)	Actual Measurements (J)
C-R	ID	22	76.4	73, 77, 79
		93	82.3	75, 85, 87
		288	85.4	76, 88, 92
	MID	22	63.3	60, 61, 69
		93	90.4	88, 88, 95
		288	98.1	96, 99, 99
	OD	22	80.9	72, 83, 88
		93	101.7	99, 103, 103
		288	113.9	111, 114, 117
L-R	ID	22	141.5	141, 141, 142
		93	163.2	155, 160, 175
		288	205.4	202, 209
	MID	22	103.9	100, 100, 111
		93	149.6	144, 152, 153
		288	169.0	161, 172, 174
	OD	22	137.8	134, 136, 144
		93	160.0	157, 157, 165
		288	176.3	174, 178, 178

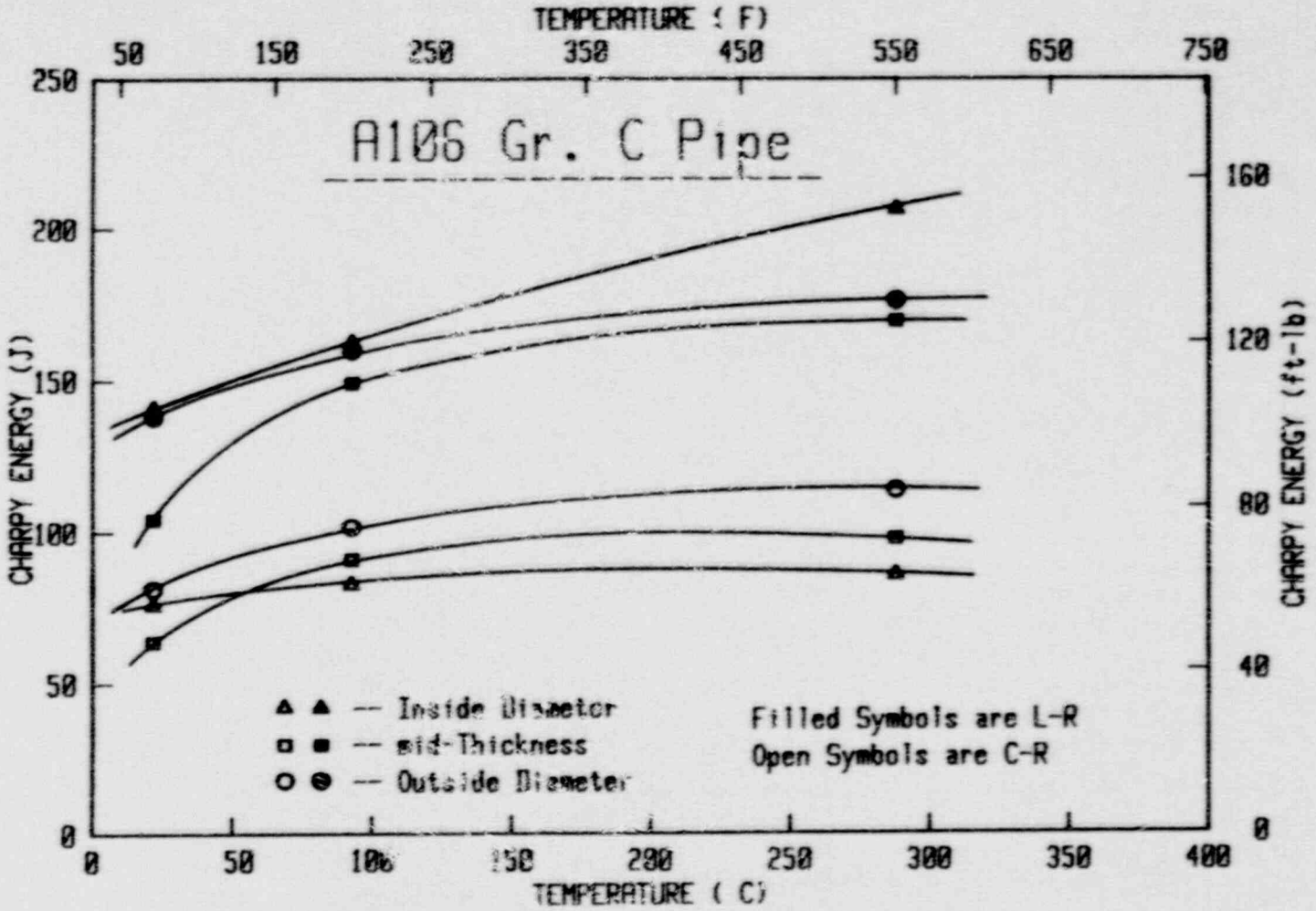

Fig. 3-1 Charpy-V data for A 106 Gr. C indicate a through-thickness sensitivity for both the C-R and the L-R orientations.

Table 3-3 Tensile Data for A 106 Grade C, Heat ZP21

Specimen Number	Test Temp. (°C)	Orientation	0.2% Offset Yield Strength (MPa)	0.2% Offset Yield Strength (ksi)	Ultimate Strength (MPa)	Ultimate Strength (ksi)	Reduction In Area (%)	Elongation (%)
A106-1L	22	L	355.8	51.6	573.6	83.2	69.7	29.4
A106-2L	22	L	354.4	51.4	569.5	82.6	68.8	30.9
A106-1C	22	C	372.3	54.0	586.1	85.0	61.3	27.9
A106-2C	22	C	348.9	50.6	572.3	83.0	61.6	28.2
A106-3L	232	L	282.0	40.9	588.1	85.3	55.7	24.6
A106-3C	232	C	328.9	47.7	608.8	88.3	54.6	24.9
A106-4L	343	L	279.9	40.6	584.0	84.7	77.8	33.9
A106-5L	343	L	286.8	41.6	586.3	85.0	76.3	35.0
A106-4C	343	C	279.9	40.6	570.9	82.8	65.2	31.5
A106-5C	343	C	322.7	46.8	592.9	86.0	71.7	37.2

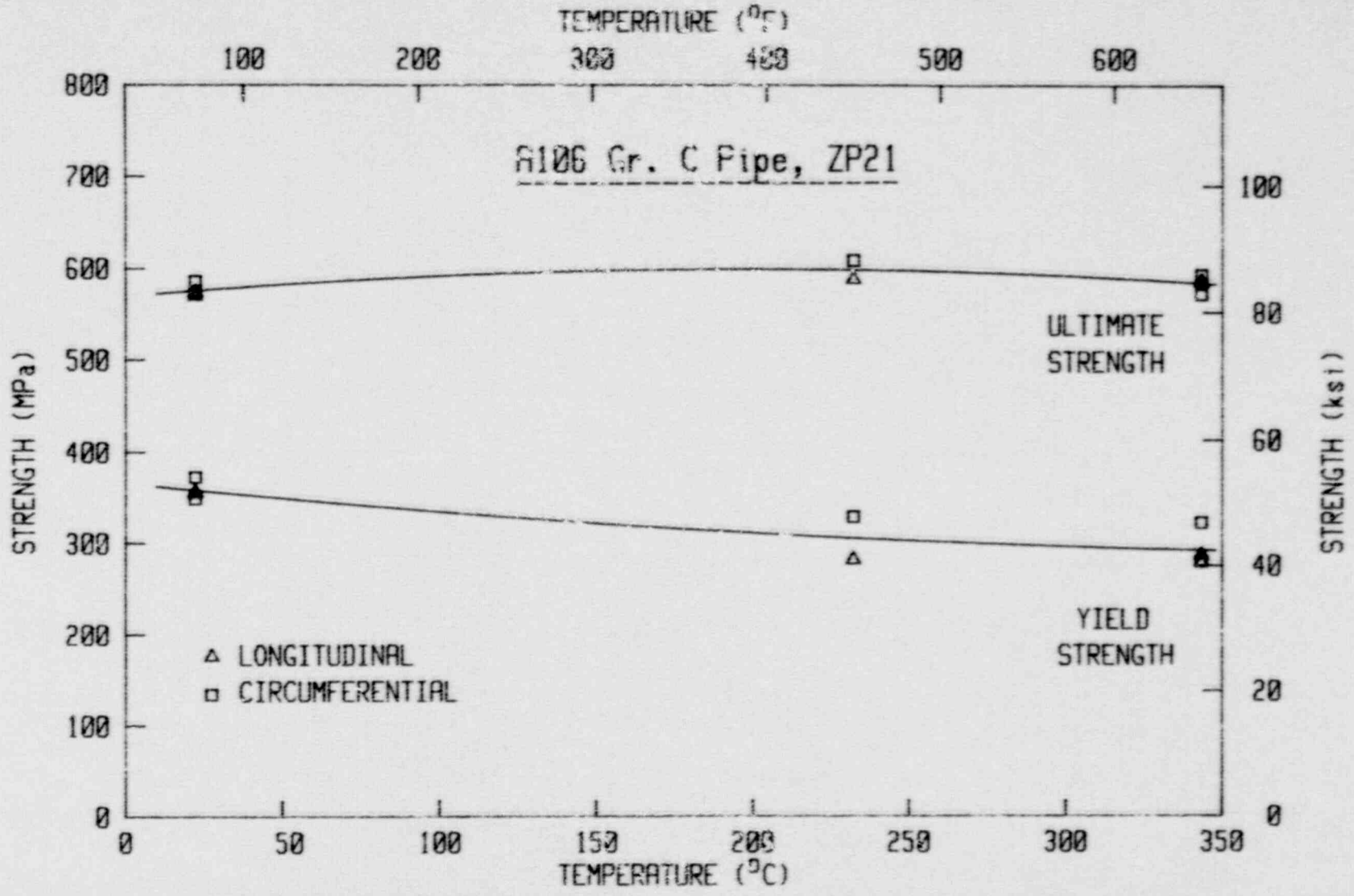

Fig. 3-2 Tensile strength data for A 106 Gr. C demonstrate minimal temperature sensitivity.

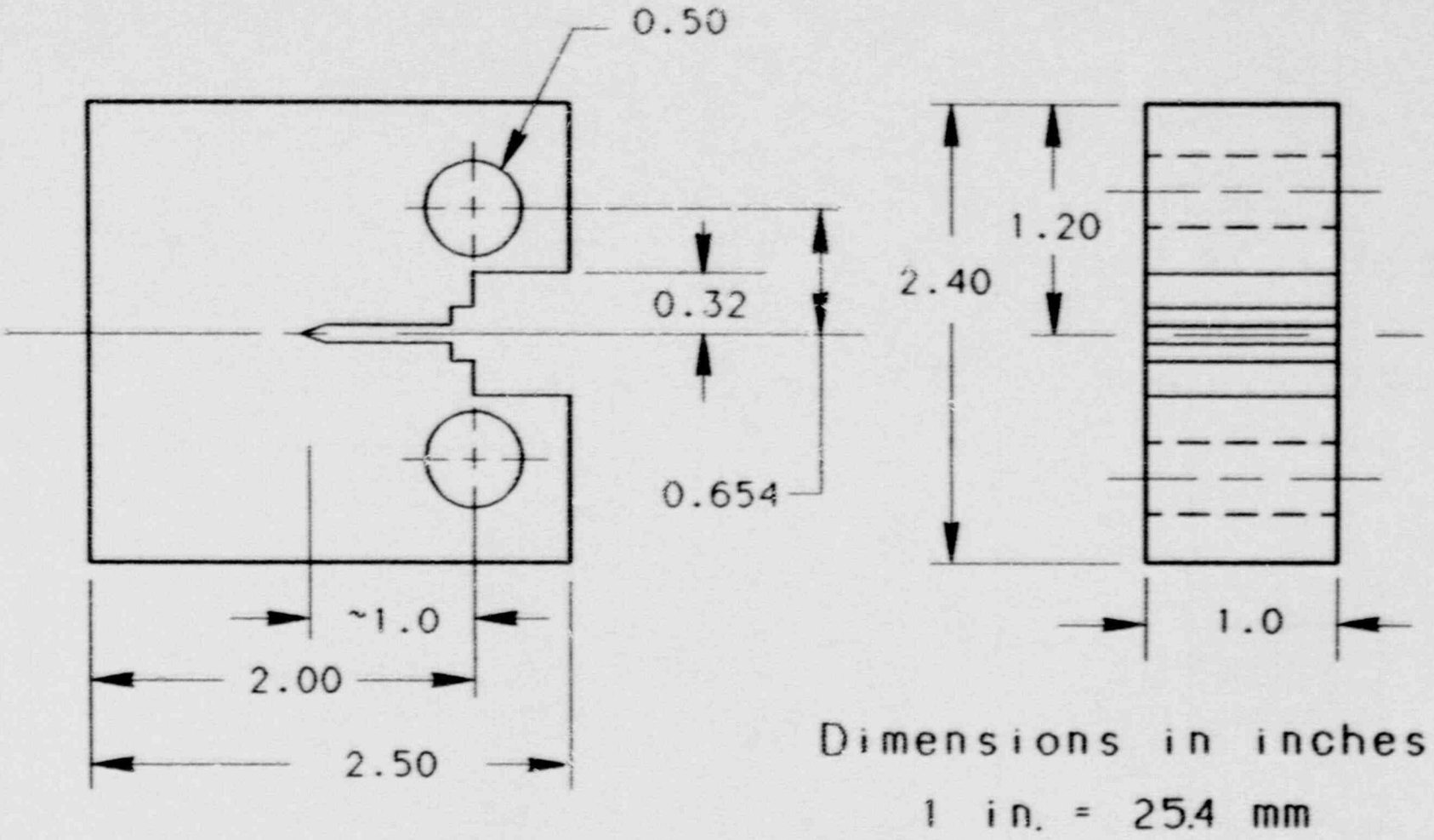

Fig. 3-3 Fracture toughness tests of A 106 Gr. C used this 1T-CT specimen design.

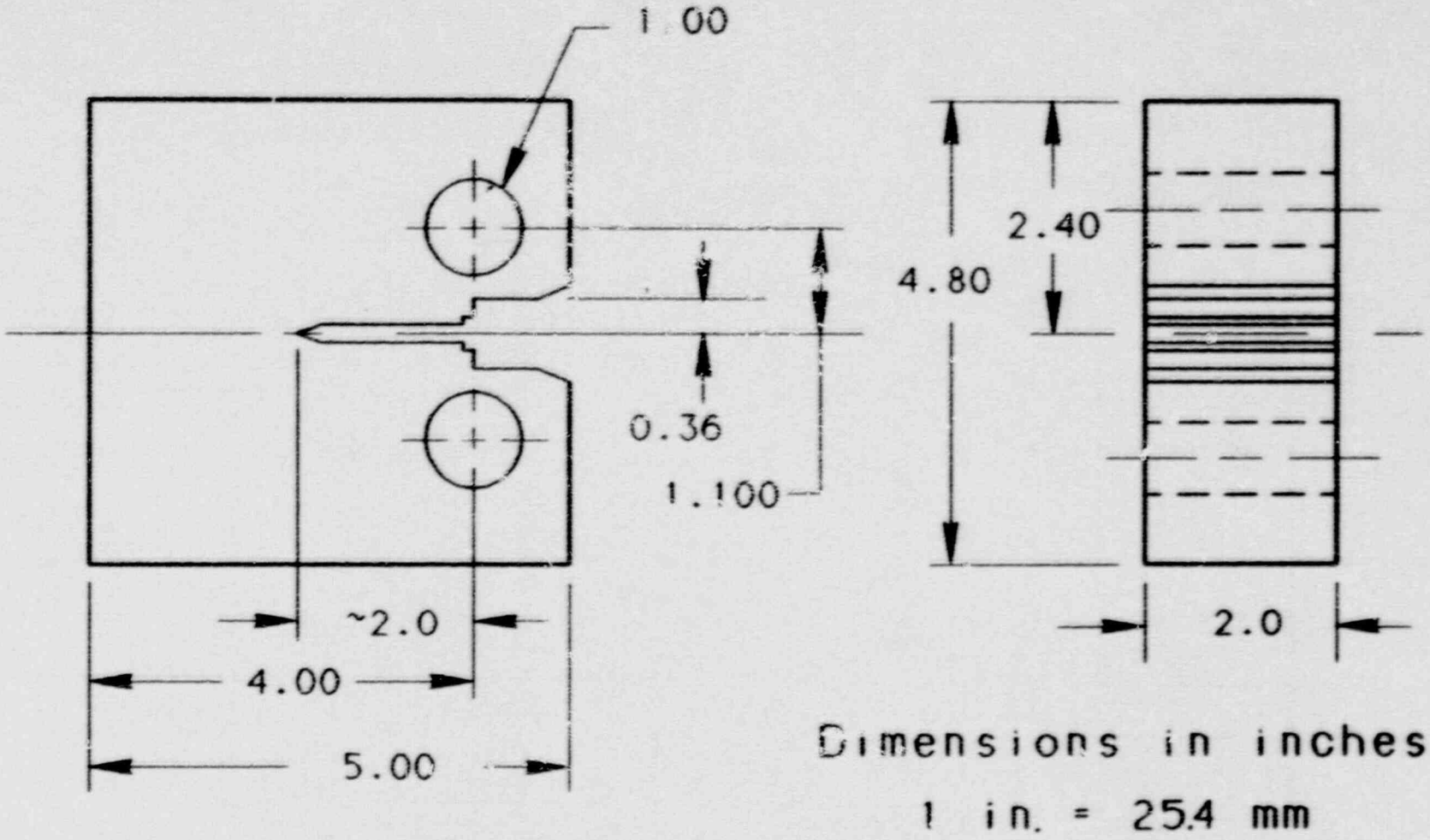

Fig. 3-4 Fracture toughness tests of A 106 Gr. C used this 2T-CT specimen design.

Table 3-4 J-R Curve Results for A 106 Grade C (20% Sideg rooved)

Specimen Number	Test Temperature (°C)	$(a/W)_o$	Δa_p (mm)	$\Delta a_p - \Delta a_b$ (mm)	J_{1c} P.L. (kJ/m^2)	J_{1c} Linear (kJ/m^2)	K_{Jc} P.L. (MPa$\sqrt{m}$)	K_{Jc} Linear (MPa$\sqrt{m}$)	T_{mat} P.L.	T_{mat} ASTM	Flow Strength (MPa)
C-R Orientation (1T-CT)											
A106-10CR	20	0.518	12.61	-0.77	112.3	89.1	159.5	142.0	164	175	469.5
A106-13CR	20	0.517	13.22	+0.08	117.0	109.0	162.7	157.1	155	163	469.5
A106-22CR	20	0.518	12.07	-0.49	108.0	105.0	156.3	154.2	161	160	469.5
A106-12CR	121	0.516	12.20	-0.66	102.9	97.4	150.5	146.4	133	132	477.8
A106-15CR	121	0.520	11.83	+0.11	131.5	124.9	170.1	165.8	116	119	477.8
A106-19CR	121	0.515	12.38	-0.77	123.2	114.9	164.7	159.0	117	121	477.8
A106-14CR	232	0.519	12.54	-0.66	74.1	98.2	125.7	144.7	100	85	468.8
A106-17CR	232	0.512	10.81	-0.10	101.7	98.3	147.2	144.7	92	95	468.8
A106-16CR	288	0.514	11.77	-0.41	126.3	119.9	162.7	158.5	102	106	457.8
A106-18CR	288	0.513	11.24	-0.24	108.2	94.6	150.6	140.8	113	120	457.8
A106-21CR	288	0.519	10.99	-0.38	125.9	103.3	167.5	147.2	106	129	457.8
A106-11CR	343	0.517	11.35	-0.74	215.5	210.7	210.8	208.4	144	145	442.0
A106-20CR	343	0.522	10.47	-0.38	202.9	189.4	204.5	197.6	157	164	442.0
A106-23CR	343	0.522	10.17	-0.45	220.3	208.7	213.1	209.4	136	144	442.0
L-R Orientation (1T-CT)											
A106-14LR	23	0.521	7.45	-0.03	214.2	192.1	220.2	211.5	301	318	463.3
A106-15LR	20	0.519	9.27	+0.05	167.1	155.1	194.5	187.4	294	282	463.3
A106-20LR	20	0.521	8.52	-0.11	222.5	190.1	224.4	207.4	304	307	463.3
A106-13LR	121	0.519	9.26	+0.16	195.6	179.8	207.5	198.9	235	237	445.4
A106-18LR	121	0.519	8.84	-0.02	154.9	149.4	184.6	181.3	276	263	445.4
A106-17LR	121	0.518	11.07	+0.25	130.0	156.9	199.0	185.9	248	252	445.4
A106-12LR	232	0.521	11.97	-0.12	112.4	90.3	154.9	141.0	141	155	435.1
A106-19LR	232	0.519	9.90	-0.22	117.6	102.0	158.3	147.4	167	174	435.1
A106-22LR	232	0.519	11.85	-0.08	122.8	119.5	161.8	159.6	167	165	435.1
A106-11LR	288	0.519	8.61	-0.37	148.4	129.3	176.4	164.7	190	196	433.0
A106-18LR	288	0.523	8.68	-0.27	174.9	148.5	191.5	176.4	243	250	433.0
A106-21LR	288	0.513	10.48	-0.18	156.0	137.0	180.6	169.5	224	229	433.0
A106-10LR	343	0.522	2.37	+0.41	406.5	342.9	289.5	265.9	371	383	434.4
A106-23LR	343	0.513	4.35	+0.36	467.2	392.0	310.3	284.3	315	344	434.4
A106-24LR	343	0.519	3.81	+0.12	451.1	422.3	305.0	295.1	378	372	434.4
L-C Orientation (2T-CT)											
A106-1LC[a]	24	0.519	12.97	-1.57	223.8	194.2	214.6	199.9	272	275	463.3
A106-2LC	121	0.517	14.32	-1.55	295.5	261.1	255.0	239.7	211	236	445.4
A106-3LC	232	0.518	23.30	-1.29	207.4	205.7	210.2	209.4	143	146	435.1
A106-4LC	288	0.518	18.13	-0.64	285.4	262.5	244.6	234.6	160	178	433.0
A106-5LC	288	0.517	16.41	-0.62	290.3	274.6	246.7	239.9	181	190	433.0
A106-6LC	343	0.505	7.77	-1.93	633.4	570.1	344.7	327.0	324	365	434.4
A106-7LC	343	0.519	8.61	-1.27	583.9	578.7	331.0	329.5	210	205	434.4
C-L Orientation (2T-CT)											
A106-ACL	343	0.517	14.33	-0.93	232.7	234.1	219.0	219.7	121	120	422.0

[a] Sideg rooved 10%.

J-R curves for the C-R, L-R and L-C orientations are illustrated in Figs. 3-5 to 3-7. In each case, the lowest J-R curves are at 232°C (450°F), with the highest J-R curves at 343°C (650°F). Overall, the toughness at ambient temperature is fairly high, with increasing temperature resulting in somewhat reduced toughness, at least to 232°C. At higher temperatures, the toughness increases substantially. For each orientation, only moderate scatter results from multiple tests at each temperature. J_M and J_D give similar comparisons for the L-C orientation (Fig. 3-7).

Comparing the curves at 343°C (Fig. 3-8), the L-R and L-C orientations exhibit much higher toughness than the C-R and C-L orientations. The closeness of results for the L-R and L-C orientations and, separately, the C-R and C-L orientations implies that, for the same loading in both orientations, flaws will tend to propagate through-thickness almost as easily as lengthwise.

Further illustration of the temperature dependence and orientation effect are given in Figs. 3-9 and 3-10 for J_{Ic} and T_{avg}, respectively. The overall temperature dependence is identical to that reported by Miglin, et al. (Ref. 16), which was attributed to dynamic strain aging (DSA). Many of the 1T-CT specimens from the L-R and the C-R orientations exhibited minor serrated tearing, indicative of DSA. Several other specimens experienced load drops, ranging from minor (20% or less) or much larger (up to 58%), also indicative of DSA. However, none of the 2T-CT specimens from the L-C and the C-L orientations exhibited any serrations or load drops. This finding is somewhat surprising since data for the L-C orientation are nearly identical to those for the L-R orientation, and data for the C-L orientation are similar to that for the C-R orientation. Although the loading rates for the 1T-CT and the 2T-CT specimens were intended to give the same $\dot{K}$ on the elastic portion of the load displacement curves, the descrepency in behavior may be due to inheret differences in the effective strain rate during plastic strain (i.e., after maximum load) for the two specimen sizes. Since no evidence of DSA has been found for the 2T-CT specimens, then DSA may not be the cause for the temperature dependence seen for this steel.

Load-deflection curves for several tests of the C-R and the L-R orientations are illustrated in Fig. 3-11. The tests at 343°C exhibit no unusual behavior, whereas the tests at 20°C exhibit only minor serrated tearing, as indicated by the extremely small "lumps" in the load-displacement curves. (The occasional large load spikes to higher loads are due to test machine noise and not due to anything from the specimen.) In contrast, the tests at 288°C exhibit large load drops, during which large crack jumps occur.

Concerning the indications of DSA, particularly the crack jumps and serrated tearing, the lowest J-R curves (at 232°C) exhibited minor serrated tearing (similar to that seen in Fig. 3-11 for the tests at 20°C) and small load drops in several cases, but in general the signs of DSA were more pronounced (i.e., greater load drops) at 288°C than at 232°C. In general the signs of DSA were less pronounced as the test temperature was reduced from 232°C, and no serrated tearing or load drops occurred at 343°C.

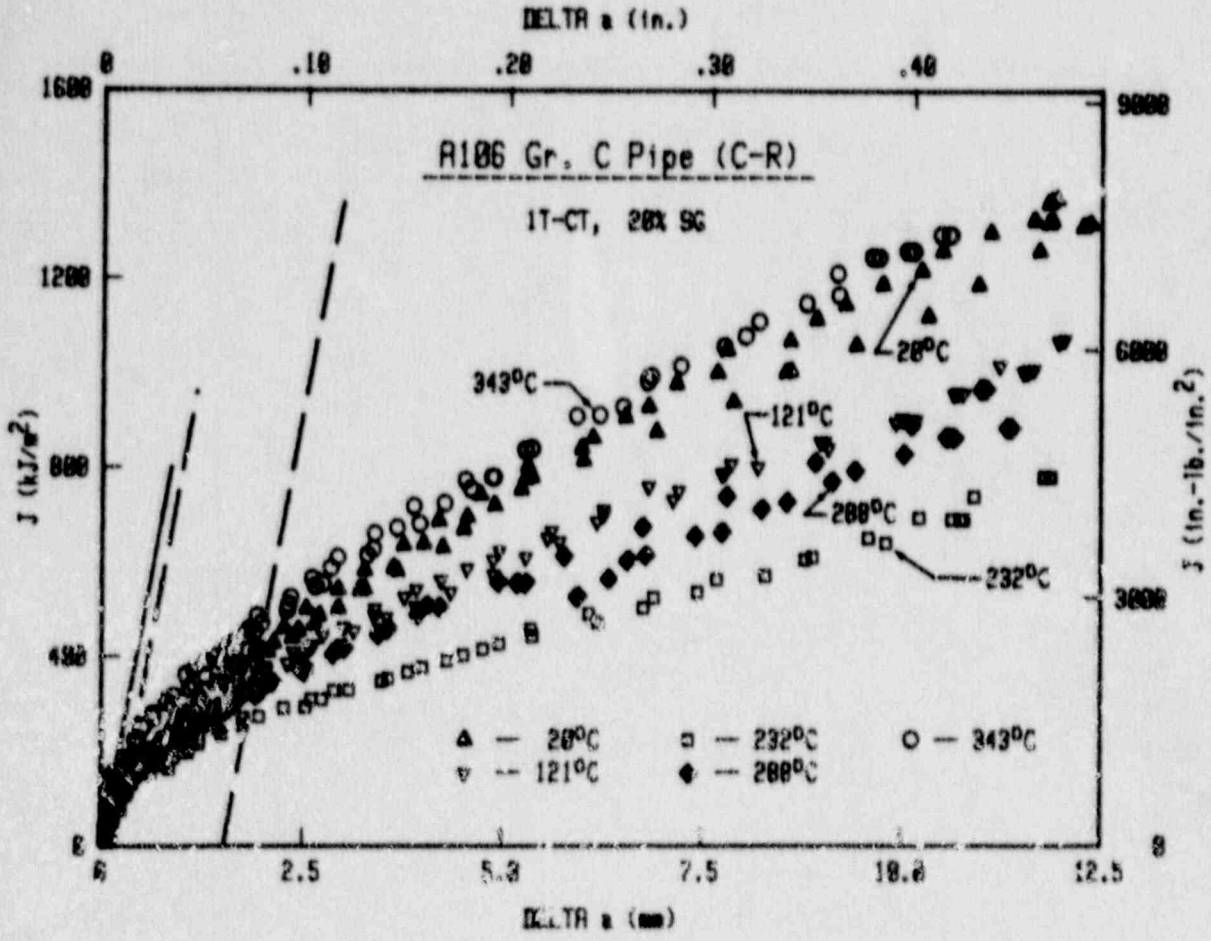

Fig. 3-5 J-R curve tests for A 106 Gr. C (C-R orientation) demonstrate strong temperature sensitivity, with the lowest J-R curves at a test temperature of 232 °C.

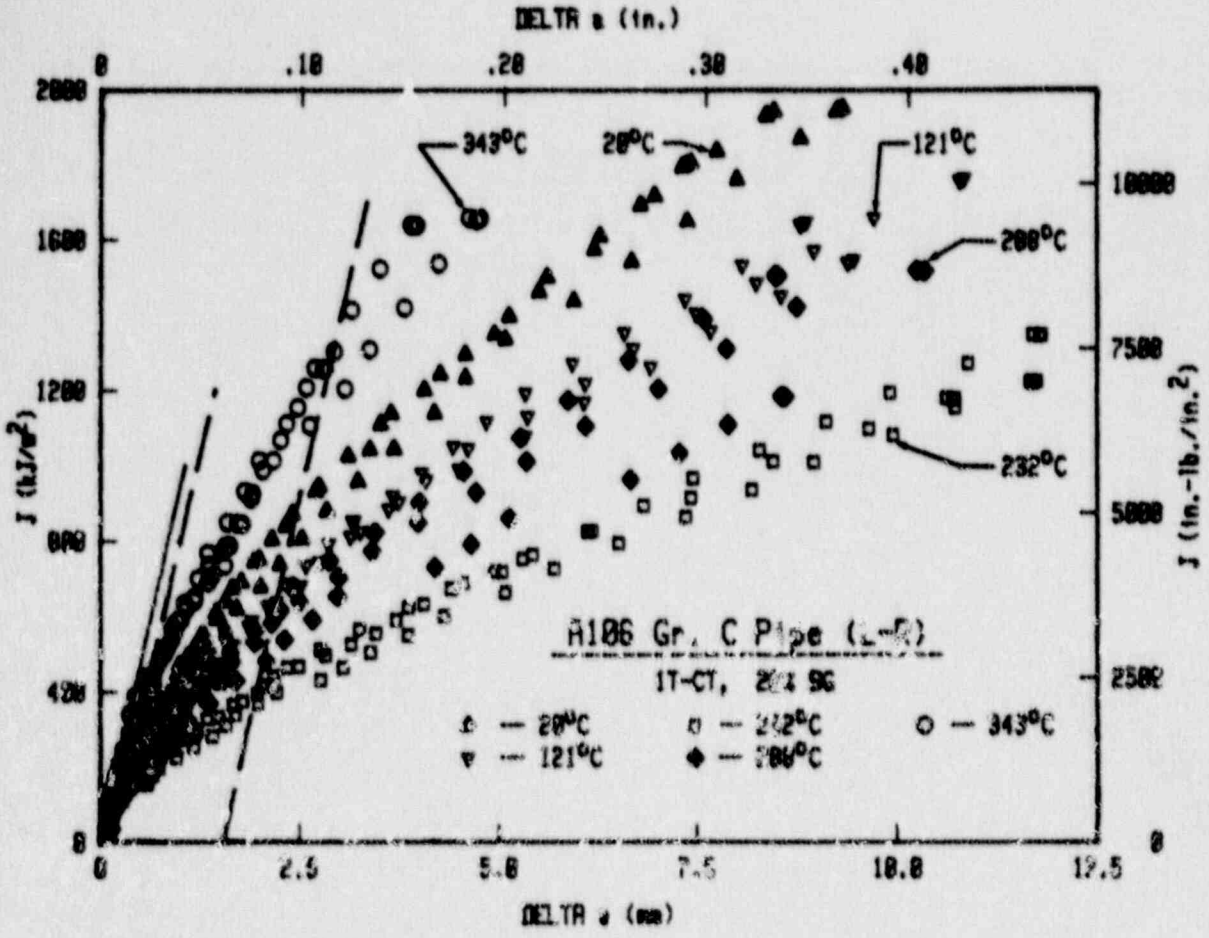

Fig. 3-6 J-R curve tests for A 106 Gr. C (L-R orientation) demonstrate strong temperature sensitivity, with the lowest J-R curves at a test temperature of 232 °C.

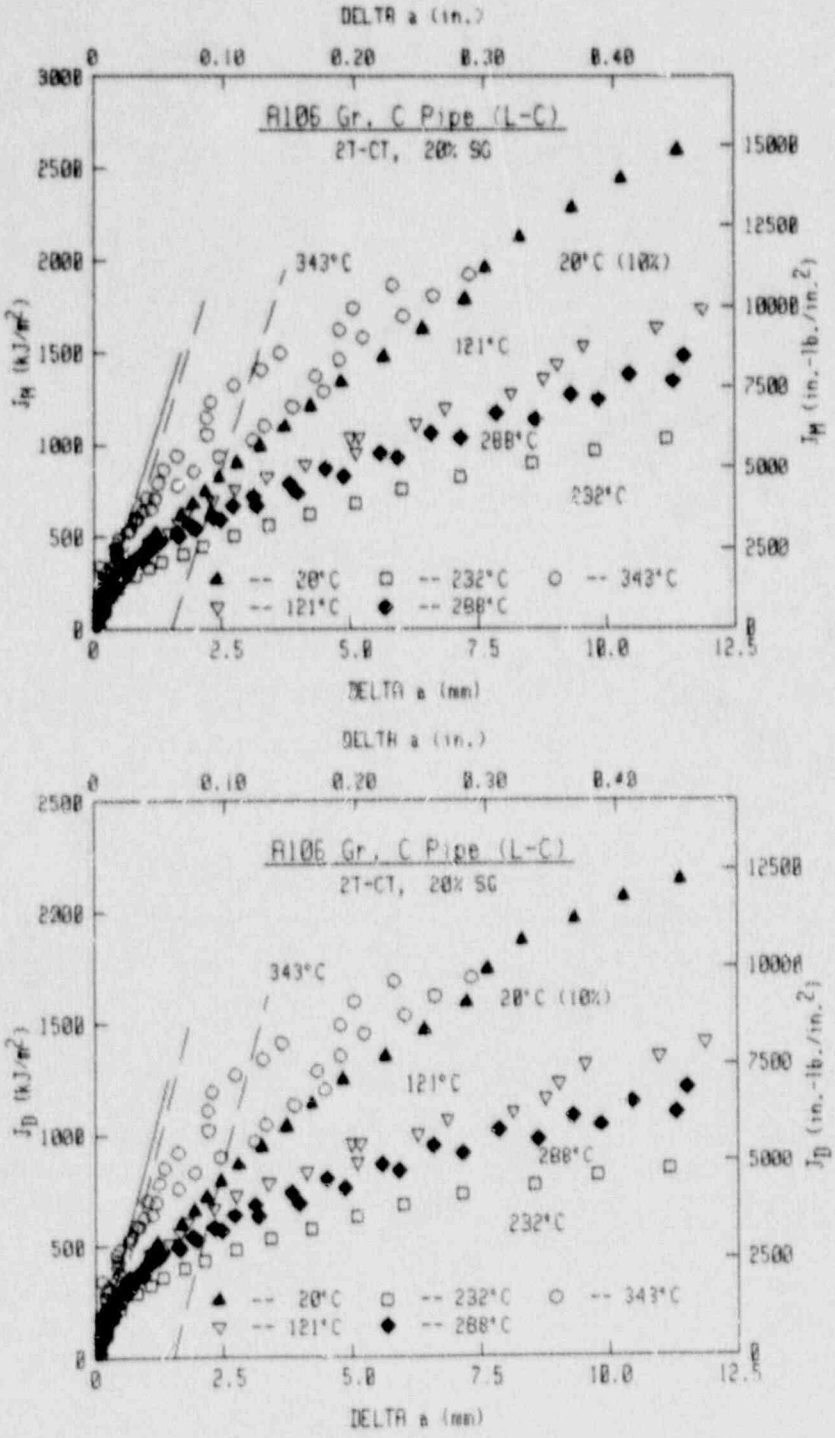

Fig. 3-7 J-R curve tests for A 106 Gr. C (L-C orientation) demonstrate strong temperature sensitivity, with the lowest J-R curves at a test temperature of 232°C. In this case, data using both J_M and J_D are illustrated.

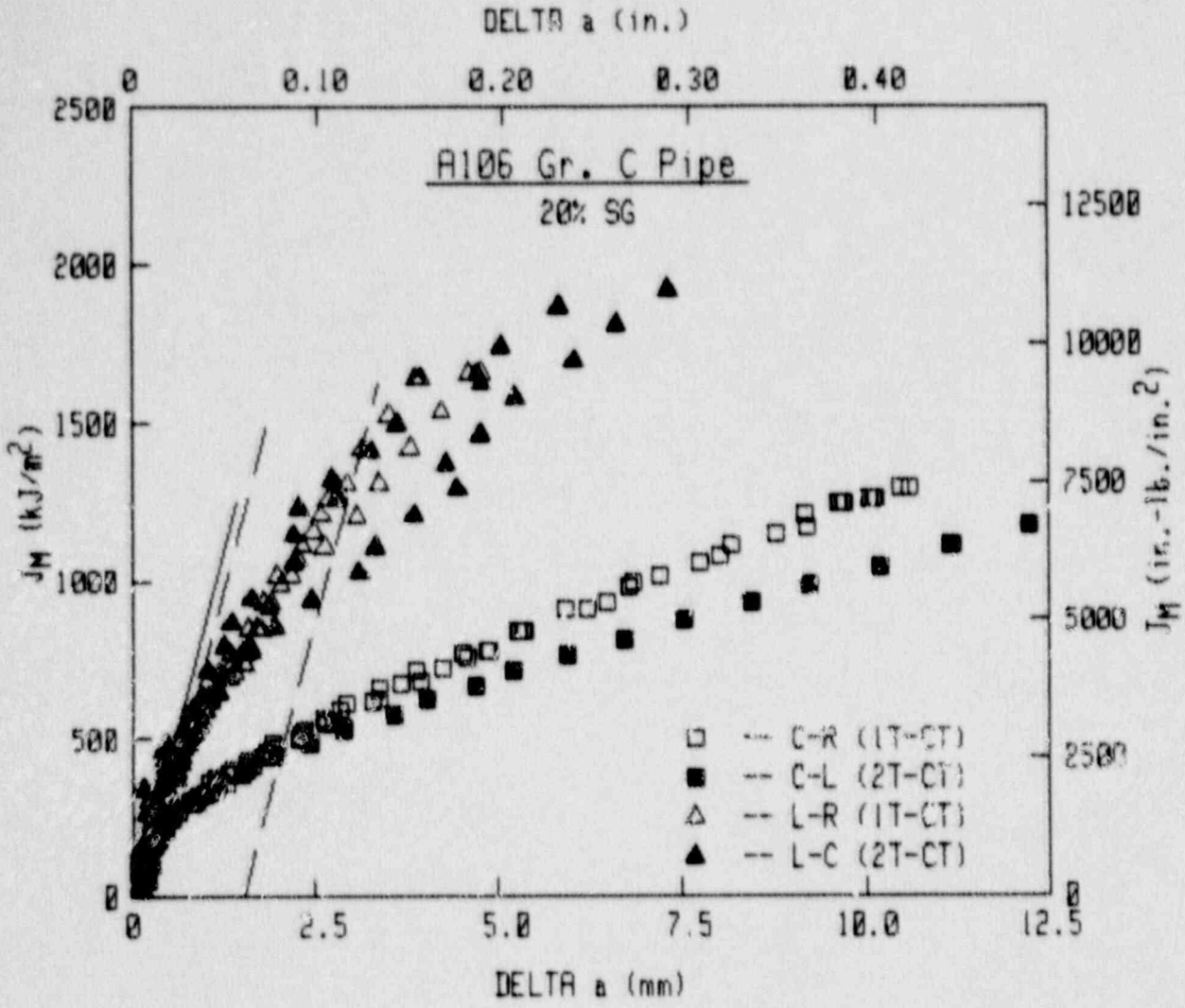

Fig. 3-8 J-R curve tests for A 106 Gr. C at 343°C demonstrate strong orientation sensitivity. Similar toughness is evident for crack growth orientations representing through-thickness crack growth and lengthwise flaw growth.

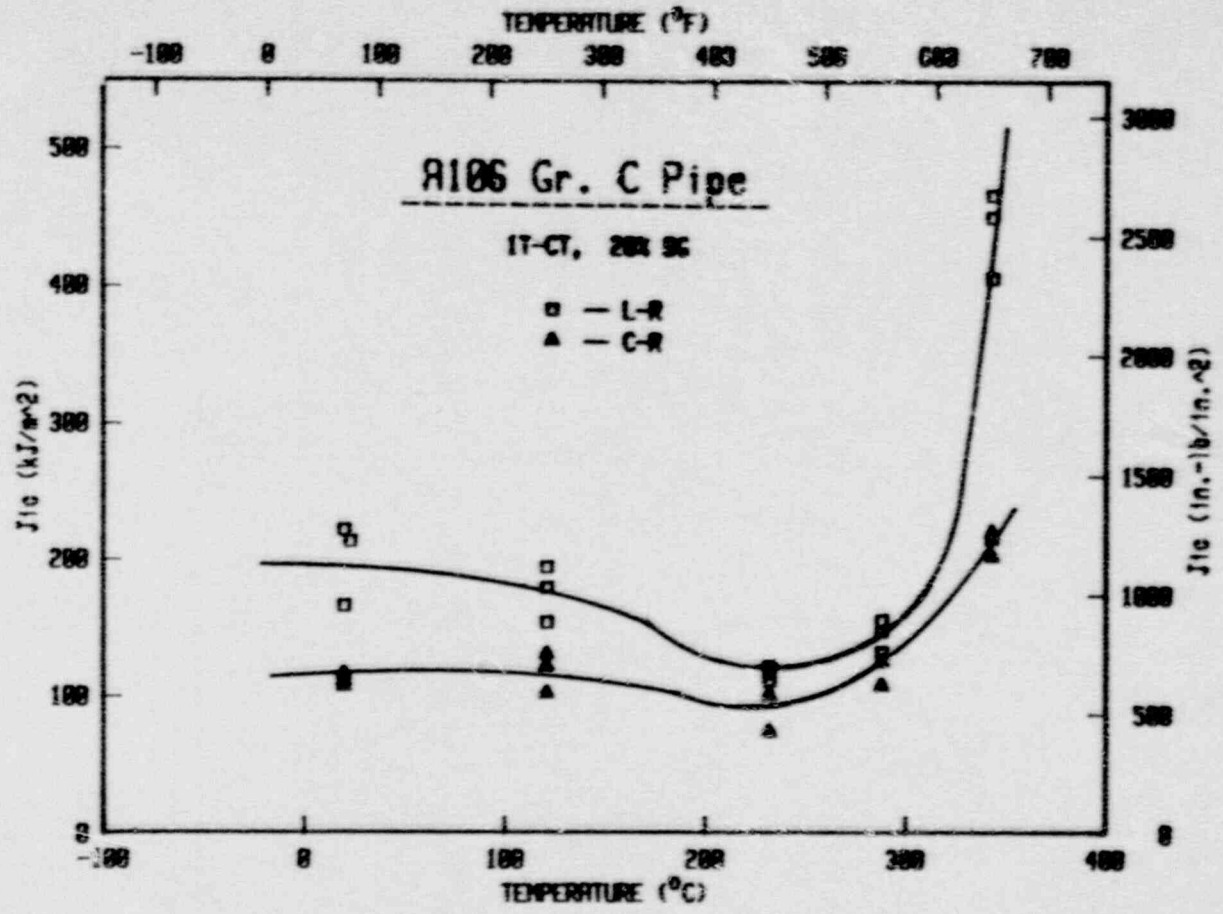

Fig. 3-9 For A 106 Gr. C, J_{IC} values for the C-R and the L-R orientation demonstrate strong temperature sensitivity.

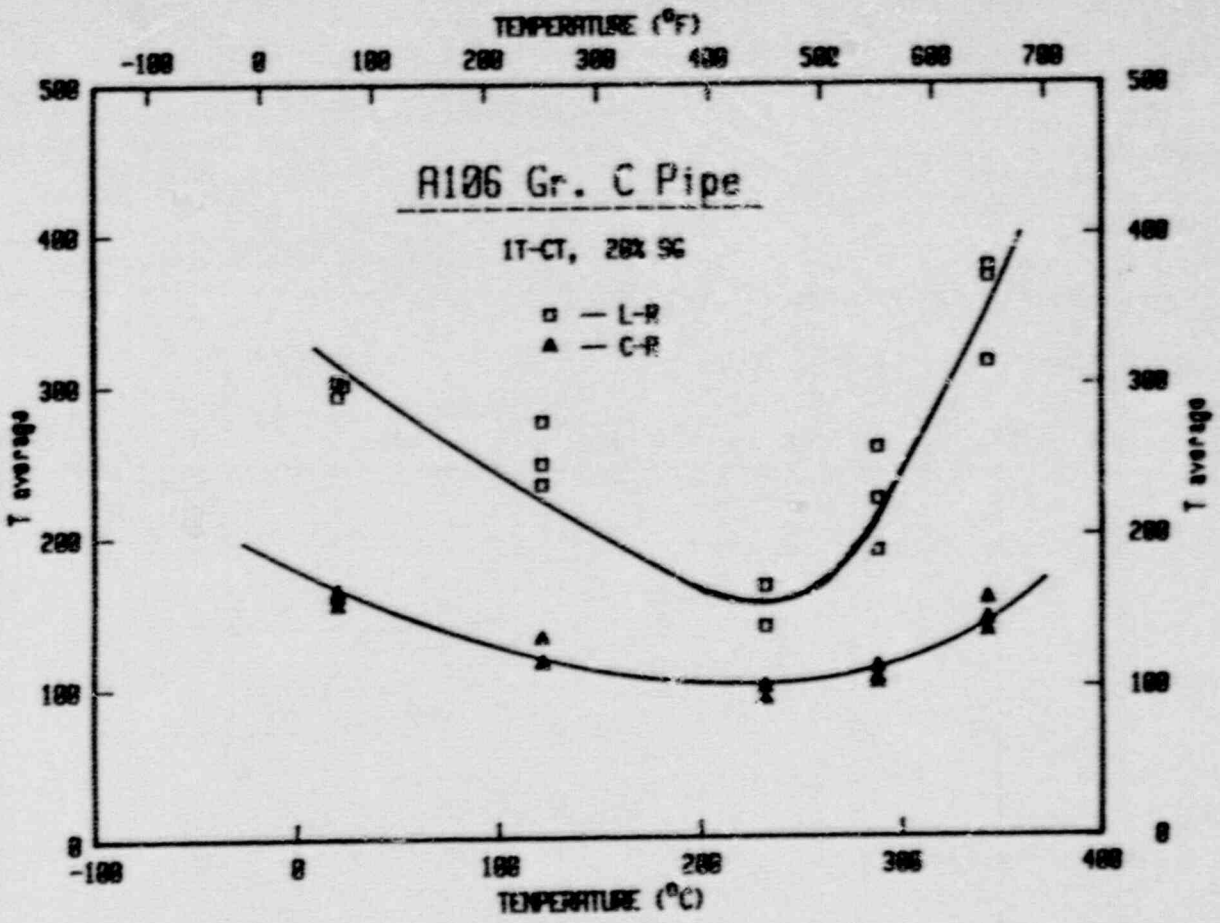

Fig. 3-17 For A 106 Gr. C, T_{avg} values for the C-R and the L-R orientation demonstrate strong temperature sensitivity.

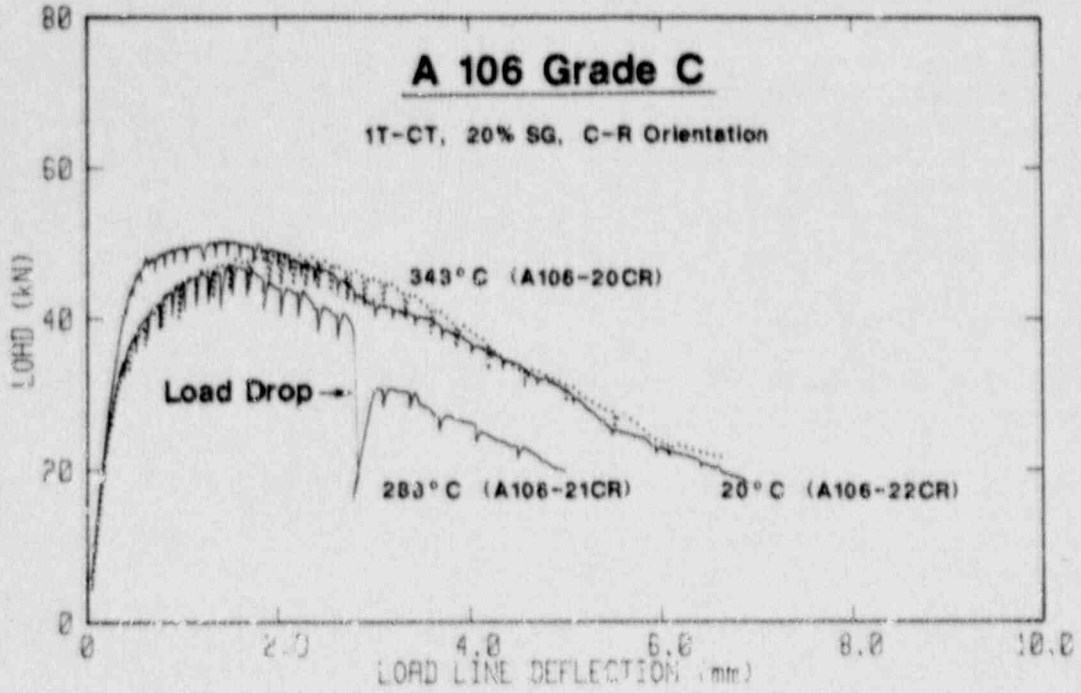

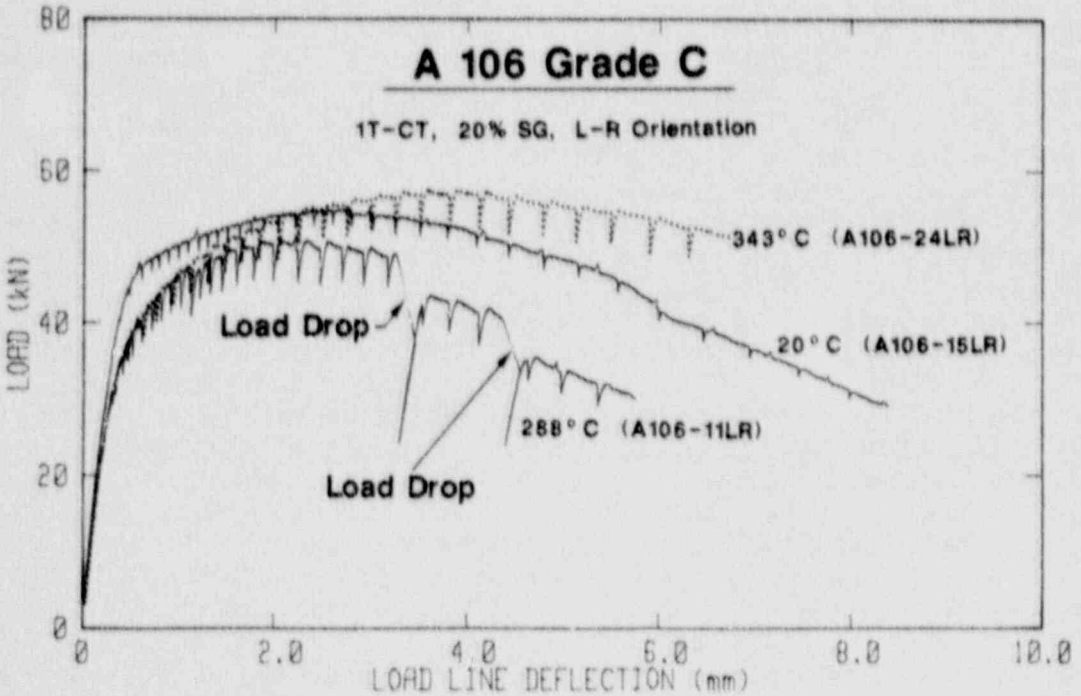

Fig. 3-11 For A 106 Gr. C, load-deflection curves for the C-R and the L-R orientations demonstrate temperature sensitivity. At 288 °C, the maximum loads are reduced from those at 20 °C and 343 °C, with load drops also evident at 288 °C.

3.2 A 106 Grade B

3.2.1 Material Description

Three different heats of A 106 Grade B were procured and tested. All three heats had a diameter of 152 mm (6 in.), where Heat ZP13 was a Schedule 40 (a wall thickness of 7.1 mm or 0.28 in.), Heat ZP15 was a Schedule 120 (a wall thickness of 14.3 mm or 0.56 in.), and Heat ZP14 was a Schedule XXS (a wall thickness of 0.86 in.). Heat ZP13 is the same heat as DP2-F1, ZP15 is the same as DP2-F30 and ZP14 is the same as DP2-F2 in Ref. 4.

3.2.2 Charpy-V Data

Due to the thin wall of Heat ZP13, C_v specimens with a reduced thickness (B) of 5.8 mm (0.23 in.) were tested from the L-C orientation only. As illustrated in Fig. 3-12 and listed in Table 3-5, this heat exhibits upper shelf behavior (as demonstrated by 100% shear) at temperatures as low as -100°C (-148°F). A sharp increase in absorbed energy occurs at 288°C (550°F), although the lateral expansion do not reflect this increase.

For Heat ZP15, full thickness C_v specimens (B = 10 mm or 0.394 in.) were tested from the L-C and C-L orientations, with one reduced thickness specimen (B = 5.8 mm or 0.23 in.) tested from the L-C orientation. Results for this heat are summarized in Table 3-6, and illustrated in Fig. 3-13. The L-C orientation is seen to have much higher upper shelf energy levels, as the TANH relation (Eq. 2-1) indicates an upper shelf energy of 153 J (113 ft-lb) for the L-C orientation, in contrast to 59 J (43 ft-lb) for the C-L orientation. For both orientations, upper shelf (as given by 100% shear) does not occur until ~ 150°C (300°F). As with ZP13, a sharp increase in absorbed energy at 288°C (550°F) for the L-C orientation is not accompanied by a similar increase in lateral expansion. For the C-L orientation, the energy increase at 288°C is reflected by the lateral expansion.

If the energy of the reduced-thickness specimen is linearily scaled (using the specimen thickness / the standard specimen thickness), then the effective energy becomes 81 J (60 ft-lb). In comparison, two full-thickness specimens tested at this same temperature had energies of 81 J (60 ft-lb) and 52 J (38 ft-lb). The lateral expansion of the reduced-thickness specimen is also nearly identical to that of the highest energy, full-thickness specimen (0.66 mm vs. 0.64 mm), implying that these two results should be comparable. In contrast, the low energy full-thickness specimen has low energy and low lateral expansion, indicating lower toughness which is not comparable to that of the reduced-thickness specimen. Therefore, a linear scaling of energy levels for reduced thickness specimens appears to be a reasonable way to simulate full-thickness behavior for materials of these toughness and strength characteristics. Scaling the results for Heat ZP13 in this manner would indicate an upper shelf level of 182 J (134 ft-lb) for the L-C orientation.

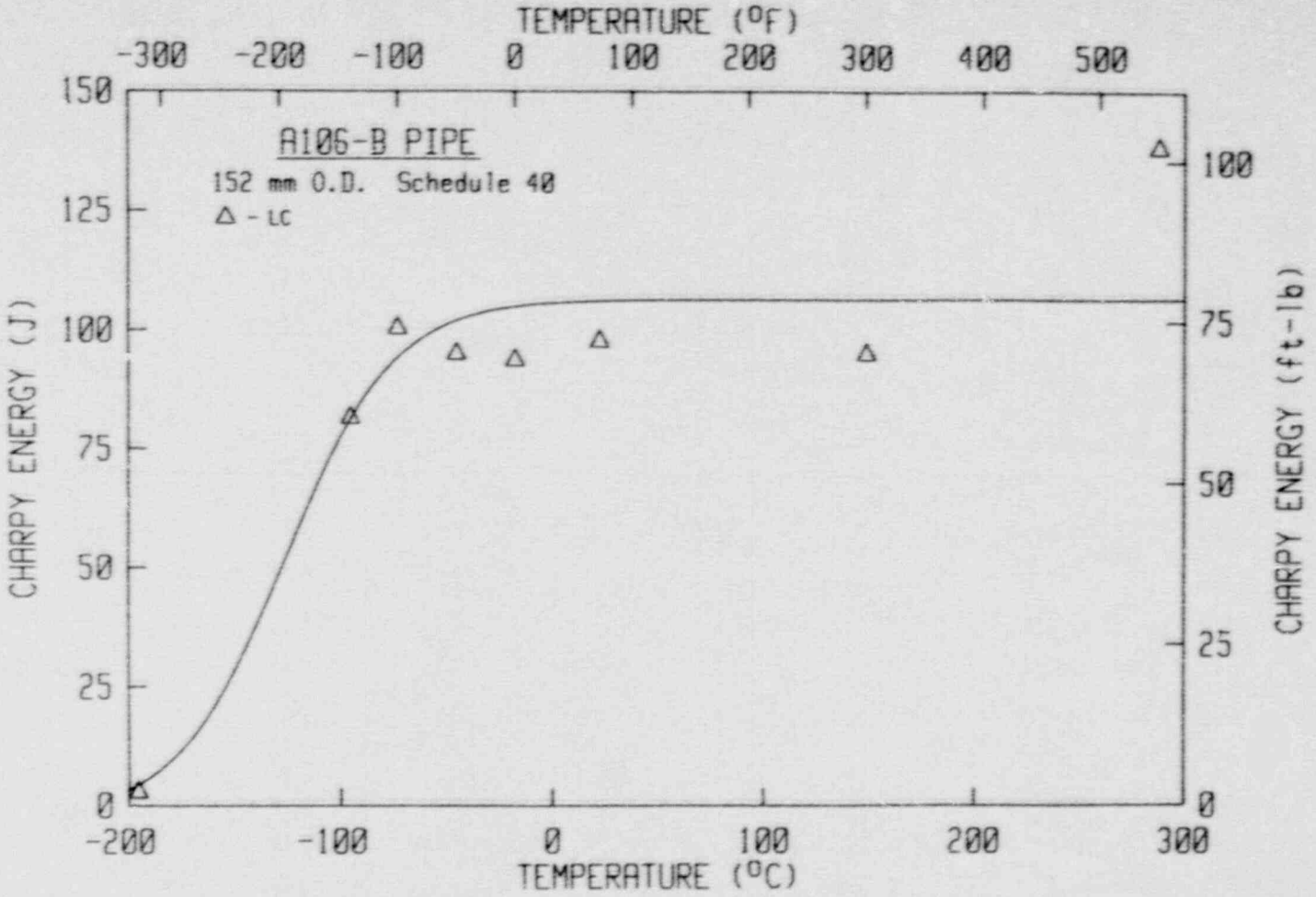

Fig. 3-12 Charpy-V data for A 106 Gr. B (Heat ZP13). In this case the specimen thickness was reduced to 5.8 mm (0.23 in.) due to the thin wall of this heat.

Table 3-5 Charpy-V Results for A 106 Grade B, Heat ZP13
(Reduced-Thickness Specimens, B = 5.8 mm or 0.23 in.)

Specimen ID	Test Temperature		Absorbed Energy		Lateral Expansion		Percent Shear
	(°C)	(°F)	(J)	(ft-lb)	(mm)	(in.)	(%)
L-C Orientation							
ZP13-2LC[a]	-196	-320	3[a]	2[a]	0.03	0.001	0
ZP13-19LC[a]	-196	-320	3[a]	2[a]	0.03	0.001	0
ZP13-1LC[a]	-96	-140	81[a]	60[a]	1.14	0.045	50
ZP13-20LC[a]	-73	-100	100[a]	74[a]	1.19	0.047	100
ZP13-3LC[a]	-46	-50	95[a]	70[a]	1.07	0.042	100
ZP13-17LC[a]	-18	0	94[a]	69[a]	1.02	0.040	100
ZP13-6LC[a]	22	72	98[a]	72[a]	1.02	0.040	100
ZP13-10LC[a]	149	300	95[a]	70[a]	1.19	0.047	100
ZP13-13LC[a]	288	550	138[a]	102[a]	1.02	0.040	100

[a] Reduced-thickness, B = 5.8 mm or 0.23 in.

Table 3-6 Charpy-V Results for A 106 Grade B, Heat ZP15
(Full-Thickness Specimens, B = 10 mm or 0.394 in.)

Specimen ID	Test Temperature		Absorbed Energy		Lateral Expansion		Percent Shear
	(°C)	(°F)	(J)	(ft-lb)	(mm)	(in.)	(%)
L-C Orientation							
ZP15-1LC	-96	-140	5	4	0.15	0.006	0
ZP15-14LC	-73	-100	5	4	0.10	0.004	0
ZP15-3LC	-46	-50	7	5	0.10	0.004	0
ZP15-17LC	-18	0	8	6	0.20	0.008	6
ZP15-12LC	-1	30	20	15	0.61	0.024	17
ZP15-11LC	10	50	81	60	1.37	0.054	47
ZP15-6LC	22	72	52	38	0.94	0.037	23
ZP15-15LC	22	72	81	60	1.35	0.053	50
ZP15-18LC[a]	22	72	47[a]	35[a]	1.32	0.052	75
ZP15-7LC	43	110	89	66	1.52	0.060	60
ZP15-16LC	43	110	102	75	1.68	0.066	61
ZP15-8LC	66	150	102	75	1.65	0.065	56
ZP15-5LC	66	150	110	81	1.73	0.068	81
ZP15-9LC	79	175	92	68	1.50	0.059	60
ZP15-4LC	93	200	121	89	1.88	0.074	96
ZP15-10LC	149	300	144	106	2.03	0.080	98
ZP15-2LC	204	400	141	104	2.03	0.080	100
ZP15-13LC	288	550	168	124	1.78	0.070	100
C-L Orientation							
ZP15-1CL	-96	-140	4	3	0.05	0.002	0
ZP15-14LC	-73	-100	4	3	0.18	0.007	0
ZP15-3CL	-46	-50	8	6	0.15	0.006	0
ZP15-17CL	-18	0	8	6	0.13	0.005	0
ZP15-12CL	-1	30	18	13	0.38	0.015	6
ZP15-18CL	4	40	16	12	0.66	0.026	12
ZP15-11CL	10	50	19	14	0.41	0.016	6
ZP15-15CL	22	72	22	16	0.48	0.019	27
ZP15-6CL	22	72	27	20	0.56	0.022	11
ZP15-7CL	43	110	27	20	0.51	0.020	27
ZP15-16CL	43	110	34	25	0.79	0.031	45
ZP15-5CL	66	150	43	32	0.94	0.037	65
ZP15-8CL	66	150	45	33	0.99	0.039	62
ZP15-9CL	79	175	46	34	1.12	0.044	85
ZP15-4CL	93	200	34	25	1.12	0.044	85
ZP15-10CL	149	300	52	38	1.19	0.047	100
ZP15-2CL	204	400	54	40	1.24	0.049	100
ZP15-13CL	288	550	65	48	1.27	0.050	100

[a] Reduced thickness, B = 5.8 mm or 0.23 in.

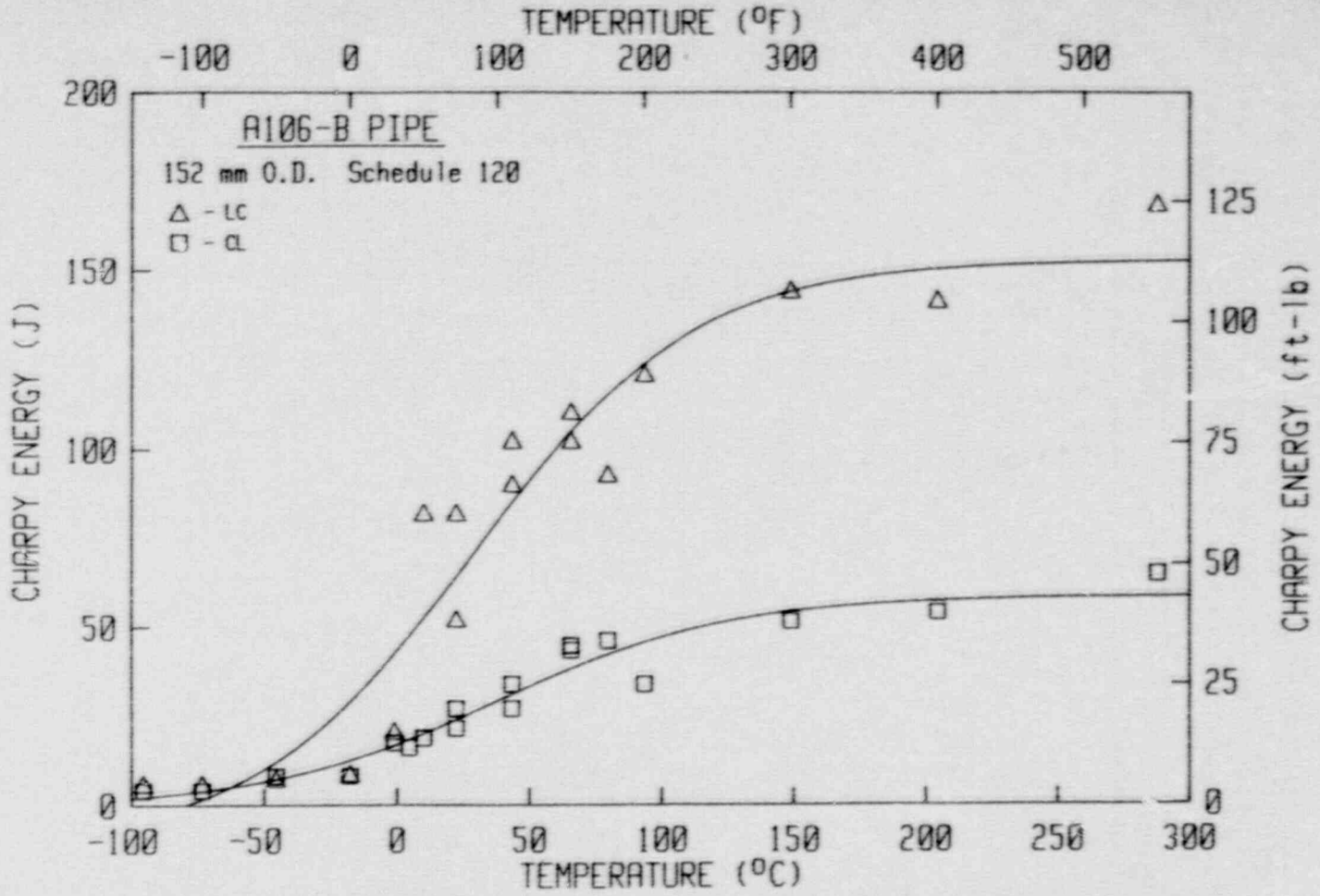

Fig. 3-13 Charpy-V data for A 106 Gr. B (Heat ZP15). Much higher toughness is evident for the L-C orientation as opposed to the C-L orientation. Upper shelf is not achieved for this heat until ~150°C (300°F).

For Heat ZP14, results from C_v tests are summarized in Table 3-7, and illustrated in Fig. 3-14. As with Heat ZP15, the L-C orientation has a higher shelf energy than does the C-L orientation, 136 J (100 ft-lb) as compared to 55 J (41 ft-lb). For this heat, several tests of the L-R orientation in the brittle-to-ductile transition region correspond well (i.e., similar energy levels) with data for the L-C orientation.

Comparison of the upper shelf energy levels (from the TANH relation, Eq. 2-1) for the L-C orientations of these heats indicates that the upper shelf energy decreases as the pipe thickness increases, for the three thicknesses studied.

3.2.3 Tensile Data

Tensile results are summarized in Tables 3-8 to 3-10, and illustrated in Figs. 3-15 to 3-17. Heat ZP13 used a specimen design with a gage diameter of 2.9 mm (0.113 in.), and a gage length of 12.7 mm (0.5 in.). The small diameter was caused by the thin wall of this heat, with only L orientation specimens possible due to pipe curvature. For Heats ZP14 and ZP15, the tensile specimen design used blanks which were the same as those used for C_v specimens. These tensile specimens had a gage diameter of 5.1 mm (0.2 in.) and a gage length of 12.7 mm (0.5 in.). The latter is subsize for calculation of elongation, therefore elongation percentages are too large for these tests in comparison to those for the proper gage length.

In all cases, the ambient temperature strengths exceed the requirements of A 106 Grade B. Temperature sensitivity is not too severe for Heats ZP13 and ZP14, although at 204°C (400°F), Heat ZP15 has an obvious peak in ultimate strength which is ~ 25% higher than that at ambient temperature. The L and C orientations have similar strength levels for both heats and at all temperatures.

All three of these heats demonstrate several characteristics of dynamic strain aging (Ref. 16). First, ductility (as given by elongation percentage) is less at elevated temperature (149°C and 204°C) than at ambient temperatures. Secondly, the ultimate strength is higher at 149°C and 204°C than at ambient temperature (except for Heat ZP13). Lastly, the stress-strain curves demonstrate serrations, principally at test temperatures of 149°C and 204°C.

In terms of the stress-strain behavior of these heats, serrated tearing, indicative of dynamic strain aging, did occur in some tests; all tests at 149°C (300°F) and 204°C (400°F) were affected to some degree, except for specimen ZP14-3L. Specific instances of frequent and large serrations are from specimens ZP13-2L, ZP14-2L, ZP14-2C, ZP14-7L, and ZP15-2L. All of these specimens were tested at 149°C (300°F). In addition, specimens ZP14-3C and ZP14-8L exhibit single serrations shortly after the yield point, and specimens ZP15-2C and ZP15-3L experienced serrations near ultimate strength. Specimens ZP13-3L and ZP13-7L exhibited less pronounced serrations. An example of a serrated stress-strain curve is given in Fig. 3-18. This curve is from an analog plot of stress-strain. The overall stress-strain curves for the L orientation of Heat ZP15 are illustrated in

Table 3-7 Charpy-V Results for A 106 Grade B, Heat ZP14
(Full-Thickness Specimens, B = 10 mm or 0.394 in.)

Specimen ID	Test Temperature		Absorbed Energy		Lateral Expansion		Percent Shear
	(°C)	(°F)	(J)	(ft-lb)	(mm)	(in.)	(%)
L-C Orientation							
ZP14-11C	-96	-140	5	4	0.10	0.004	0
ZP14-14LC	-73	-100	9	7	0.18	0.007	0
ZP14-3LC	-46	-50	14	10	0.20	0.008	0
ZP14-17LC	-18	0	27	20	0.48	0.019	6
ZP14-16LC	-7	20	47	35	0.79	0.031	17
ZP14-12LC	4	40	57	42	0.91	0.036	33
ZP14-11LC	10	50	87	64	1.35	0.053	52
ZP14-6LC	22	72	84	62	1.40	0.055	55
ZP14-15LC	22	72	92	68	1.45	0.057	60
ZP14-18LC[a]	22	72	43[a]	32[a]	1.12	0.044	70
ZP14-9LC	32	90	117	86	1.83	0.072	82
ZP14-5LC	43	110	111	82	1.70	0.067	77
ZP14-7LC	43	110	114	84	1.70	0.067	72
ZP14-8LC	66	150	134	99	1.93	0.076	100
ZP14-4LC	93	200	138	102	2.06	0.081	100
ZP14-10LC	149	300	130	96	2.06	0.081	100
ZP14-2LC	204	400	132	97	1.98	0.078	100
ZP14-13LC	288	550	141	104	1.88	0.074	100
C-L Orientation							
ZP14-1CL	-96	-140	7	5	0.10	0.004	0
ZP14-14CL	-73	-100	5	4	0.03	0.001	0
ZP14-3CL	-46	-50	12	9	0.18	0.007	0
ZP14-15CL	-18	0	19	14	0.33	0.013	6
ZP14-12CL	4	40	19	14	0.46	0.018	21
ZP14-11CL	22	72	27	20	0.51	0.020	50
ZP14-6CL	22	72	30	22	0.64	0.025	31
ZP14-9CL	32	90	52	38	0.79	0.031	58
ZP14-5CL	43	110	33	24	0.74	0.029	58
ZP14-7CL	43	110	38	28	0.74	0.029	55
ZP14-8CL	66	150	49	36	0.97	0.038	94
ZP14-4CL	93	200	43	32	1.12	0.044	100
ZP14-10CL	149	300	49	36	1.22	0.048	100
ZP14-2CL	204	400	50	37	1.30	0.051	100
ZP14-13CL	288	550	65	48	1.35	0.053	100
L-R Orientation							
ZP14-2LR	-7	20	41	30	0.66	0.026	12
ZP14-1LR	-1	30	76	56	1.19	0.047	27
ZP14-3LR	4	40	98	72	1.45	0.057	55
ZP14-4LR	22	72	115	85	1.73	0.068	68
ZP14-5LR	32	90	122	90	1.80	0.071	74
ZP14-6LR	43	110	113	83	1.68	0.066	75

[a] Reduced thickness, B = 5.8 mm or 0.23 in.

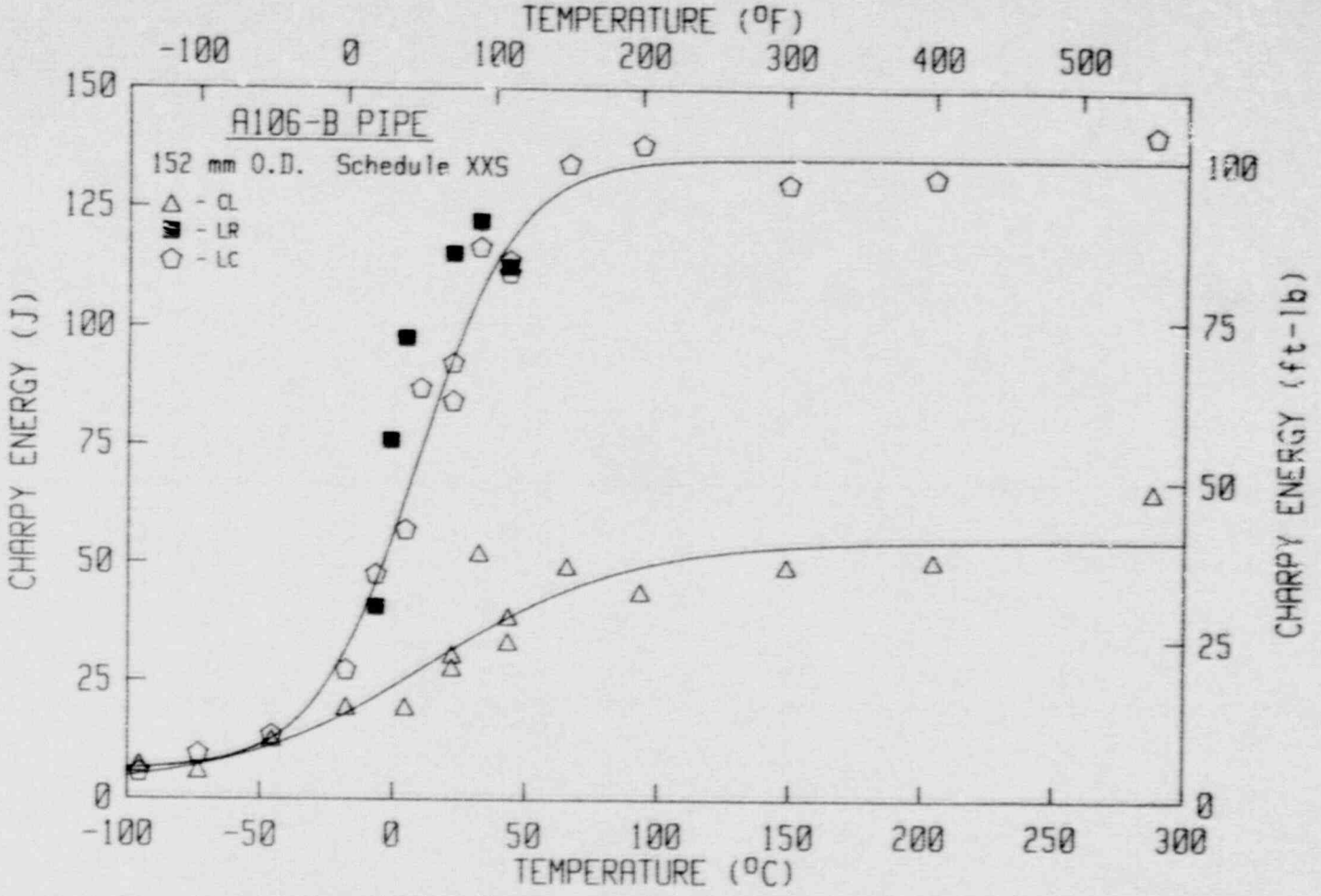

Fig. 3-14 Charpy-V data for A 106 Gr. B (Heat ZP14). As with Heat ZP15, the L-C orientation exhibits much higher toughness than the C-L orientation, and similar toughness to the L-R orientation in the transition region. Upper shelf is achieved at ~66°C (150°F).

Table 3-8 Tensile Strength of A 106 Grade B (Heat ZP13)

Specimen Number	Test Temperature (°C)	Test Temperature (°F)	Orientation	0.2% Offset Yield Strength (MPa)	0.2% Offset Yield Strength (ksi)	Ultimate Strength (MPa)	Ultimate Strength (ksi)	Reduction In Area (%)	Elongation (%)
ZP13-1L	24	75	L	293.6	42.6	467.9	67.9	70.9	42.4
ZP13-6L	24	75	L	295.5	42.9	470.1	68.2	58.3	35.0
ZP13-2L	149	300	L	253.1	36.7	429.5	62.3	70.9	32.8
ZP13-3L	204	400	L	256.7	37.2	448.5	65.1	49.8	24.8
ZP13-7L	204	400	L	259.0	37.6	453.7	65.8	65.9	34.8
ZP13-4L	288	550	L	212.0	30.8	467.7	67.8	54.7	25.0
ZP13-5L	343	650	L	201.2	29.2	454.0	65.9	54.7	26.6
ZP13-8L	343	650	L	258.5	37.5	458.2	66.5	76.2	46.6

Table 3-9 Tensile Strength of A 106 Grade B (Heat ZP15)

Specimen Number	Test Temperature (°C)	Test Temperature (°F)	Orientation	0.2% Offset Yield Strength (MPa)	0.2% Offset Yield Strength (ksi)	Ultimate Strength (MPa)	Ultimate Strength (ksi)	Reduction In Area (%)	Elongation (%)
ZP15-1L	25	77	L	314.5	46.0	520.1	75.4	62.2	38.6
ZP15-1C	25	77	C	320.3	46.6	510.9	74.1	45.2	3[illegible].6
ZP15-2L	149	300	L	308.0	44.8	628.0	91.1	3[illegible].6	2[illegible].6
ZP15-3L	204	400	L	340.7	49.6	659.5	95.7	33.5	16.[illegible]
ZP15-2C	204	400	C	333.9	48.6	652.5	94.6	34.4	20.[illegible]
ZP15-4L	288	550	L	319.7	46.5	620.7	90.0	34.4	24.[illegible]
ZP15-5L	343	650	L	315.2	45.9	586.1	85.0	41.5	35.[illegible]
ZP15-3C	343	650	C	322.5	46.9	565.5	82.0	16.2	1[illegible].6

Table 3-10 Tensile Strength of A 106 Grade B (Heat ZP14)

Specimen Number	Test Temperature (°C)	Test Temperature (°F)	Orientation	0.2% Offset Yield Strength (MPa)	0.2% Offset Yield Strength (ksi)	Ultimate Strength (MPa)	Ultimate Strength (ksi)	Reduction In Area (%)	Elongation (%)
ZP14-1L	25	77	L	295.0	42.8	[illegible]	74.9	40.5	46.8
ZP14-6L	25	77	L	270.4	39.2	51[illegible].1	74.1	60.9	42.4
ZP14-1C	25	77	C	275.0	39.9	512.2	74.3	63.4	48.0
ZP14-2L	149	300	L	255.0	37.0	529.6	76.8	39.9	22.8
ZP14-7L	149	300	L	251.0	36.4	537.0	77.9	54.4	30.4
ZP14-2C	149	300	C	248.6	36.1	533.7	77.4	42.2	19.4
ZP14-3L	204	400	L	277.0	40.2	572.2	83.0	37.6	22.6
ZP14-8L	204	400	L	261.4	37.9	570.7	82.8	44.5	28.4
ZP14-3C	204	400	C	258.4	37.5	573.8	83.2	40.7	24.4
ZP14-4L	288	550	L	262.3	38.0	568.6	82.5	44.5	31.8
ZP14-9L	288	550	L	254.5	36.9	571.2	82.8	53.1	28.4
ZP14-4C	288	550	C	255.0	37.0	567.8	82.4	51.0	28.0
ZP14-5L	343	650	L	257.9	37.4	537.8	78.0	51.2	34.6
ZP14-10L	343	650	L	242.2	35.1	532.1	77.2	60.0	43.4
ZP14-5C	343	650	C	238.8	34.6	534.4	77.5	62.8	49.0

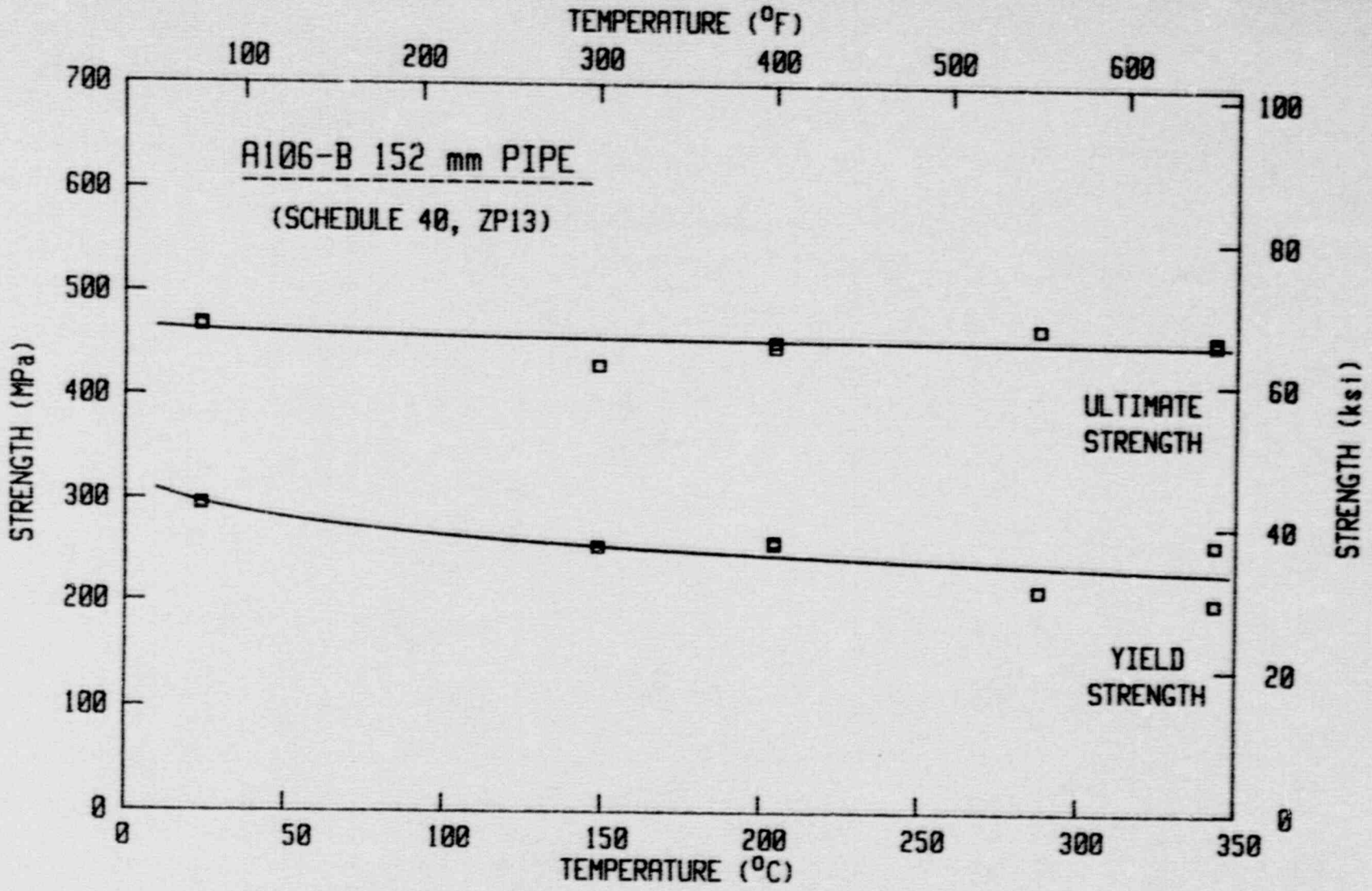

Fig. 3-15 Tensile strength data for A 106 Gr. B (Heat ZP13) are essentially invariant with temperature.

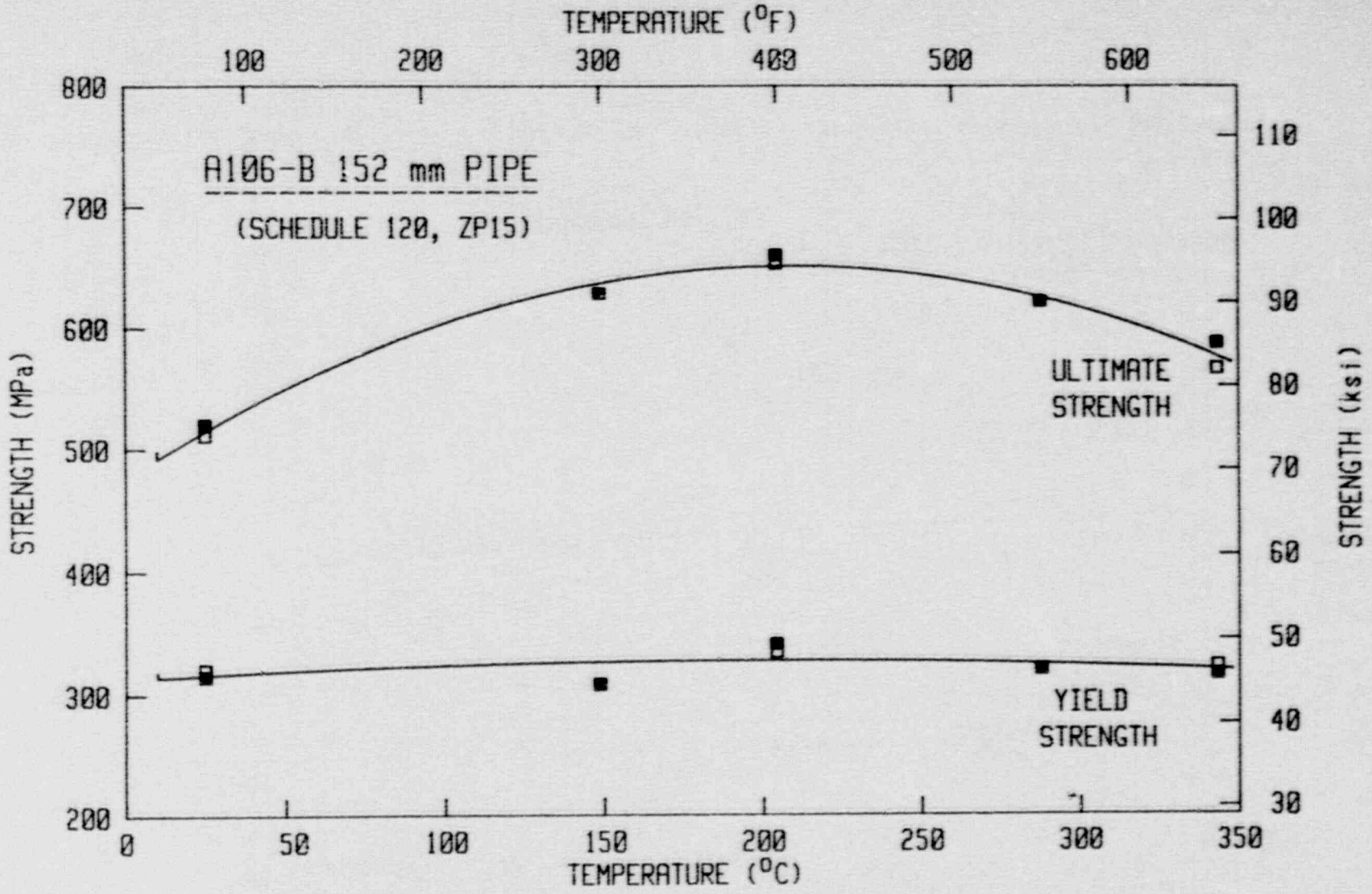

Fig. 3-16 Tensile strength data for A 106 Gr. B (Heat ZP15). These data are more sensitive to temperature than that for Heat ZP13, with both the yield and the ultimate strengths higher than those for Heat ZP13.

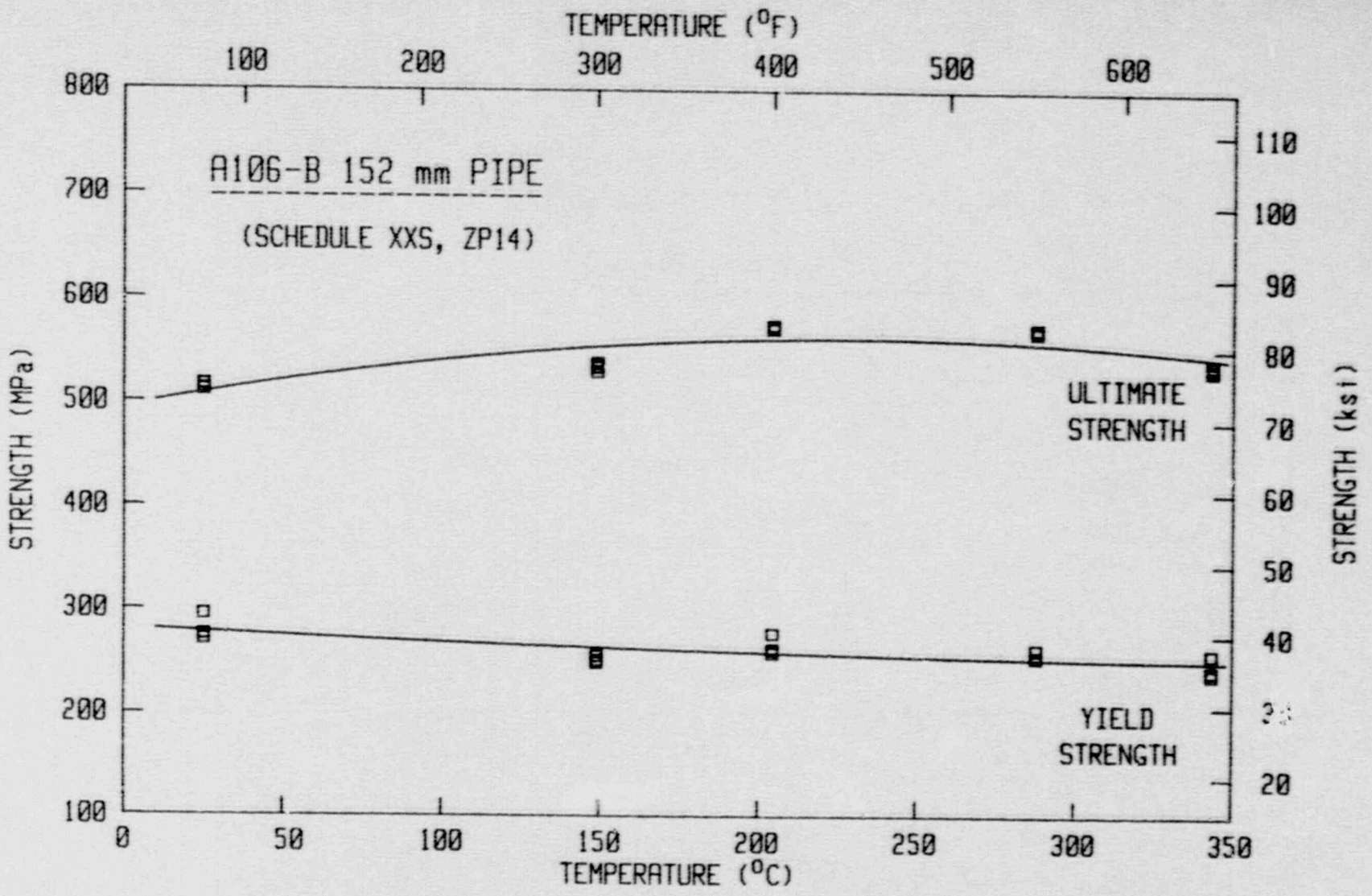

Fig. 3-17 Tensile strength data for A 106 Gr. B (Heat ZP14). The yield strength levels for this heat are similar to those for Heat ZP13 and the ultimate strength levels are somewhat lower than those for Heat ZP15.

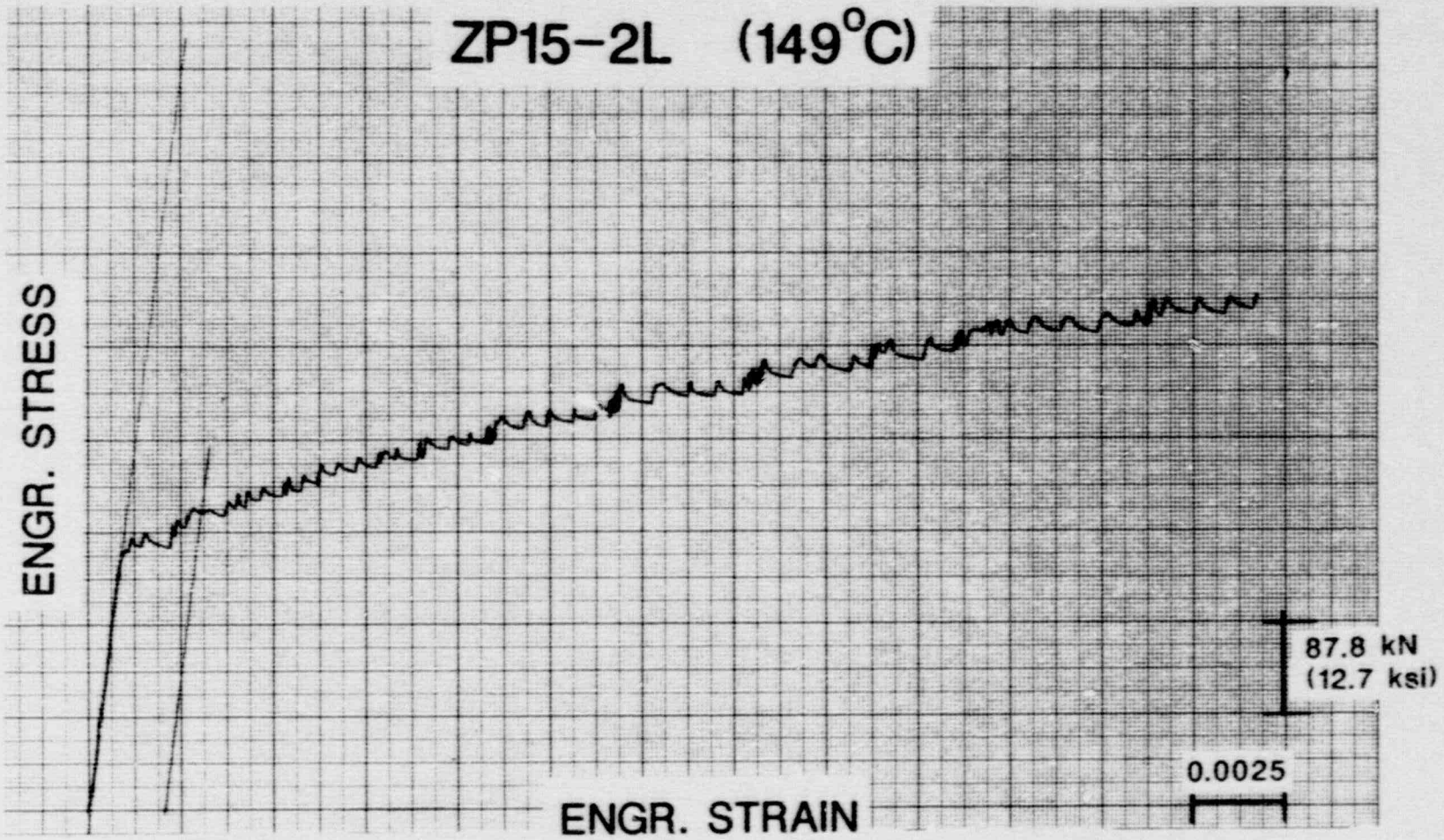

Fig. 3-18 Example of a serrated stress-strain curve for A 106 Grade B.

Fig. 3-19. These curves illustrate the serrations at 149°C and 204°C, and the lack thereof at the other test temperatures.

3.2.4 Fracture Toughness Data

With the different geometries available for the three heats (due to wall thickness differences), each heat used different specimen designs, intending to optimize the specimen thickness and unbroken ligament in each case.

For Heat ZP13, the specimen design was a 0.4T-CT specimen, with a thickness of 5.8 mm or 0.23 in. (Fig. 3-20). Results for this heat are summarized in Table 3-11. From Fig. 3-21, J-R curves for the L-C orientation (using plane-sided specimens) at 149°C and 288°C demonstrate no temperature sensitivity at these two temperatures. Similarly, results for A 106 Grade C (Figs. 3-5 to 3-7), likewise demonstrated little or no difference in these same two temperatures. However, additional tests at ambient temperature and at ~ 204°C (400°F) would probably indicate temperature sensitivity, with a minimum in J-R curve at ~ 204°C (400°F).

Comparing data from plane-sided and side-grooved specimens at 200°C (Fig. 3-22) demonstrates the J-R curve reductions normally associated with side-grooving, as has been found with reactor pressure vessel steels. In particular, J_{Ic} levels are generally unchanged with side grooving, with the major reduction in toughness occurring as reduced J-R curve slopes (i.e., tearing resistance). For the case of thin wall pipes in particular, data from plane-sided specimens may be appropriate in comparison to the fracture behavior of actual pipe, but the use of data from side-grooved specimens would give some additional conservatism in the measured toughness.

Of the two orientations for which J-R curves were determined at 288°C (Fig. 3-23), the L-C orientation is seen to have much higher toughness than the C-L orientation. In the case of the C-L orientation, J_{Ic} levels are very low, from 45 to 57 kJ/m² (250 to 325 in.-lb/in.²), and the tearing resistance is also quite low.

For Heat ZP15, a 0.5T-CT specimen design with a thickness of 9.1 mm (0.36 in.) was used (Fig. 3-24). Results for this heat are summarized in Table 3-12. As indicated, tests at 24°C for both orientations resulted in brittle fracture after some amount of stable crack growth (Fig. 3-25). For the stable crack growth data available, the L-C orientation demonstrates much higher toughness than the C-L orientation.

Similarly at 149°C and 288°C (Figs. 3-26 and 3-27, respectively), the L-C orientation demonstrates much higher toughness than the C-L orientation. The higher toughness is exemplified by higher J_{Ic} levels and higher tearing resistance (J-R curve slopes).

For both the L-C and C-L orientations (Figs. 3-28 and 3-29, respectively), the highest J-R curves are at 24°C (although these curves terminate in cleavage fracture), whereas the J-R curves at

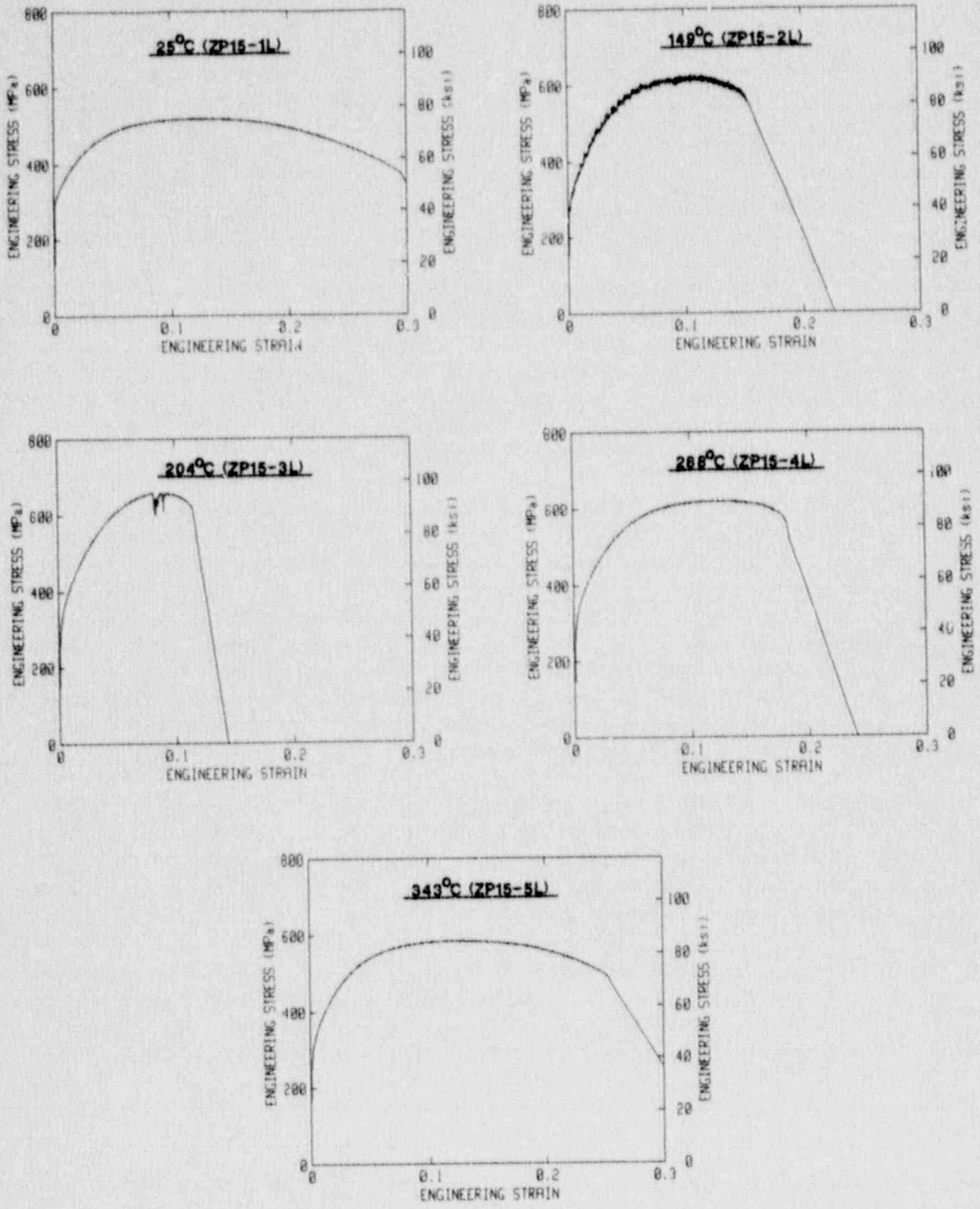

Fig. 3-19 Stress-strain curves for the L orientation of Heat ZP15.

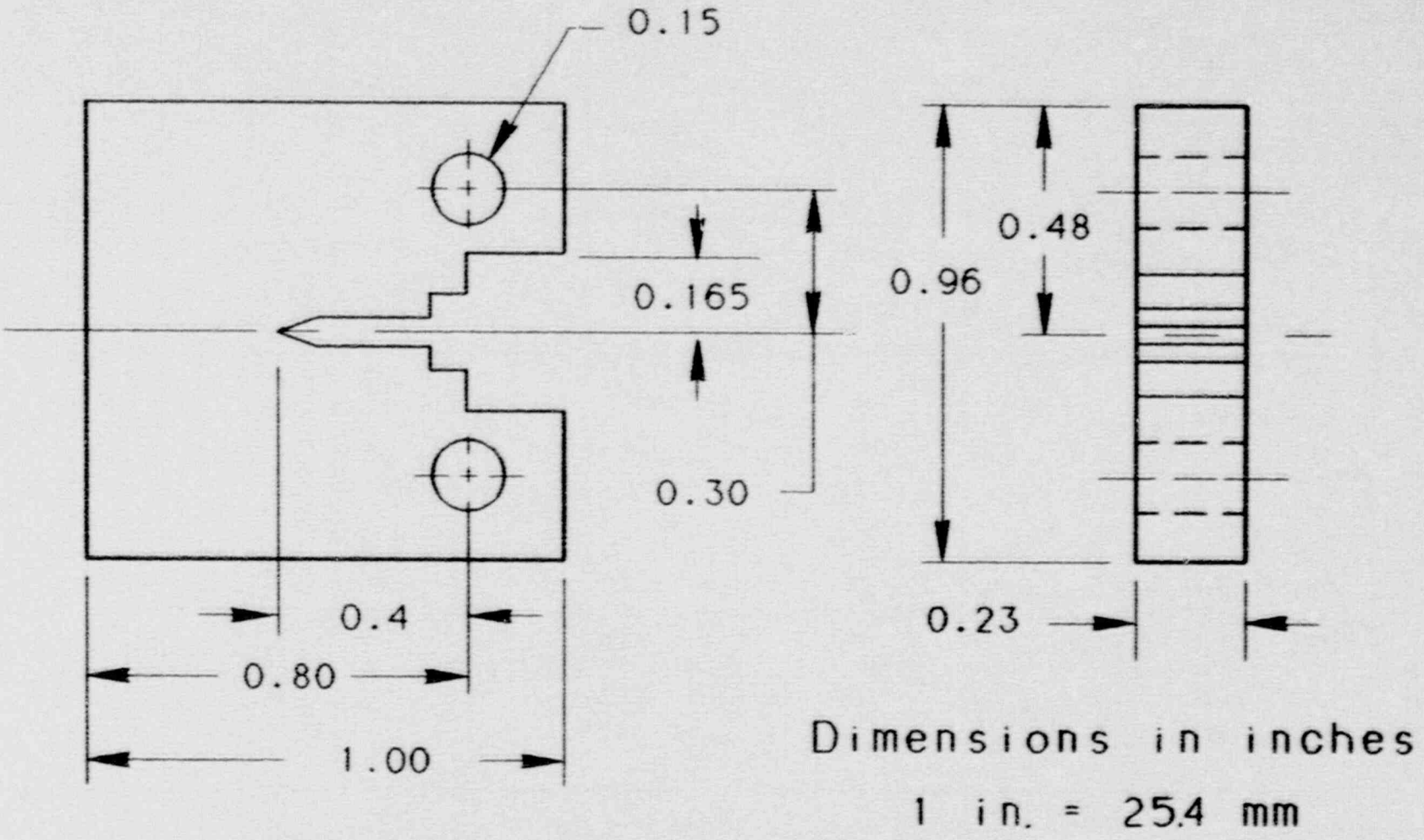

Fig. 3-20 Fracture toughness tests of A 106 Gr. B (Heat ZP13) used this 0.5T-CT specimen design with a thickness of 5.8 mm (0.23 in.).

Table 3-11 J-R Curve Results for A 106 Grade B (Heat ZP13)

Specimen Number	Test Temp. (°C)	Side Groove (%)	$(a/W)_o$	Δa_m (mm)	$\Delta a_p - \Delta a_m$ (mm)	J_{Ic} P.L. (kJ/m^2)	J_{Ic} Linear (kJ/m^2)	K_{Jc} P.L. ($MPa\sqrt{m}$)	K_{Jc} Linear ($MPa\sqrt{m}$)	T_{avg} P.L.	T_{avg} ASTM	Flow Strength (MPa)
L-C Orientation												
ZP13-1LC	149	0	0.527	5.46	-0.48	402.5	376.9	282.8	273.7	364	378	341.3
ZP13-2LC	149	0	0.524	5.55	-0.63	331.4	300.8	256.6	244.5	395	413	341.3
ZP13-3LC	288	0	0.511	4.41	-2.09	454.6	425.6	294.5	285.0	518	519	339.9
ZP13-4LC	288	0	0.522	7.10	-3.47	387.7	381.4	271.9	269.7	411	402	339.9
ZP13-7LC	288	20	0.519	5.50	-2.30	274.2	269.4	228.7	226.7	227	228	339.9
ZP13-8LC	288	20	0.522	5.92	-0.78	244.1	216.7	215.8	203.3	282	303	339.9
C-L Orientation												
ZP13-1CL	288	20	0.518	6.57	-0.42	48.6	44.8	96.2	92.5	41	59	339.9
ZP13-2CL	288	20	0.515	5.86	-0.69	56.6	52.0	103.9	99.6	103	111	339.9

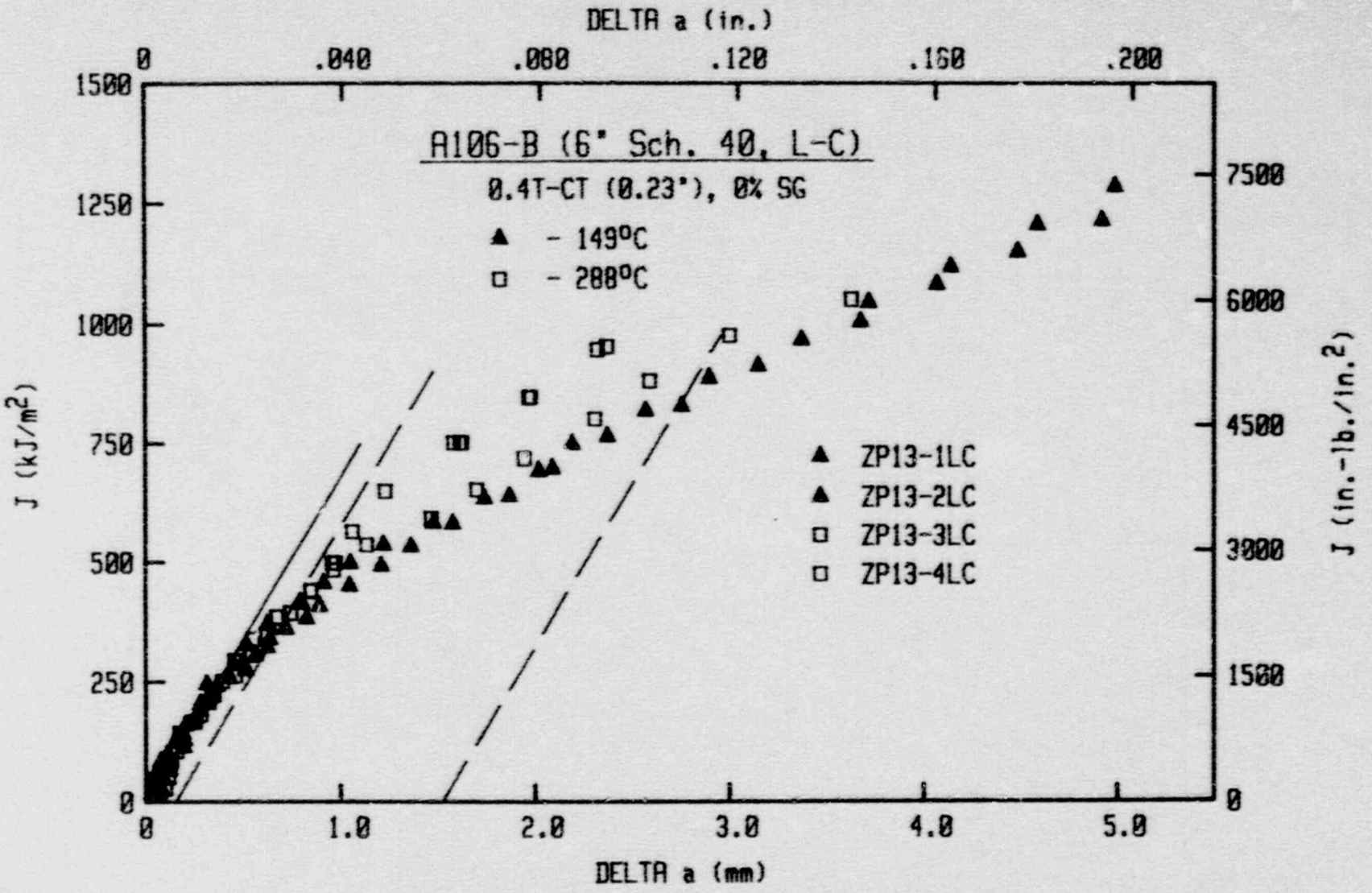

Fig. 3-21 J-R curves for the L-C orientation of A 106 Gr. B (Heat ZP13), using plane-sided specimens. Data at 288°C are only slightly lower than that at 149°C.

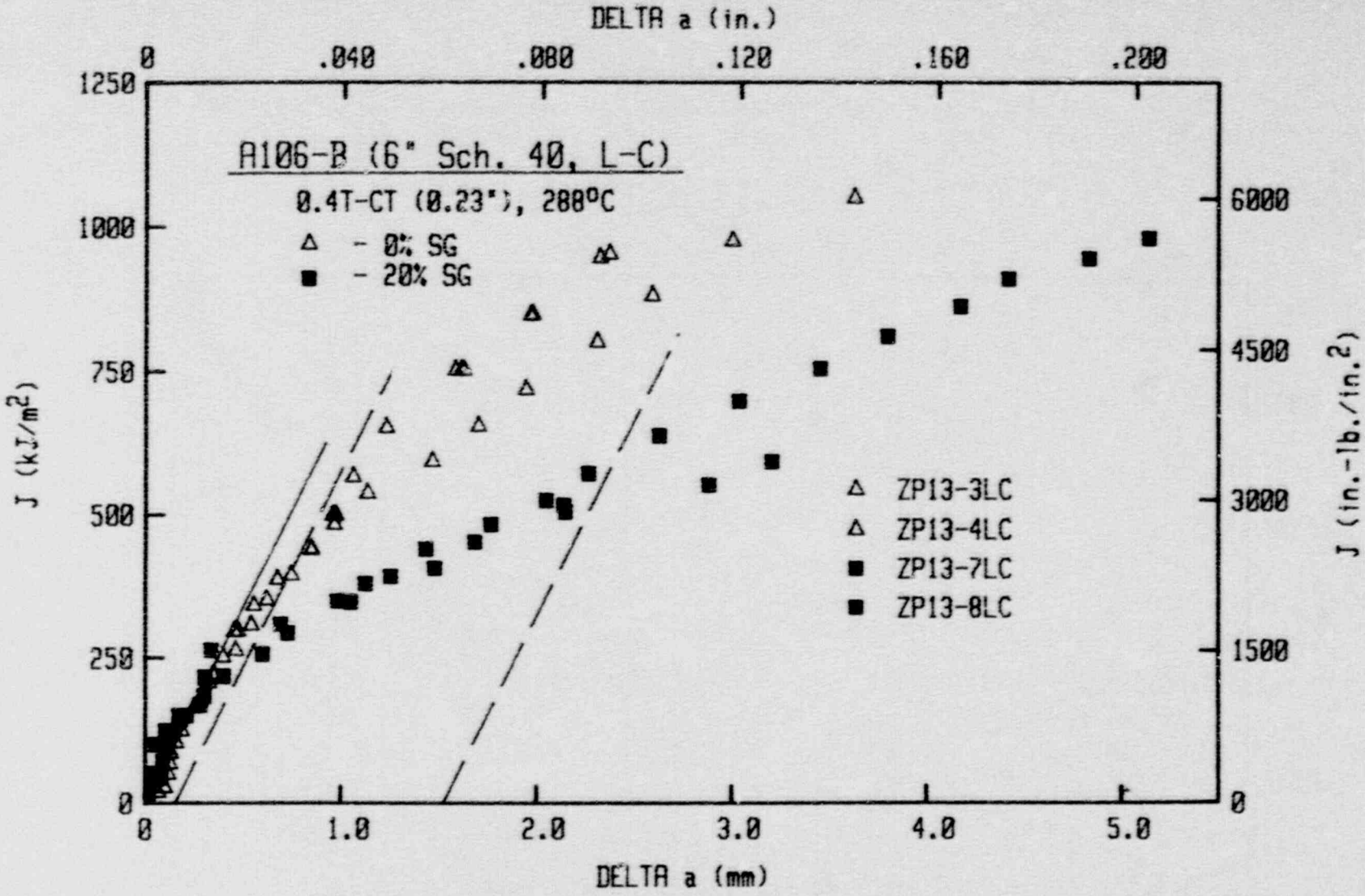

Fig. 3-22 J-R curves for the L-C orientation of A 106 Gr. B (Heat ZP13) at 288°C. Data from sidegrooved specimens are somewhat lower than that from plane-sided specimens.

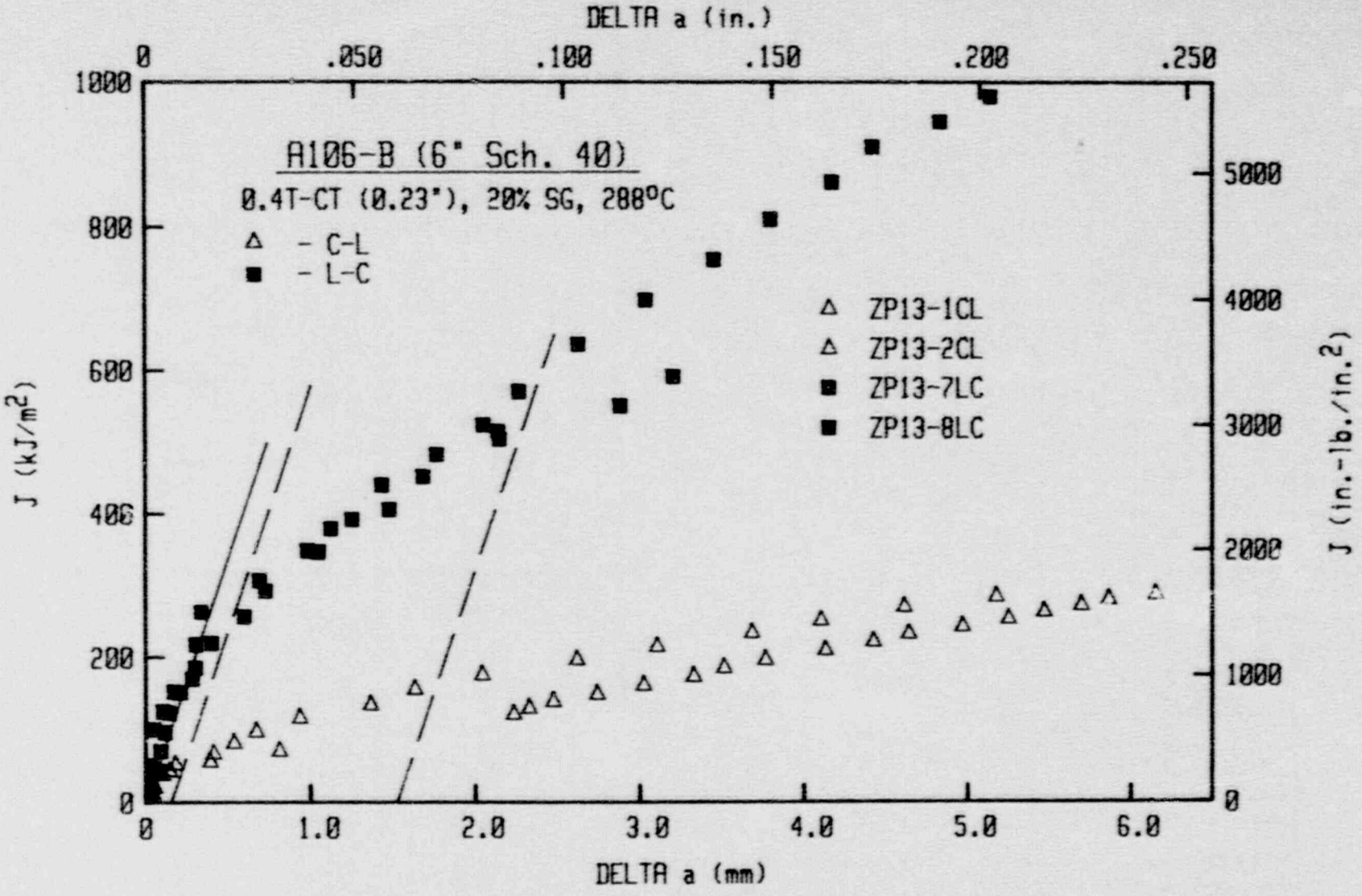

Fig. 3-23 J-R curves for the L-C and C-L orientations of A 106 Gr. B (Heat ZP13) at 288°C. The L-C orientation has much higher toughness, consistent with the C_v results.

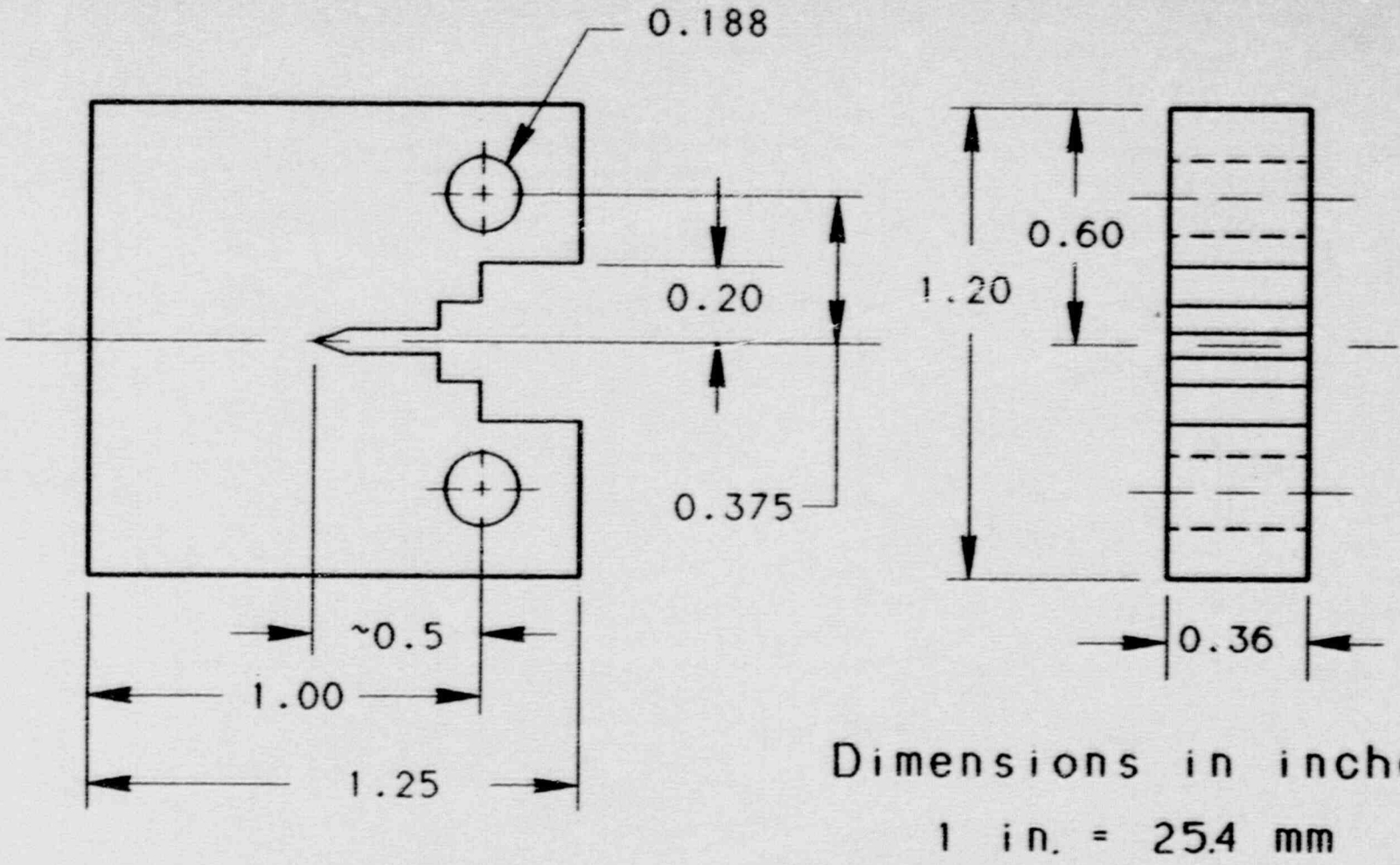

Fig. 3-24 Fracture toughness tests of A 106 Gr. B (Heat ZP15) used this 0.5T-CT specimen design with a thickness of 9.1 mm (0.36 in.).

Table 3-12 J-R Curve Results for A 106 Grade B (Heat ZP15)

Specimen Number	Test Temp. (°C)	Side Groove (%)	$(a/W)_o$	Δa_m (mm)	$\Delta a_p - \Delta a_m$ (mm)	J_{Ic} P.L. (kJ/m^2)	J_{Ic} Linear (kJ/m^2)	K_{Jc} P.L. ($MPa\sqrt{m}$)	K_{Jc} Linear ($MPa\sqrt{m}$)	T_{avg} P.L.	T_{avg} ASTM	Flow Strength (MPa)
L-C Orientation												
ZP15-7LC	24	20	0.532	——[a]	——[a]	336.0	——[a]	263.0	——[a]	—[a]	—[a]	416.4
ZP15-8LC	149	20	0.501	6.94	-0.07	112.4	113.4	149.5	150.1	96	95	468.0
ZP15-1LC	149	0	0.520	6.80	-1.13	122.6	115.8	156.1	151.7	131	133	468.0
ZP15-2LC	149	0	0.522	6.50	-1.35	133.8	124.0	163.0	157.0	111	116	468.0
ZP15-3LC	288	0	0.531	6.97	-1.07	125.4	123.8	154.6	153.7	117	116	470.2
ZP15-4LC	288	0	0.513	6.56	-0.80	125.6	114.1	154.8	147.5	108	118	470.2
ZP15-5LC	288	20	0.530	6.22	-0.21	104.2	100.8	141.0	138.6	93	95	470.2
ZP15-6LC	288	20	0.522	6.29	-0.35	110.5	104.9	145.2	141.5	85	90	470.2
C-L Orientation												
ZP15-3CL	24	20	0.511	——[a]	——[a]	96.7	94.4	147.9	146.1	86	88	416.4
ZP15-4CL	149	20	0.523	6.95	-0.50	60.0	60.0	109.2	109.2	33	34	468.0
ZP15-1CL	288	20	0.563	5.45	-0.24	54.2	56.0	101.7	103.3	31	31	470.2
ZP15-2CL	288	20	0.523	5.52	-0.31	59.7	52.5	106.8	100.0	46	60	470.2

[a] Cleavage fracture precluded determination of this quantity.

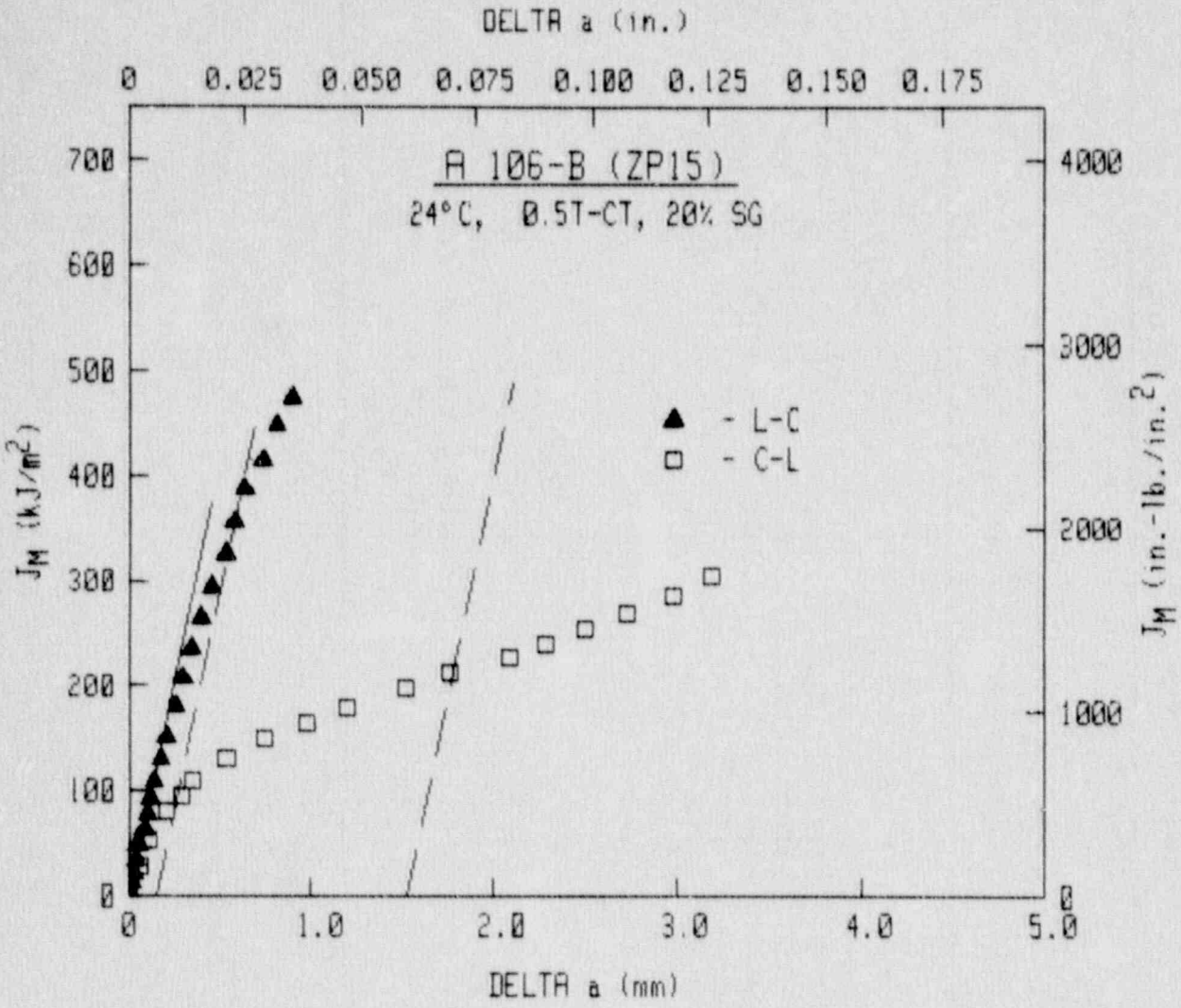

Fig. 3-25 J-R curves for A 106 Gr. B (Heat ZP15) at 24°C.

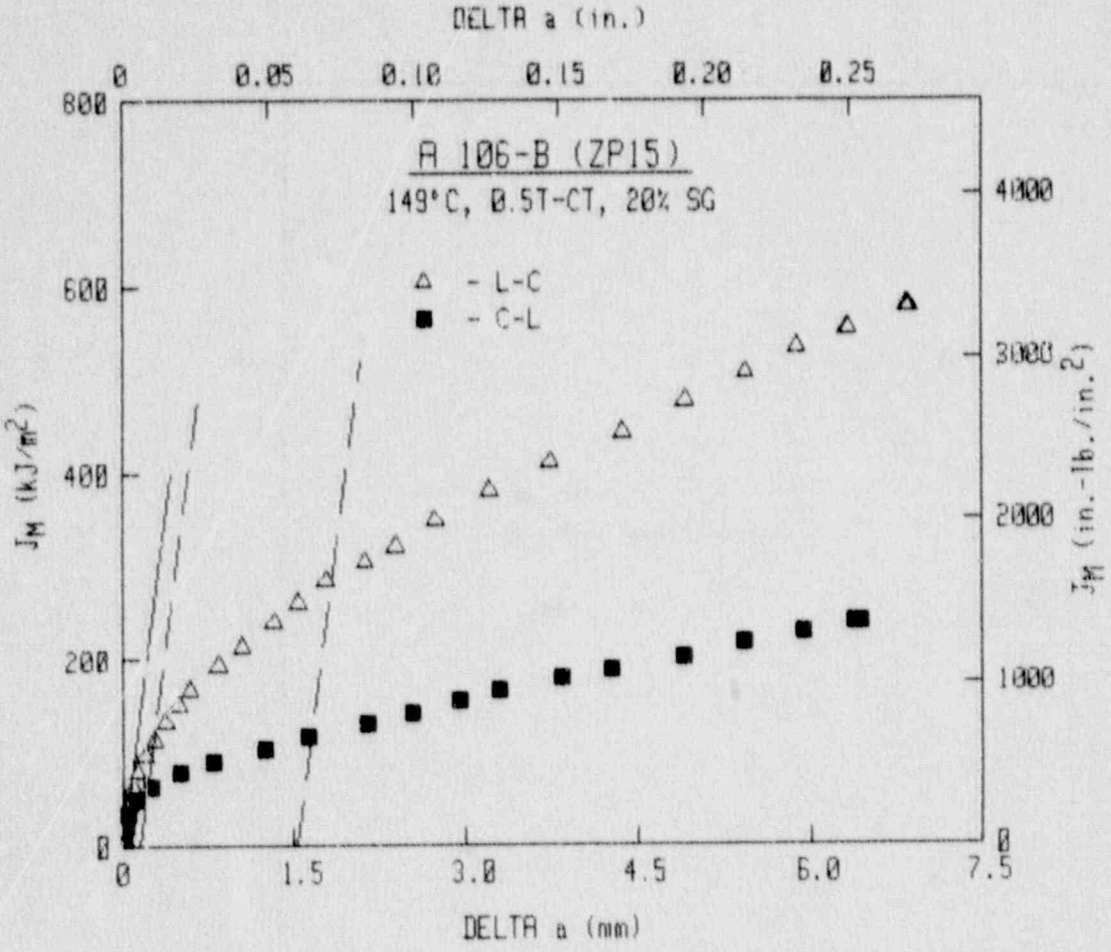

Fig. 3-26 J-R curves for A 106 Gr. B (Heat ZP15) at 149°C.

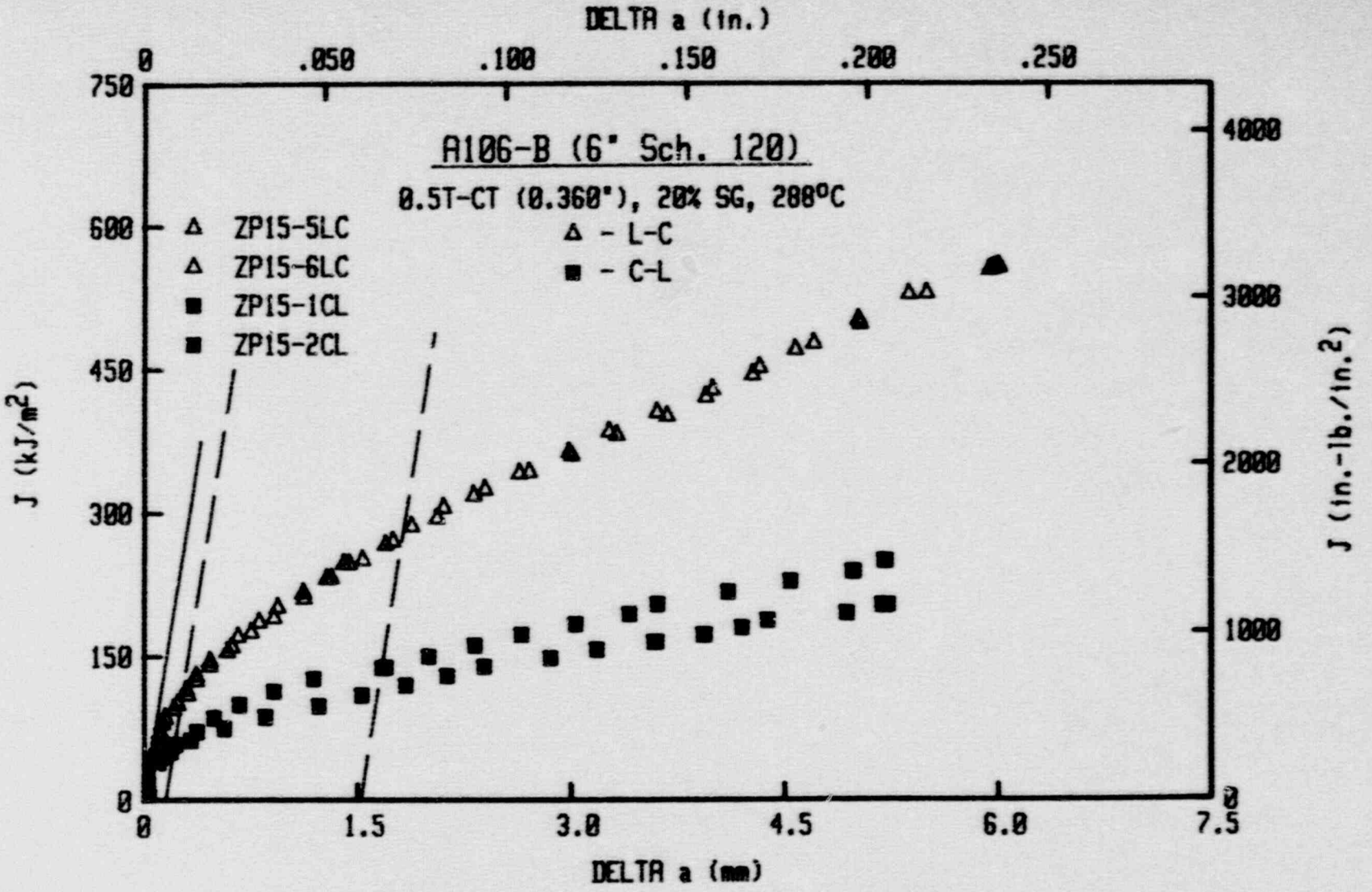

Fig. 3-27 J-R curves for A 106 Gr. B (Heat ZP15) at 288°C.

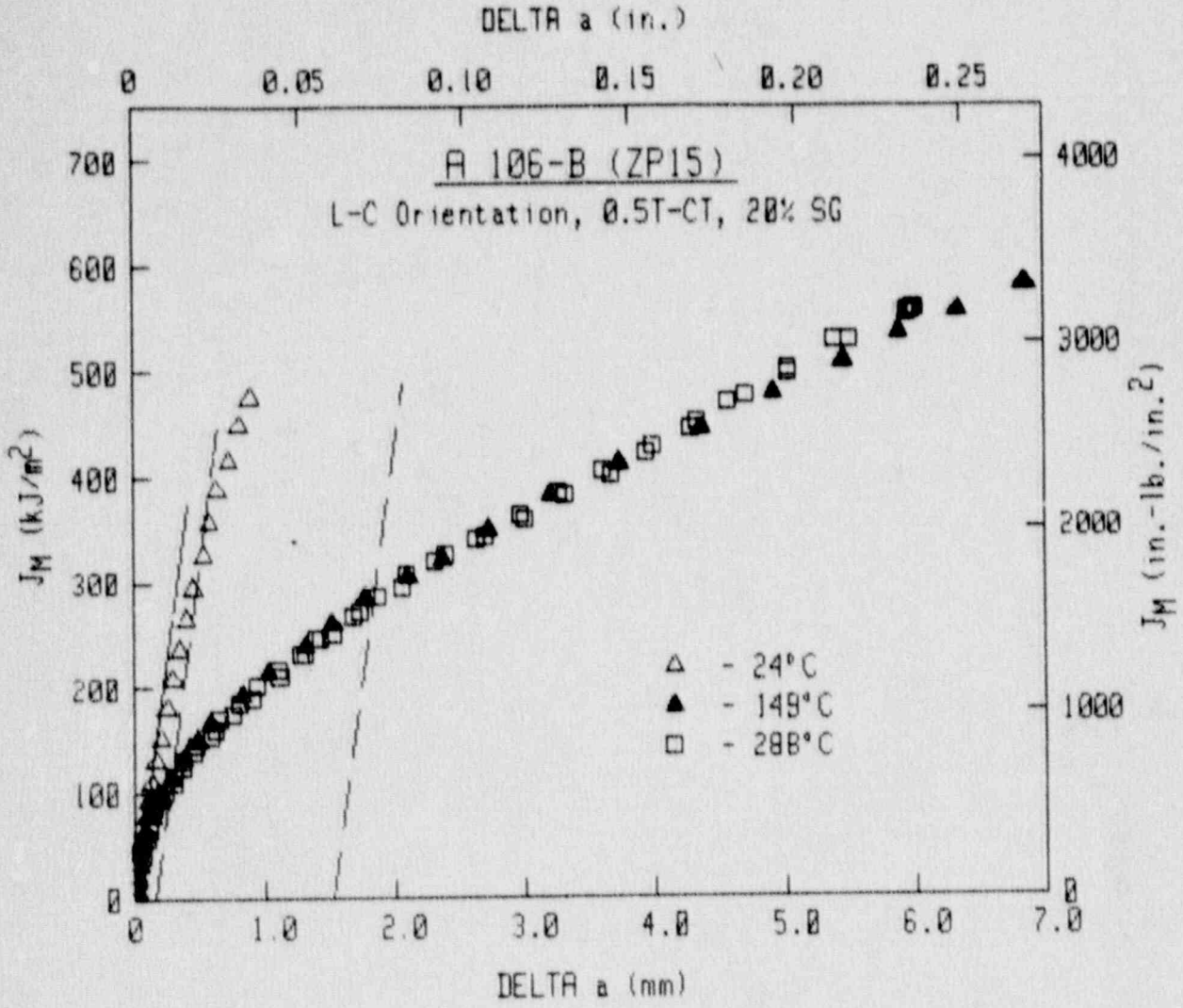

Fig. 3-28 J-R curves for the L-C orientation of A 106 Gr. B (Heat ZP15), using sidegrooved specimens.

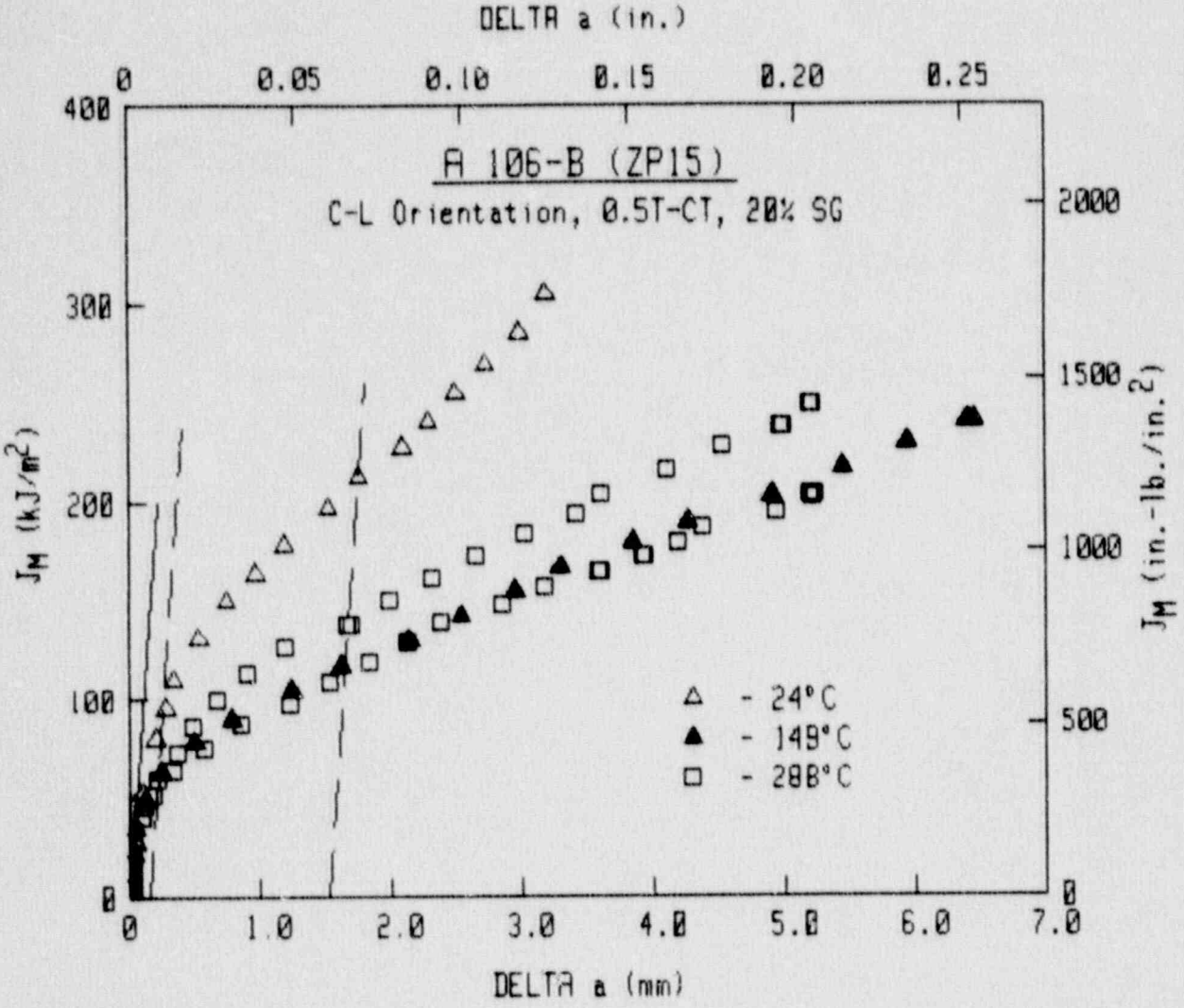

Fig. 3-29 J-R curves for the C-L orientation of A 106 Gr. B (Heat ZP15), using sidegrooved specimens.

149°C and 288°C are remarkably close to one another. The latter trend is likewise followed by plane-sided tests of the L-C orientation as well (Fig. 3-30).

Lastly, comparisons of data from plane-sided and side-grooved specimens for the L-C orientation at 149°C and 288°C indicate a fairly moderate effect of side-grooving in these cases (Figs. 3-31 and 3-32), especially as compared to the larger decreases found for Heat ZP13 in Fig. 3-22.

For Heat ZP14, tests of the C-L and L-C orientations were made using side-grooved 0.8T-CT specimens with a thickness of 18 mm or 0.7 in. (Fig. 3-33). Some additional tests of the L-C orientation were made with plane-sided 1T-CT specimens with a thickness of 15 mm or 0.6 in. (Fig. 3-34).

Results for the J-R curve tests are summarized in Table 3-13. As illustrated for the L-C and C-L orientations using side-grooved specimens (Figs. 3-35 and 3-36, respectively), and the L-C orientation using plane-sided specimens (Fig. 3-37), the highest J-R curve levels occur at a test temperature of 25°C and the lowest occur at 149°C. In contrast to results for Heats ZP13 and ZP15, tests at 288°C give J-R curves which are between the curves at 25°C and 149°C. In addition, the test at 343°C for the C-L orientations exhibits similar toughness to that at 288°C. This trend is not consistent with that found for A 106 Grade C (see Section 3.1.4).

For the C-L orientation tests, serrated tearing is evident on the load-displacement traces of the two tests at 288°C (Fig. 3-38). The serrated tearing is thought to be indicative of dynamic strain aging (DSA), which can cause reduced toughness (Ref. 16). For the test at 343°C, the load-displacement curve demonstrates two large load drops, the first of which occurred just after maximum load (Fig. 3-39). These two load drops do cause minor discontinuities on the J-R curves (Fig. 3-36); the first load drop is evident on the J-R curve as a crack jump (with only a small increase in J) from Δa of ~ 0.8 mm to Δa of ~ 1.5 mm. The second load drop results in a crack jump from ~ 3.8 mm to ~ 5 mm. Although these load drops result in a large increase in crack length with only a small increase in J, the tearing resistance (J-R slope) does not appear to be adversely affected by the load drops, as the J-R curve for this test is similar to those for the tests at 288°C. One additional point is that no serrated tearing occurs for this test, only the load drops.

As illustrated in Fig. 3-40 at 25°C and 288°C, the L-C orientation exhibits much higher toughness than the C-L orientation. This trend is consistent with that found for the other heats of A 106. The differences in J levels, ranging from a factor of two to three, are similar to the difference in C_v upper shelf energy, a ratio of 2.5:1 (based on the TANH results).

As with the other heats of A 106 Grade B, side-grooving results in moderate to large reductions in J levels for the L-C orientation of this heat, as illustrated at 25°C and 288°C (Fig. 3-41).

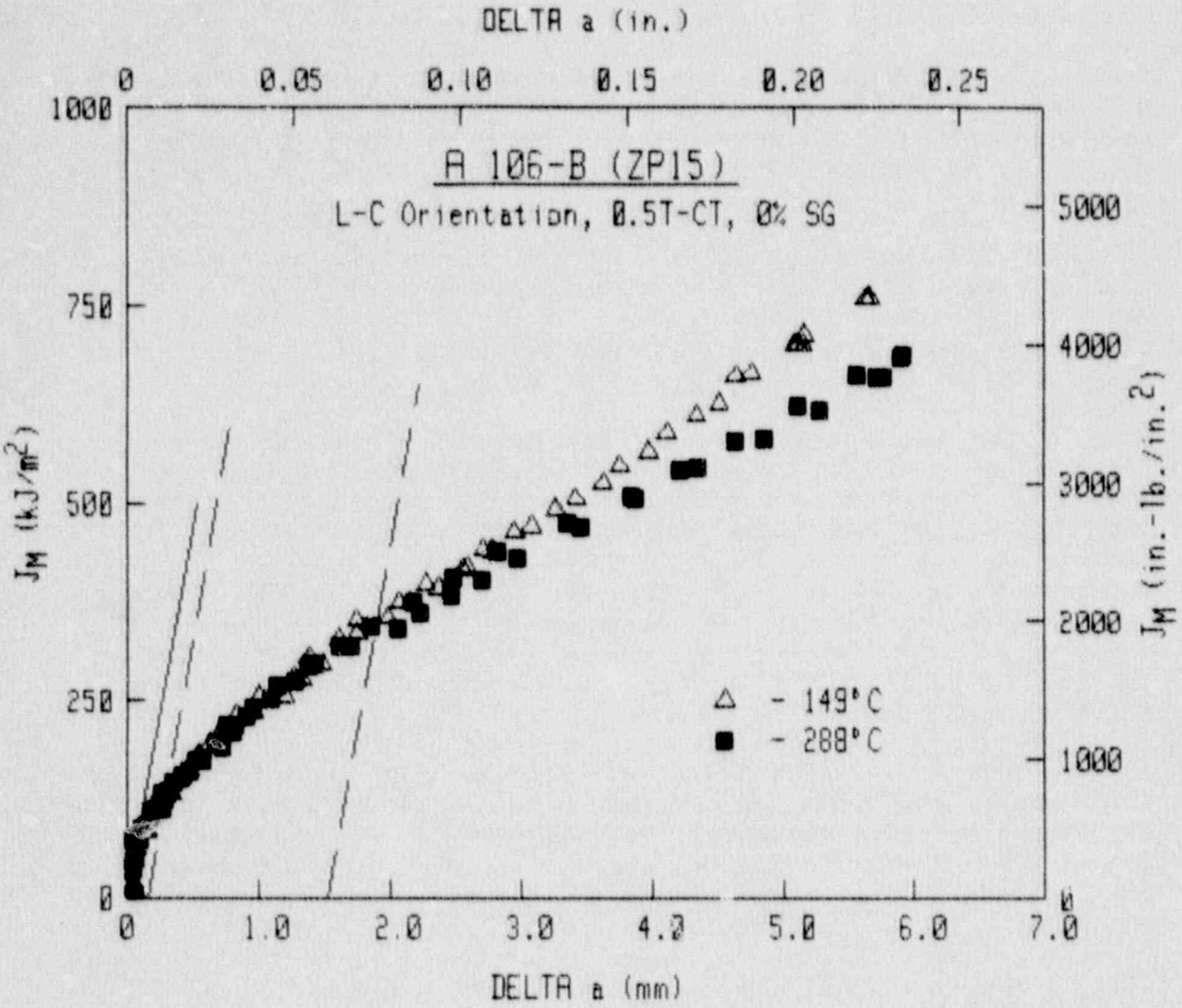

Fig. 3-30 J-R curves for the L-C orientation of A 106 Gr. B (Heat ZP15), using plane-sided specimens.

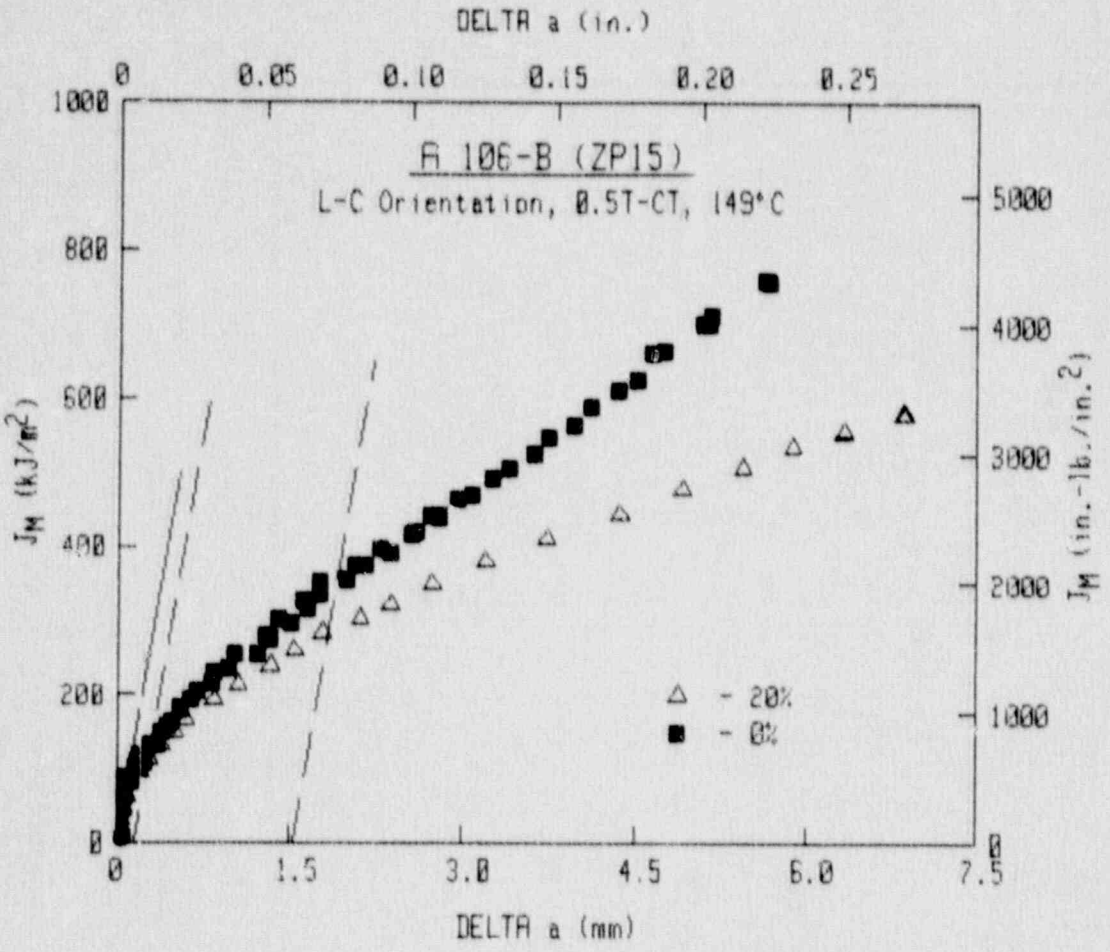

Fig. 3-31 J-R curves for the L-C orientation of A 106 Gr. B (Heat ZP15) at 149°C. Data from sidegrooved specimens are somewhat lower than that from plane-sided specimens.

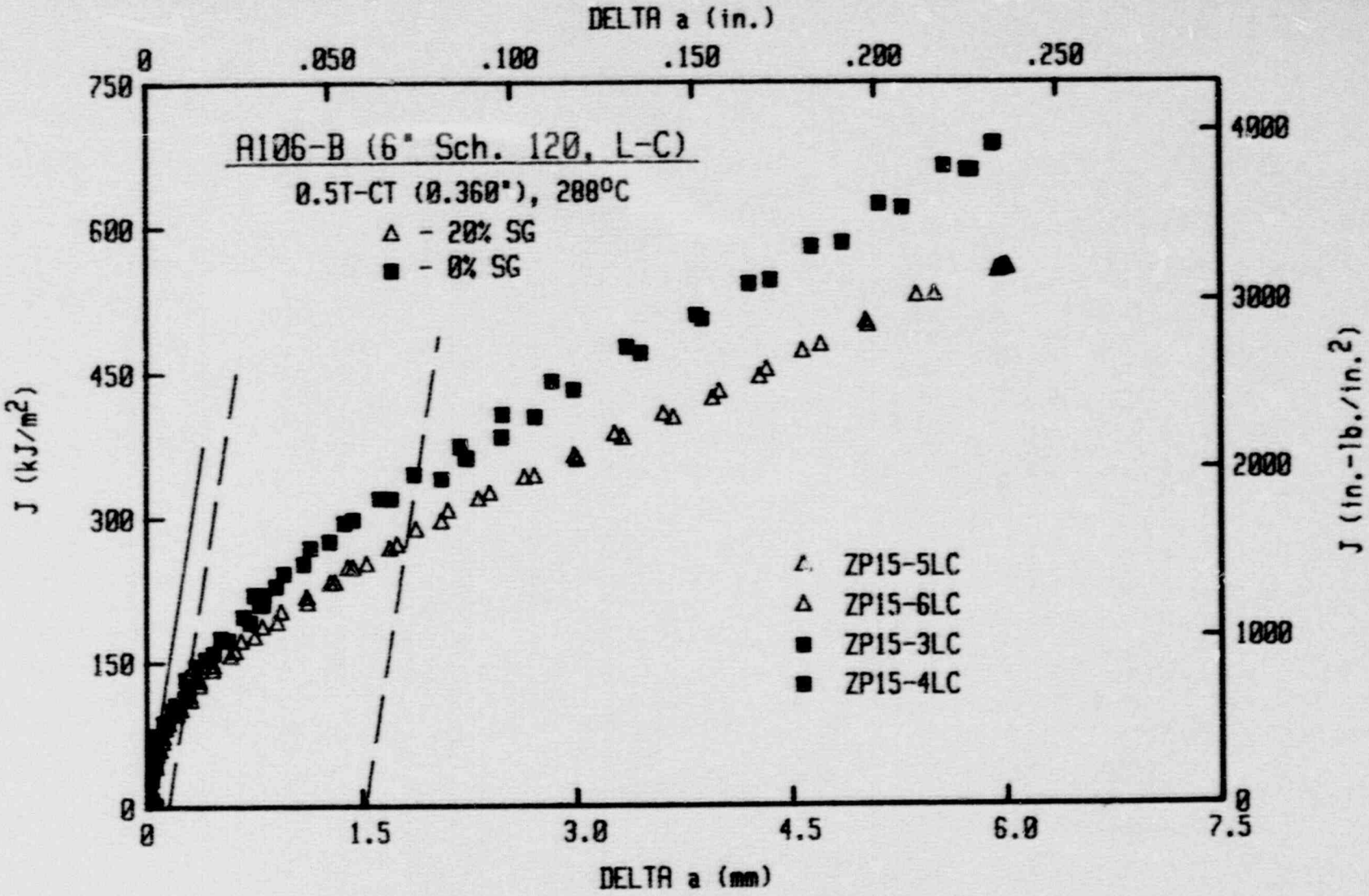

Fig. 3-32 J-R curves for the L-C orientation of A 106 Gr. B (Heat ZP15) at 288°C. Data from sidegrooved specimens are somewhat lower than that from plane-sided specimens.

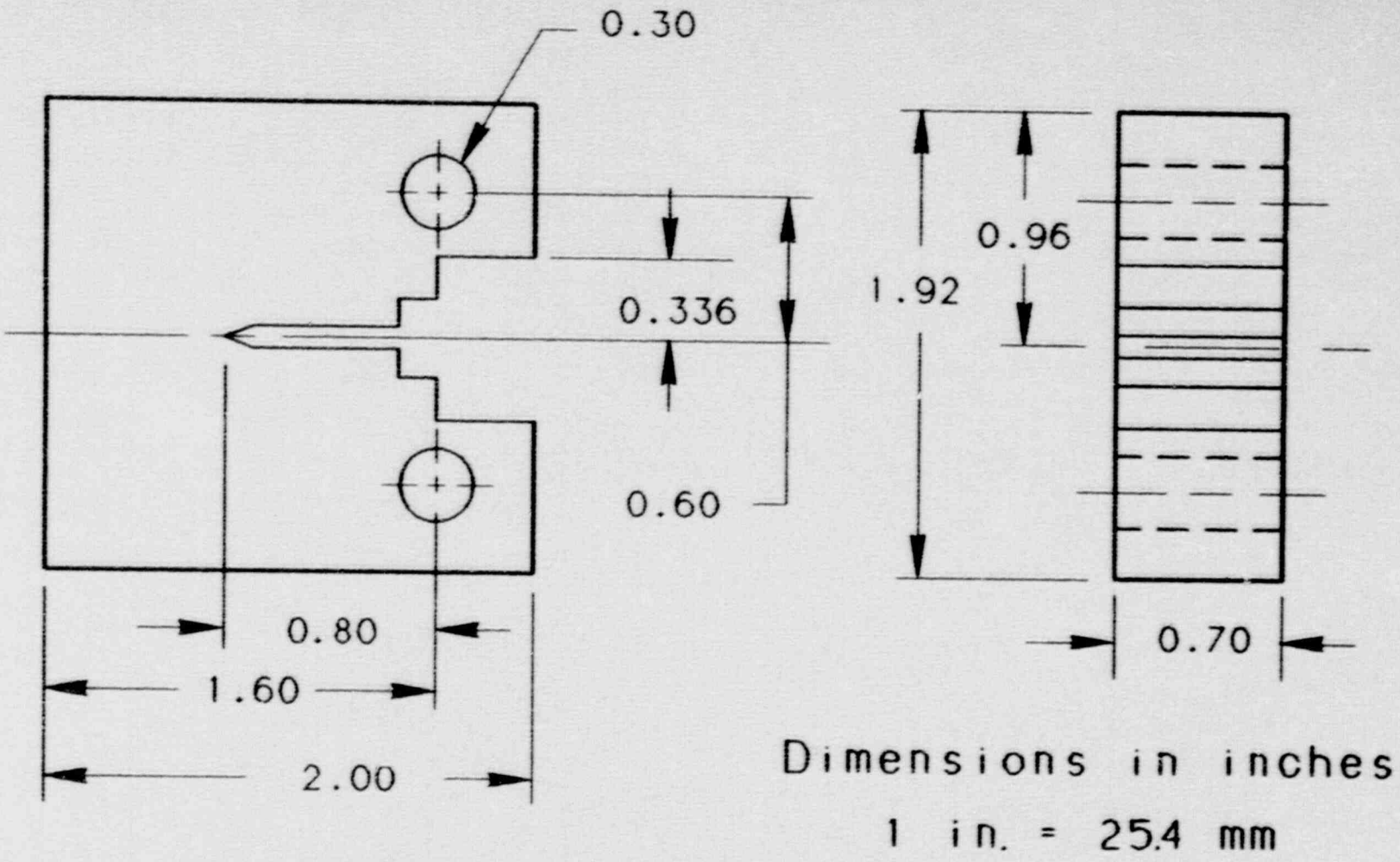

Fig. 3-33 Fracture toughness tests of A 106 Gr. B (Heat ZP14) used this 0.8T-CT specimen design with a thickness of 18 mm (0.7 in.).

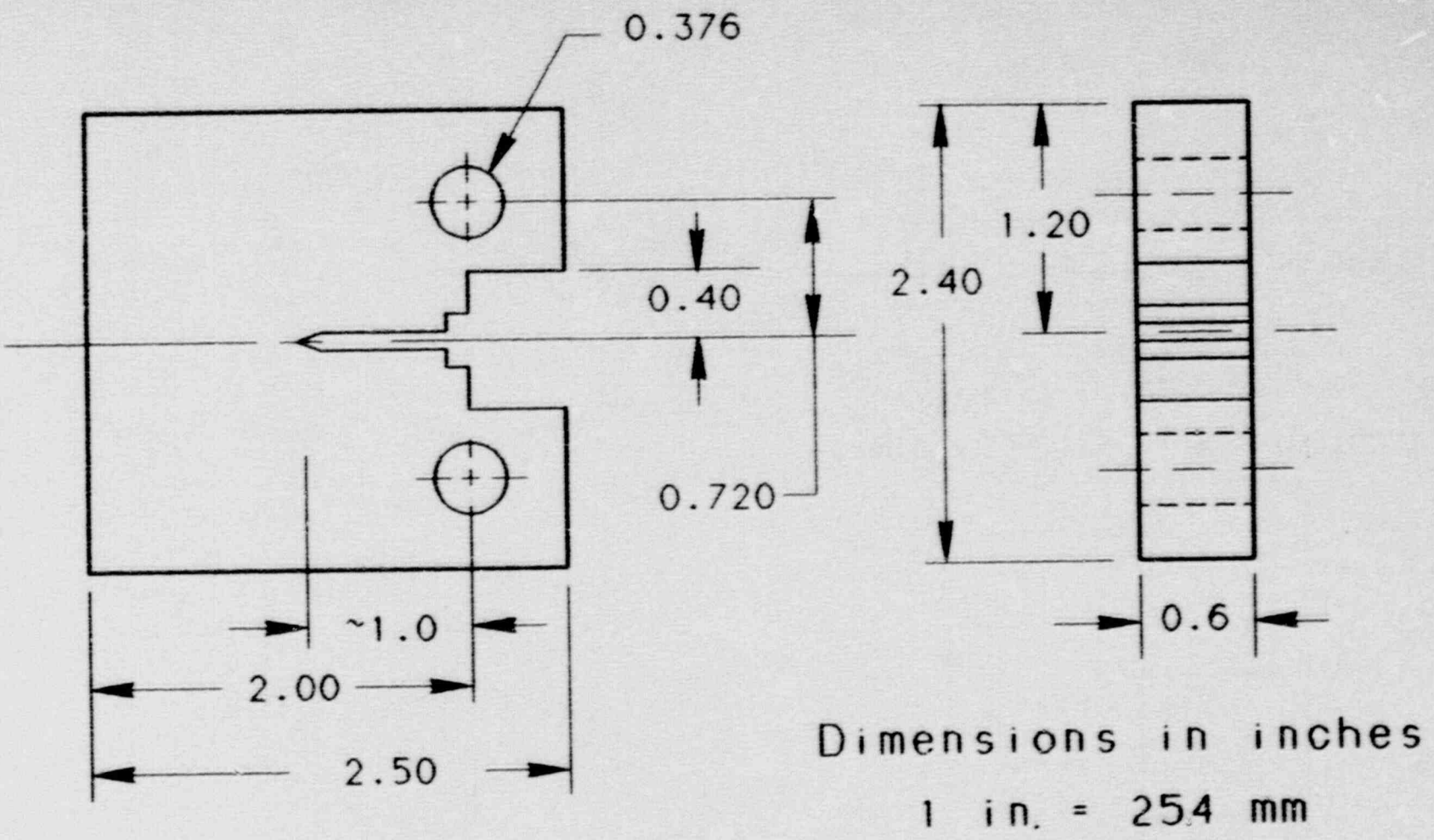

Fig. 3-34 Fracture toughness tests of A 106 Gr. B (Heat ZP14) used this 1T-CT specimen design with a thickness of 15 mm (0.6 in.).

Table 3-13 J-R Curve Results for A 106 Grade B (Heat ZP14)

Specimen Number	Test Temp. (°C)	Side Groove (%)	$(a/W)_o$	Δa_m (mm)	$\Delta a_p - \Delta a_m$ (mm)	J_{Ic} P.L. (kJ/m^2)	J_{Ic} Linear (kJ/m^2)	K_{Jc} P.L. (MPa$\sqrt{m}$)	K_{Jc} Linear (MPa$\sqrt{m}$)	T_{avg} P.L.	T_{avg} ASTM	Flow Strength (MPa)
L-C Orientation												
ZP14-1LC	25	0	0.509	5.26	-0.37	417.9	392.9	293.2	284.3	374	370	398.2
ZP14-2LC	149	0	0.515	12.33	-1.78	161.7	127.8	179.3	159.3	175	206	393.1
ZP14-4LC	149	0	0.521	13.88	-2.74	136.2	136.4	164.5	164.6	170	167	393.1
ZP14-3LC	288	0	0.518	7.78	-0.51	322.1	323.3	247.9	248.4	230	224	414.0
ZP14-5LC	288	0	0.513	7.69	-0.47	245.7	229.4	216.5	209.2	245	251	414.0
ZP14-1LC	25	20	0.521	8.65	-0.90	270.1	250.0	235.7	226.8	262	266	398.2
ZP14-6LC	25	20	0.505	8.90	+0.11	193.4	156.5	199.5	179.4	274	303	398.2
ZP14-2LC	149	20	0.531	10.02	-0.32	108.9	109.6	147.1	147.5	103	104	393.1
ZP14-7LC	149	20	0.467	11.20	-0.16	89.2	94.4	133.2	137.0	106	103	393.1
ZP14-4LC	288	20	0.539	10.20	-0.48	197.4	204.3	194.1	197.4	145	135	414.0
ZP14-3LC	288	20	0.519	10.02	-0.06	183.2	157.6	186.9	173.4	152	181	414.0
C-L Orientation												
ZP14-1CL	25	20	0.526	10.61	-1.10	81.3	84.3	129.4	131.7	99	93	393.6
ZP14-2CL	149	20	0.529	10.16	-0.69	53.1	56.1	102.8	105.6	48	44	391.1
ZP14-3CL	288	20	0.567	9.49	-0.55	64.9	63.9	111.3	110.4	55	57	411.4
ZP14-4CL	288	20	0.515	10.43	-0.55	78.3	78.4	122.2	122.3	53	55	411.4
ZP14-5CL	343	20	0.524	10.95	-0.80	92.4	96.3	131.6	134.6	59	51	386.7

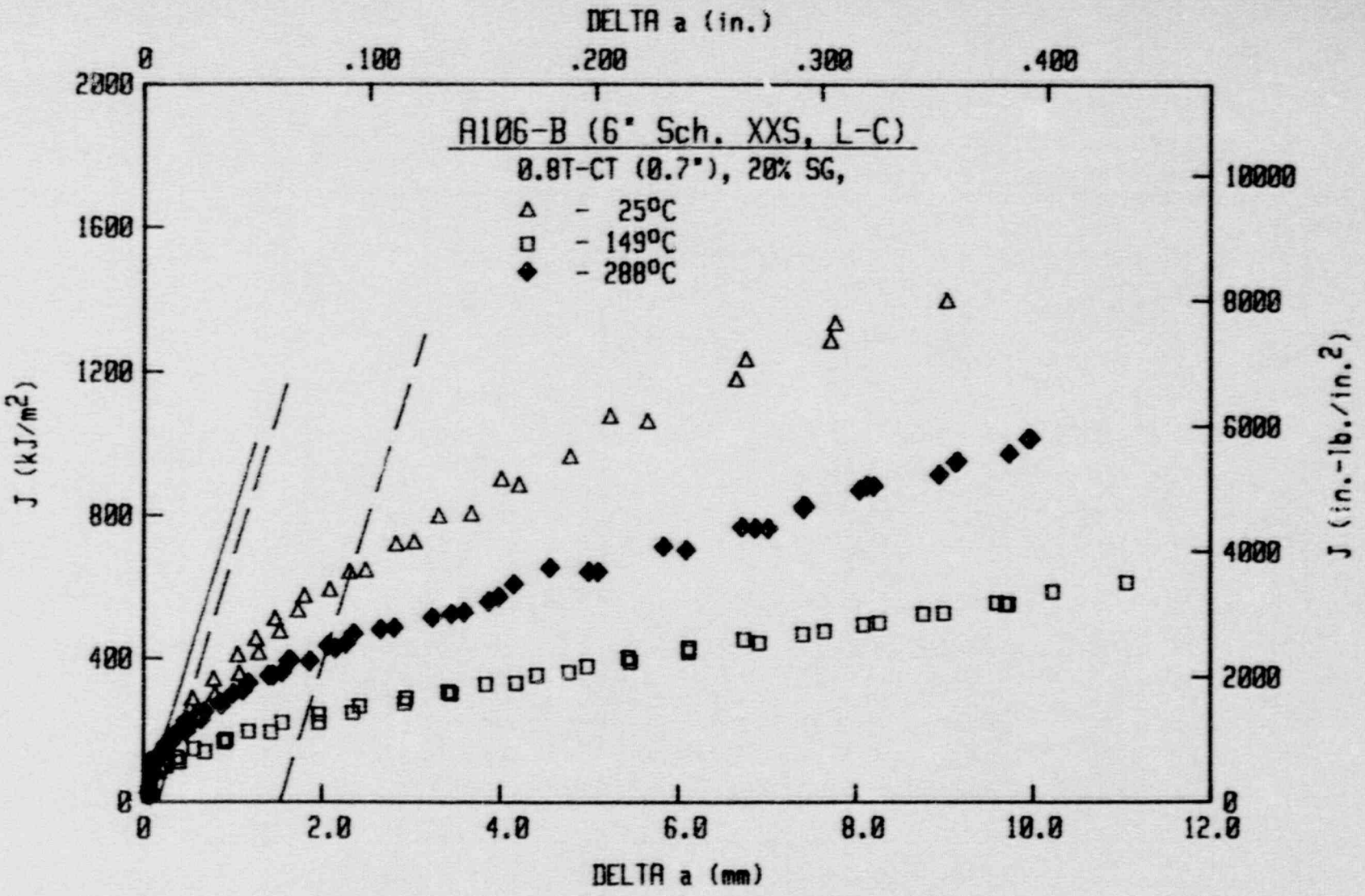

Fig. 3-35 J-R curves for the L-C orientation of A 106 Gr. B (Heat ZP14), using sidegrooved specimens.

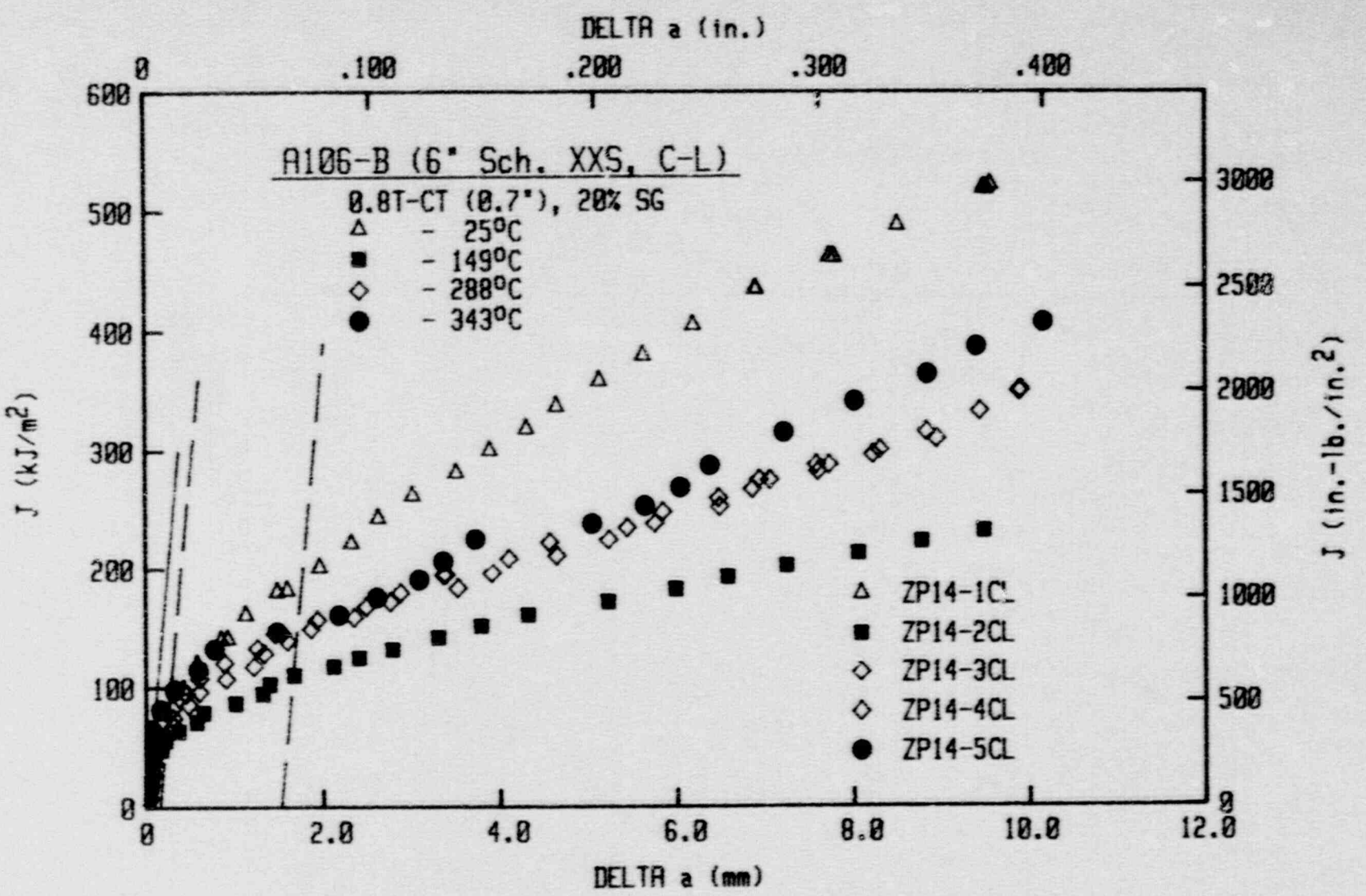

Fig. 3-36 J-R curves for the C-L orientation of A 106 Gr. B (Heat ZP14), using sidegrooved specimens.

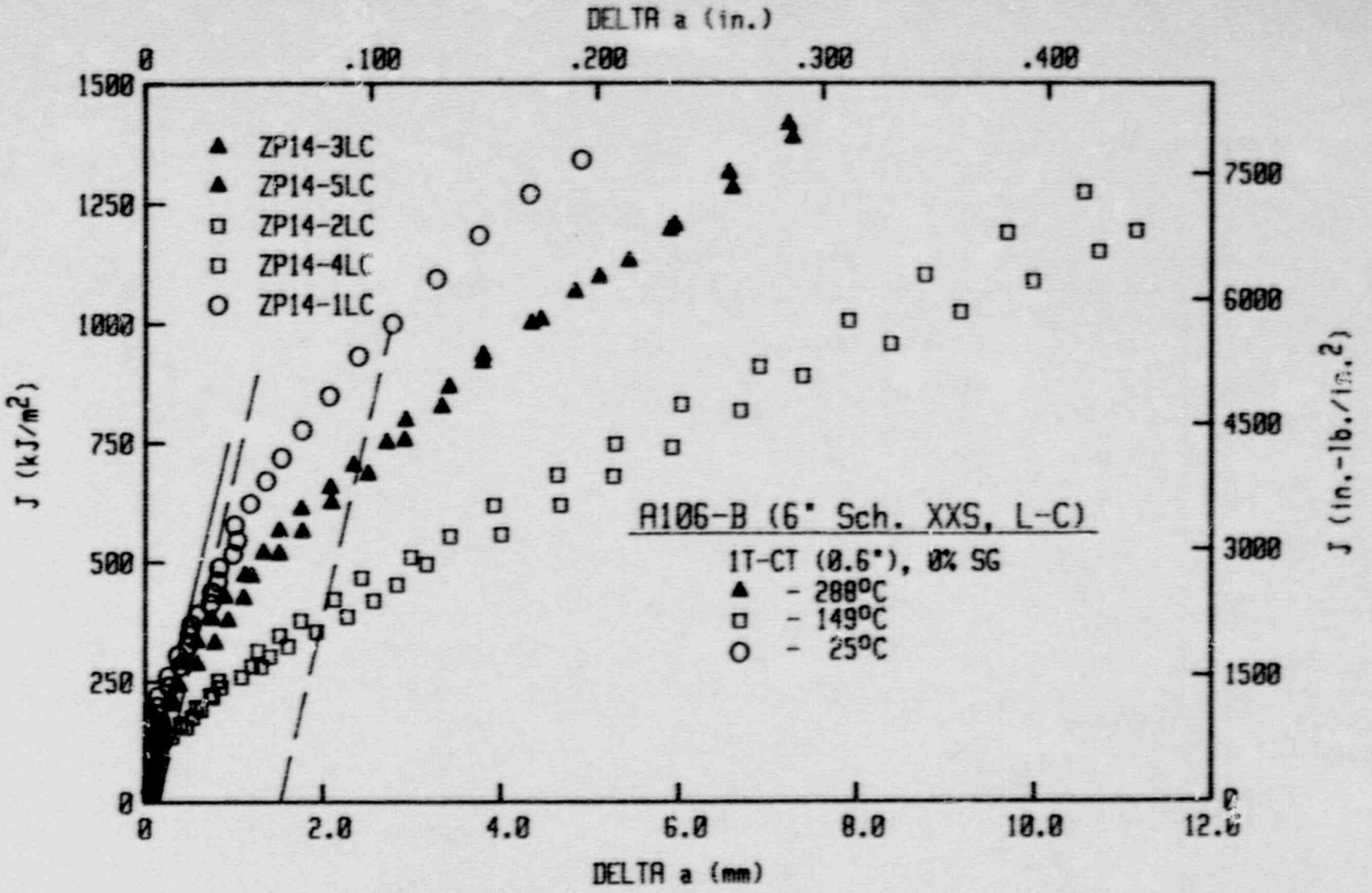

Fig. 3-37 J-R curves for the L-C orientation of A 106 Gr. B (Heat ZP14), using plane-sided specimens.

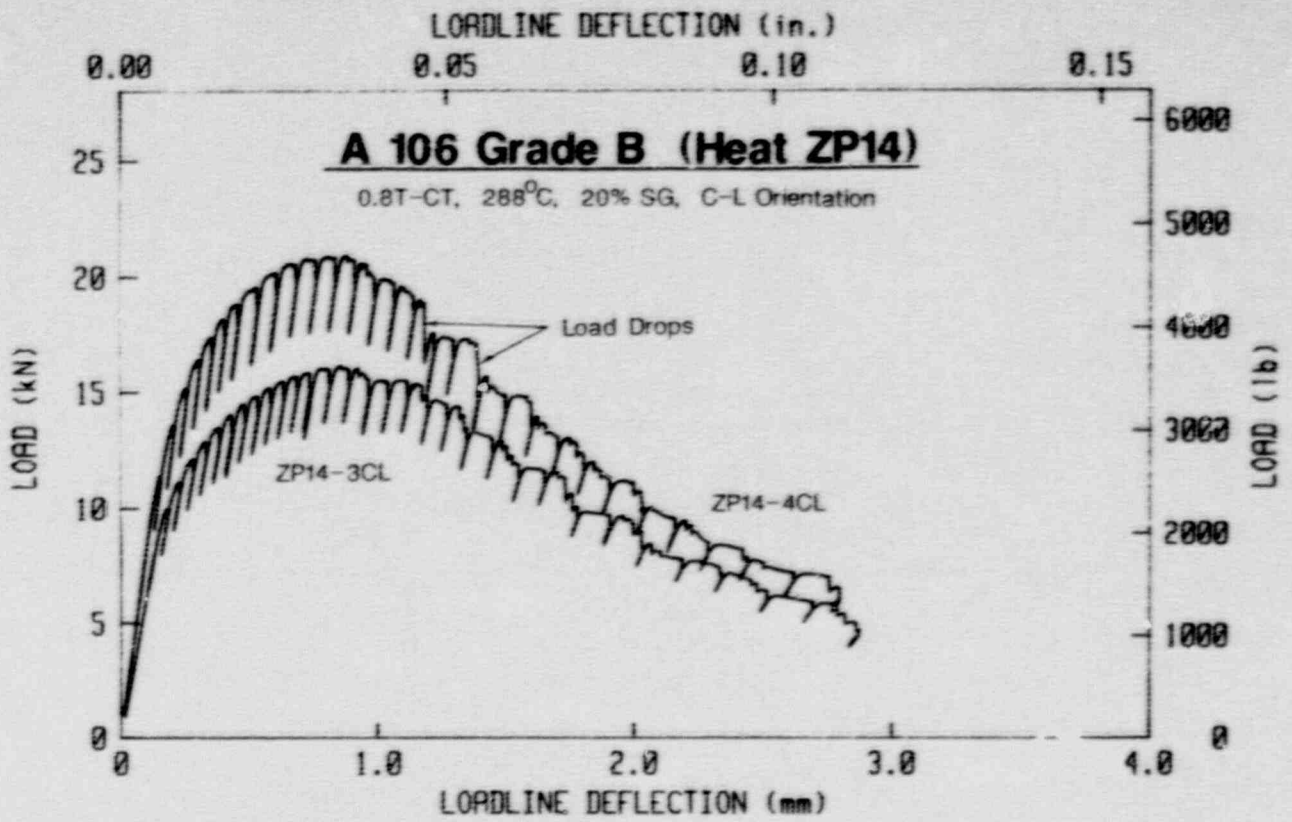

Fig. 3-38 Load-displacement curves for the C-L orientation of A 106 Gr. B at 288°C. Note the load drops in the higher of the two curves, along with the serrated tearing after maximum load.

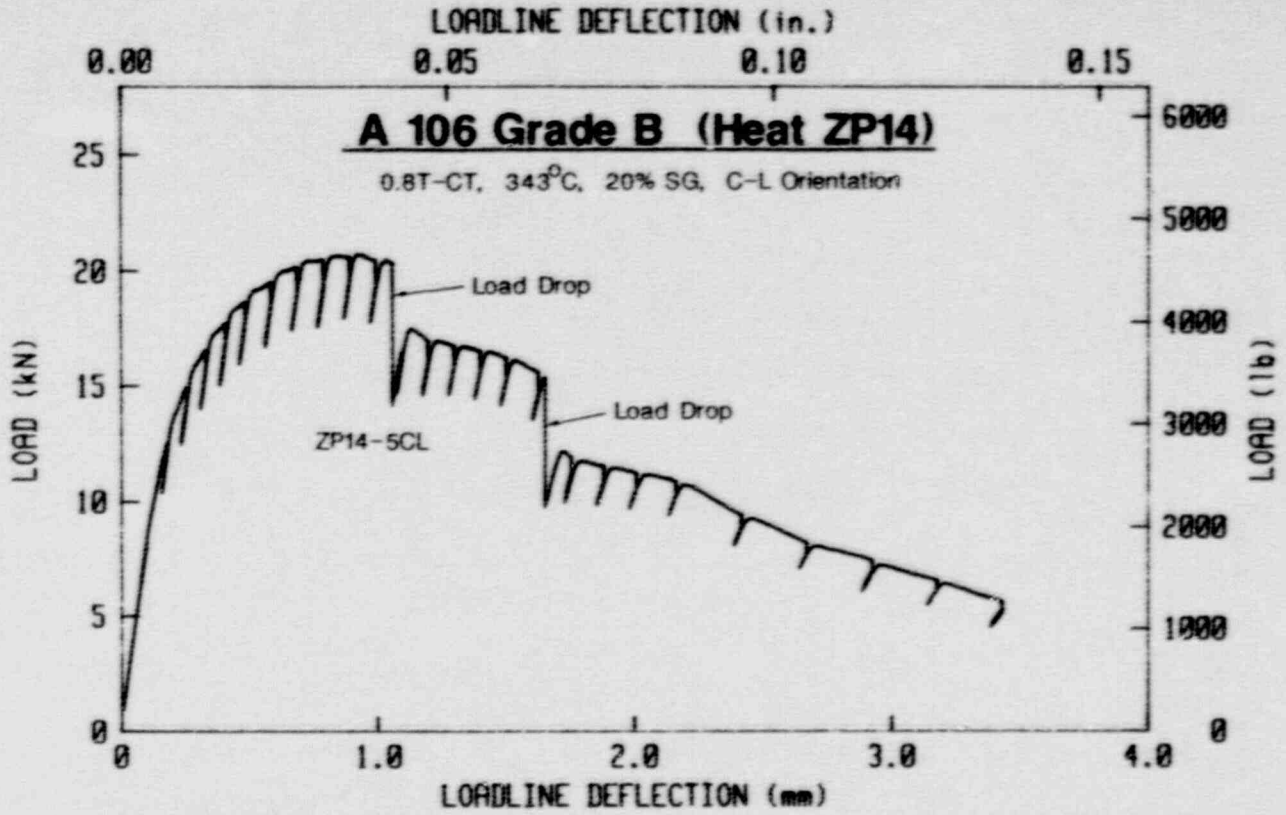

Fig. 3-39 Load-displacement curve for the C-L orientation of A 106 Gr. B at 343°C. Note the two load drops in this curve.

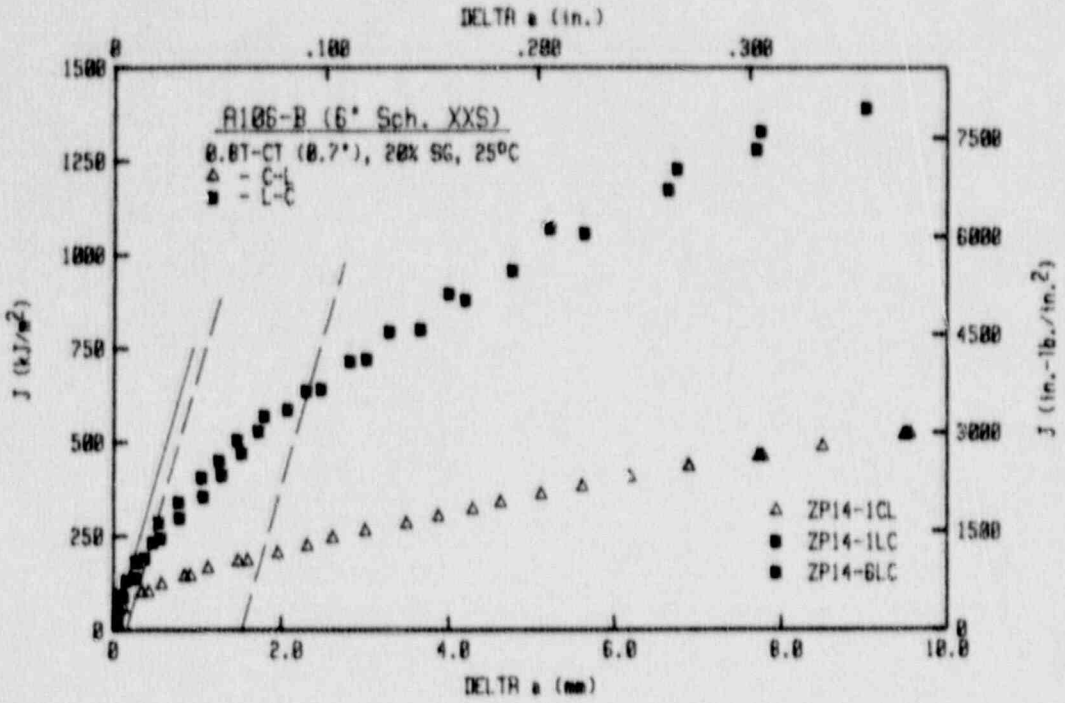

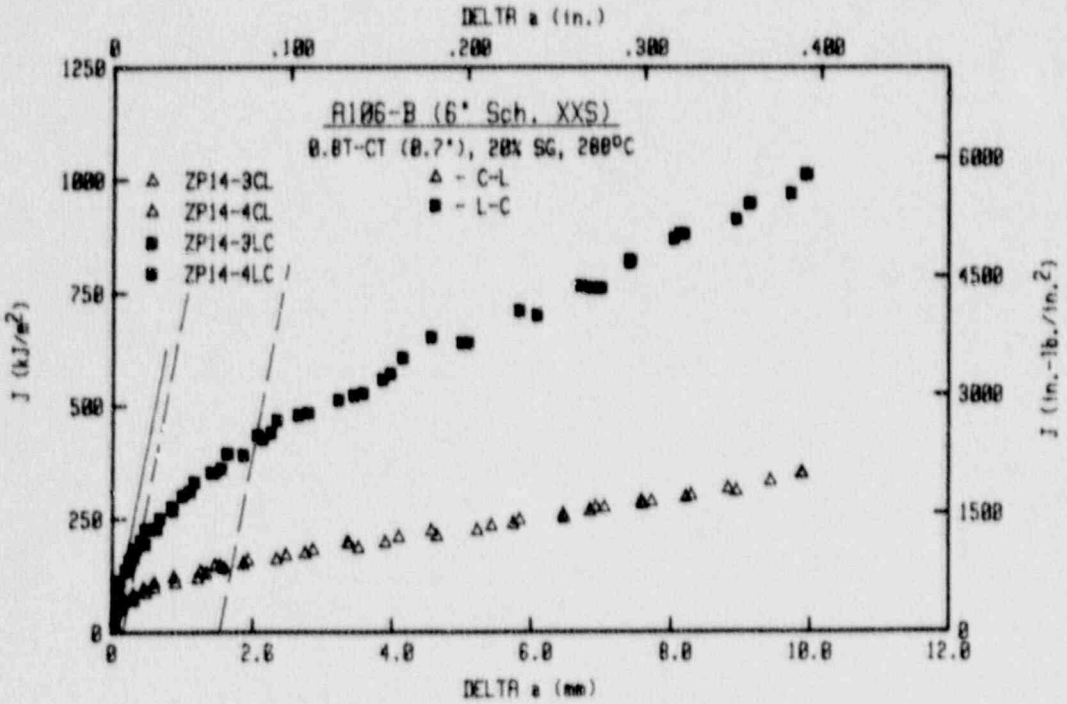

Fig. 3-40 J-R curves for the L-C and C-L orientations of A 106 Gr. B (Heat ZP13) at 25°C and 288°C. The L-C orientation has much higher toughness, consistent with the C_V results.

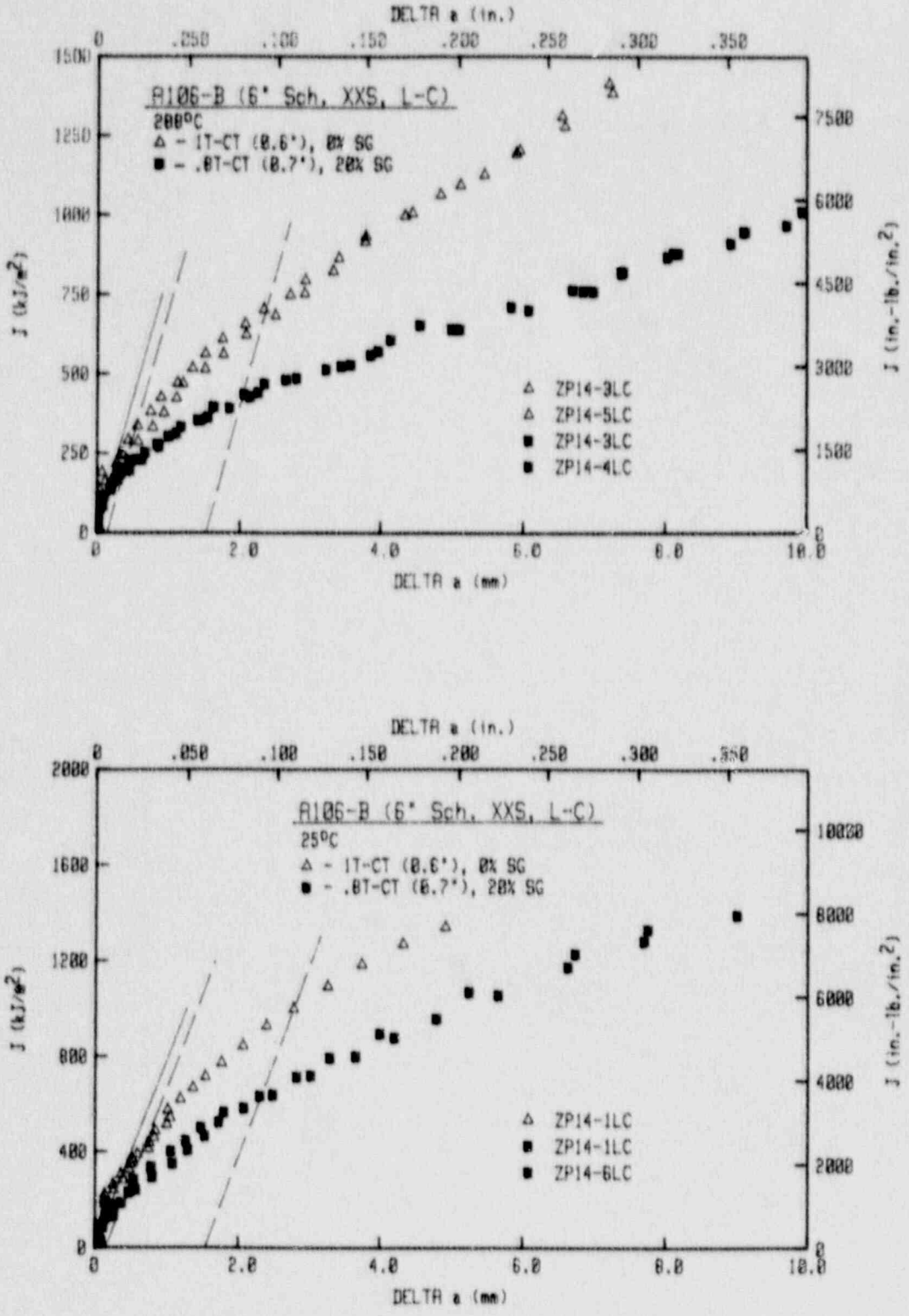

Fig. 3-41 J-R curves for the L-C orientation of A 106 Gr. B (Heat ZP15) at 25°C and 288°C. Data from sidegrooved specimens are somewhat lower than that from plane-sided specimens.

3.3 A 516 Grade 70

3.3.1 Material Description

The heat of A 516 Grade 70 was procured as a 940 mm (37 in.) diameter by 82.5 mm (3.25 in.) thick pipe. This pipe was originally intended for use in the cold leg of a pressurized water reactor (PWR). This heat is the same as DP2-F34 in Ref. 4. A weld of this same pipe has also been characterized (see Secton 3.4).

Data from slow strain rate testing of this heat are given in Ref. 17.

3.3.2 Charpy-V Data

Full-thickness C_v specimens were used from this heat. All four test orientations were sampled. For the L-C and C-L orientations, specimens were located at the nominal inside diameter (ID), the mid-thickness (MID), and the nominal outside diameter (OD). Only the pipe mid-thickness was sampled for the C-R and L-R orientations.

Results from the C_v tests are given in Table 3-14, with the TANH curve-fitting results summarized in Table 3-15 (the lower shelf has been forced to 6.8 J or 5 ft-lb). For all orientations, the onset of upper shelf (as determined by 100% shear) occurs at ~ 93°C (200°F), with several of the data sets exhibiting 100% shear at somewhat lower temperatures. As illustrated in Fig. 3-42 for the L-C orientation, all three thickness locations exhibit similar energy levels within the transition region. However, the ID location exhibits much higher upper shelf energy levels. From the TANH curve-fitting, the ID exhibits an average upper shelf energy of 200 J (147 ft-lb), in contrast to 143 J (106 ft-lb) for OD and 132 J (97 ft-lb) for MID.

A similar trend holds for the C-L orientation (Fig. 3-43), although the differences in the energy levels for the various thickness levels are much smaller. The ID has an average upper shelf energy of 98 J (72 ft-lb), the OD has an average energy of 87 J (64 ft-lb) and the MID has an average energy of 79 J (58 ft-lb).

Comparison of the curve-fit trend lines for the mid-thickness location (Fig. 3-44) indicates similar toughness for the C-L and the C-R orientations, with the midthickness of the L-R orientation exhibiting much higher toughness than the L-C orientation.

3.3.3 Tensile Data

Tensile tests of this heat were made using threaded-end specimens with a gage diameter of 12.83 mm (0.505 in.) and a gage length of ~ 50.8 mm (2 in.) used for elongation measurements. The pipe ID, OD and MID locations were sampled for both the circumferential (C) and the longitudinal (L) orientations.

The strength data are given in Table 3-16. In general the two orientations give quite similar strength levels, as illustrated in Fig. 3-45 and summarized in Table 3-17.

Table 3-14 Charpy-V Data for A 516 Grade 70 Base Metal

Specimen Number	Test Temp.		Absorbed Energy		Lateral Expansion		Shear Percent
	(°C)	(°F)	(J)	(ft-lb)	(mm)	(in.)	(%)
			L-C Orientation (O.D.)				
BLO-18	-51	-60	6.8	5	0.13	0.005	0
BLO-5	-40	-40	8.1	6	0.18	0.007	0
BLO-4	-18	0	23.0	17	0.48	0.019	11
BLO-13	-18	0	38.0	28	0.71	0.028	17
BLO-11	4	40	65.1	48	1.19	0.047	36
BLO-14	16	60	56.9	42	1.17	0.046	53
BLO-1	22	72	81.3	60	1.40	0.055	50
BLO-7	22	72	93.6	69	1.63	0.064	62
BLO-17	66	150	135.6	100	2.21	0.087	100
BLO-2	93	200	157.3	116	2.41	0.095	100
BLO-12	93	200	157.3	116	2.34	0.092	100
BLO-10	149	300	136.9	101	2.16	0.085	100
BLO-16	149	300	141.0	104	2.29	0.090	99
BLO-3	218	425	135.6	100	2.21	0.087	100
BLO-9	218	425	149.1	110	2.16	0.085	100
BLO-8	288	550	132.9	98	2.06	0.081	100
BLO-15	288	550	134.2	99	1.85	0.073	100
			L-C Orientation (MID)				
BLM-18	-51	-60	6.8	5	0.10	0.004	0
BLM-5	-40	-40	9.5	7	0.25	0.010	0
BLM-4	-18	0	39.3	29	0.76	0.030	17
BLM-13	-18	0	44.7	33	0.86	0.034	21
BLM-11	4	40	67.8	50	1.27	0.050	50
BLM-14	16	60	61.0	45	1.22	0.048	52
BLM-1	22	72	81.3	60	1.42	0.056	60
BLM-7	22	72	84.1	62	1.52	0.060	55
BLM-6	52	125	116.6	86	1.98	0.078	97
BLM-17	66	150	122.0	90	2.06	0.081	100
BLM-2	93	200	130.2	96	1.98	0.078	100
BLM-12	93	200	124.7	92	1.98	0.078	100
BLM-10	149	300	119.3	88	2.03	0.080	100
BLM-16	149	300	126.1	93	2.08	0.082	100
BLM-3	218	425	134.2	99	2.03	0.080	100
BLM-9	218	425	135.6	100	1.98	0.078	100
BLM-8	288	550	130.2	96	1.93	0.076	100
BLM-15	288	550	142.4	105	1.68	0.066	100
			L-C Orientation (I.D.)				
BLI-18	-51	-60	6.8	5	0.13	0.005	0
BLI-5	-40	-40	8.1	6	0.10	0.004	5
BLI-4	-18	0	38.0	28	0.61	0.024	17
BLI-13	-18	0	43.4	32	0.76	0.030	17
BLI-11	4	40	61.0	45	1.09	0.043	33
BLI-14	16	60	70.5	52	1.22	0.048	44
BLI-1	22	72	97.6	72	1.63	0.064	55
BLI-7	22	72	107.1	79	1.70	0.067	60
BLI-6	52	125	160.0	118	2.24	0.088	100
BLI-17	66	150	157.3	116	2.18	0.086	100
BLI-2	93	200	162.7	120	2.18	0.086	100
BLI-12	93	200	157.3	116	2.16	0.085	100
BLI-10	149	300	161.3	119	2.18	0.086	100
BLI-16	149	300	174.9	129	2.11	0.083	100
BLI-3	218	425	211.5	156	1.68	0.066	100
BLI-9	218	425	219.6	162	1.75	0.069	100
BLI-8	288	550	227.8	168	1.60	0.063	100
BLI-15	288	550	206.1	152	1.52	0.060	100

Table 3-14 Charpy-V Data for A 516 Grade 70 Base Metal (cont.)

Specimen Number	Test Temp.		Absorbed Energy		Lateral Expansion		Shear Percent
	(°C)	(°F)	(J)	(ft-lb)	(mm)	(in.)	(%)
C-L Orientation (O.D.)							
BCO-18	-51	-60	8.1	6	0.07	0.003	0
BCO-5	-40	-40	6.8	5	0.07	0.003	0
BCO-4	-18	0	29.8	22	0.64	0.025	21
BCO-13	-18	0	29.8	22	0.64	0.025	21
BCO-11	4	40	43.4	32	0.89	0.035	50
BCO-14	16	60	46.1	34	0.94	0.037	44
BCO-1	22	72	50.2	37	1.12	0.044	69
BCO-7	22	72	48.8	36	1.09	0.043	56
BCO-6	52	125	75.9	56	1.55	0.061	96
BCO-17	66	150	78.6	58	1.50	0.059	96
BCO-2	93	200	78.6	58	1.55	0.061	100
BCO-12	93	200	78.6	58	1.63	0.064	100
BCO-19	121	250	75.9	56	1.63	0.064	100
BCO-20	121	250	75.9	56	1.68	0.066	100
BCO-10	149	300	88.1	65	1.75	0.069	100
BCO-16	149	300	81.3	60	1.65	0.065	100
BCO-3	218	425	90.8	67	1.73	0.068	100
BCO-9	218	425	88.1	65	1.68	0.066	100
BCO-8	288	550	97.6	72	1.75	0.069	100
BCO-15	288	550	94.9	70	1.70	0.067	100
C-L Orientation (MID)							
BCM-18	-51	-60	13.6	10	0.23	0.009	0
BCM-5	-40	-40	12.2	9	0.23	0.009	5
BCM-4	-18	0	27.1	20	0.56	0.022	26
BCM-13	-18	0	21.7	16	0.46	0.018	30
BCM-11	4	40	38.0	28	0.81	0.032	39
BCM-14	16	60	46.1	34	1.02	0.040	56
BCM-1	22	72	48.8	36	1.04	0.041	62
BCM-7	22	72	51.5	38	1.02	0.040	65
BCM-6	52	125	65.1	48	1.32	0.052	94
BCM-17	66	150	67.8	50	1.37	0.054	100
BCM-2	93	200	70.5	52	1.47	0.058	100
BCM-12	93	200	71.9	53	1.47	0.058	100
BCM-19	121	250	71.9	53	1.52	0.060	100
BCM-20	121	250	73.2	54	1.50	0.059	100
BCM-10	149	300	71.9	53	1.42	0.056	100
BCM-16	149	300	63.7	47	1.35	0.053	100
BCM-3	218	425	88.1	65	1.52	0.060	100
BCM-9	218	425	84.1	62	1.47	0.058	100
BCM-8	288	550	88.1	65	1.55	0.061	100
BCM-15	288	550	84.1	62	1.45	0.057	100
C-L Orientation (I.D.)							
BCI-18	-51	-60	17.6	13	0.33	0.013	0
BCI-5	-40	-40	21.7	16	0.36	0.014	6
BCI-4	-18	0	23.0	17	0.46	0.018	16
BCI-13	-18	0	27.1	20	0.53	0.021	17
BCI-11	4	40	36.6	27	0.76	0.030	40
BCI-14	16	60	50.2	37	1.02	0.040	50
BCI-1	22	72	42.0	31	0.91	0.036	50
BCI-7	22	72	48.8	36	0.94	0.037	45
BCI-6	52	125	70.5	52	1.32	0.052	76
BCI-17	66	150	88.1	65	1.60	0.063	99
BCI-2	93	200	94.9	70	1.83	0.072	100
BCI-12	93	200	93.6	69	1.75	0.069	100
BCI-19	121	250	88.1	65	1.73	0.068	100
BCI-20	121	250	84.1	62	1.68	0.066	100
BCI-10	149	300	89.5	66	1.78	0.070	100
BCI-16	149	300	92.2	68	1.73	0.068	100
BCI-3	218	425	105.8	78	1.68	0.066	100
BCI-9	218	425	100.3	74	1.63	0.064	100
BCI-8	288	550	97.6	72	1.55	0.061	100
BCI-15	288	550	101.7	75	1.57	0.062	100

Table 3-14 Charpy-V Data for A 516 Grade 70 Base Metal (cont.)

Specimen Number	Test Temp.		Absorbed Energy		Lateral Expansion		Shear Percent
	(°C)	(°F)	(J)	(ft-lb)	(mm)	(in.)	(%)
L-R Orientation (MID)							
BLR-18	-51	-60	5.4	4	0.13	0.005	0
BLR-5	-40	-40	12.2	9	0.28	0.011	0
BLR-4	-18	0	17.6	13	0.43	0.017	16
BLR-13	-18	0	43.4	32	0.79	0.031	21
BLR-11	4	40	84.1	62	1.37	0.054	50
BLR-14	16	60	119.3	88	1.91	0.075	70
BLR-1	22	72	107.1	79	1.68	0.066	69
BLR-7	22	72	105.8	78	1.70	0.067	74
BLR-6	52	125	157.3	116	2.21	0.087	100
BLR-17	66	150	141.0	104	2.01	0.079	100
BLR-2	93	200	146.4	108	2.06	0.081	100
BLR-12	93	200	146.4	108	2.13	0.084	100
BLR-10	149	300	158.6	117	1.98	0.078	100
BLR-16	149	300	168.8	123	2.16	0.085	100
BLR-3	218	425	235.9	174	1.73	0.068	100
BLR-9	218	425	176.3	130	1.68	0.066	100
BLR-8	288	550	219.6	162	[a]	[a]	100
BLR-15	288	550	229.1	169	1.73	0.068	100
C-R Orientation (MID)							
BCR-18	-51	-60	10.8	8	0.10	0.004	0
BCR-5	-40	-40	14.9	11	0.28	0.011	6
BCR-4	-18	0	38.0	28	0.74	0.029	26
BCR-13	-18	0	29.8	22	0.63	0.025	26
BCR-11	4	40	43.4	32	0.84	0.033	61
BCR-14	16	60	51.5	38	0.86	0.034	63
BCR-1	22	72	84.1	62	1.50	0.059	98
BCR-7	22	72	62.4	46	1.24	0.049	85
BCR-6	52	125	78.6	58	1.60	0.063	98
BCR-17	66	150	84.1	62	1.37	0.054	100
BCR-2	93	200	80.0	59	1.62	0.064	100
BCR-12	93	200	78.6	58	1.63	0.064	100
BCR-19	121	250	77.3	57	1.52	0.060	100
BCR-20	121	250	78.6	58	1.63	0.064	100
BCR-10	149	300	84.1	62	1.73	0.068	100
BCR-16	149	300	93.6	69	1.63	0.064	100
BCR-3	218	425	100.3	74	1.60	0.063	100
BCR-9	218	425	101.7	75	1.57	0.062	100
BCR-8	288	550	90.8	67	1.42	0.056	100
BCR-15	288	550	96.3	71	1.47	0.058	100

[a] Specimen did not fully fracture.

Table 3-15 Curve-fit Results for Charpy Data from A 516 Gr. 70

Thickness Location	Upper Shelf		$C_v = A + B \tanh (T-T_o)/C$							
			A		B		C		T_o	
	(J)	(ft-lb)	(J)	(ft-lb)	(J)	(ft-lb)	(°C)	(°F)	(°C)	(°F)
L-C Orientation										
OD	143.4	105.8	75.08	55.38	68.30	50.38	37.38	67.28	16.06	60.91
MID	131.7	97.1	69.23	51.06	62.46	46.06	47.41	85.34	11.48	52.66
ID	199.6	147.2	103.19	76.11	96.41	71.11	61.71	111.08	29.38	84.89
C-L Orientation										
OD	87.2	64.3	47.00	34.66	40.22	29.66	56.71	102.07	15.35	59.63
MID	78.8	58.1	42.76	31.54	35.99	26.54	60.67	109.20	13.36	56.04
ID	98.1	72.3	52.41	38.66	45.64	33.66	62.26	112.07	24.39	75.90
L-R Orientation										
MID	198.0	146.0	102.40	75.53	95.62	70.53	74.79	134.62	27.30	81.14
C-R Orientation										
MID	88.9	65.5	47.82	35.27	41.04	30.27	45.82	82.47	2.09	35.76

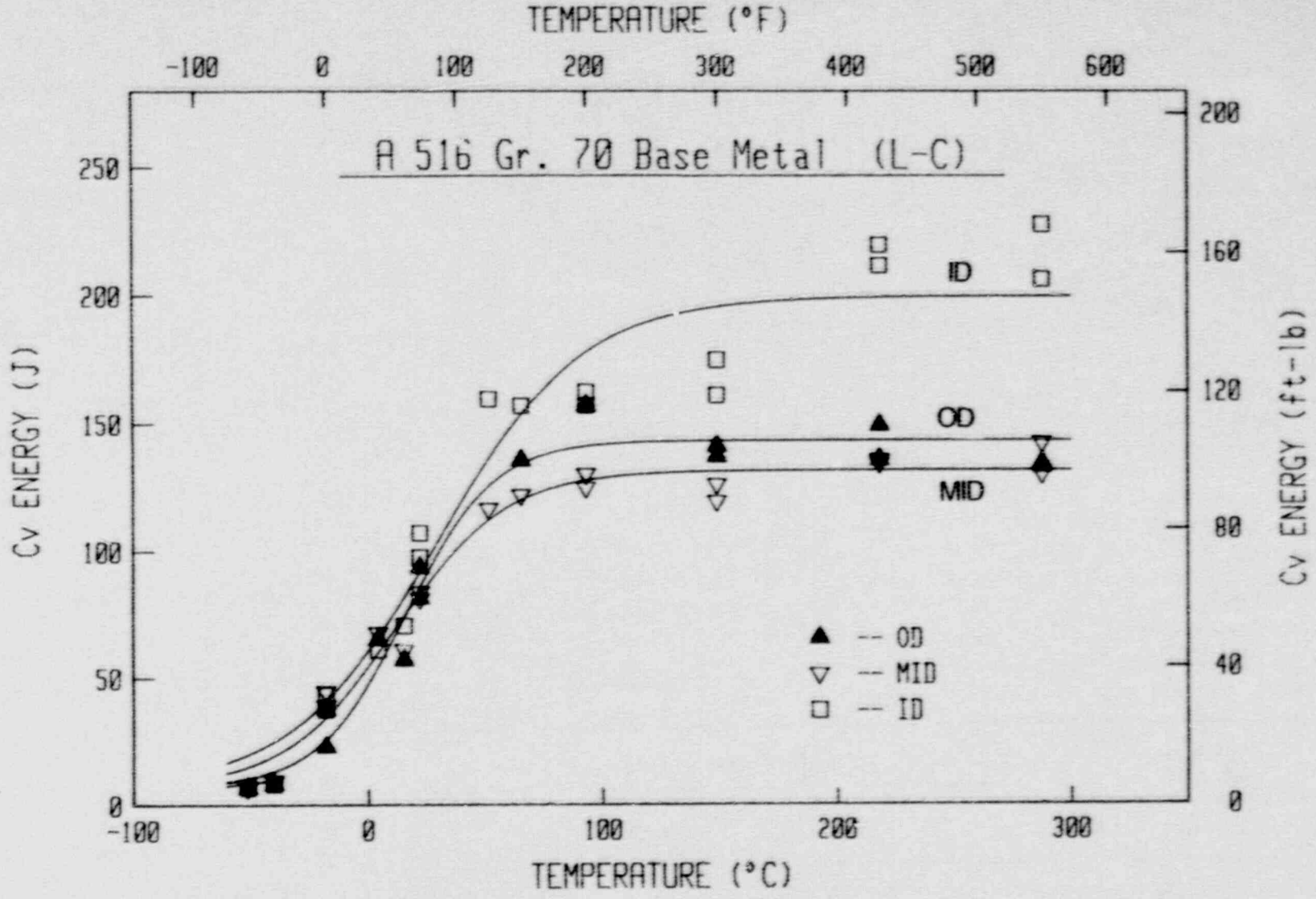

Fig. 3-42 Charpy-V data for the L-C orientation of the A 516 Gr. 70 base metal.

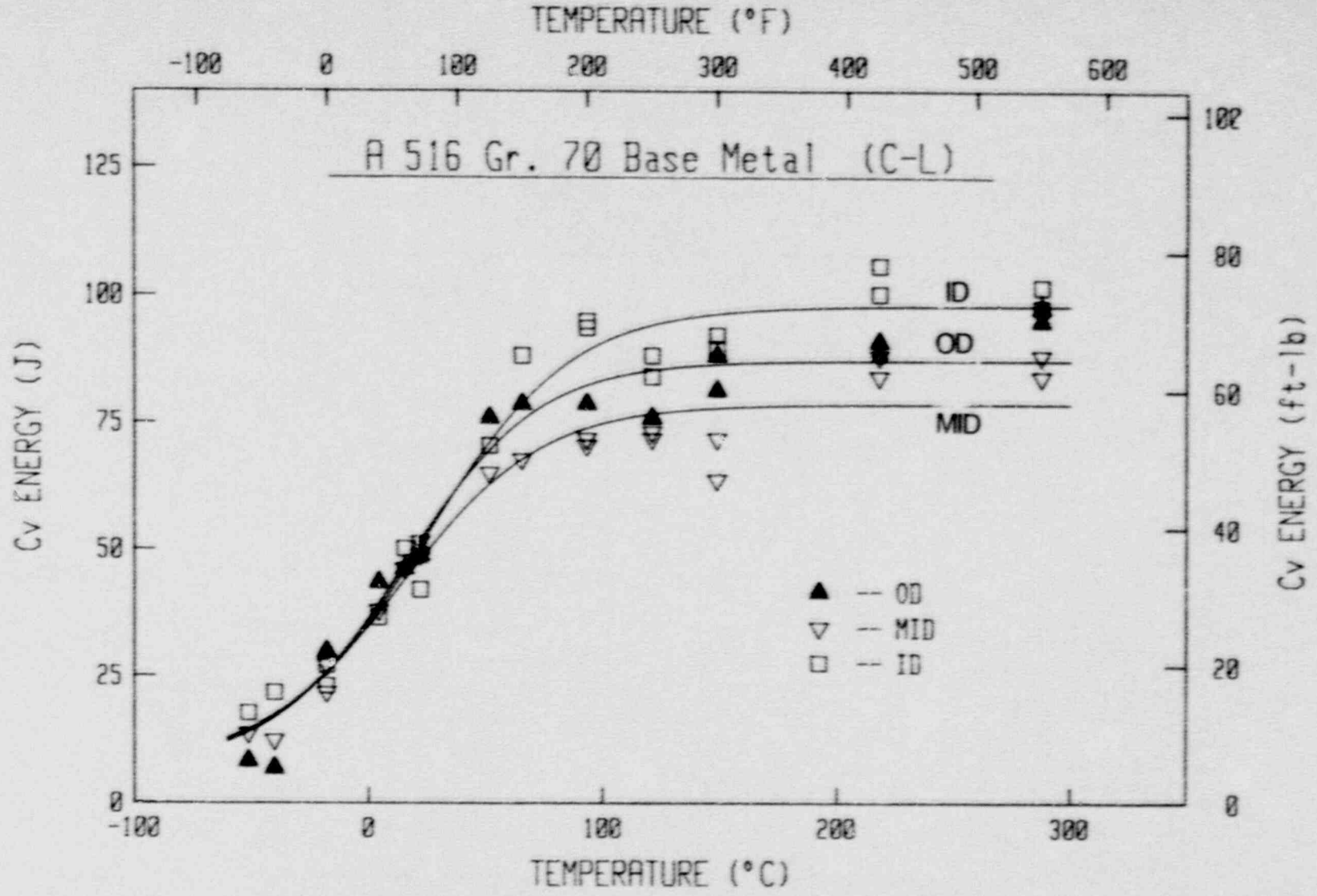

Fig. 3-43 Charpy-V data for the C-L orientation of the A 516 Gr. 70 base metal.

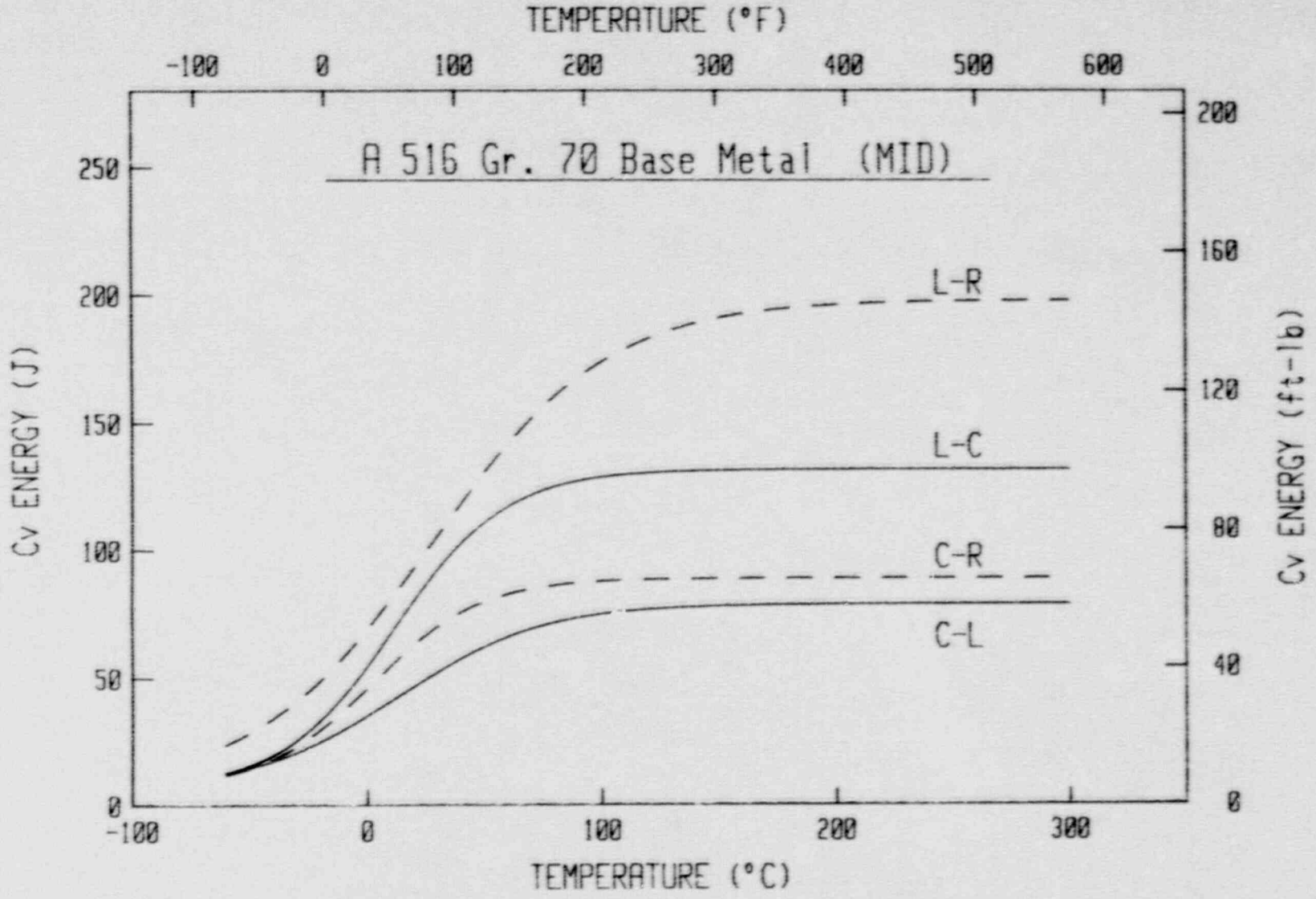

Fig. 3-44 The curve-fits to the Charpy-V data for the A 516 Gr. 70 base metal.

Table 3-16 Tensile Data for A 516 Grade 70 Base Metal

Specimen Number	Orient.	Thickness Location	Test Temp.		0.2% Offset Yield Strength		Ultimate Strength		Elongation	Reduction In Area
			(°C)	(°F)	(MPa)	(ksi)	(MPa)	(ksi)	(%)	(%)
BC-03	C	OD	24	75	291.5	42.3	503.6	73.0	31.2	57.2
BC-M3	C	MID	24	75	292.4	42.4	518.6	75.2	29.0	54.3
BC-I3	C	ID	24	75	282.4	41.0	495.7	71.9	32.8	60.8
BC-01	C	OD	149	300	256.3	37.2	454.4	65.9	31.9	56.7
BC-M1	C	MID	149	300	246.3	35.7	465.3	67.5	26.7	53.8
BC-I1	C	ID	149	300	241.8	35.1	446.6	64.8	28.1	60.3
BC-05	C	OD	204	400	234.4	34.0	460.9	66.9	27.8	54.4
BC-M5	C	MID	204	400	217.3	31.5	469.2	68.1	24.7	50.3
BC-I5	C	ID	204	400	223.7	32.5	455.5	66.1	29.2	57.8
BC-02	C	OD	288	550	241.2	35.0	488.0	70.8	29.5	55.7
BC-M2	C	MID	288	550	201.3	29.2	502.1	72.8	28.0	59.1
BC-I2	C	ID	288	550	223.8	32.5	478.9	69.5	28.3	55.9
BC-M4	C	MID	288	550	206.2	29.9	504.6	73.2	29.1	44.9
BC-I4	C	ID	288	550	227.9	33.1	478.5	69.4	28.8	56.5
BL-03	L	OD	24	75	308.5	44.7	506.4	73.5	34.6	67.4
BL-M3	L	MID	24	75	297.0	43.1	521.0	75.6	33.0	64.7
BL-I3	L	ID	24	75	290.3	42.1	501.0	72.7	34.4	66.7
BL-01	L	OD	149	300	272.3	39.5	459.1	66.6	29.5	68.8
BL-M1	L	MID	149	300	261.3	37.9	475.5	69.0	31.1	64.7
BL-I1	L	ID	149	300	245.6	35.6	450.5	65.3	31.0	68.8
BL-05	L	OD	204	400	241.9	35.1	467.0	67.7	30.6	64.8
BL-M5	L	MID	204	400	222.4	32.3	484.1	70.2	22.7	57.6
BL-I5	L	ID	204	400	224.3	32.5	458.7	66.5	30.1	65.2
BL-02	L	OD	288	550	263.8	38.3	494.4	71.7	30.2	63.7
BL-M2	L	MID	288	550	210.4	30.5	509.5	73.9	31.0	59.8
BL-I2	L	ID	288	550	230.2	33.4	484.4	70.3	32.5	64.4
BL-04	L	OD	288	550	250.9	36.4	495.3	71.8	30.2	63.9
BL-M4	L	MID	288	550	207.0	30.0	511.5	74.2	29.8	59.8
BL-I4	L	ID	288	550	209.6	30.4	479.2	69.5	33.7	66.5

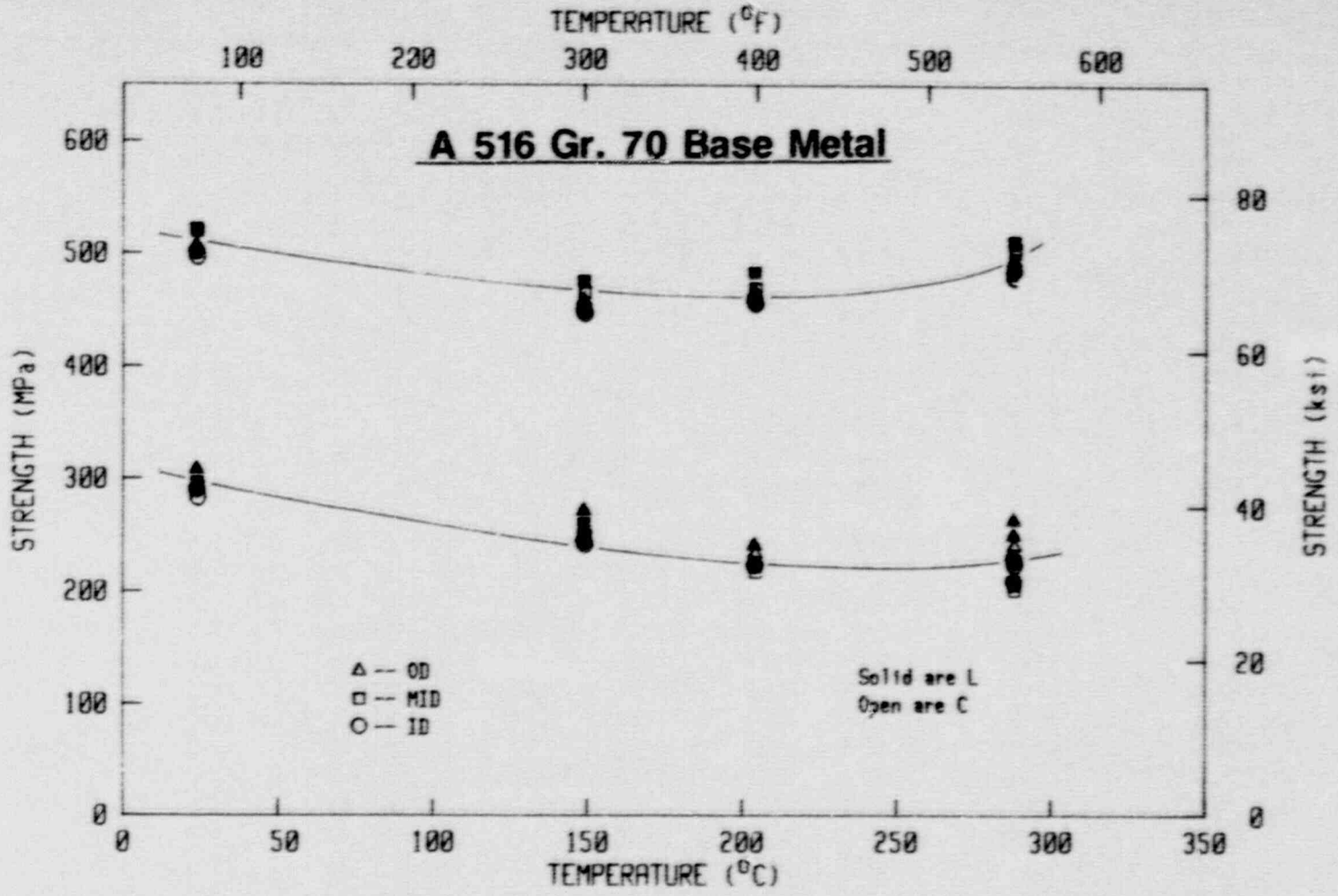

Fig. 3-45 Tensile data for the A 516 Gr. 70 base metal.

Table 3-17 Summary of Strength Results for A 516 Gr. 70 Base Metal

Test Temperature		Orientation	0.2% Offset Yield Strength		Ultimate Strength	
(°C)	(°F)		(MPa)	(ksi)	(MPa)	(ksi)
24	75	C	288.8	41.9	506.0	73.4
		L	298.6	43.3	509.5	73.9
149	300	C	248.1	36.0	455.4	66.1
		L	259.7	37.7	461.7	67.0
204	400	C	225.1	32.7	461.9	67.0
		L	229.5	33.3	469.9	68.2
288	550	C	220.1	31.9	490.4	71.1
		L	228.7	33.2	495.7	71.9

3.3.4 Fracture Toughness Data

J-R curves were evaluated for the L-C orientation of this material at 288°C (550°F) using 4T-CT plan-form specimens with a thickness of 66 mm (2.6 in.), as illustrated in Fig. 3-46. Two specimens of this geometry were tested, with one of the specimens side-grooved by 20% and the other specimen plane-sided. Results from these tests are summarized in Table 3-18, and illustrated in Figs. 3-47 and 3-48 for J_M and J_D, respectively. As with other ferritic steels described previously, both specimens exhibit similar J levels at low crack growth levels (i.e., for $\Delta a < 2.5$ mm or 0.1 in.), with the J levels for the plane-sided specimen greatly exceeding those of the sidegrooved specimen at larger crack growth levels.

Photographs of these two specimens are given in Fig. 3-49. Large shear lips are evident on the plane-sided specimen, with a large split obvious on the fracture surface of the side-grooved specimen. The latter is probably caused by the increased triaxiality and constraint resulting from the side-grooves.

3.4 Weld of A 516 Gr. 70 to A 516 Gr. 70

3.4.1 Material Description

This weld was made using the base metal described in Section 3.3. One observation of this weld was the presence of a large repaired region (Fig. 3-50). The presence of this repair posed some problems in finding "good" (i.e., unrepaired) metal for machining of specimens. In addition, testing of the repair weld metal was much desired but could not be completed within the available time schedule.

This weld is included in Ref. 4 as DP2-F34W.

3.4.2 Charpy-V Data

This weld was characterized using full-size C_v specimens, with the L-C and the L-R orientations tested. For the L-C orientation, the pipe ID, OD and the MID location were characterized; for the L-R orientation, the ID and OD locations were tested.

Results for the C_v tests are given in Table 3-19 and illustrated in Figs. 3-51 and 3-52, with results from TANH curve-fitting summarized in Table 3-20. The TANH curve-fitting has been accomplished by forcing a lower bound of 6.8 J (5 ft-lb). As with the base metal, the ID exhibits the highest upper shelf levels for each orientation. For all test temperatures below 288°C (550°F), the ID of the L-R orientation exhibits much higher energy levels than the OD of this orientation. In contrast, at 288°C (550°F) the OD exhibits much higher energy levels than the ID, with the energy levels for the OD at this temperature far exceeding anything expected for this orientation. Causes for this extremely high energy absorption are not known.

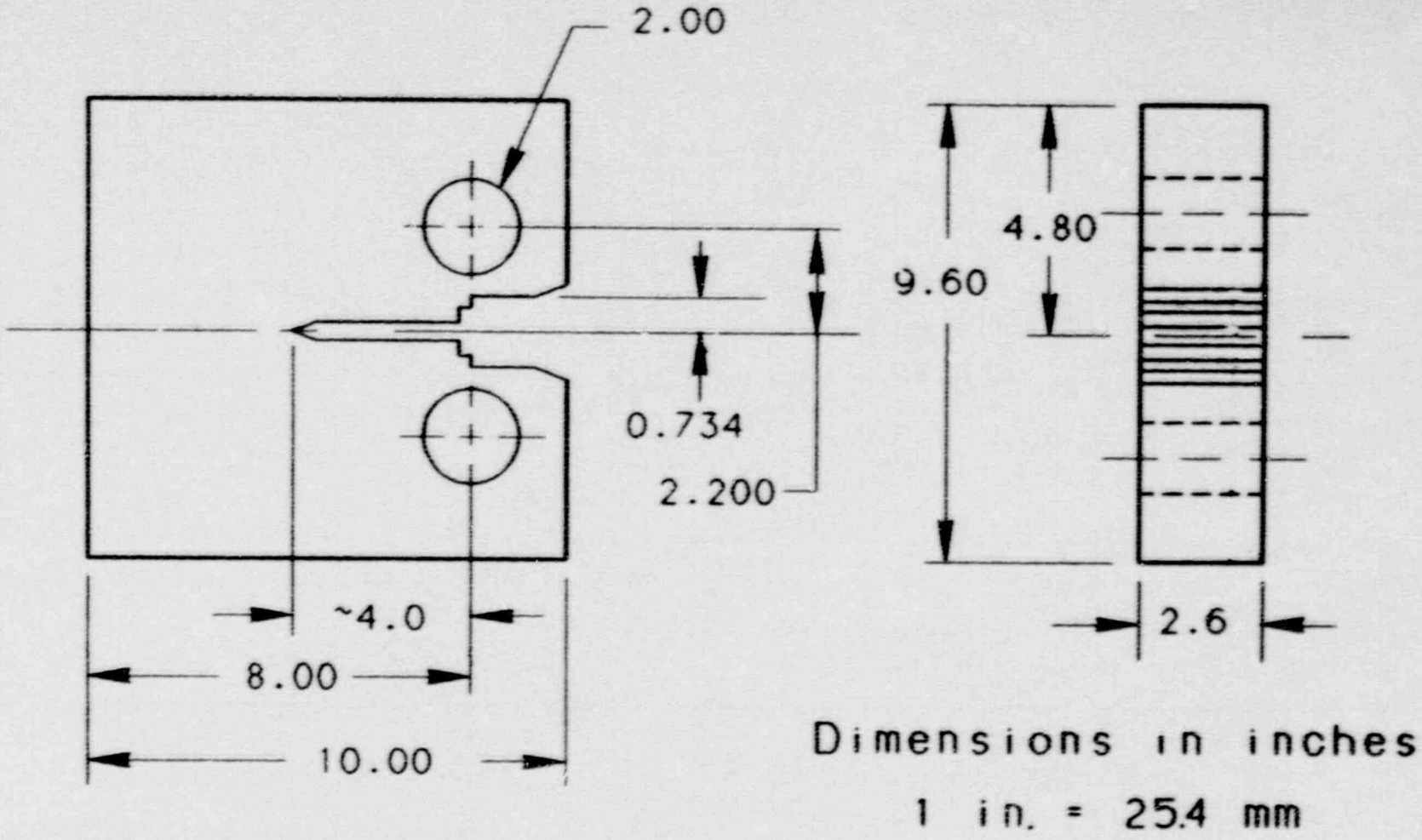

Fig. 3-46 Fracture toughness tests of A 516 Gr. 70 base metal used this 4T-CT specimen design with a thickness of 66 mm (2.6 in.).

Table 3-18 J-R Curve Results for A 516 Grade 70 Base Metal (L-C Orientation)

Specimen Number	Test Temperature (°C)	$(a/W)_o$	Δa_m (mm)	$\Delta a_p - \Delta a_m$ (mm)	J_{Ic} P.L. (kJ/m^2)	J_{Ic} Linear (kJ/m^2)	K_{Jc} P.L. ($MPa\sqrt{m}$)	K_{Jc} Linear ($MPa\sqrt{m}$)	T_{avg} P.L.	T_{avg} ASTM	Flow Strength (MPa)
B1 (20%)[a]	288	0.529	40.67	-1.80	190.4	191.6	199.8	200.4	228	228	362.2
B2 (0%)[a]	288	0.527	29.73	2.50	96.7	84.2	142.4	132.9	335	320	362.2

[a] Side-groove percentage.

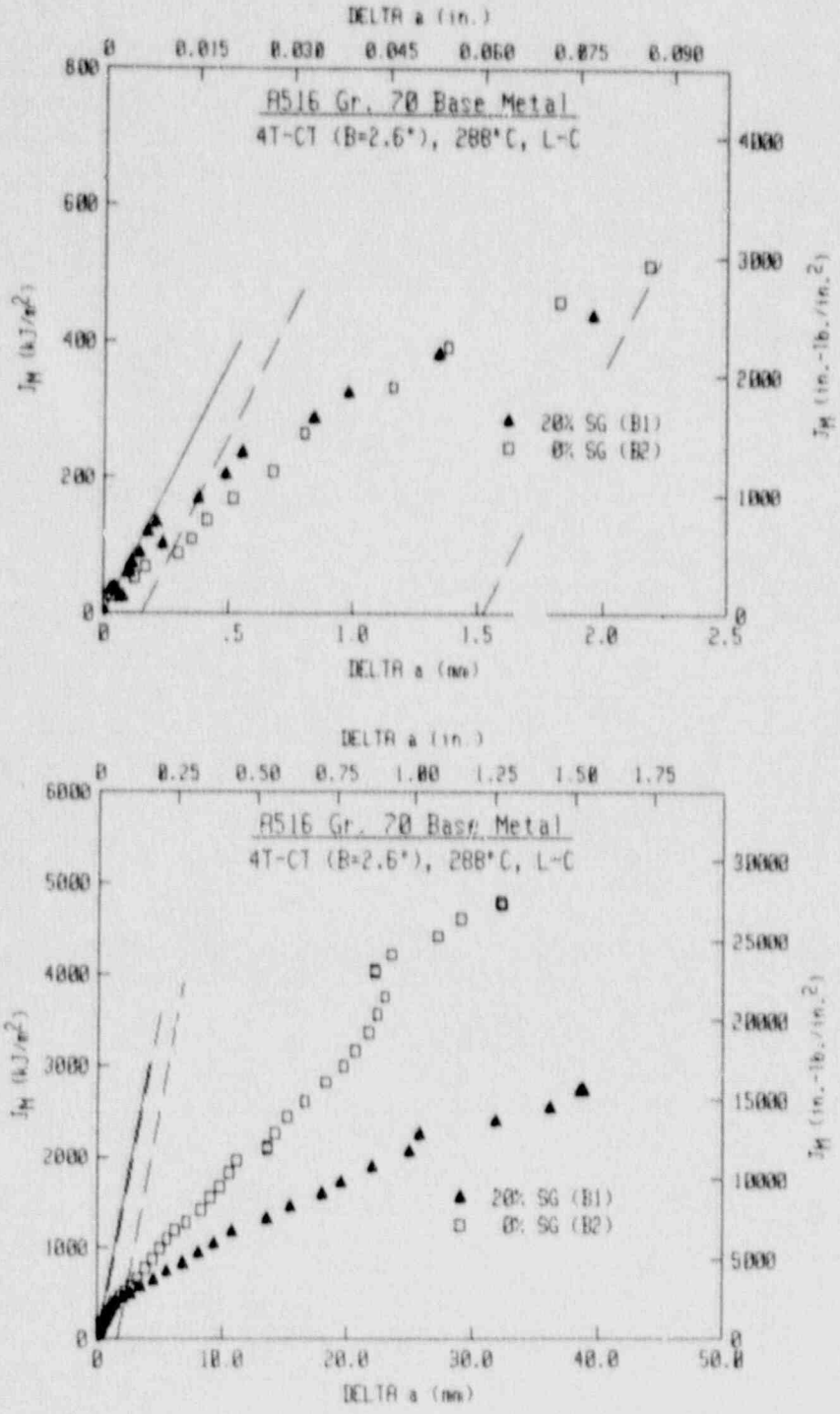

Fig. 3-47 J_M-R curves for the L-C orientation of A 516 Gr. 70 at 288 °C. Data from the sidegrooved specimen are somewhat lower than that from the plane-sided specimen.

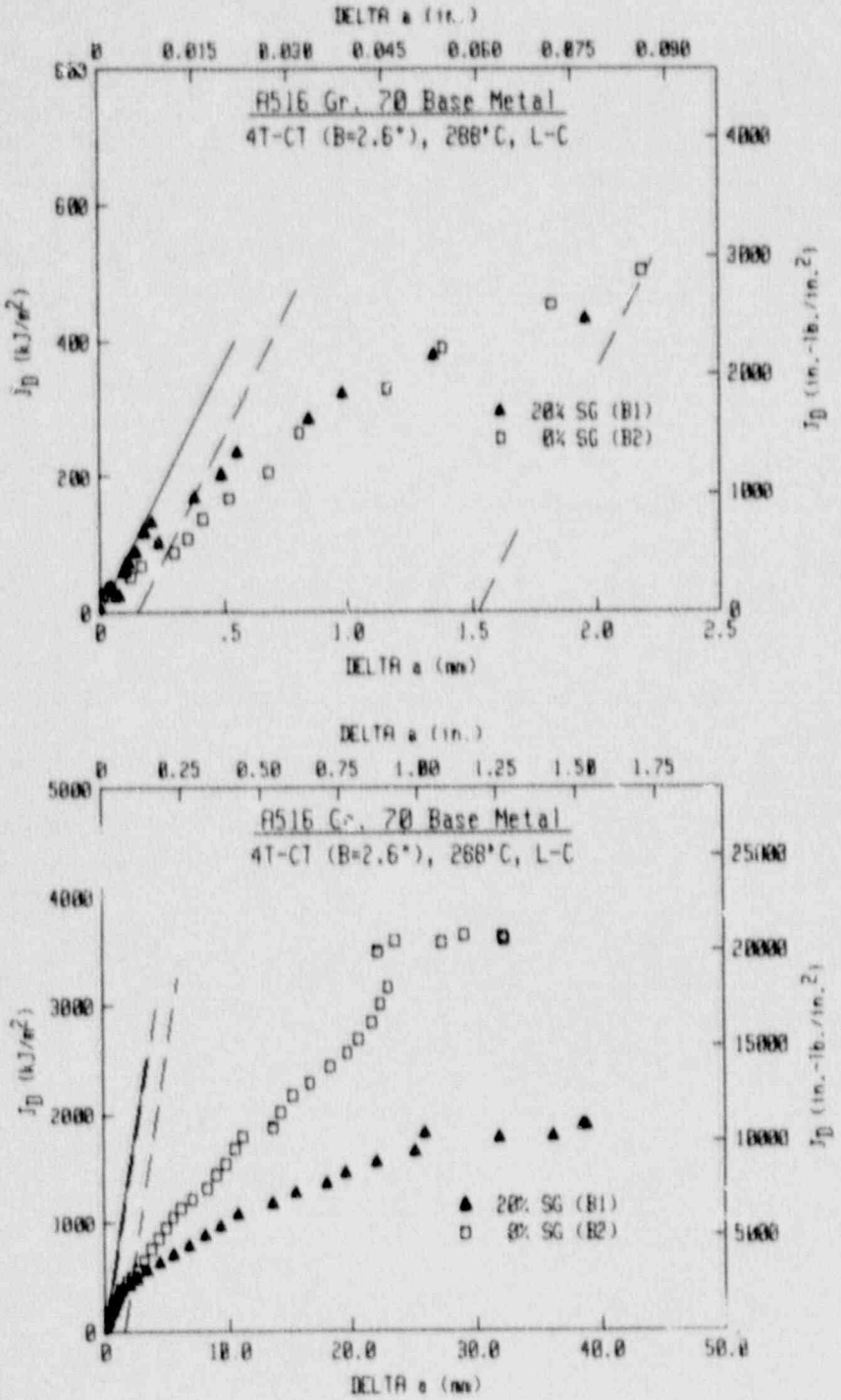

Fig. 3-48 J_D-R curves for the L-C orientation of A 516 Gr. 70 at 288°C. Data from the sidegrooved specimen are somewhat lower than that from the plane-sided specimen.

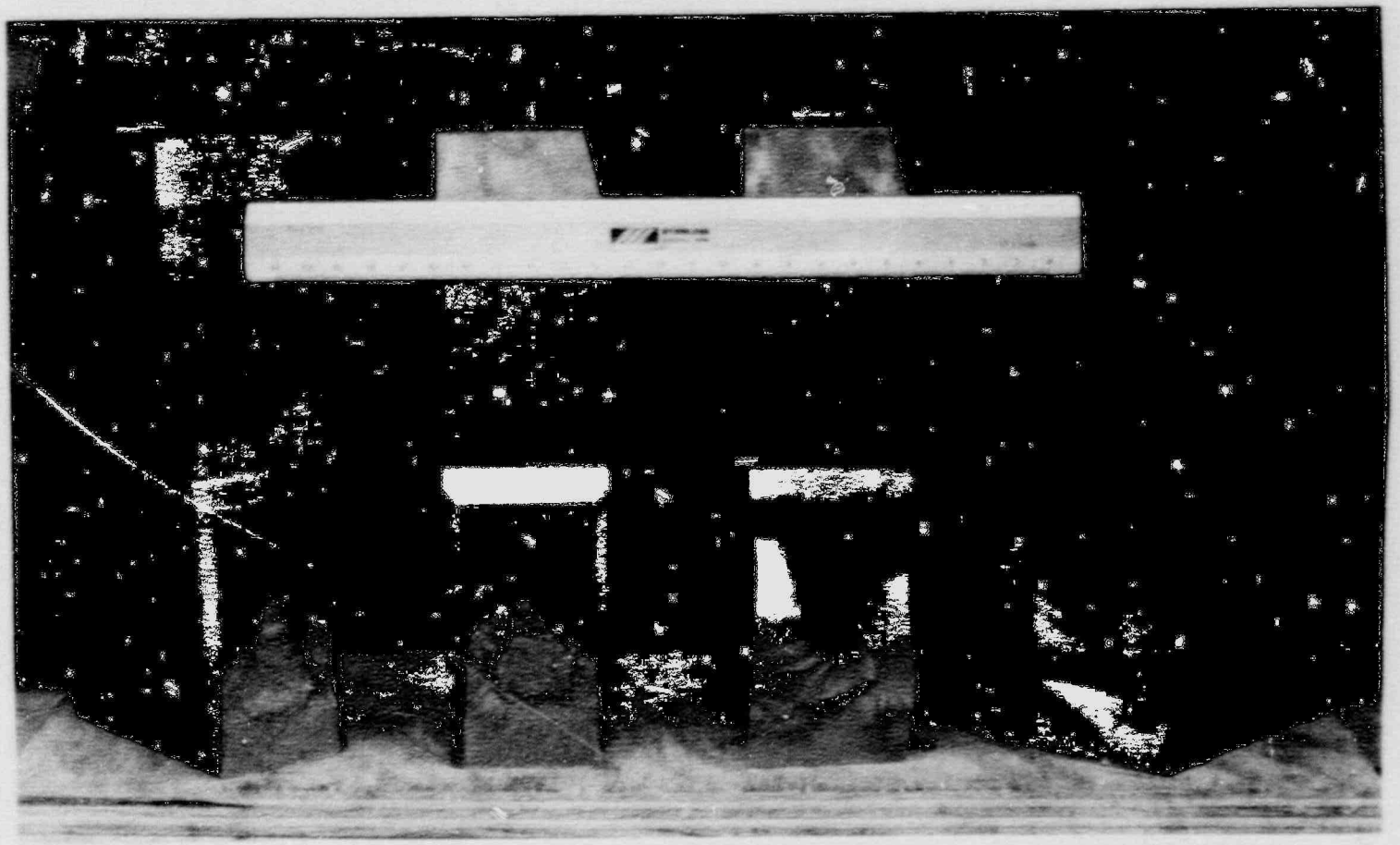

Fig. 3-49 Fracture surfaces from the A 516 Gr. 70 base metal tests.

Fig. 3-50 Portions of the A 516 Gr. 70 weld exhibited weld repairs similar to that illustrated here.

Table 3-18 Charpy-V Data for A 516 Grade 70 Weld Metal

Specimen Number	Test Temp.		Absorbed Energy		Lateral Expansion		Shear Percent
	(°C)	(°F)	(J)	(ft-lb)	(mm)	(in.)	(%)
			L-C Orientation (O.D.)				
CW-17C	-90	-130	8.1	6	0.23	0.009	10
CW-15C	-62	-80	16.3	12	0.18	0.007	21
CW-16C	-62	-80	13.6	10	0.23	0.009	34
CW-13C	-40	-40	32.5	24	0.53	0.021	30
CW-14C	-40	-40	21.7	16	0.43	0.017	30
CW-11C	-18	0	69.1	51	0.71	0.028	40
CW-12C	-18	0	84.1	62	1.47	0.058	61
CW-18C	4	40	61.0	45	0.84	0.033	72
CW-1C	22	71	103.0	76	1.65	0.065	88
CW-2C	22	71	108.5	80	1.70	0.067	94
CW-3C	93	200	126.1	93	2.01	0.079	99
CW-4C	93	200	120.7	89	1.96	0.077	99
CW-5C	149	300	138.3	102	2.21	0.087	100
CW-6C	149	300	130.2	96	2.01	0.079	100
CW-7C	218	425	168.1	124	2.26	0.089	100
CW-8C	218	425	165.4	122	2.03	0.080	100
CW-9C	288	550	172.2	127	1.85	0.073	100
CW-10C	288	550	160.0	118	1.85	0.073	100
			L-C Orientation (MID)				
CW-36C	-90	-130	5.4	4	0.13	0.005	10
CW-34C	-62	-80	19.0	14	0.25	0.010	30
CW-35C	-62	-80	13.6	10	0.18	0.007	30
CW-32C	-40	-40	43.8	36	0.84	0.033	59
CW-33C	-40	-40	32.5	24	0.61	0.024	47
CW-30C	-18	0	65.1	48	1.07	0.042	66
CW-31C	-18	0	56.9	42	1.09	0.043	63
CW-37C	4	40	84.1	62	1.35	0.053	85
CW-20C	22	71	113.9	84	1.75	0.069	97
CW-21C	22	71	119.3	88	1.80	0.071	98
CW-22C	93	200	120.7	89	1.93	0.076	100
CW-23C	93	200	119.3	88	1.98	0.078	99
CW-24C	149	300	130.2	96	1.91	0.075	100
CW-25C	149	300	143.7	106	2.08	0.082	100
CW-26C	218	425	165.4	122	1.91	0.075	100
CW-27C	218	425	169.5	125	1.78	0.070	100
CW-28C	288	550	162.7	120	1.70	0.067	100
CW-29C	288	550	164.1	121	1.73	0.068	100
			L-C Orientation (I.D.)				
CW-56C	-90	-130	8.1	6	0.23	0.009	0
CW-54C	-62	-80	28.5	21	0.71	0.028	30
CW-55C	-62	-80	42.0	31	0.66	0.026	26
CW-52C	-40	-40	75.9	56	1.17	0.046	56
CW-53C	-40	-40	89.5	66	1.57	0.062	56
CW-50C	-18	0	128.8	95	1.93	0.076	80
CW-51C	-18	0	143.7	106	2.03	0.080	87
CW-57C	4	40	130.2	96	1.88	0.074	81
CW-40C	22	71	130.2	96	1.98	0.078	98
CW-41C	22	71	149.1	110	2.11	0.083	95
CW-42C	93	200	203.4	150	2.26	0.089	100
CW-43C	93	200	207.4	153	2.13	0.084	100
CW-44C	149	300	195.2	144	2.26	0.089	100
CW-45C	149	300	189.8	140	2.08	0.082	100
CW-46C	218	425	227.8	168	1.75	0.069	100
CW-47C	218	425	244.0	180	1.63	0.064	100
CW-48C	288	550	290.1	214	1.65	0.065	100
CW-49C	288	550	298.3	220	1.73	0.068	100

Table 3-19 Charpy-V Data for A 516 Grade 70 Weld Metal (cont.)

Specimen Number	Test Temp.		Absorbed Energy		Lateral Expansion		Shear Percent
	(°C)	(°F)	(J)	(ft-lb)	(mm)	(in.)	(%)
L-R Orientation (O.D.)							
CW-15R	-62	-80	5.4	4	0.03	0.001	0
CW-16R	-62	-80	6.8	5	0.05	0.002	0
CW-13R	-40	-40	14.9	11	0.25	0.010	21
CW-14R	-40	-40	10.8	8	0.23	0.009	21
CW-11R	-18	0	70.5	52	1.30	0.051	45
CW-12R	-18	0	78.6	58	1.57	0.062	44
CW-17R	4	40	94.9	70	1.57	0.062	40
CW-18R	4	40	88.1	65	1.47	0.058	50
CW-1R	22	71	111.2	82	1.73	0.068	79
CW-2R	22	71	104.4	77	1.47	0.058	88
CW-3R	93	200	118.0	87	1.83	0.072	99
CW-4R	93	200	119.3	88	1.80	0.071	100
CW-5R	149	300	127.4	94	1.88	0.074	100
CW-6R	149	300	119.3	88	1.85	0.073	100
CW-7R	218	425	151.9	112	1.80	0.071	100
CW-8R	218	425	160.0	118	1.91	0.075	100
CW-9R	288	550	328.1	242	1.45	0.057	100
CW-10R	288	550	328.1	242	[a]	[a]	100
L-R Orientation (I.D.)							
CW-36R	-90	-130	4.1	3	0.08	0.003	0
CW-34R	-62	-80	24.4	18	0.41	0.016	21
CW-35R	-62	-80	10.8	8	0.15	0.006	11
CW-32R	-40	-40	134.2	99	1.98	0.078	55
CW-33R	-40	-40	126.1	93	1.96	0.077	50
CW-30R	-18	0	146.4	108	2.08	0.082	69
CW-31R	-18	0	162.7	120	2.11	0.083	72
CW-37R	4	40	203.4	150	2.36	0.093	100
CW-20R	22	71	139.6	103	2.24	0.088	90
CW-21R	22	71	153.2	113	2.13	0.084	95
CW-22R	93	200	202.0	149	2.03	0.080	100
CW-23R	93	200	235.9	174	2.39	0.094	99
CW-24R	149	300	225.1	166	2.18	0.086	100
CW-25R	149	300	214.2	158	2.31	0.091	100
CW-26R	218	425	260.3	192	1.65	0.065	100
CW-27R	218	425	225.1	166	1.65	0.065	100
CW-28R	288	550	218.3	161	1.60	0.063	100
CW-29R	288	550	284.7	210	1.65	0.065	100

[a] Specimen did not fully fracture.

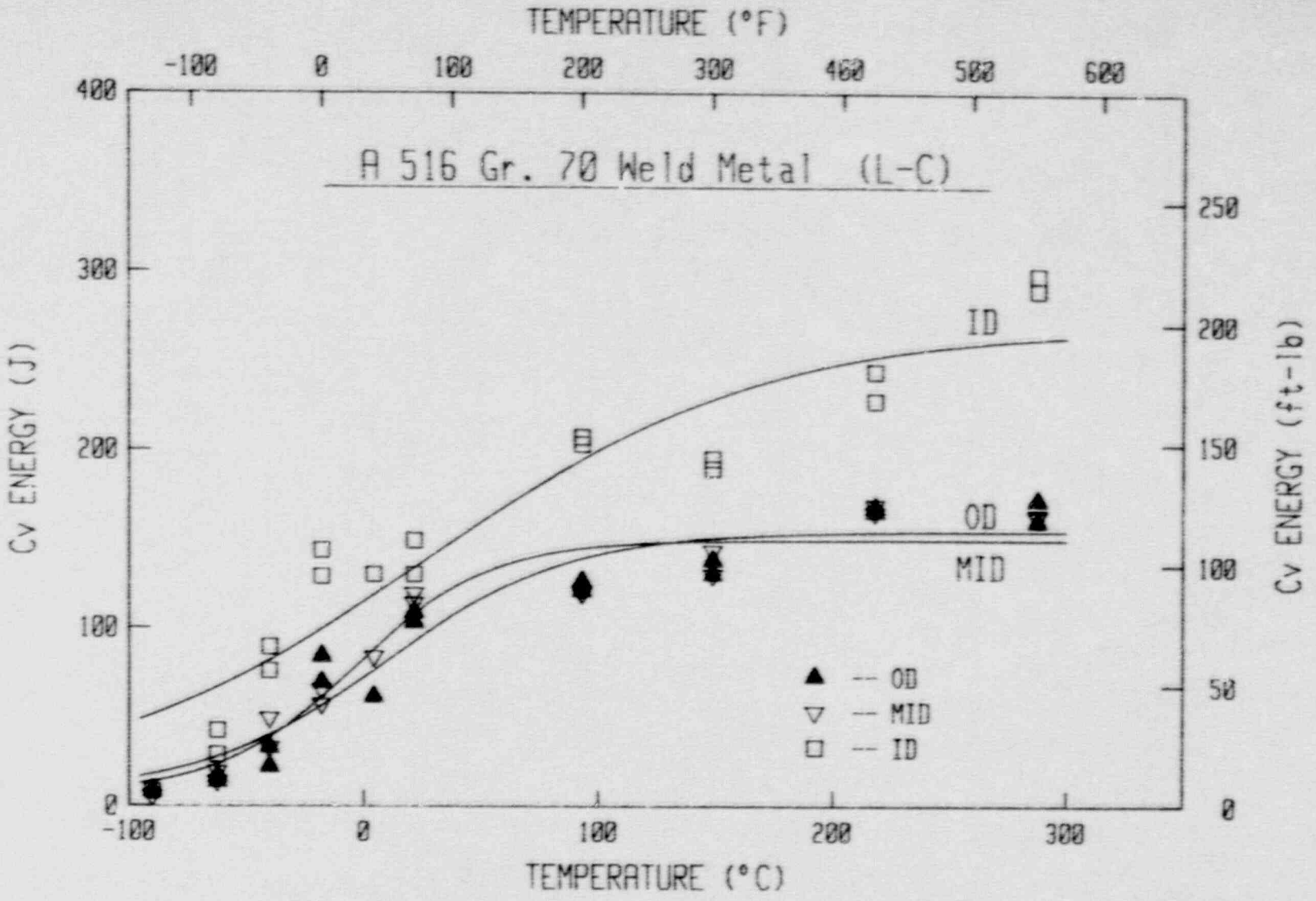

Fig. 3-51 Charpy-V data for the L-C orientation of the A 516 Gr. 70 weld metal.

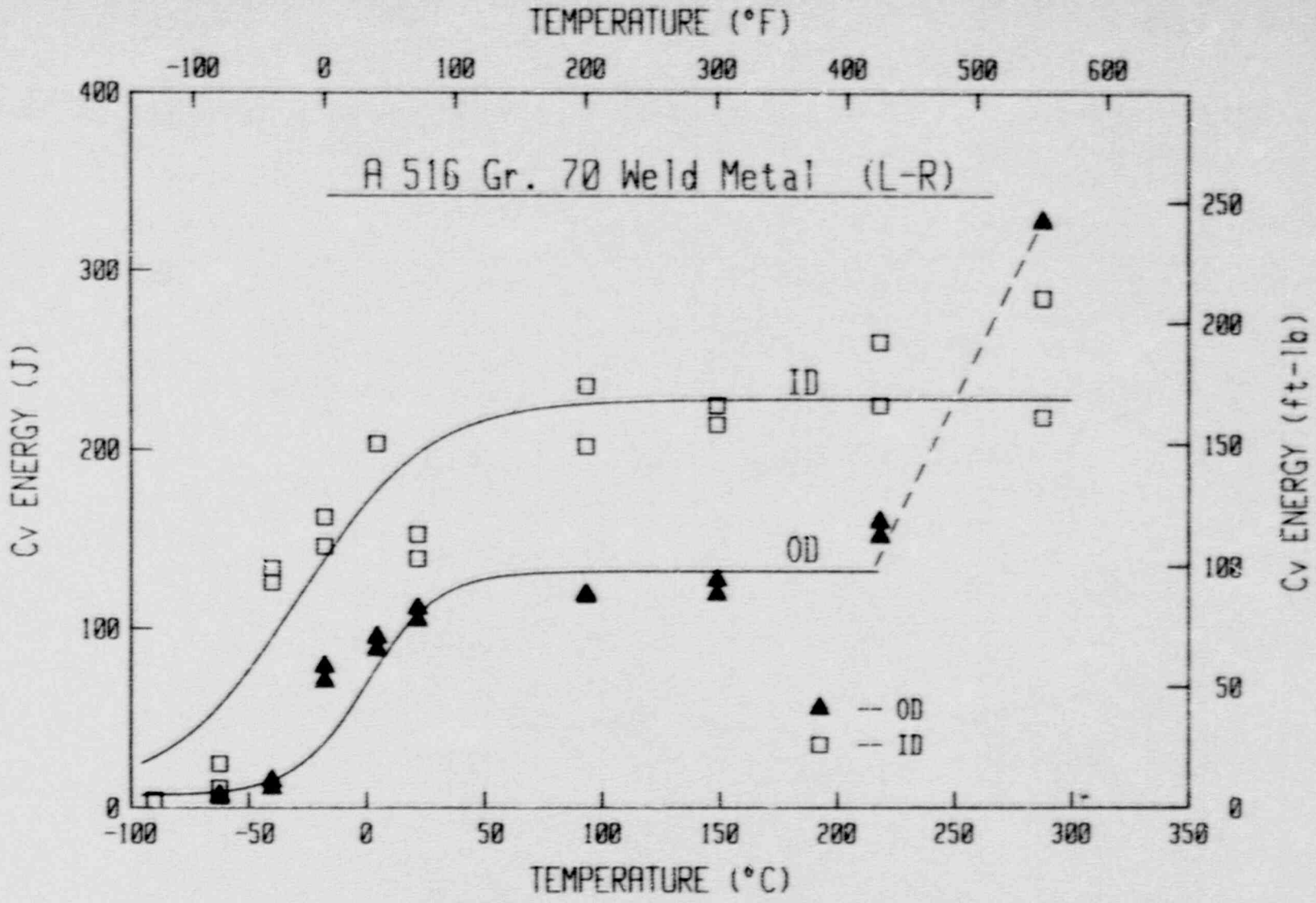

Fig. 3-52 Charpy-V data for the L-R orientation of the A 516 Gr. 70 weld metal.

Table 3-20 Curve-fit Results for Charpy Data from A 516 Gr. 70 Weld Metal

Thickness Location	Upper Shelf		$C_V = A + B \tanh (T-T_o)/C$							
			A		B		C		T_o	
	(J)	(ft-lb)	(J)	(ft-lb)	(J)	(ft-lb)	(°C)	(°F)	(°C)	(°F)
L-C Orientation										
OD	154.7	114.1	80.76	59.56	73.98	54.56	78.41	141.14	9.18	48.53
MID	149.8	110.5	78.27	57.73	71.49	52.73	57.82	104.08	-3.52	25.67
ID	269.8	199.0	138.27	101.99	131.50	96.99	145.26	261.47	26.43	79.57
L-R Orientation										
OD	132.7	97.9	69.75	51.44	62.97	46.44	30.50	54.89	0.11	32.20
ID	228.6	168.6	117.68	86.79	110.90	81.79	54.99	98.99	-28.67	-19.60

3.4.3 Tensile Data

Tensile tests of this heat were made using threaded-end specimens with an overall size similar to that used for the base metal tests (see Section 3.3.3), although for the weld the gage diameter was reduced within the weld to force fracture to occur within the weld metal. As illustrated in Fig. 3-53, the overall specimen diameter of 12.83 mm (0.505 in.) was reduced to 9.07 mm (0.357 in.) for a length of 9.65 mm (0.38 in.), with a total length of 12.7 mm (0.5 in.) for the reduced section. The gage length used for total elongation evaluation was ~ 8.4 mm (0.33 in.), totally within the weld metal. However, the gage length used for measurement of specimen displacement and calculation of strain was 14.7 mm (0.58 in.). The latter encompasses the weld metal and some portion of the base metal, with the reduced diameter, the larger overall diameter and the fillet transition between the two diameters also enclosed by the displacement measurements. To approximate strain from these measurements of displacement, an elastic analysis (i.e., PL/AE) was used to sum the displacement contributions from the various sections and extract that which occurs for the section with a diameter of 9.07 mm (0.357 in.). With the gage length of 14.7 mm (0.58 in.) used for displacement measurement, a correction factor of 0.97 can be applied to the measured displacements to obtain an approximation to the displacement over the gage length of 9.65 mm (0.38 in.). This correction factor applies only up to the yield strength. After yield strength, an assumption is made that all additional strain (primarily plastic strain) occurs within the gage length of 9.65 mm (0.38 in.).

The strength data are given in Table 3-21 and illustrated in Fig. 3-54. In comparison to the strength for the base metal (from Section 3.3.3), the weld exhibits much higher yield and ultimate strength levels. The yield strength levels for the weld are about twice those of the base metal, and the ultimate strengths are about 173 MPa (25 ksi) higher than those for the base metal.

3.4.4 Fracture Toughness Data

As with the base metal, J-R curves for this weld were evaluated for the L-C orientation at 288°C (550°F) using 4T-CT plan-form specimens with a thickness of 66 mm (2.6 in.). Two specimens of this geometry were used, with one specimen side-grooved by 20% and the other specimen tested in a plane-sided condition. Results from these tests are summarized Table 3-22 and illustrated in Figs. 3-55 and 3-56 for J_M and J_D, respectively. As for the base metal, the two specimens yield similar J levels at low Δa levels, with data for the plane-sided specimen exhibiting much higher J levels at large Δa levels.

As with the base metal, the plane-sided specimen exhibits large shear lips (Fig. 3-57), with minimal crack growth obvious on the surface of the specimen. In addition, the crack growth in the middle of this specimen starts off planar but then begins to progress outside of the expected crack growth plane. In this case the side-grooved specimen exhibits a relatively small split, with the crack growth appearing to grow outside of the anticipated plane and probably deviating into the HAZ or the base metal.

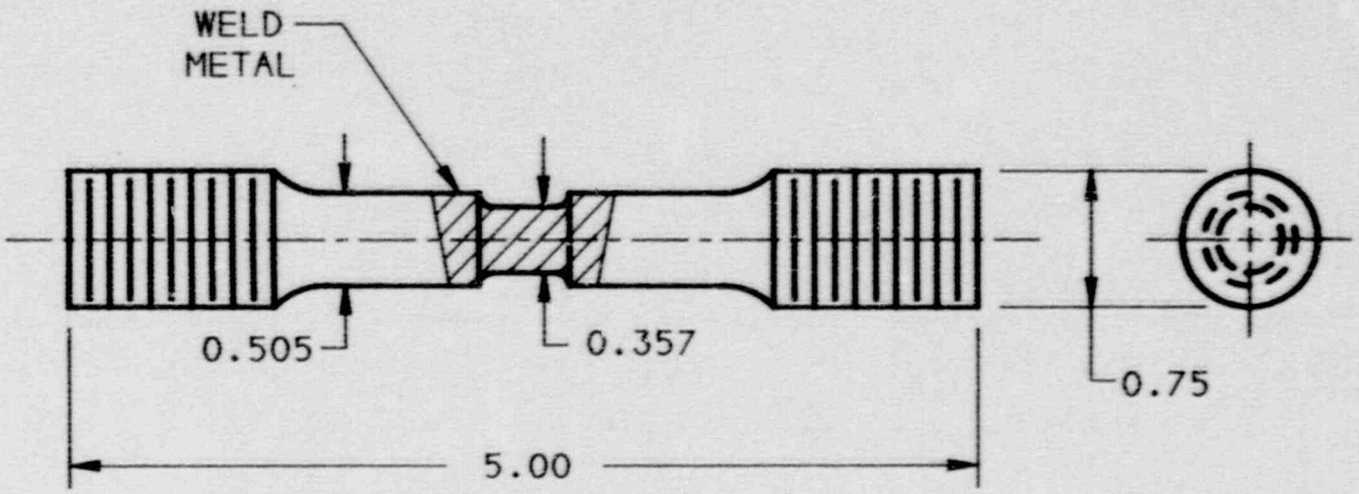

Fig. 3-53 Illustration of the tensile specimen used for testing of the A 516 Gr. 70 weld.

Table 3-21 Tensile Data for A 516 Grade 70 Weld Metal

Specimen Number	Orient.	Thickness Location	Test Temp.		0.2% Offset Yield Strength		Ultimate Strength		Elongation	Reduction In Area
			(°C)	(°F)	(MPa)	(ksi)	(MPa)	(ksi)	(%)	(%)
CW-O3	L	OD	24	75	554.5	80.4	674.2	97.8	59.6	63.4
CW-M3	L	MID	24	75	578.7	83.9	695.5	100.9	54.1	64.7
CW-I3	L	ID	24	75	620.5	90.0	697.8	101.2	52.8	66.4
CW-O1	L	OD	149	300	527.1	76.5	642.5	93.2	53.4	62.4
CW-M1	L	MID	149	300	545.4	79.1	651.8	94.5	49.4	63.1
CW-I1	L	ID	149	300	460.9	66.9	569.6	82.6	58.5	68.3
CW-O4	L	OD	204	400	500.3	72.6	628.0	91.1	53.6	61.1
CW-M4	L	MID	204	400	518.3	75.2	643.1	93.3	52.9	61.6
CW-I4	L	ID	204	400	550.6	79.9	657.4	95.4	55.6	61.7
CW-O2	L	OD	288	550	515.9	74.8	658.5	95.5	45.9	59.2
CW-M2	L	MID	288	550	506.4	73.5	670.5	97.3	53.4	58.9
CW-I2	L	ID	288	550	514.3	74.6	675.5	98.0	45.5	54.0
CW-O5	L	OD	288	550	496.2	72.0	654.2	94.9	50.3	57.7
CW-M5	L	MID	288	550	530.3	76.9	663.8	96.3	54.8	59.2
CW-I5	L	ID	288	550	543.3	78.8	673.9	97.7	47.0	53.6

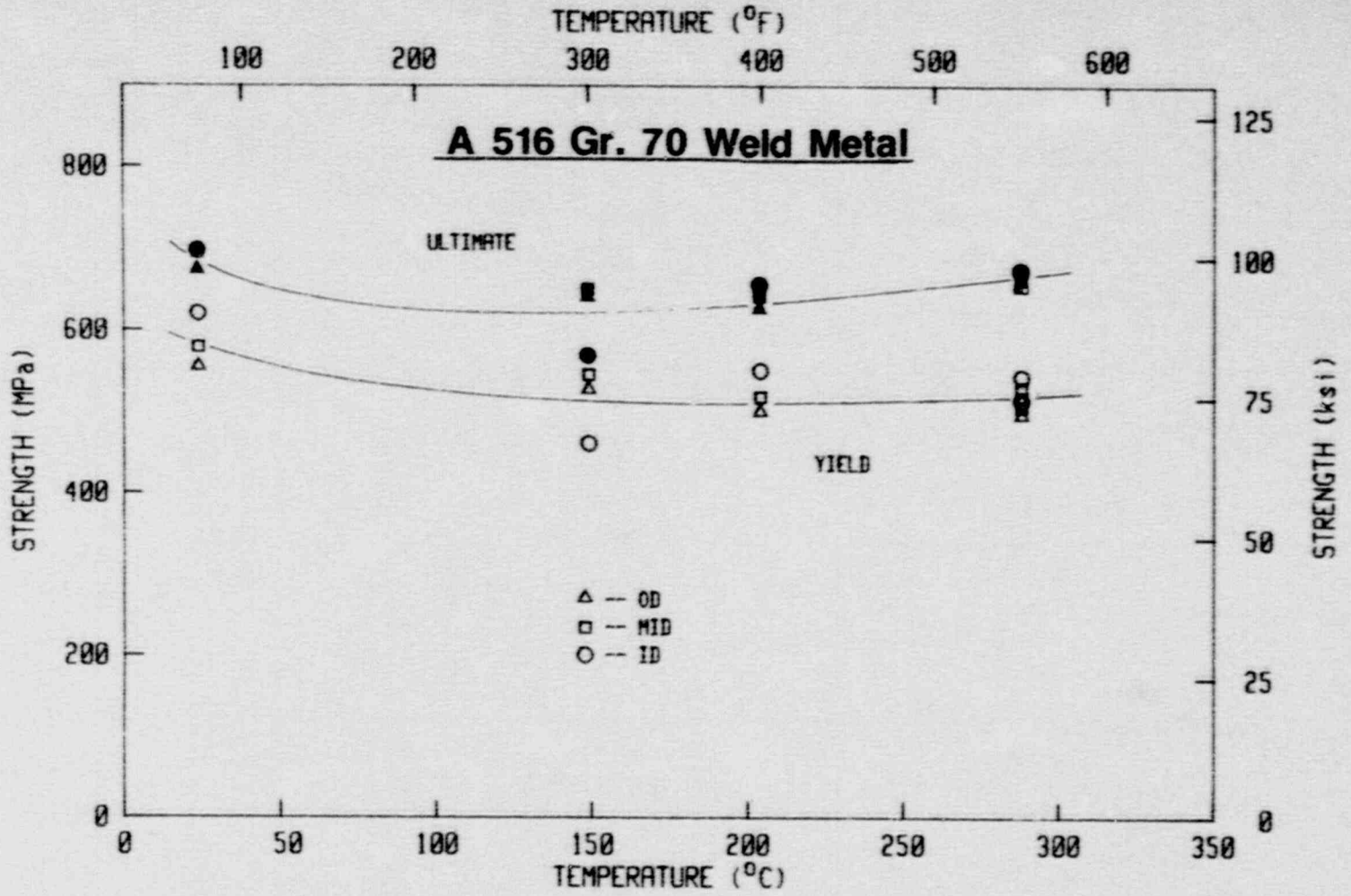

Fig. 3-54 Tensile data for the A 516 Gr. 70 weld metal.

Table 3-22 J-R Curve Results for A 516 Grade 70 Weld Metal (L-C Orientation)

Specimen Number	Test Temperature (°C)	$(a/W)_o$	Δa_m (mm)	$\Delta a_p - \Delta a_m$ (mm)	J_{Ic}		K_{Jc}		T_{avg}		Flow Strength (MPa)
					P.L. (kJ/m^2)	Linear (kJ/m^2)	P.L. ($MPa\sqrt{m}$)	Linear ($MPa\sqrt{m}$)	P.L.	ASTM	
W1 (20%)[a]	288	0.519	51.05	-3.46	268.0	234.6	237.1	221.8	120	139	591.9
W2 (0%)[a]	288	0.515	17.50	5.15	388.4	379.6	285.4	282.1	83	86	591.9

[a] Side-groove percentage.

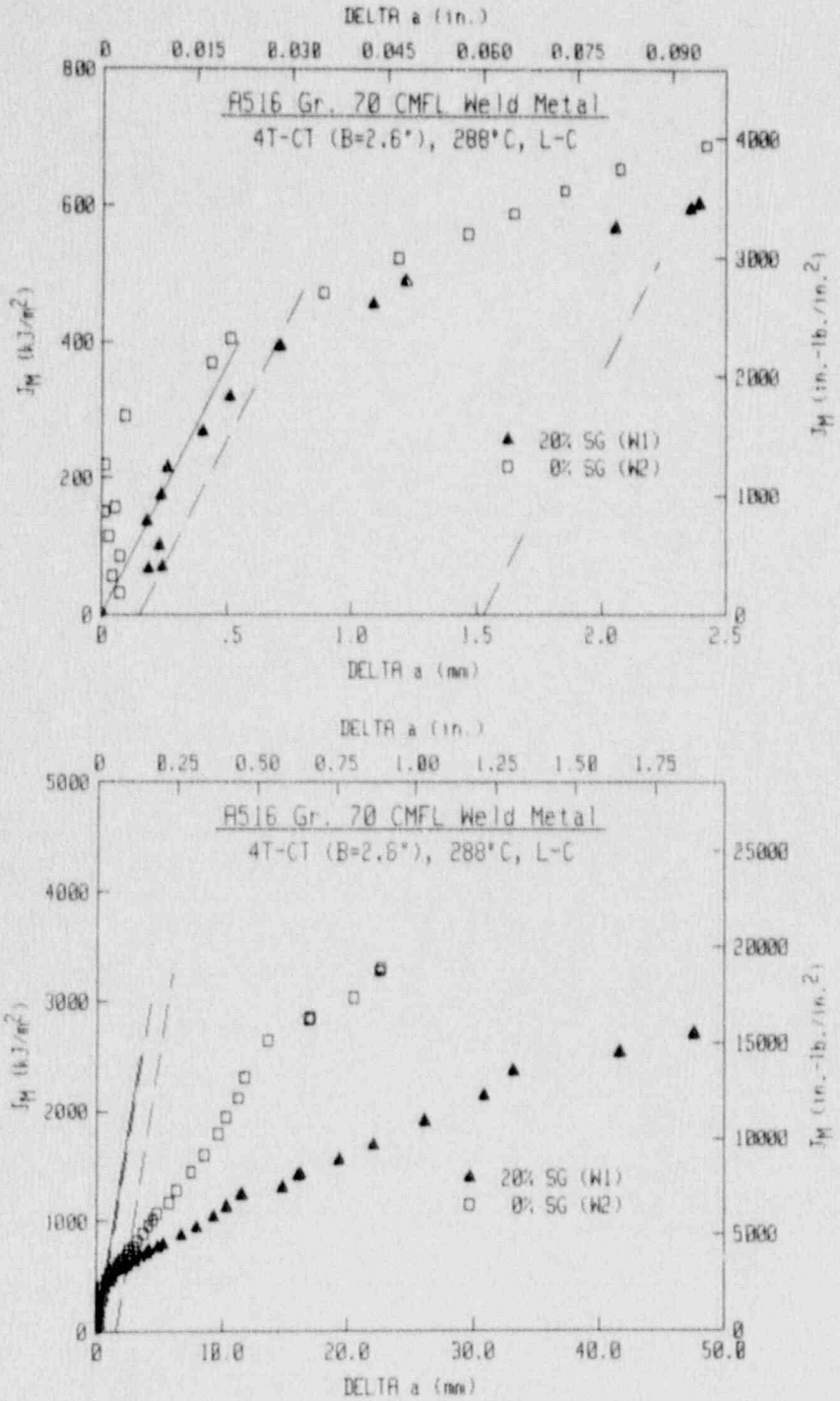

Fig. 3-55 J_M-R curves for the L-C orientation of A 516 Gr. 70 weld metal at 288 °C. Data from the sidegrooved specimen are somewhat lower than that from the plane-sided specimen.

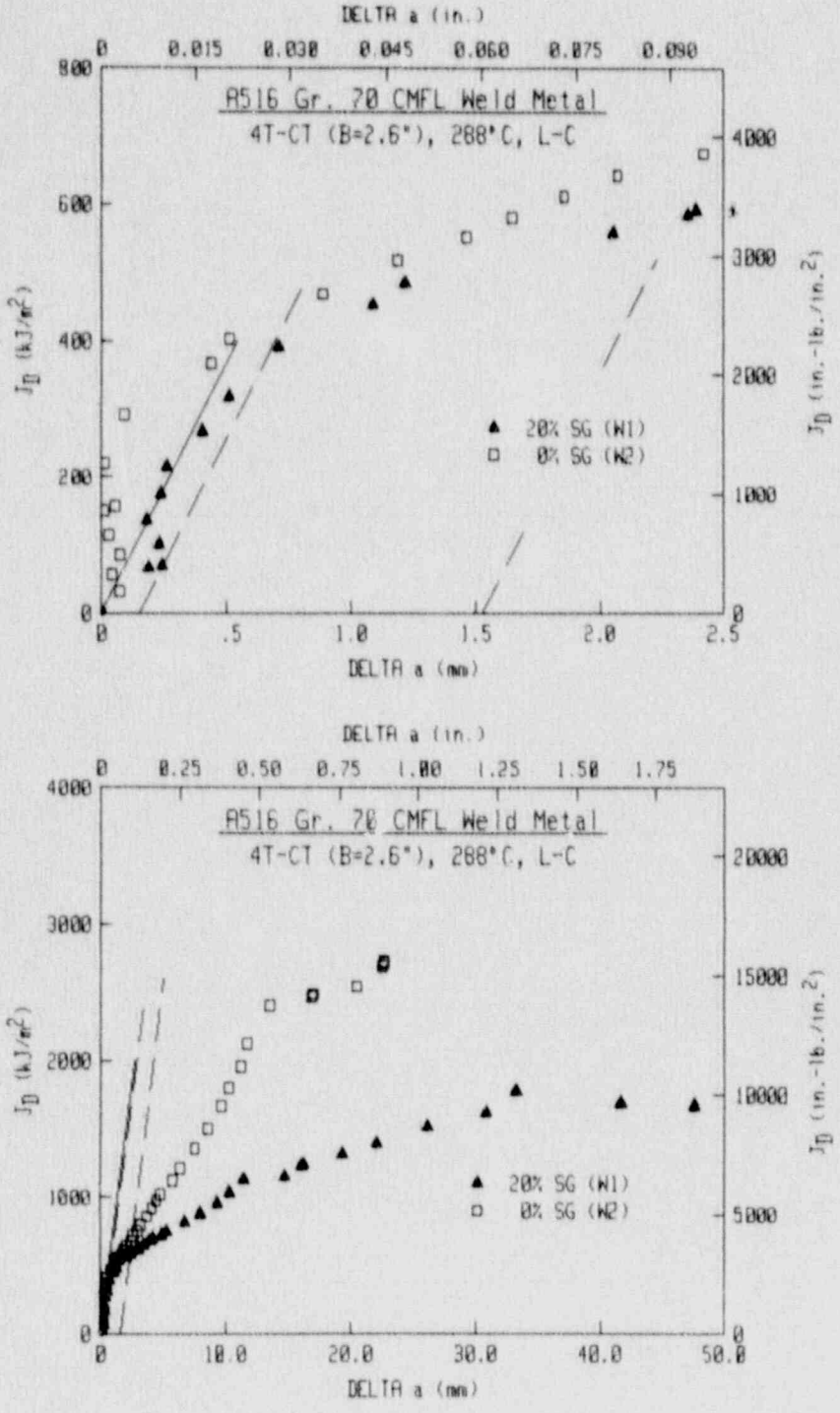

Fig. 3-56 J_D-R curves for the L-C orientation of A 516 Gr. 70 weld metal at 288 °C. Data from the sidegrooved specimen are somewhat lower than that from the plane-sided specimen.

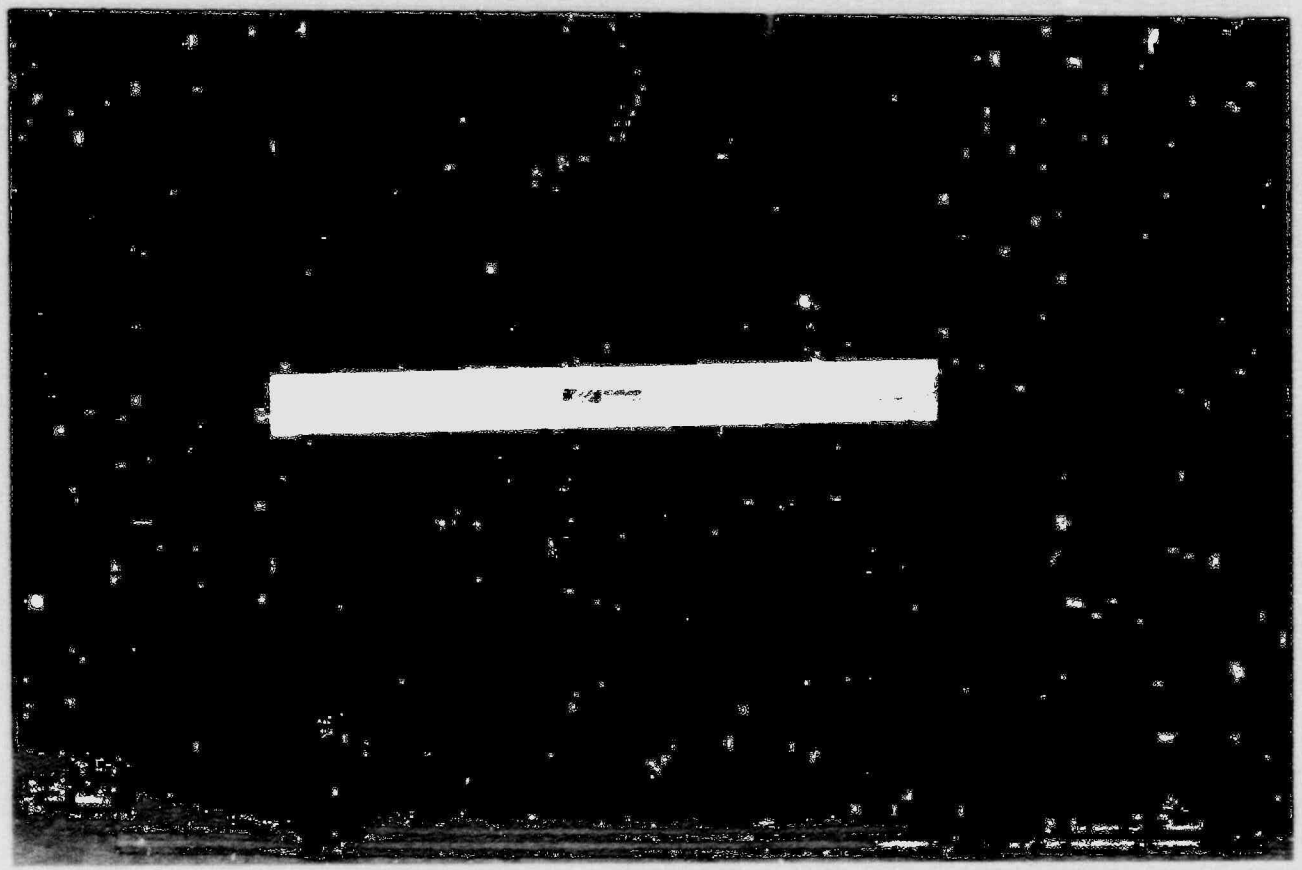

Fig. 3-57 Fracture surfaces from the A 516 Gr. 70 weld metal tests.

Comparisons of the J-R curves for the base metal and the weld metal indicate similar J levels at large crack growth intervals, but much higher J levels at small crack growth intervals for the weld metal (Figs. 3-58 to 3-61). Comparison of the profiles of these specimens indicates substantial differences (Fig. 3-62). Specifically, the side-grooved weld specimen exhibits considerable crack growth outside of the intended crack plane. In contrast, the side-grooved base metal specimen only exhibits out-of-plane growth due to the split in the fracture surface. The shear lips on the plane-sided base metal specimen have almost grown back upon themselves, in contrast to the minimal crack growth evident for the plane-sided weld metal specimen.

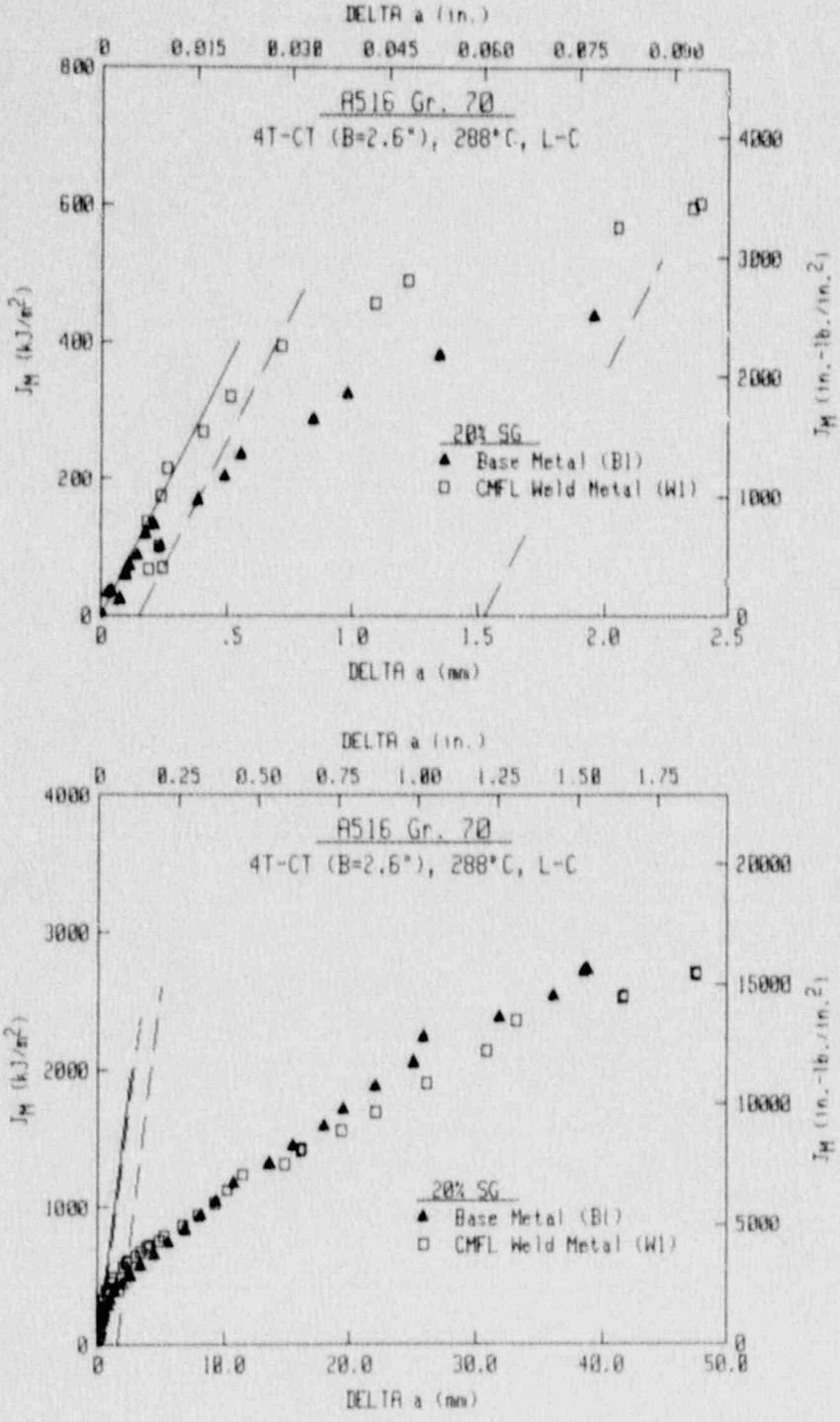

Fig. 3-58 Comparison of J_M-R curves from A 516 Gr. 70 base and weld metals at 288 °C, using side-grooved specimens.

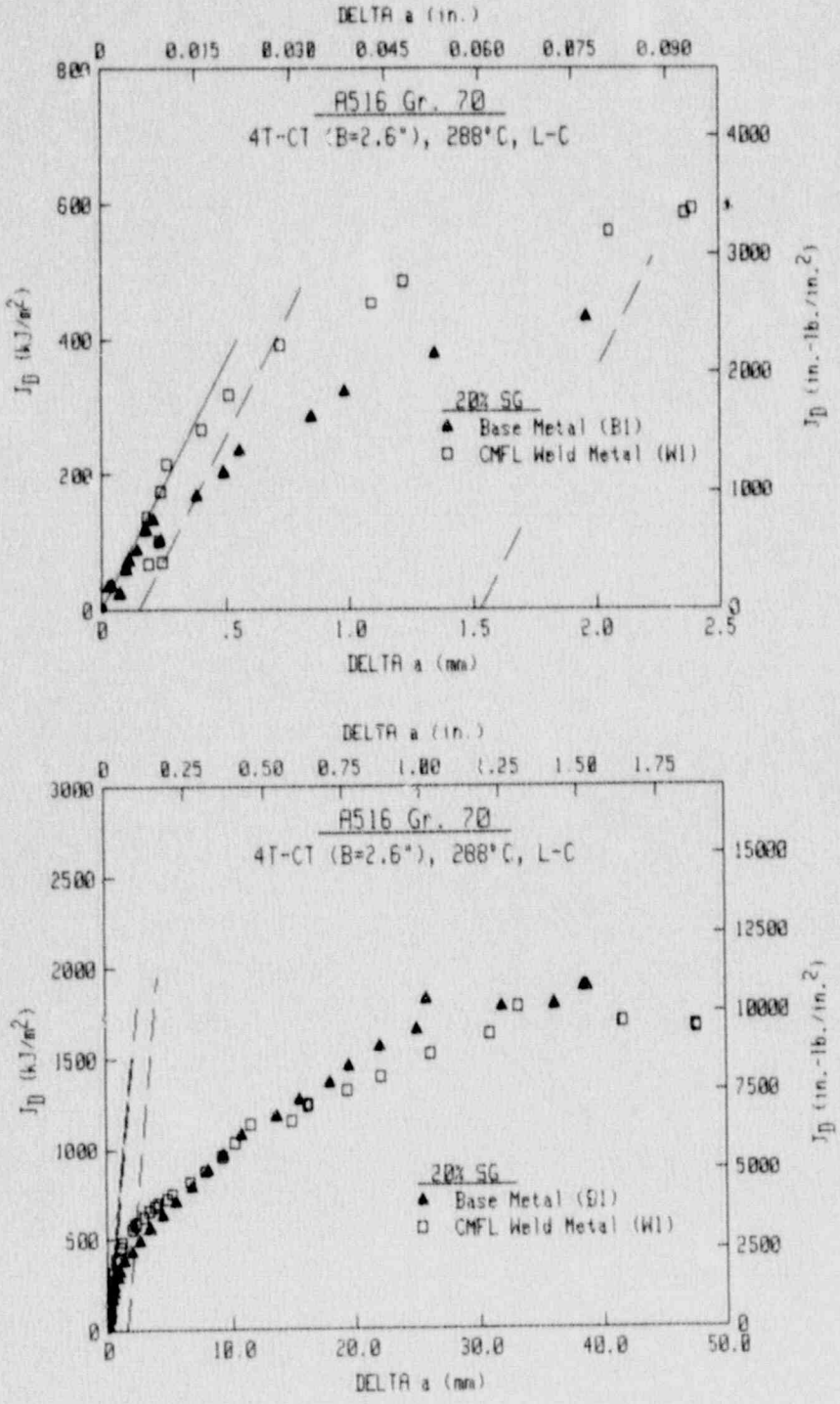

Fig. 3-59 Comparison of J_D-R curves from A 516 Gr. 70 base and weld metals at 288 °C, using side-grooved specimens.

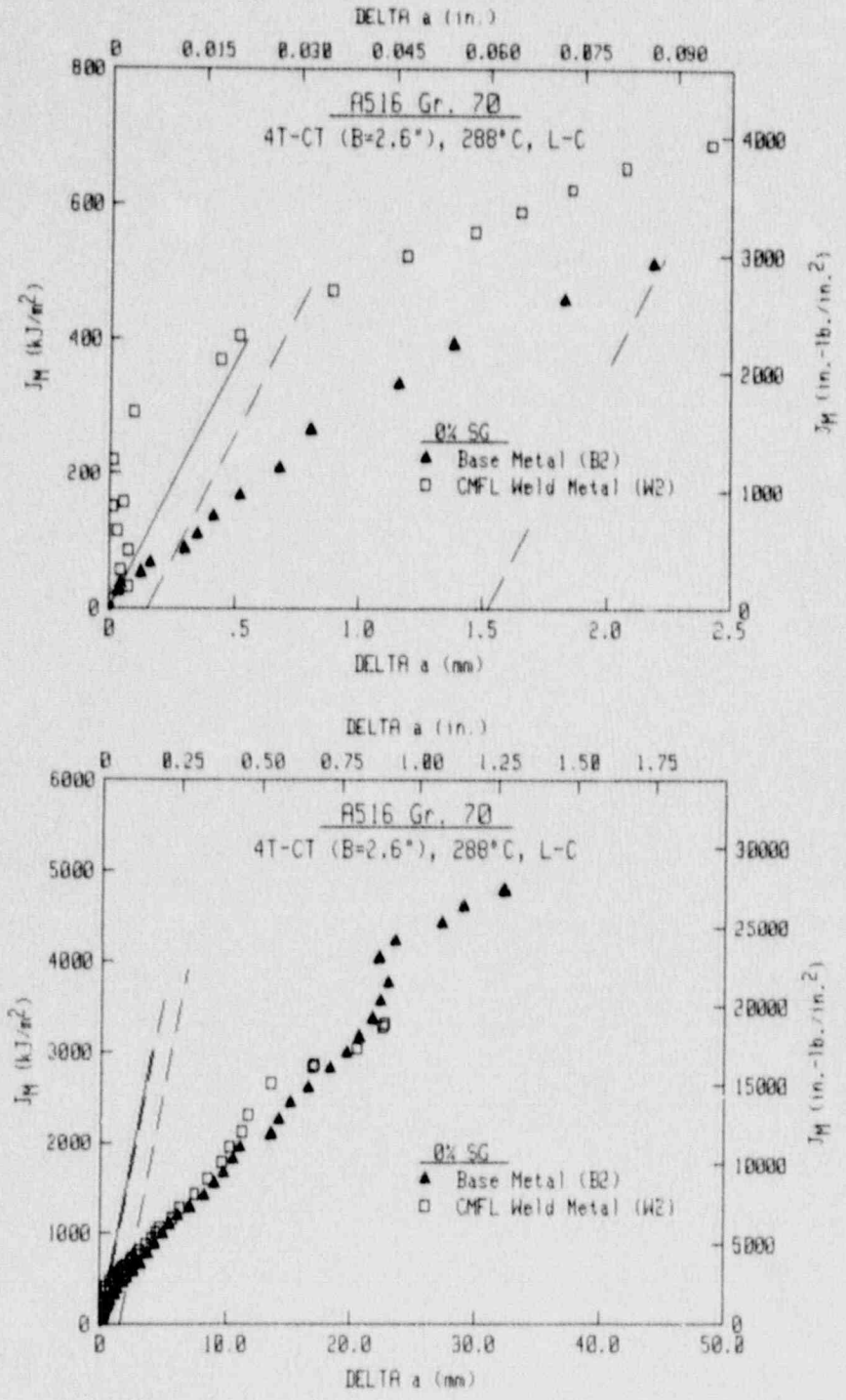

Fig. 3-60 Comparison of J_M-R curves from A 516 Gr. 70 base and weld metals at 288°C, using plane-sided specimens.

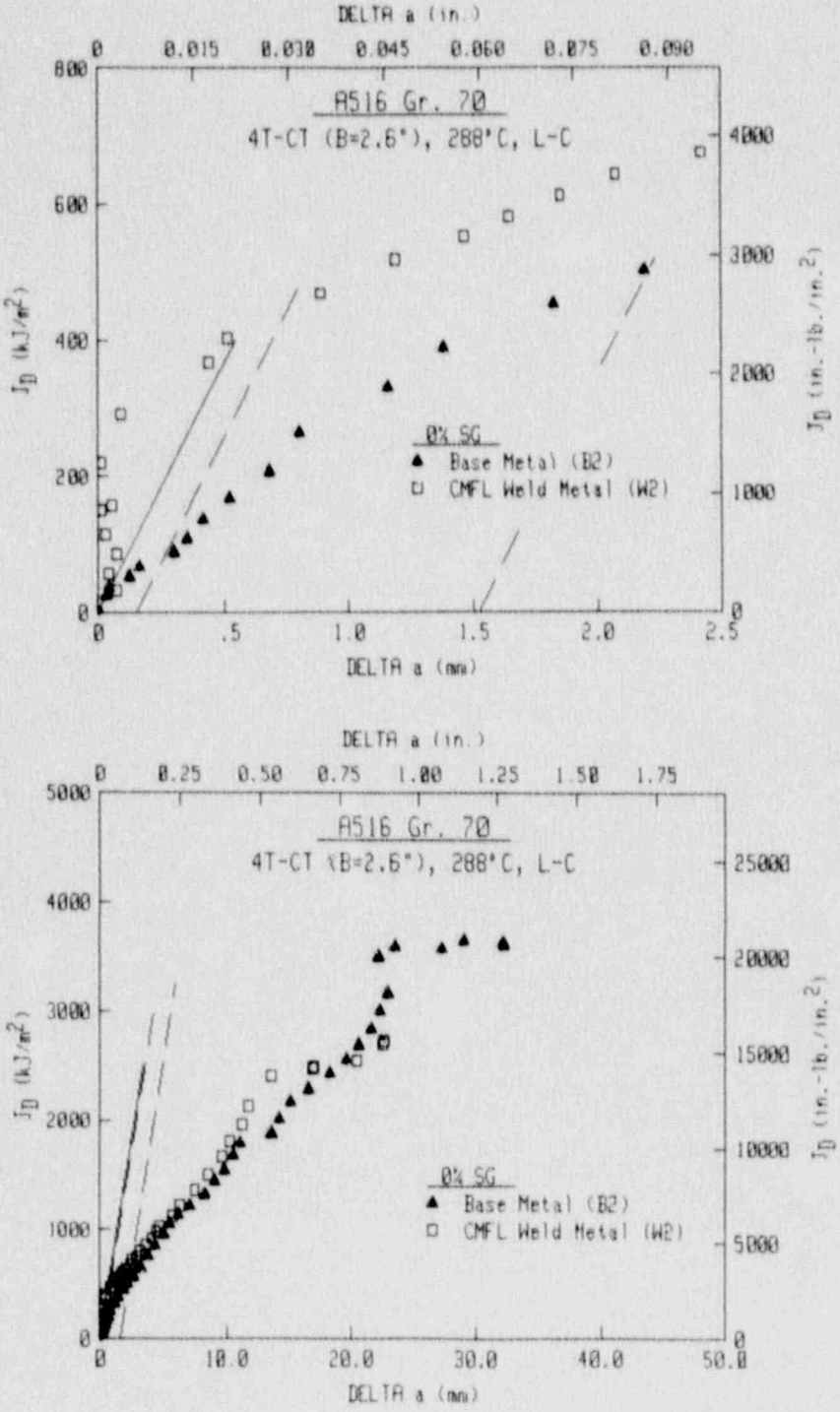

Fig. 3-61 Comparison of J_D-R curves from A 516 Gr. 70 base and weld metals at 288 °C, using plane-sided specimens.

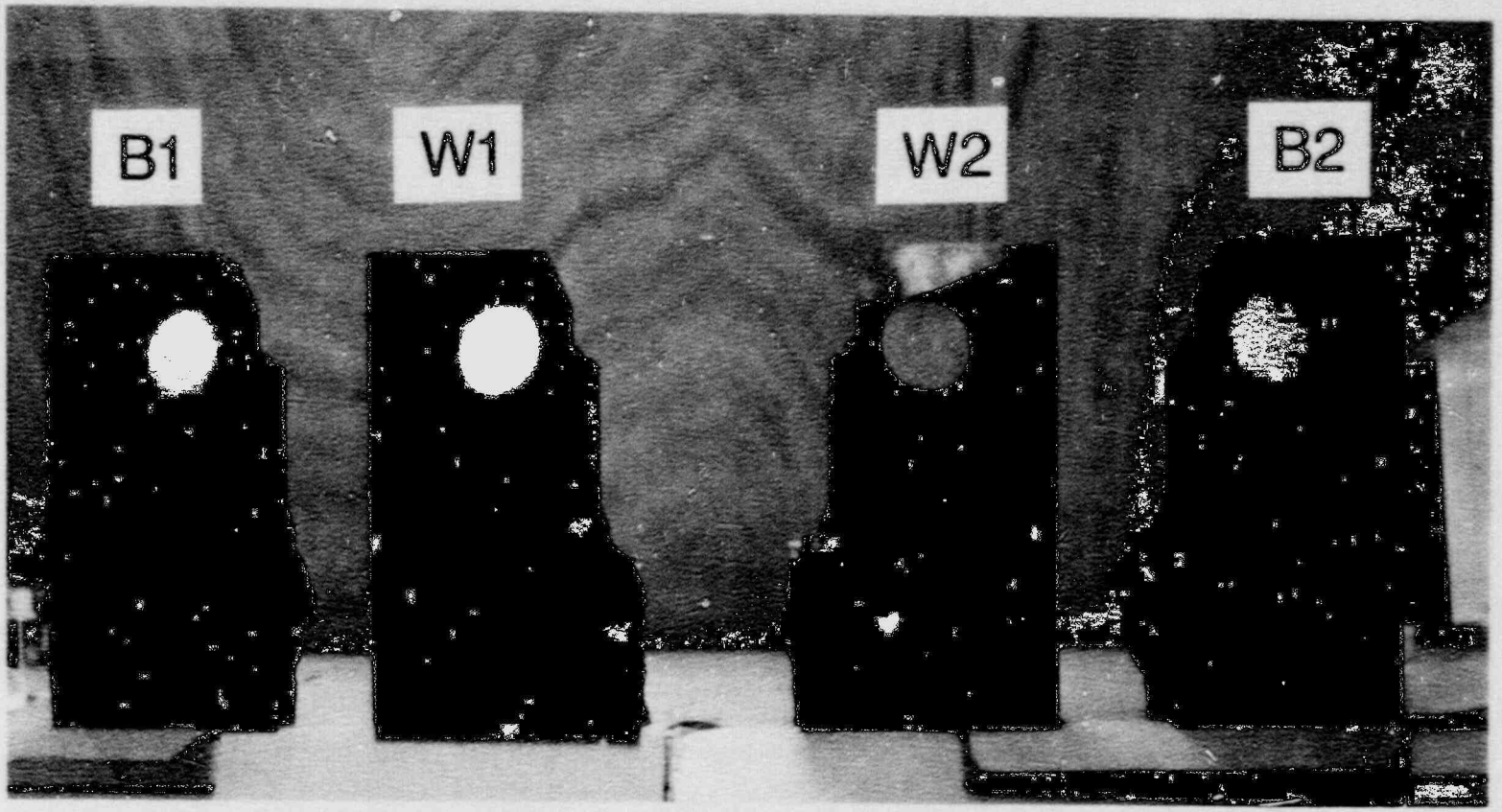

Fig. 3-62 Comparison of profile views of the A 516 Gr. 70 weld and base metal specimens, illustrating the shear lip formation on the plane-sided specimens and the out-of-plane growth on the side-grooved specimens.

4. WROUGHT STAINLESS STEELS

The wrought stainless steels tested are all Type 304 stainless, with one heat from a safe end and the other two heats from pipe products. Chemical compositions of these heats are given in Table 4-1.

4.1 SA 182 Type 304

4.1.1 Material Description

The heat of SA 182 Type 304 was procured as a nominal 20-in. Schedule 100 safe end, with a diameter of 508 mm (20 in.) and a wall thickness of 31 mm (1.25 in.).

4.1.2 Charpy-V Data

Several C_v specimens were tested from this heat, with two specimens each of the C-L, L-C, L-R and C-R orientations. The first test of each orientation was made at -73°C (-100°F). All of the specimens yielded very high energy levels. The absorbed energy for the L-C orientation was 354 J (261 ft-lb), for the C-R orientation 351 J (259 ft-lb), for the L-R orientation 347 J (256 ft-lb), and that for the C-L orientation was 319 J (235 ft-lb). The second test of each orientation was made at -18°C (0°F), and in each case a stalled hammer resulted. The capacity of the test machine used is 354 J (261 ft-lb).

4.1.3 Tensile Data

The strength properties of this heat were determined using threaded-end specimens with a gage diameter of 6.35 mm (0.25 in.) and a gage length of 25.4 mm (1.0 in.) for elongation measurements.

The strength data are summarized in Table 4-2 and illustrated in Fig. 4-1. The two orientations tested (i.e., the L and the C orientations) exhibit similar strength levels at all test temperatures, although the longitudinal orientation exhibited slightly higher yield strengths at several temperatures. Both ultimate and yield strength are invariant with temperature over the range from 150°C (300°F) to 343°C (650°F), with higher strength levels exhibited at ambient temperature for both strengths.

4.1.4 Fracture Toughness Data

The fracture toughness tests of this heat were made using 1T-CT specimens with a thickness of 25.4 mm or 1.0 in. (Fig. 4-2). All specimens were side-grooved by 20%. Results from these tests are summarized in Table 4-3. From this table, J_{Ic} and T_{avg} values are reported for few of the tests. As illustrated in the J-R curves, the lack of J_{Ic} and T_{avg} values is due to very high J-R curves and the failure of the data to cross through the ASTM exclusion zone.

As illustrated in Figs. 4-3 and 4-4, both the L-C and the C-L orientations exhibit some temperature dependence between ambient temperature and the elevated temperatures of 288°C and 343°C. In

Table 4-1 Chemical Composition (Wt. %) of the Wrought Stainless Steel Piping Materials

Heat ID	Specification	Chemical Composition (Wt. %)												
		C	Mn	P	S	Si	Ni	Cr	Mo	Cu	V	Ti	Al	Co
ZP6	SA 182 (Type 304)	0.030	1.140	0.017	0.009	0.430	9.810	18.920	0.290	0.160	0.004	0.003	ND[a]	0.120
ZP17	SA 376 (Type 304)	0.058	1.530	0.019	0.014	0.480	9.300	18.740	0.150	ND[a]	ND[a]	0.004	ND[a]	ND[a]
ZP12	SA 376 (Type 304)	0.052	1.740	0.020	0.011	0.410	10.430	19.230	0.220	ND[a]	ND[a]	0.003	ND[a]	ND[a]

[a] Not determined.

Table 4-2 Tensile Properties of SA 182 (Type 304)

Specimen Number	Test Temperature (°C)	Test Temperature (°F)	Orientation	0.2% Offset Yield Strength (MPa)	0.2% Offset Yield Strength (ksi)	Ultimate Strength (MPa)	Ultimate Strength (ksi)	Reduction In Area (%)	Elongation (%)
ZP6-1L	27	81	L	226.4	32.84	554.7	80.45	84.3	68.8
ZP6-2L	149	300	L	166.6	24.17	424.0	61.50	83.7	52.2
ZP6-3L	204	400	L	154.4	22.40	406.0	58.89	79.6	45.1
ZP6-4L	288	550	L	140.7	20.41	391.1	56.72	77.3	46.9
ZP6-6L	288	550	L	141.4	20.51	390.0	56.56	78.1	42.6
ZP6-5L	343	650	L	138.8	20.13	401.4	58.22	75.6	46.8
ZP6-1C	29	84	C	210.4	30.51	552.9	80.19	85.3	78.6
ZP6-2C	149	300	C	158.0	22.91	421.3	61.10	82.5	47.1
ZP6-3C	204	400	C	158.0	22.91	407.2	59.06	79.2	49.1
ZP6-4C	288	550	C	143.1	20.76	397.1	57.59	61.4	43.4
ZP6-6C	288	550	C	148.8	21.58	399.2	57.90	77.2	43.7
ZP6-5C	343	650	C	134.7	19.53	398.9	57.86	73.6	45.7

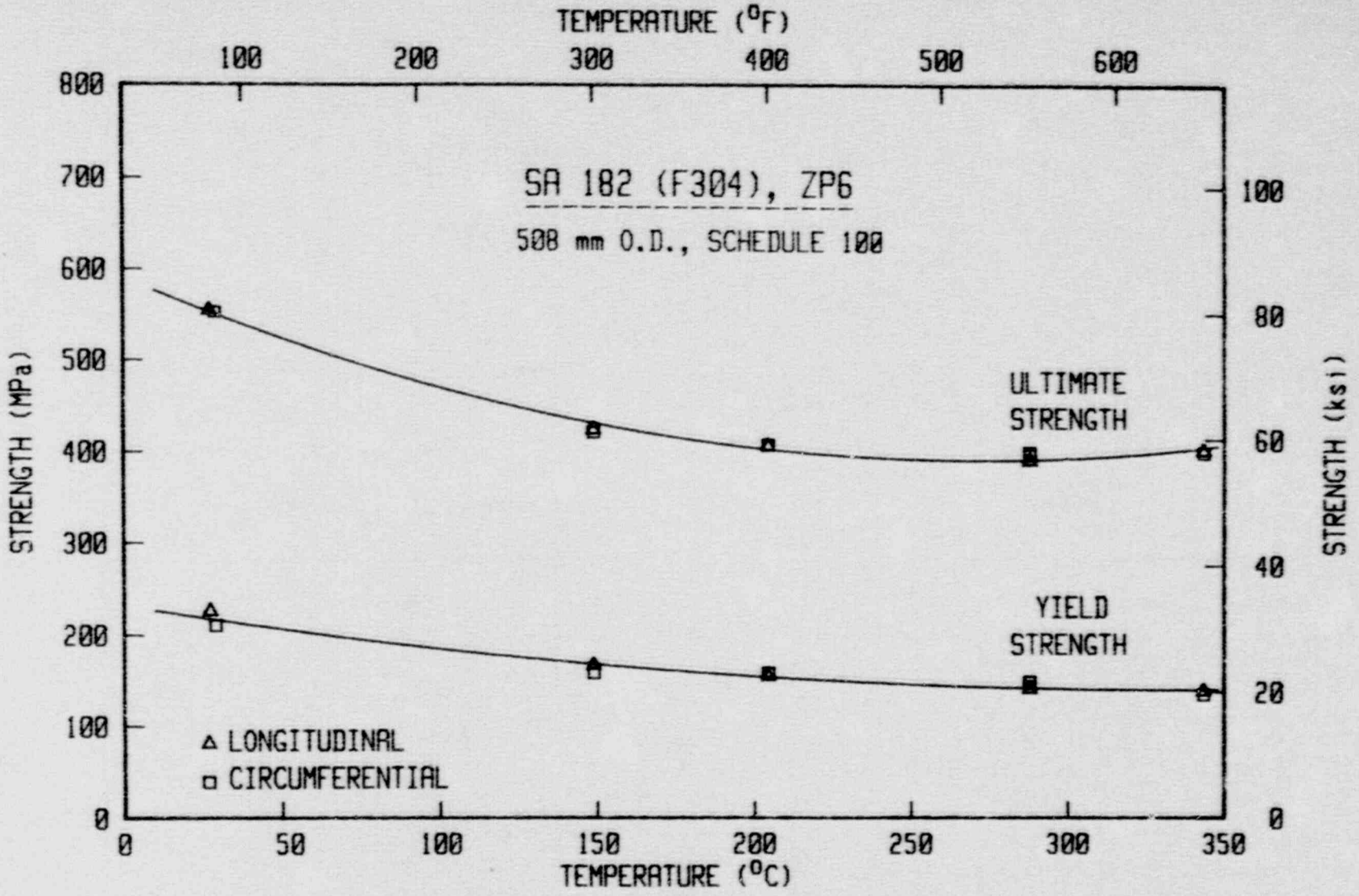

Fig. 4-1 Tensile strength data for the SA 182 Type 304 stainless steel (Heat ZP6).

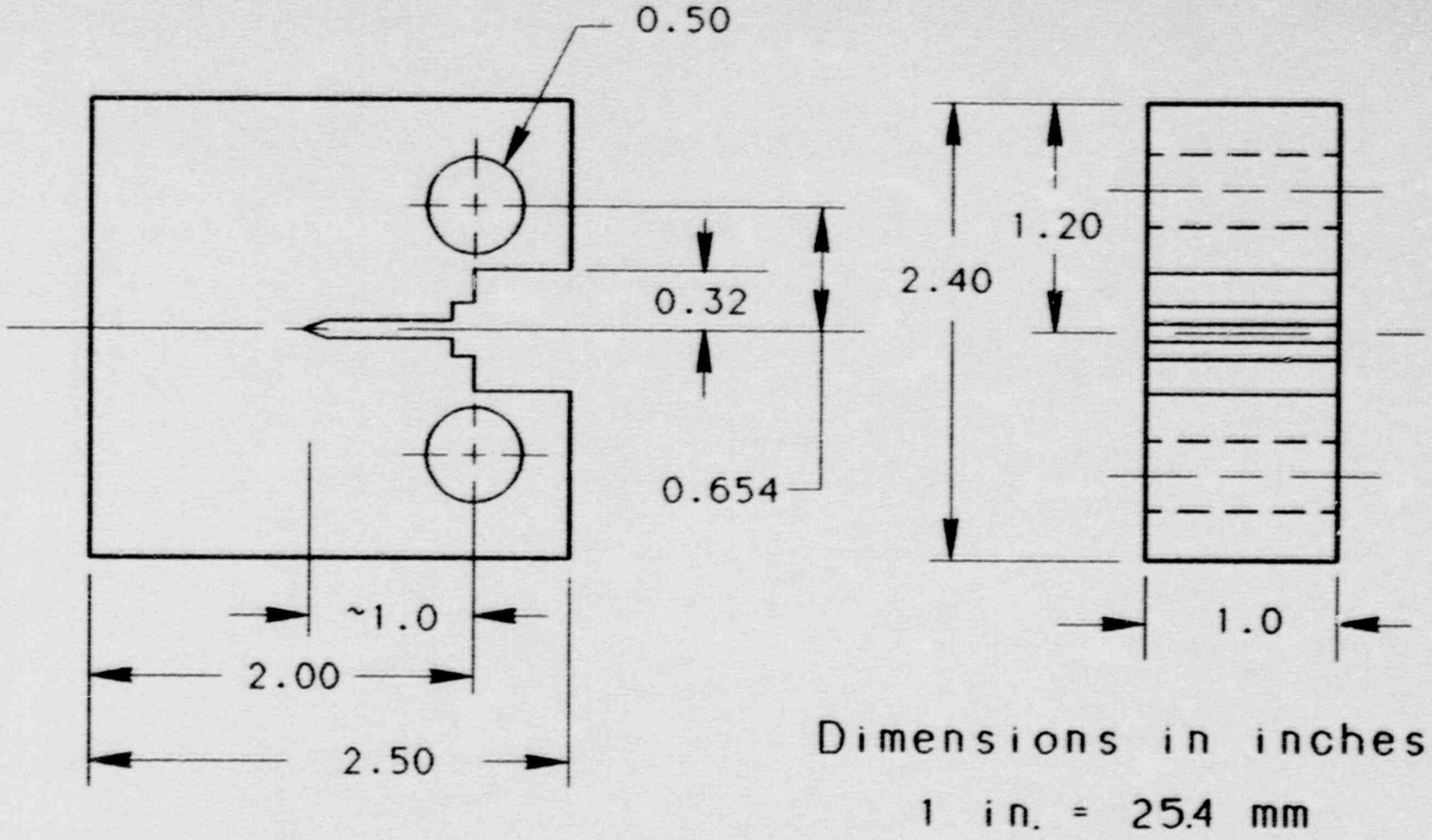

Fig. 4-2 Fracture toughness tests of SA 182 Type 304 (Heat ZP6) used this 1T-CT specimen design.

Table 4-3 J-R Curve Results for SA 182 (Type 304)

Specimen Number	Orient.	Test Temp.	Side Groove	$(a/W)_o$	Δa_m	$\Delta a_p - \Delta a_m$	J_{Ic}		K_{Jc}		T_{avg}		Flow Strength
							P.L.	Linear	P.L.	Linear	P.L.	Linear	
		(°C)	(%)		(mm)	(mm)	(kJ/m^2)	(kJ/m^2)	($MPa\sqrt{m}$)	($MPa\sqrt{m}$)			(MPa)
ZP6-1LC	L-C	25	20	0.555	7.08	-0.98	------	------	-----	-----	---	---	387.5
ZP6-6LC	L-C	24	20	0.552	5.76	-1.04	------	------	-----	-----	---	---	387.5
ZP6-4LC	L-C	288	20	0.542	2.96	+0.12	------	------	-----	-----	---	---	266.1
ZP6-7LC	L-C	288	20	0.550	8.51	-1.09	3126.9	------	772.4	-----	---	---	266.1
ZP6-5LC	L-C	343	20	0.548	5.39	-0.58	------	------	-----	-----	---	---	272.3
ZP6-1CL	C-L	25	20	0.548	7.99	-0.90	4235.9	------	933.5	-----	---	---	387.5
ZP6-6CL	C-L	25	20	0.575	6.39	-1.63	------	------	-----	-----	---	---	387.5
ZP6-4CL	C-L	288	20	0.552	8.75	-1.27	2192.6	1973.0	646.8	613.5	686	789	266.1
ZP6-5CL	C-L	343	20	0.549	5.62	-1.59	------	------	-----	-----	---	---	272.3

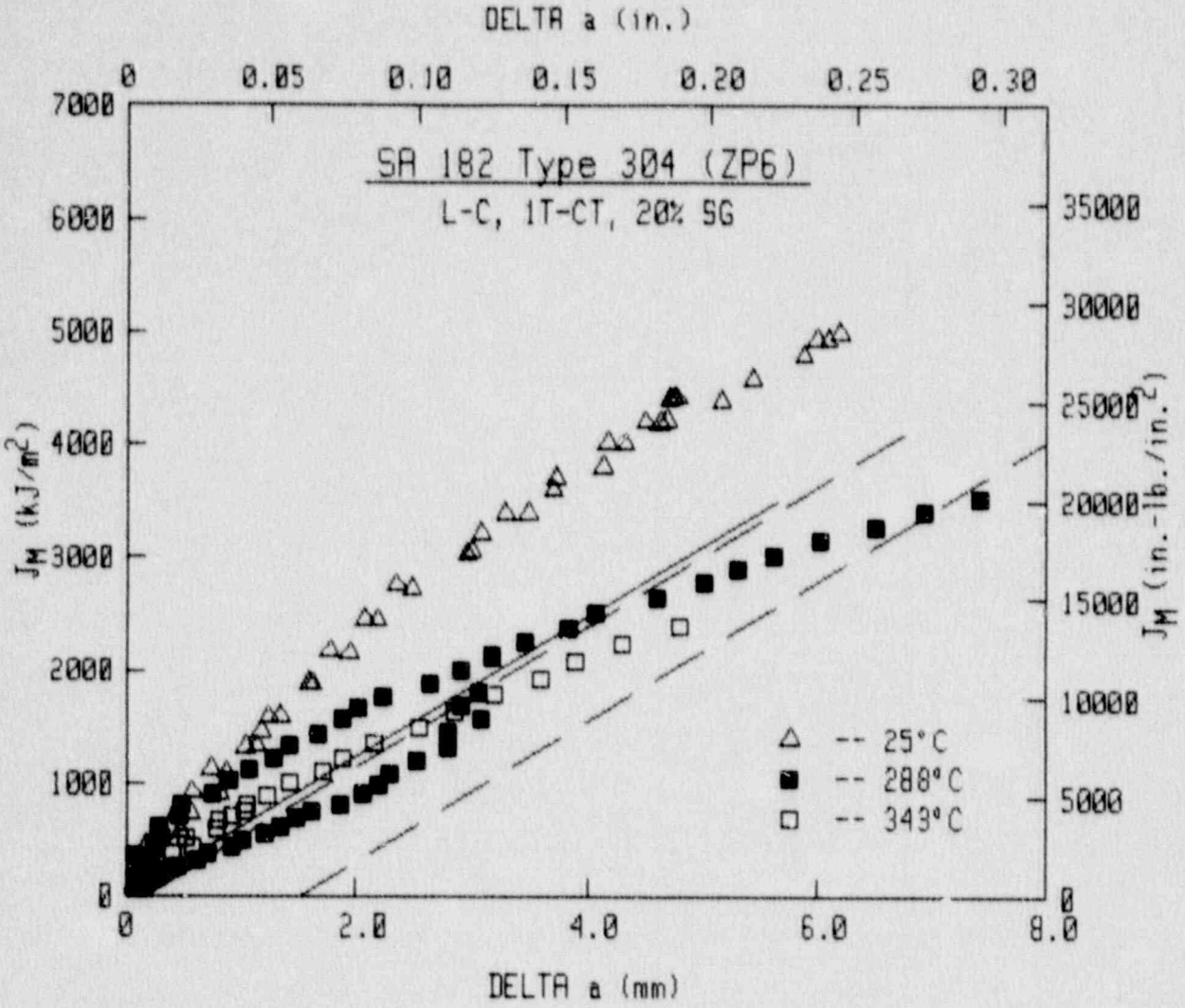

Fig. 4-3 J-R curves for the L-C orientation of SA 182 Type 304 (Heat ZP6). The highest J-R curve is at a test temperature of 25°C.

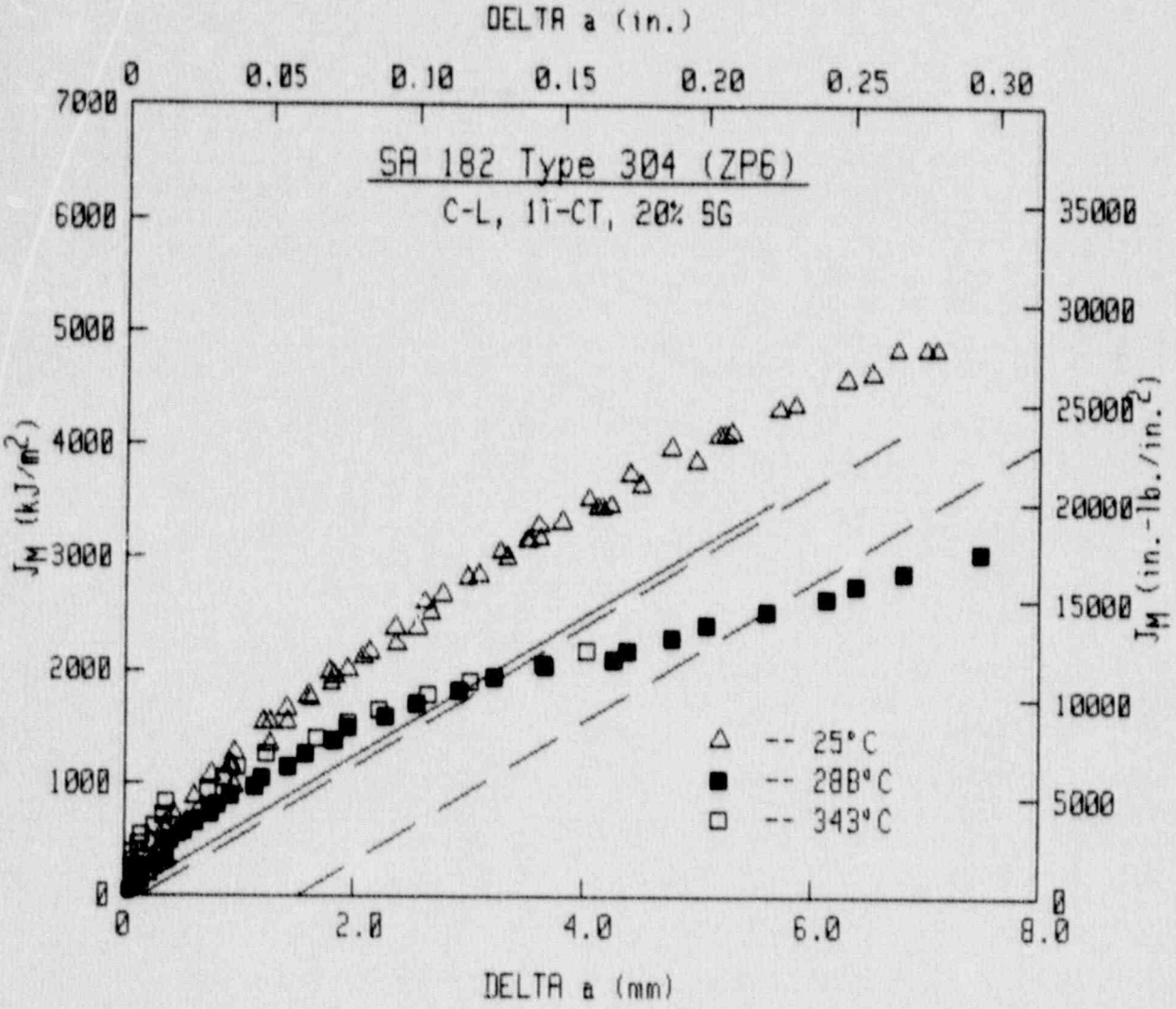

Fig. 4-4 J-R curves for the C-L orientation of SA 182 Type 304 (Heat ZP6). The highest J-R curve is at a test temperature of 25°C.

contrast, there are no significant differences in the J-R curves at 288°C and 343°C. Similarly, there are no significant differences in the J-R curves for the L-C and the C-L orientations at any of the three test temperatures (Figs. 4-5 to 4-7).

In all of the cited plots of J-R curve data, the illustrated blunting and exclusion lines are evaluated as in the ASTM method, using a slope of twice the flow strength (2 σ_f). As observed in these figures, the data are generally not well represented by the 2 σ_f blunting line, as the beginning portions of each curve generally lie exclusively to the left of the blunting line. Similar observations have been made by Mills (Ref. 18) and Landes and McCabe (Ref. 19) for Type 304 stainless, and also for cast stainless steels (Ref. 1). In the cited cases, the use of a slope twice that of the ASTM method (i.e., 4 σ_f) has been found to give a better definition of the blunting behavior of such high toughness materials. The use of 4 σ_f for this material would cause intersection of the data with the exclusion lines such that J_{Ic} values could be defined. However, such values would still be quite large (generally > 1000 kJ/m^2).

4.2 SA 376 Type 304

4.2.1 Material Description

Two heats of SA 376 Type 304 were procured and tested. Both heats had a diameter of 152 mm (6 in.), where Heat ZP12 was Schedule 40 (a wall thickness of 7.1 mm or 0.28 in.) and Heat ZP17 was a Schedule 120 (a wall thickness of 14.3 mm or 0.56 in.).

Heat ZP12 is the same as DP2-A7 and Heat ZP17 is the same as DP2-A23, in Ref. 4.

4.2.2 Charpy-V Data

Owing to the high toughness exhibited by Heat ZP6 at low temperatures (Section 4.1.2), no Charpy-V specimens were tested of these heats. It is anticipated that these heats would result in a stalled hammer condition at temperatures significantly below ambient temperature.

4.2.3 Tensile Data

Tensile results are summarized in Tables 4-4 and 4-5 and illustrated in Figs. 4-8 and 4-9. Heat ZP12 used a specimen design with a gage diameter of 2.9 mm (0.113 in.) and a gage length of 12.7 mm (0.5 in.). Heat ZP17 used a specimen design with a gage diameter of 5.1 mm (0.2 in.) and a gage length of 12.7 mm (0.5 in.). The latter is too small for calculation of elongation, therefore elongation percentages are too large for these tests in comparison to those for the proper gage length.

Each heat exhibits similar strength levels for the C and the L orientations, with both materials also exhibiting similar strength levels.

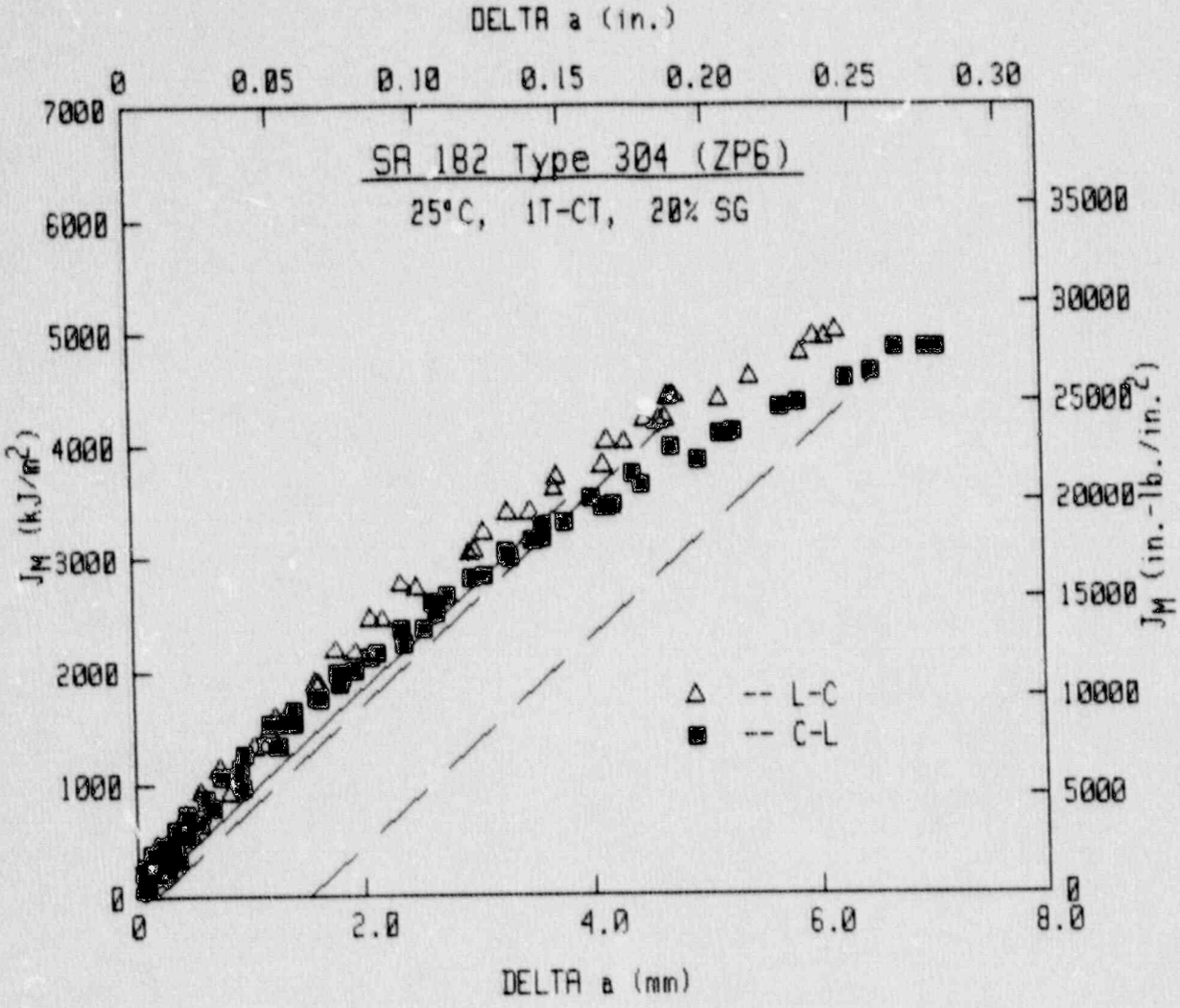

Fig. 4-5 Comparison of J-R curves for the L-C and the C-L orientations of SA 182 Type 304 (Heat ZP6) at 25°C. Little orientation dependence is apparent.

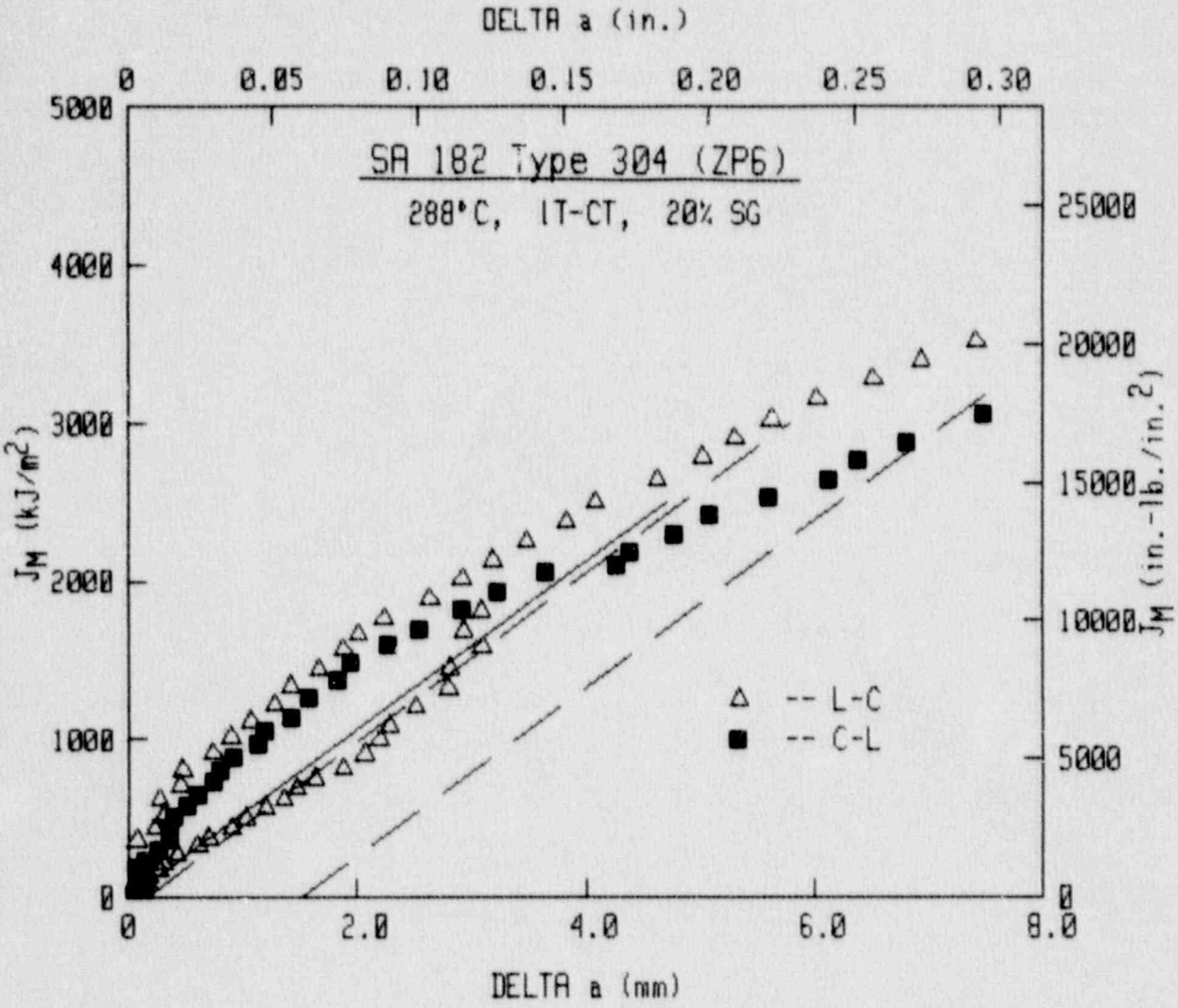

Fig. 4-6 Comparison of J-R curves for the L-C and the C-L orientations of SA 182 Type 304 (Heat ZP6) at 288°C. Little orientation dependence is apparent.

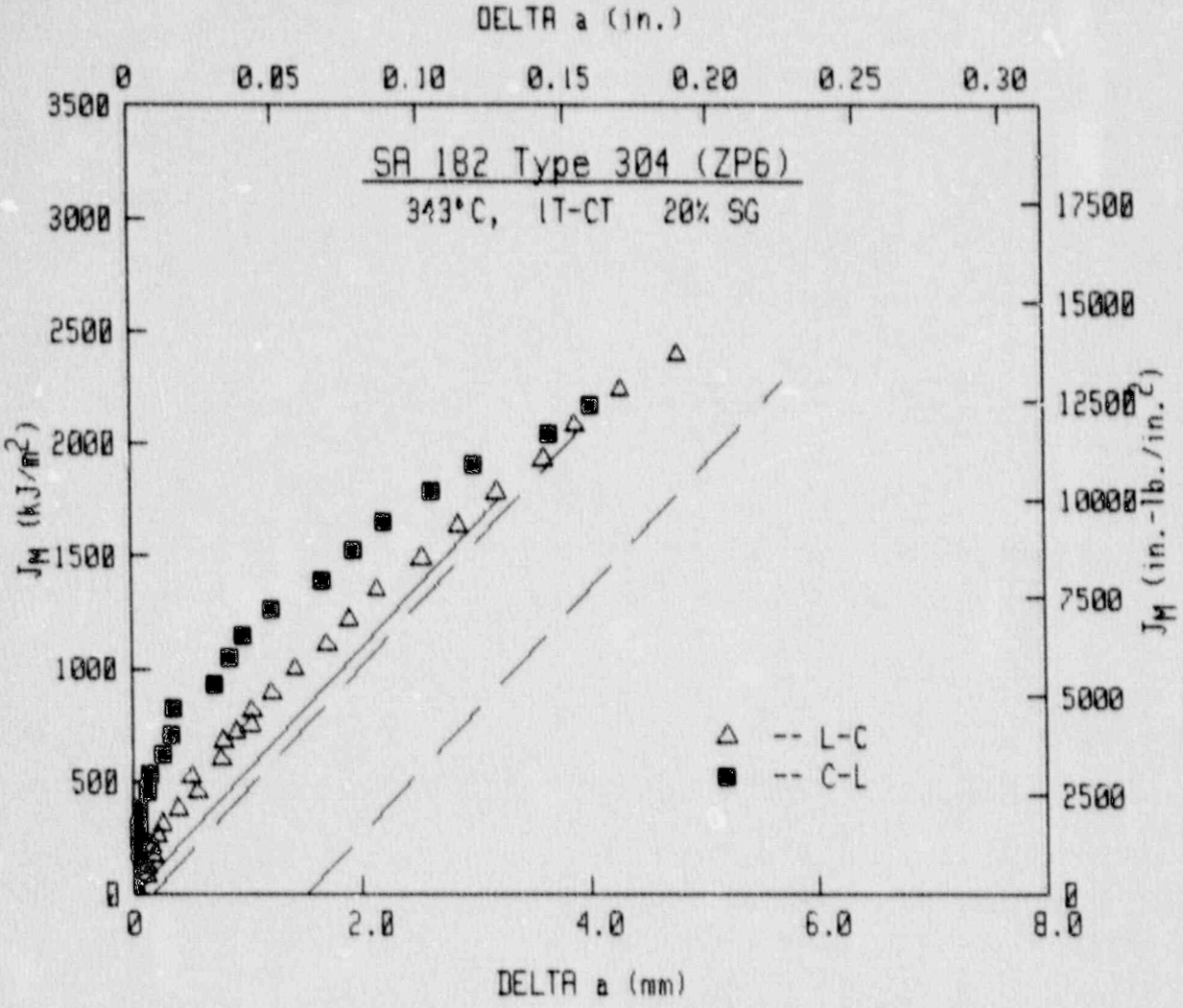

Fig. 4-7 Comparison of J-R curves for the L-C and the C-L orientations of SA 182 Type 304 (Heat ZP6) at 343°C. Little orientation dependence is apparent.

Table 4-4 Tensile Properties of SA 376-Type 304 (Heat ZP12)

Specimen Number	Test Temperature (°C)	Test Temperature (°F)	Orientation	0.2% Offset Yield Strength (MPa)	0.2% Offset Yield Strength (ksi)	Ultimate Strength (MPa)	Ultimate Strength (ksi)	Reduction In Area (%)	Elongation (%)
ZP12-9L	27	80	L	194.7	28.24	595.1	86.31	79.7	75.4
ZP12-14L	26	79	L	237.7	34.48	593.3	86.05	79.7	84.8
ZP12-10L	149	300	L	176.6	25.61	463.9	67.29	77.2	54.0
ZP12-15L	149	300	L	174.5	25.31	467.3	67.77	78.9	56.4
ZP12-12L	288	550	L	147.7	21.42	445.2	64.57	60.5	40.8
ZP12-16L	288	550	L	-----	-----	447.3	64.87	60.5	41.4
ZP12-11L	288	550	L	146.3	21.22	453.5	65.77	69.9	48.0
ZP12-13L	343	650	L	142.2	20.62	453.7	65.81	74.6	50.2
ZP12-17L	343	650	L	134.9	19.56	452.8	65.67	70.9	48.8
ZP12-1C	27	80	C	258.5	37.49	585.1	84.86	40.8	57.0
ZP12-2C	149	300	C	179.3	26.01	462.8	67.13	64.9	50.6
ZP12-4C	343	650	C	135.4	19.64	444.5	64.47	60.9	44.0

Table 4-5 Tensile Properties of SA 376-Type 304 (Heat ZP17)

Specimen Number	Test Temperature (°C)	Test Temperature (°F)	Orientation	0.2% Offset Yield Strength (MPa)	0.2% Offset Yield Strength (ksi)	Ultimate Strength (MPa)	Ultimate Strength (ksi)	Reduction In Area (%)	Elongation (%)
ZP17-1L	21	69	L	247.7	35.92	601.1	87.19	64.0	92.8
ZP17-15L	26	78	L	249.9	36.24	607.1	88.06	83.2	102.6
ZP17-17L	149	300	L	169.6	24.60	466.2	67.62	79.3	72.8
ZP17-11L	149	300	L	182.1	26.41	467.1	67.75	64.0	46.6
ZP17-12L	204	400	L	156.0	22.63	448.2	65.01	73.5	65.2
ZP17-16L	288	550	L	146.7	21.27	448.4	65.03	62.6	51.0
ZP17-13L	288	550	L	145.3	21.07	452.6	65.65	75.0	57.0
ZP17-18L	343	650	L	134.2	19.47	456.2	66.17	70.8	59.6
ZP17-14L	343	650	L	147.7	21.42	460.1	66.73	71.4	60.2
ZP17-8C	26	78	C	253.7	36.80	599.9	87.01	74.5	96.8
ZP17-1C	26	78	C	250.5	36.33	612.9	88.90	75.0	98.4
ZP17-6C	149	300	C	184.2	26.72	457.8	66.40	70.0	67.0
ZP17-7C	204	400	C	169.7	24.61	446.5	64.76	65.8	60.6
ZP17-9C	288	550	C	152.9	22.17	449.1	65.14	56.9	50.0

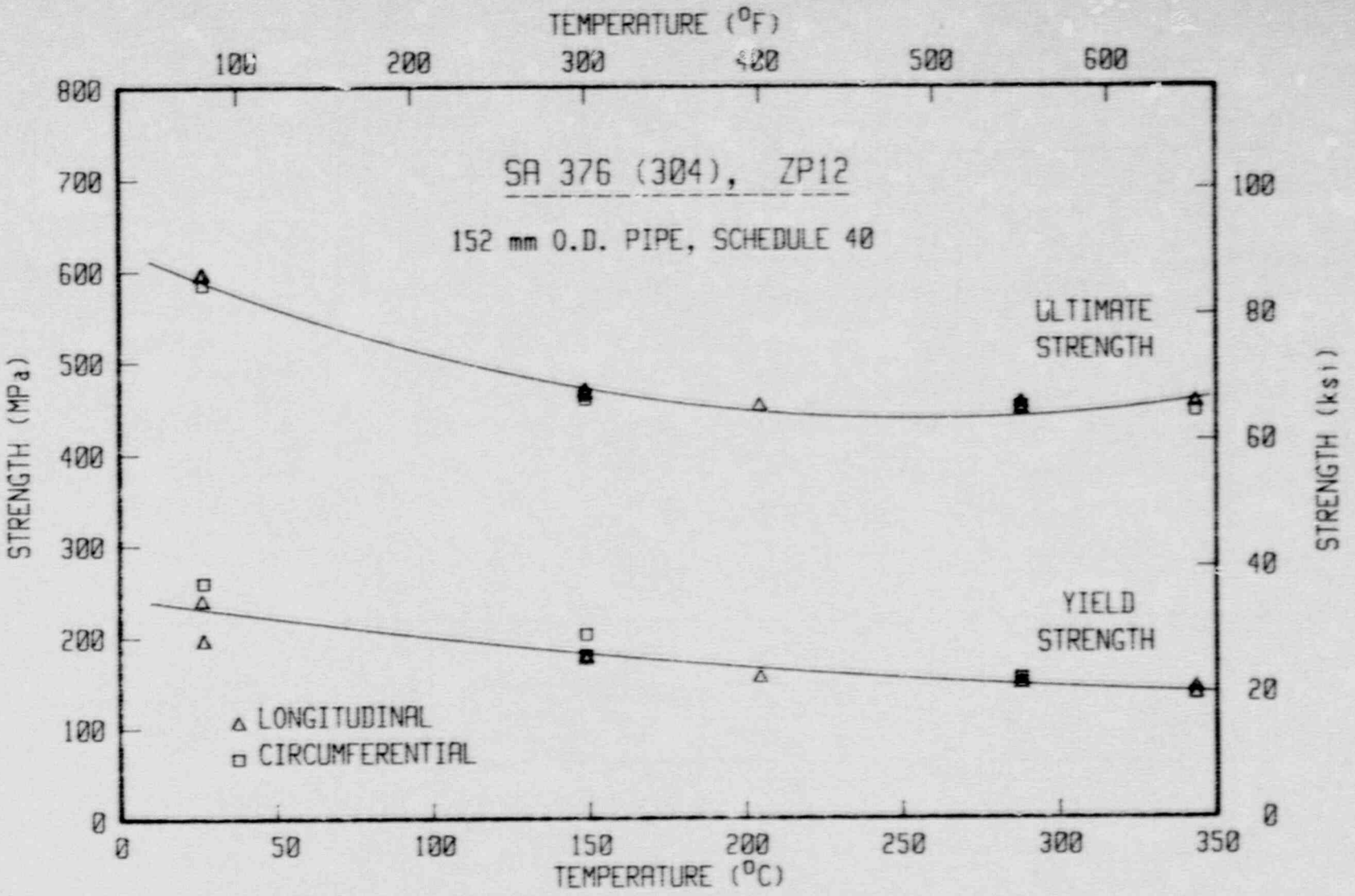

Fig. 4-8 Tensile strength data for SA 376 Type 304 (Heat ZP12).

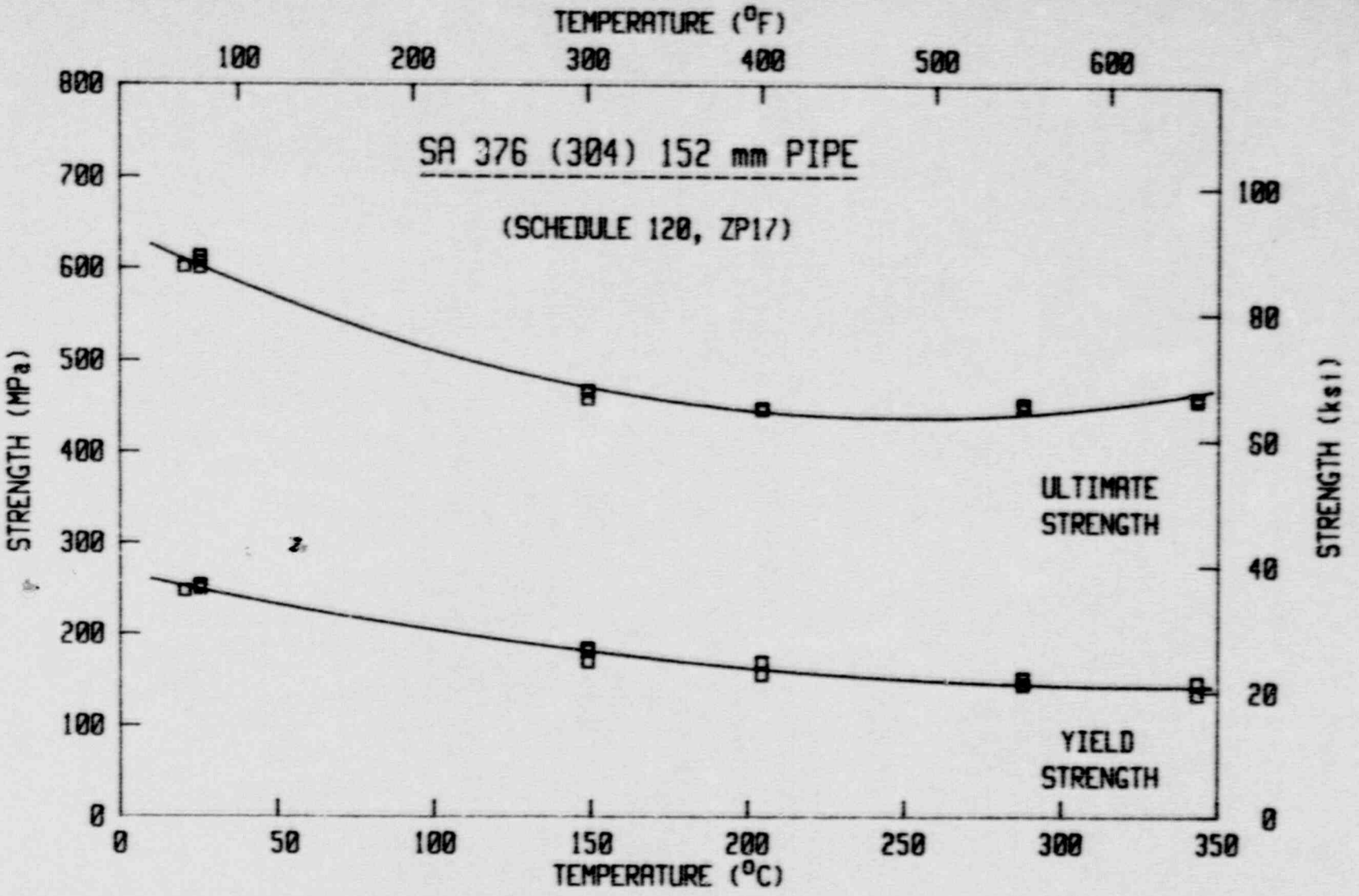

Fig. 4-9 Tensile strength data for SA 376 Type 304 (Heat ZP17) are quite similar to those for Heat ZP12.

4.2.4 Fracture Toughness Data

For Heat ZP12, the specimen design was identical to that used for Heat ZP13 in Fig. 3-20, specifically that of a 0.4T-CT specimen, with a thickness of 5.8 mm (0.23 in.). Results for this heat are summarized in Table 4-6. From Fig. 4-10 for plane-sided specimens, this heat exhibits only minor temperature sensitivity, as data at 149°C are somewhat higher than that at 288°C. At the higher test temperature of 288°C, some variability is apparent, with the higher curve exhibiting similar toughness to the tests at 149°C, and the lower curve indicating somewhat lower toughness at the higher test temperature. The latter point is noteworthy when comparing data from plane-sided and side-grooved specimens at 288°C. As illustrated in Fig. 4-11, the curve from a side-grooved specimen is similar to the lower of the curves from the plane-sided specimens, but significantly lower than that the higher curve from the plane-sided specimens. Since a lowering of the J-R curve would be expected with side-grooving, then the curve from the side-grooved specimen should probably be compared to the average of the curves from plane-sided specimens.

For Heat ZP17, the specimen design was that of a 0.5T-CT specimen with a thickness of 12.7 mm or 0.5 in. (Fig. 4-12). Results for this heat are summarized in Table 4-7. For the L-C orientation with plane-sided and side-grooved specimens and the C-L orientation with side-grooved specimens (Figs. 4-13 to 4-15), increasing the test temperature from ambient tended to give reduced J-R curve levels, at least up to 204°C. At 204°C and higher (up to 343°C), no significant change in toughness is apparent. Comparisons at test temperatures of 25°C and 288°C (Figs. 4-16 and 4-17) indicate a moderate effect of side-grooving on J level, with plane-sided specimens giving somewhat higher J levels than side-grooved specimens. However, the largest decrease in toughness occurs when comparing the L-C orientation and the C-L orientation, as illustrated in Figs. 4-16 and 4-17 for 25°C and 288°C, respectively, and in Fig. 4-18 at 343°C. Such differences are in direct conflict with those found with SA 182 Type 304 (Heat ZP6) in Figs. 4-5 to 4-7, where the L-C and the C-L orientations gave similar J-R curves. These differences are probably due to Heat ZP6 being a forged heat.

Table 4-6 J-R Curve Results for SA 376-Type 304 (Heat ZP12)

Specimen Number	Orient.	Test Temp.	Side Groove	$(a/W)_o$	Δa_m	$\Delta a_p - \Delta a_m$	J_{Ic}		K_{Jc}		T_{avg}		Flow Strength
							P.L.	ASTM	P.L.	ASTM	P.L.	ASTM	
		(°C)	(%)		(mm)	(mm)	(kJ/m^2)	(kJ/m^2)	($MPa\sqrt{m}$)	($MPa\sqrt{m}$)			(MPa)
ZP12-1LC	L-C	149	0	0.526	3.87	-0.55	2396.2	------	690.0	-----	769	----	321
ZP12-3LC	L-C	149	0	0.521	5.07	-0.80	1967.4	1797.3	625.2	597.6	742	799	321
ZP12-2LC	L-C	288	0	0.522	2.82	-0.49	999.9	------	436.8	-----	467	----	301
ZP12-4LC	L-C	288	0	0.518	3.03	-0.55	1681.4	------	556.0	-----	525	----	301
ZP12-5LC	L-C	288	20	0.527	4.47	-0.44	923.8	873.3	419.8	408.2	602	609	301
ZP12-2CL	C-L	149	20	0.510	4.57	+0.16	214.1	209.8	206.3	204.2	7	251	324

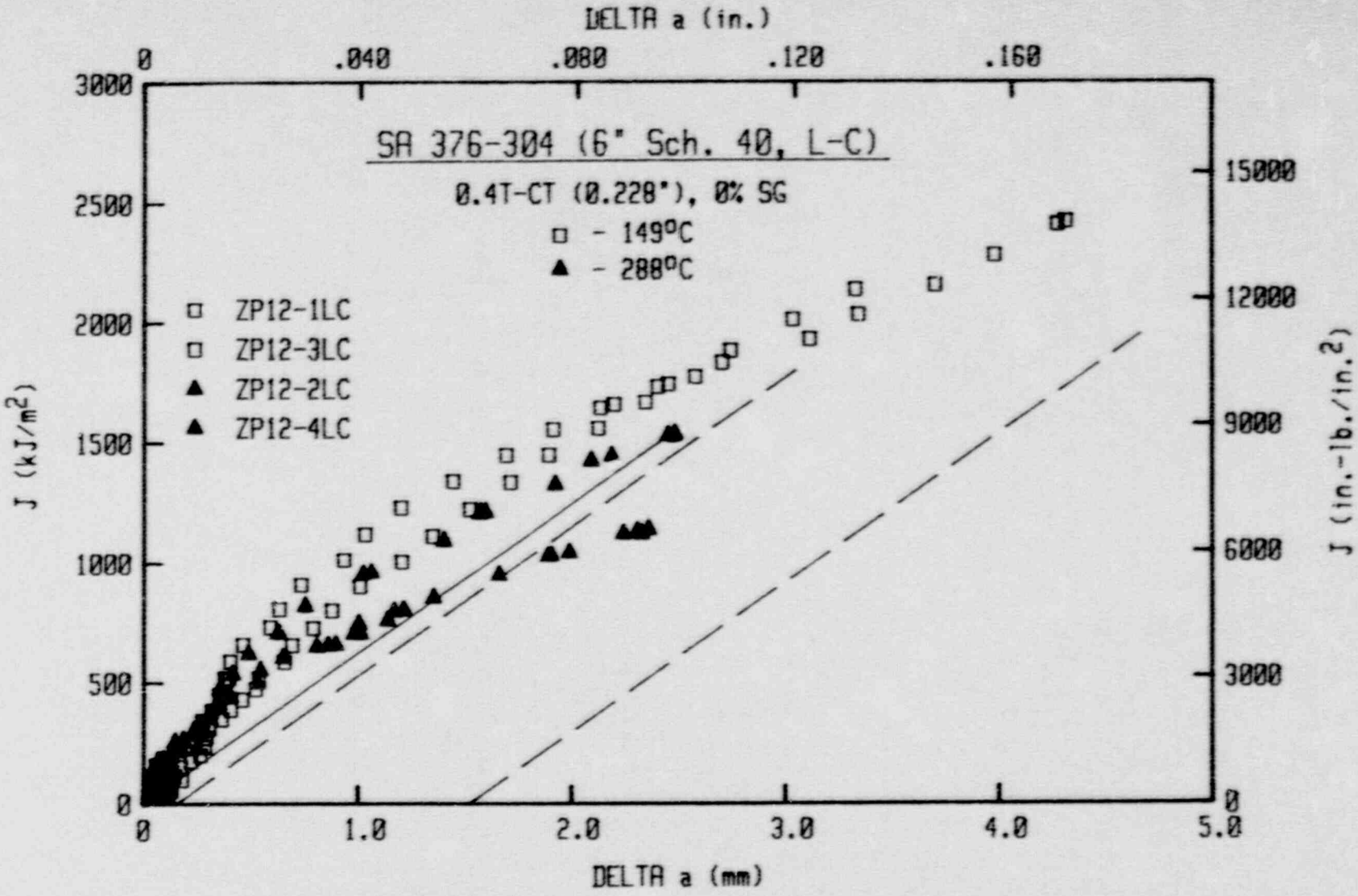

Fig. 4-10 J-R curves for the L-C orientation of SA 376 Type 304 (Heat ZP12), using plane-sided specimens. Data at 288°C are only slightly lower than that at 149°C.

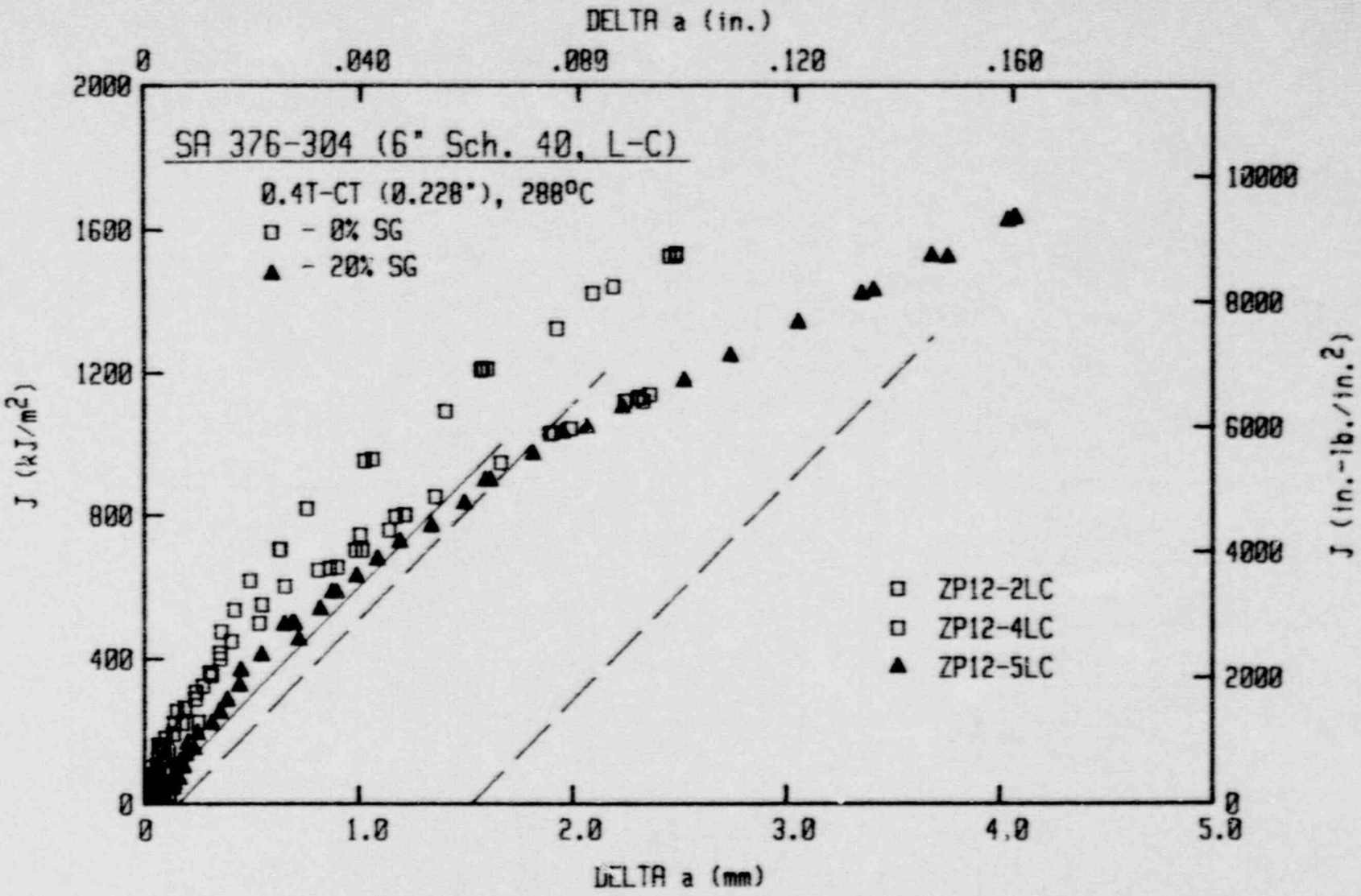

Fig. 4-11 J-R curves for the L-C orientation of SA 376 Type 304 (Heat ZP12) at 288°C. Data from sidegrooved specimens are somewhat lower than that from plane-sided specimens.

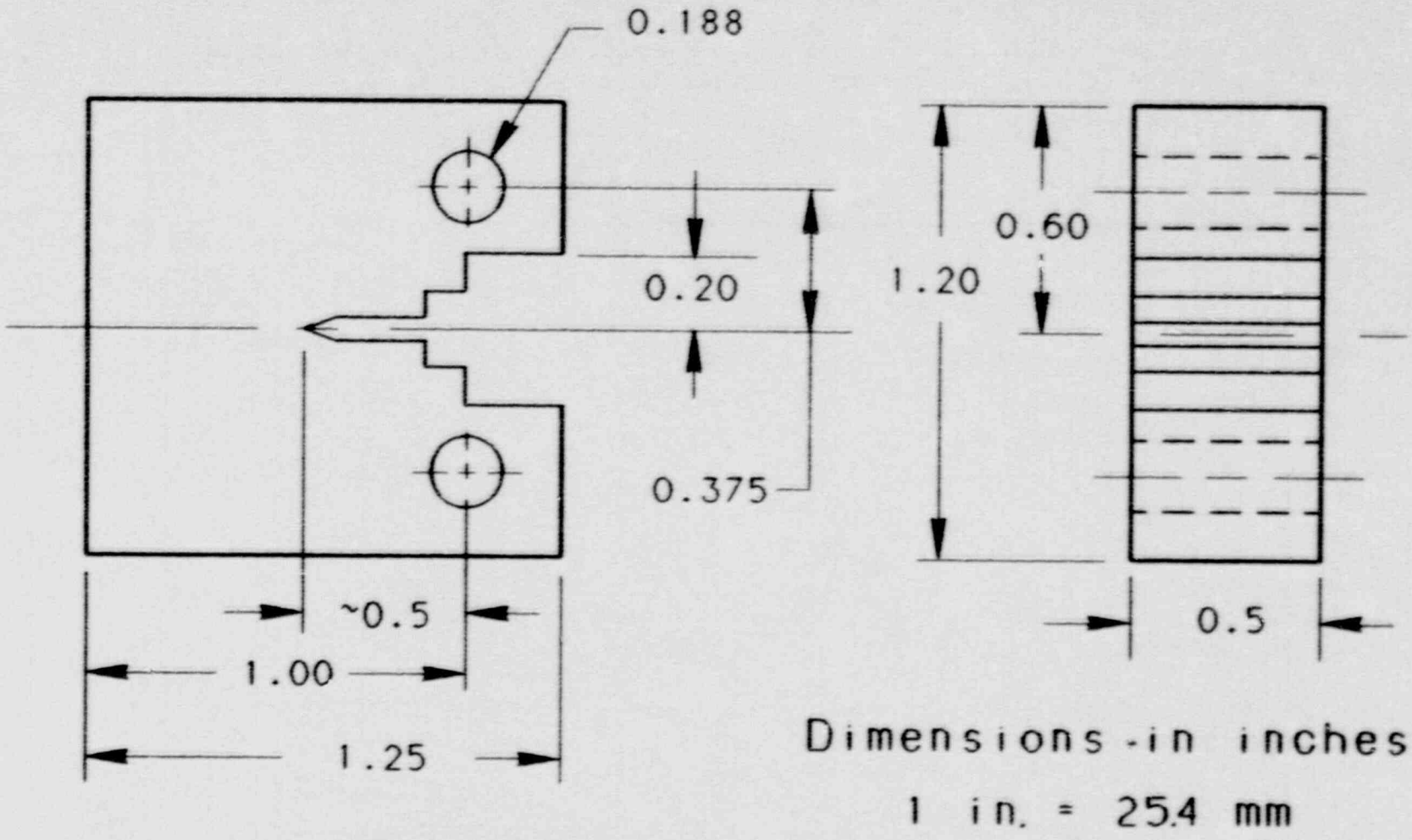

Fig. 4-12 Fracture toughness tests of SA 376 Type 304 (Heat ZP17) used this 0.5T-CT specimen design with a thickness of 12.7 mm (0.5 in.).

Table 4-7 J-R Curve Results for SA 376-Type 304 (Heat ZP17)

Specimen Number	Orient.	Test Temp.	Side Groove	$(a/W)_o$	$/a_m$	$\delta A_p - \delta A_m$	J_{Ic}		K_{Jc}		T_{avg}		Flow Strength
							P.L.	ASTM	P.L.	ASTM	P.L.	ASTM	
		(°C)	(%)		(mm)	(mm)	(kJ/m^2)	(kJ/m^2)	(MPa$\sqrt{m}$)	(MPa$\sqrt{m}$)			(MPa)
ZP17-2LC	L-C	149	0	0.556	3.50	-0.85	-----	-----	-----	-----	---	---	324.6
ZP17-4LC	L-C	149	0	0.547	1.56	-0.50	-----	-----	-----	-----	---	---	324.6
ZP17-3LC	L-C	288	0	0.557	1.52	-0.32	-----	-----	-----	-----	---	---	298.2
ZP17-5LC	L-C	288	0	0.543	2.34	-0.25	-----	-----	-----	-----	---	---	298.2
ZP17-7LC	L-C	23	20	0.563	5.22	-0.70	-----	-----	-----	-----	---	---	426.5
ZP17-11LC	L-C	23	20	0.557	5.42	-0.89	-----	-----	-----	-----	---	---	426.5
ZP17-12LC	L-C	204	20	0.534	4.93	-1.05	-----	-----	-----	-----	---	---	302.1
ZP17-9LC	L-C	288	20	0.536	3.12	-0.73	-----	-----	-----	-----	---	---	298.2
ZP17-13LC	L-C	288	20	0.544	3.84	-0.79	-----	-----	-----	-----	---	---	298.2
ZP17-10LC	L-C	343	20	0.545	3.56	-1.60	-----	-----	-----	-----	---	---	303.9
ZP17-6LC	L-C	343	20	0.540	3.82	-0.80	-----	-----	-----	-----	---	---	303.9
ZP17-1CL	C-L	22	20	0.534	7.73	-0.98	460.1	435.5	307.8	299.4	323	328	429.3
ZP17-2CL	C-L	149	20	0.539	7.51	-0.99	497.8	453.1	314.5	300.1	358	379	321.0
ZP17-3CL	C-L	204	20	0.573	7.27	-1.14	302.7	280.6	255.0	245.6	409	421	308.1
ZP17-4CL	C-L	288	20	0.535	5.77	-0.48	405.9	383.2	278.3	270.4	301	322	301.0
ZP17-5CL	C-L	343	20	0.538	6.86	-0.90	280.6	260.1	240.5	231.5	387	397	301.0

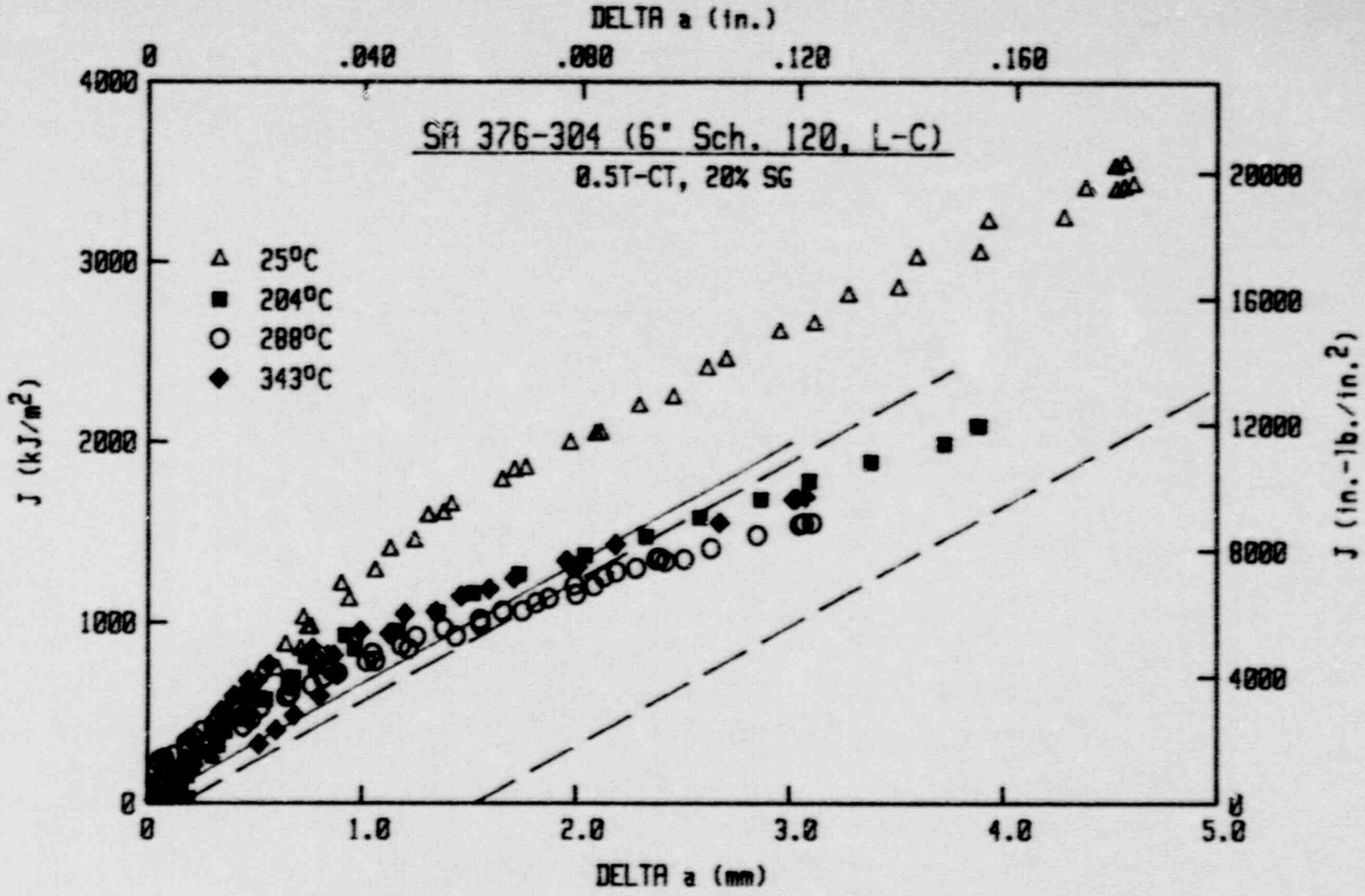

Fig. 4-13 J-R curves for the L-C orientation of SA 376 Type 304 (Heat ZP17), using side-grooved specimens. Data at 25°C are much higher than that at the other test temperatures.

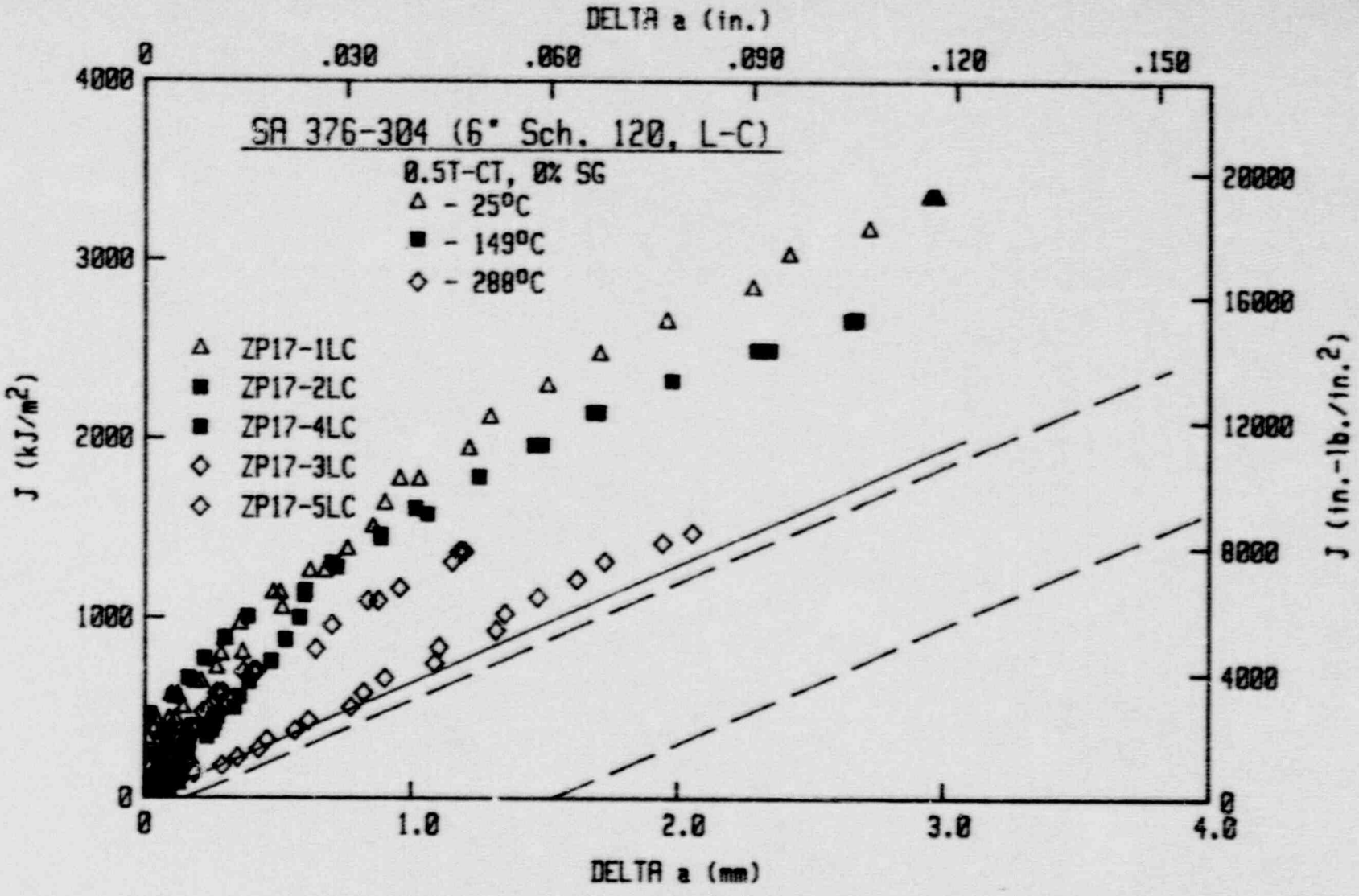

Fig. 4-14 J-R curves for the L-C orientation of SA 376 Type 304 (Heat ZP17), using plane-sided specimens.

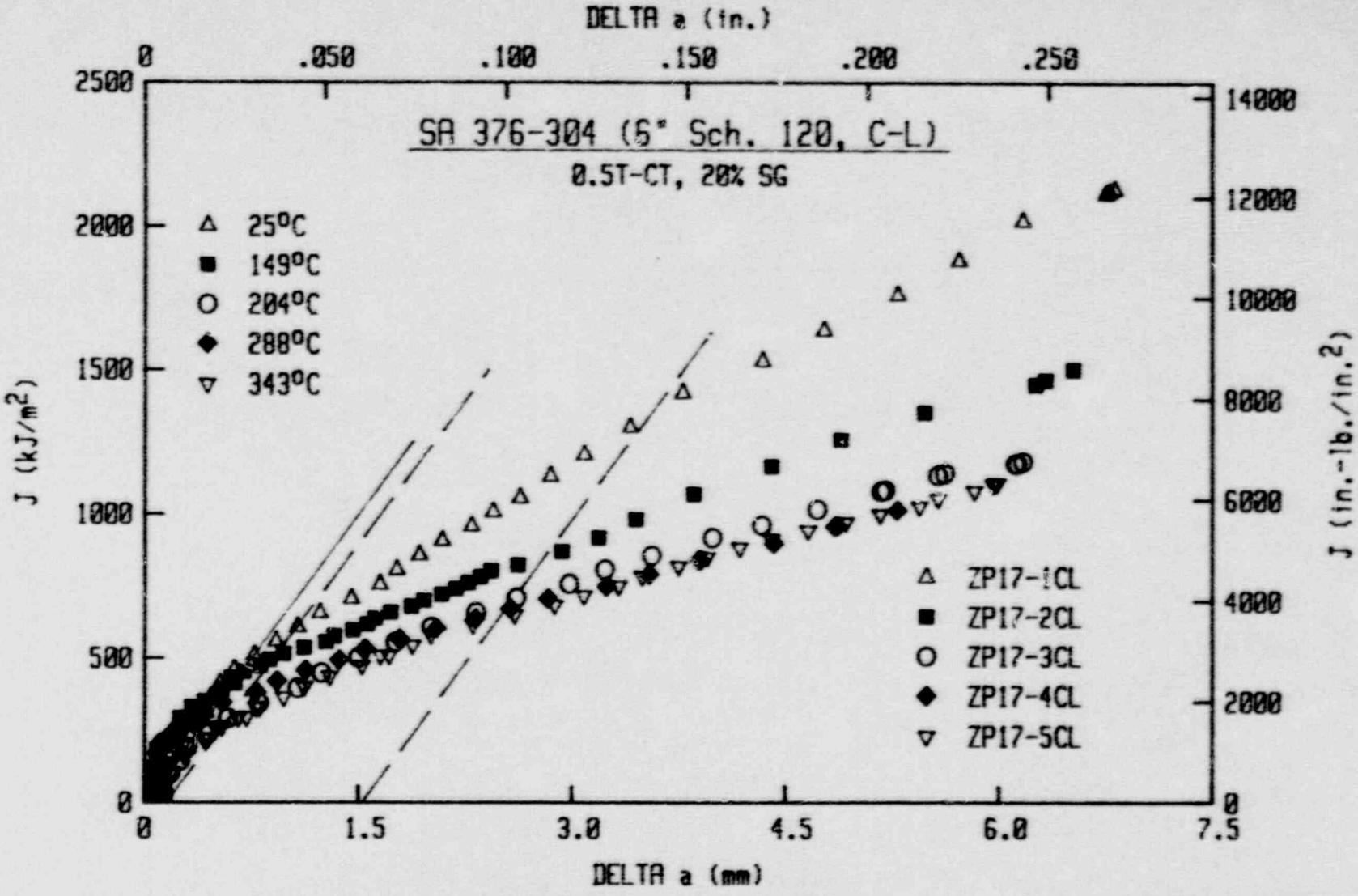

Fig. 4-15 J-R curves for the C-L orientation of SA 376 Type 304 (Heat ZP17), using side-grooved specimens. Data at 25°C are higher than that at the other test temperatures.

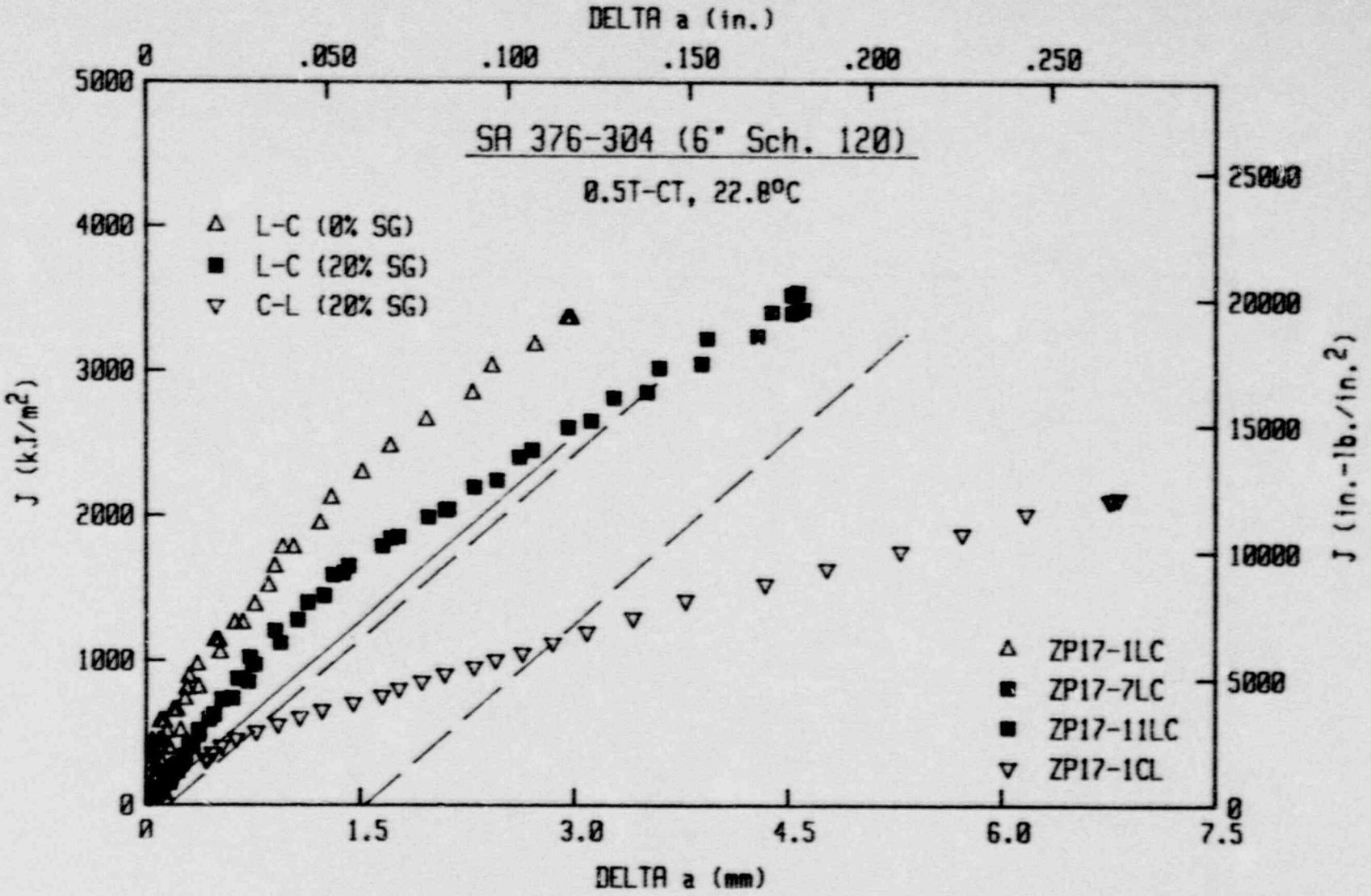

Fig. 4-16 J-R curves for SA 376 Type 304 (Heat ZP17) at 25°C. The L-C orientation exhibits much higher toughness than the C-L orientation.

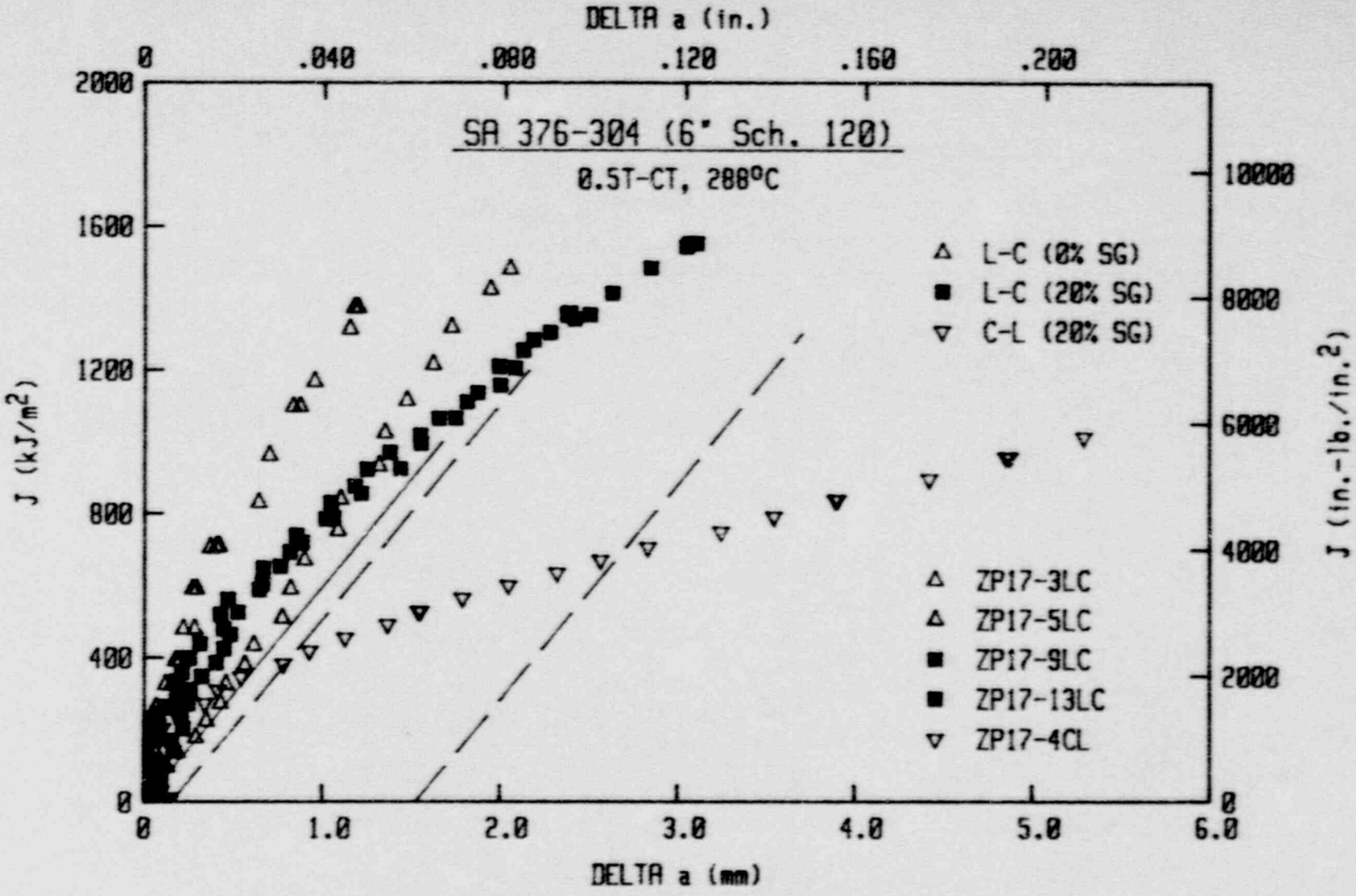

Fig. 4-17 J-R curves for SA 376 Type 304 (Heat ZP17) at 288°C. The L-C orientation exhibits much higher toughness than the C-L orientation.

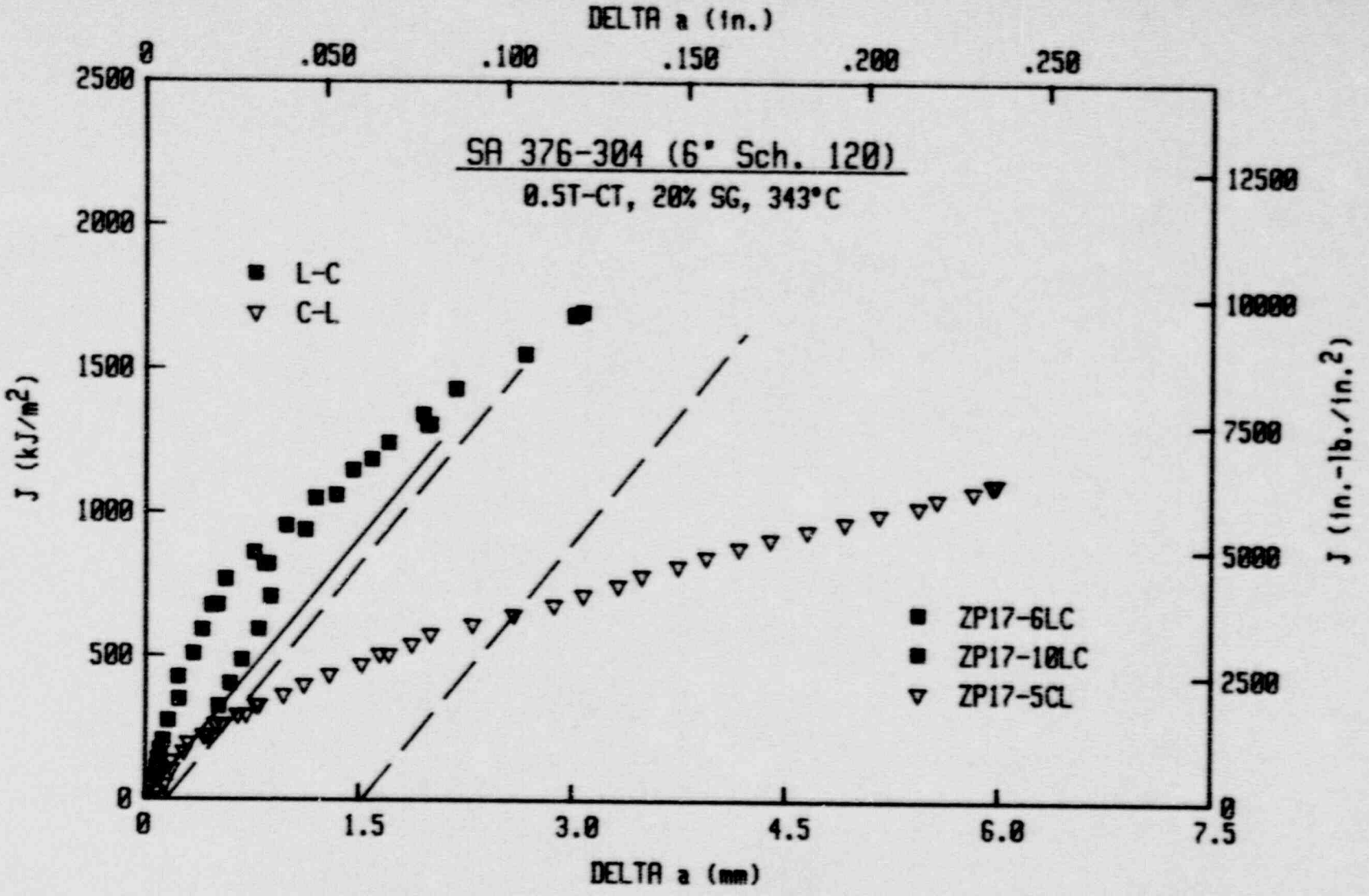

Fig. 4-18 J-R curves for SA 376 Type 304 (Heat ZP17) at 343°C. The L-C orientation exhibits much higher toughness than the C-L orientation.

5. NICKEL-BASED ALLOY

5.1 Inconel 600

5.1.1 Material Description

The nickel-based alloy is a single heat of Inconel 600. This material was procured as a pipe with a diameter of 152 mm (6 in.) and Schedule 80 (a wall thickness of 11 mm or 0.432 in.). Chemistry information on this heat is given in Table 5-1.

This heat is the same as DP2-I1 in Ref. 4.

5.1.2 Charpy-V Data

No Charpy-V specimens were tested from this pipe.

5.1.3 Tensile Data

Strength properties for this heat were determined using threaded-end specimens with a gage diameter of 2.9 mm (0.113 in.) and a gage length of 12.7 mm (0.5 in.). Tensile results are summarized in Table 5-2 and illustrated in Fig. 5-1. As with the other heats of piping materials, no significant different between the L and the C orientations were found. In addition, no significant temperature sensitivity was found.

5.1.4 Fracture Toughness Data

The specimen design used for this heat is the same as that used for Heat ZP15, specifically that of a 0.5T-CT specimen with a thickness of 9.1 mm or 0.36 in., as illustrated in Fig. 3-24. Results for this heat are summarized in Table 5-3.

From Figs. 5-2 to 5-4, temperature sensitivity for this heat is not too severe for the C-L or the L-C orientations using side-grooved specimens, or for the L-C orientation using plane-sided specimens. This trend is most evident for the C-L orientation, with the L-C orientation demonstrating some temperature sensitivity with reductions in J levels with increasing test temperature.

Comparisons at 25°C and 288°C (Figs. 5-5 and 5-6) indicate only a minimal and an inconsistent effect of side-grooving, as the plane-sided specimens give higher J levels at 25°C and lower J levels at 288°C. Likewise, the C-L orientation gives somewhat lower toughness than the L-C orientation at 25°C and 288°C, but toughness (J levels) similar to those for the L-C orientation at 343°C (Fig. 5-7).

Table 5-1 Chemical Composition (Wt. %) of the Nickel-Based Alloy

Heat	Specification	Chemical Composition (Wt. %)												
		C	Mn	P	S	Si	Ni	Cr	Mo	Cu	V	Ti	Al	Co
ZP16	Inconel 600	0.030	0.350	ND[a]	0.003	0.200	75.010	15.530	0.056	0.023	ND[a]	0.250	0.150	0.021

[a] Not determined.

Table 5-2 Tensile Properties of Inconel 600 (Heat ZP16)

Specimen Number	Test Temperature (°C)	Test Temperature (°F)	Orientation	0.2% Offset Yield Strength (MPa)	0.2% Offset Yield Strength (ksi)	Ultimate Strength (MPa)	Ultimate Strength (ksi)	Reduction In Area (%)	Elongation (%)
ZP16-1L	25	77	L	238.8	34.63	644.8	93.52	73.0	63.0
ZP16-5L	25	77	L	237.7	34.48	644.7	93.51	74.0	64.8
ZP16-2L	149	300	L	217.1	31.49	604.7	87.70	69.7	59.8
ZP16-6L	149	300	L	213.3	30.94	605.7	87.85	73.0	57.2
ZP16-3L	288	550	L	197.0	28.57	608.9	88.31	60.9	52.2
ZP16-7L	288	550	L	196.1	28.44	614.5	89.13	69.7	60.0
ZP16-9L	288	550	L	196.0	28.43	605.0	87.75	68.1	63.6
ZP16-4L	343	650	L	189.3	27.46	613.9	89.04	68.6	59.6
ZP16-8L	343	650	L	191.2	27.73	613.2	88.94	68.1	61.0
ZP16-1C	25	77	C	261.1	37.87	687.6	99.73	56.4	42.6
ZP16-2C	149	300	C	224.3	32.53	603.4	87.51	68.9	44.4
ZP16-3C	288	550	C	203.5	29.52	614.7	89.16	62.0	50.4
ZP16-4C	343	650	C	196.4	28.48	603.5	87.53	53.6	49.4

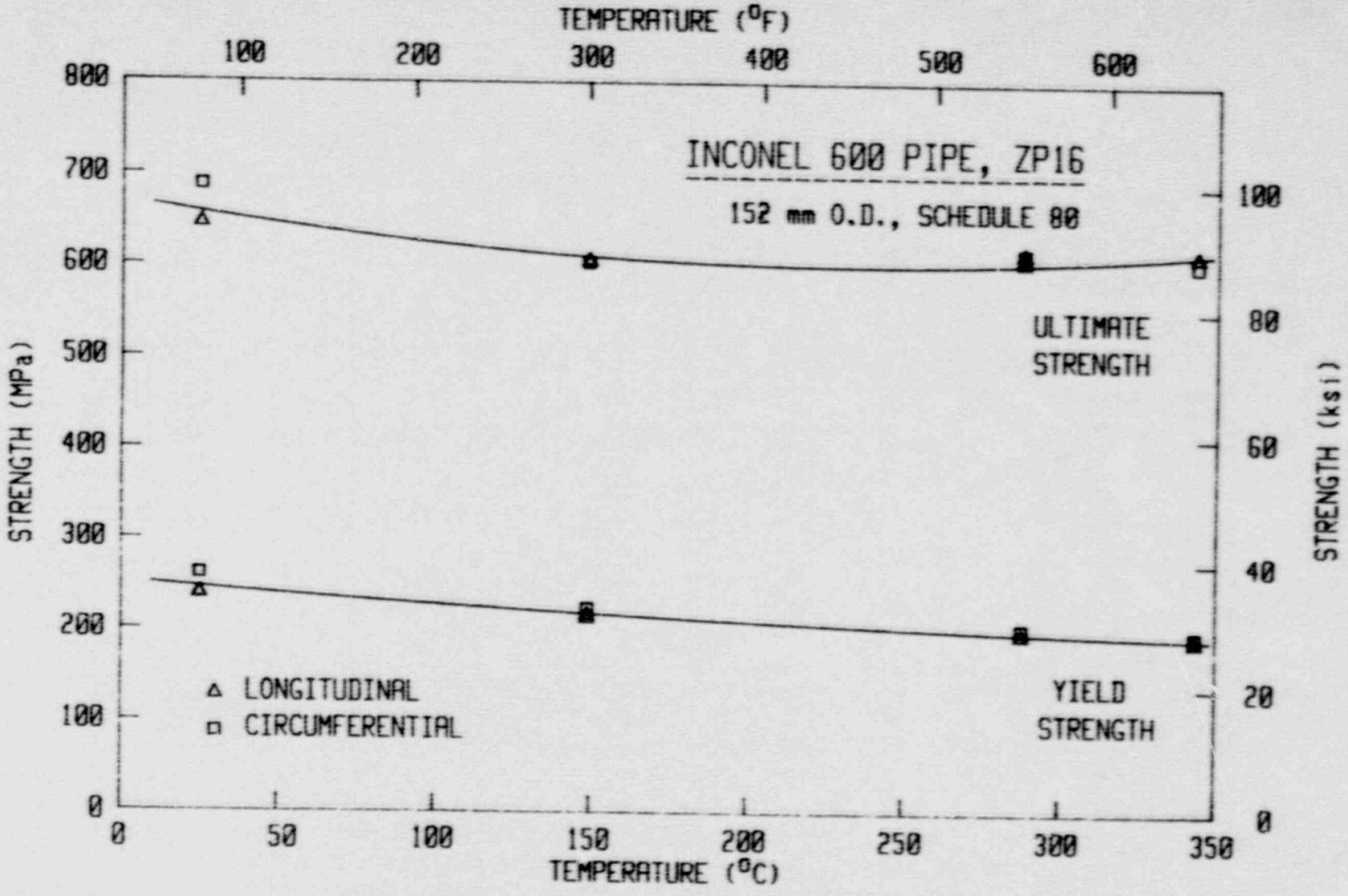

Fig. 5-1 Tensile strength data for Inconel 600 (Heat ZP16).

Table 5-3 J-R Results for Inconel 600 (Heat ZP16)

Specimen Number	Orient.	Test Temp.	Side Groove	$(a/W)_o$	δa_m	$\delta a_p - \delta a_m$	J_{Ic}		K_{Jc}		T_{avg}		Flow Strength
							P.L.	ASTM	P.L.	ASTM	P.L.	ASTM	
		(°C)	(%)		(mm)	(mm)	(kJ/m^2)	(kJ/m^2)	($MPa\sqrt{m}$)	($MPa\sqrt{m}$)			(MPa)
ZP16-1LC	L-C	24	0	0.527	3.07	-0.07	3958.3	------	887.3	-----	567	---	441.5
ZP16-2LC	L-C	149	0	0.518	----	-----	2170.2	1988.8	656.7	628.6	436	---	410.2
ZP16-4LC	L-C	149	0	0.534	3.06	-0.11	2746.0	------	738.7	-----	531	---	410.2
ZP16-3LC	L-C	288	0	0.512	----	-----	1929.2	1631.5	606.7	557.9	281	494	402.9
ZP16-7LC	L-C	24	20	0.535	4.29	-0.33	2676.3	2369.3	742.2	698.3	575	574	441.5
ZP16-12LC	L-C	24	20	0.535	4.39	-0.26	2328.1	2146.5	692.2	664.6	516	552	441.5
ZP16-8LC	L-C	149	20	0.546	4.44	-0.47	2146.7	1929.4	653.1	619.2	488	564	410.2
ZP16-9LC	L-C	204	20	0.536	4.82	-0.44	2074.0	1870.1	636.8	604.7	486	548	405.4
ZP16-13LC	L-C	204	20	0.547	4.28	-0.45	1959.5	------	618.9	-----	452	---	405.4
ZP16-10LC	L-C	288	20	0.567	4.26	-0.32	2161.0	1819.5	642.1	589.2	482	594	402.9
ZP16-6LC	L-C	343	20	0.534	4.75	-0.84	2054.9	1684.0	620.9	562.1	489	590	401.9
ZP16-11LC	L-C	343	20	0.532	5.31	-0.58	1662.8	1562.6	558.5	541.4	483	460	401.9
ZP16-1CL	C-L	24	20	0.559	4.76	-0.46	1475.4	1420.5	551.0	540.7	430	427	474.4
ZP16-2CL	C-L	149	20	0.541	5.32	-0.57	1428.6	1351.4	532.8	518.2	426	435	413.9
ZP16-3CL	C-L	204	20	0.553	5.28	-0.72	1464.7	1292.9	535.1	502.7	472	476	405.4
ZP16-4CL	C-L	288	20	0.568	2.80	-0.44	1452.9	1348.2	526.5	507.2	480	395	409.1
ZP16-5CL	C-L	343	20	0.536	4.26	-1.04	1590.6	1331.2	546.2	499.7	479	577	400.0

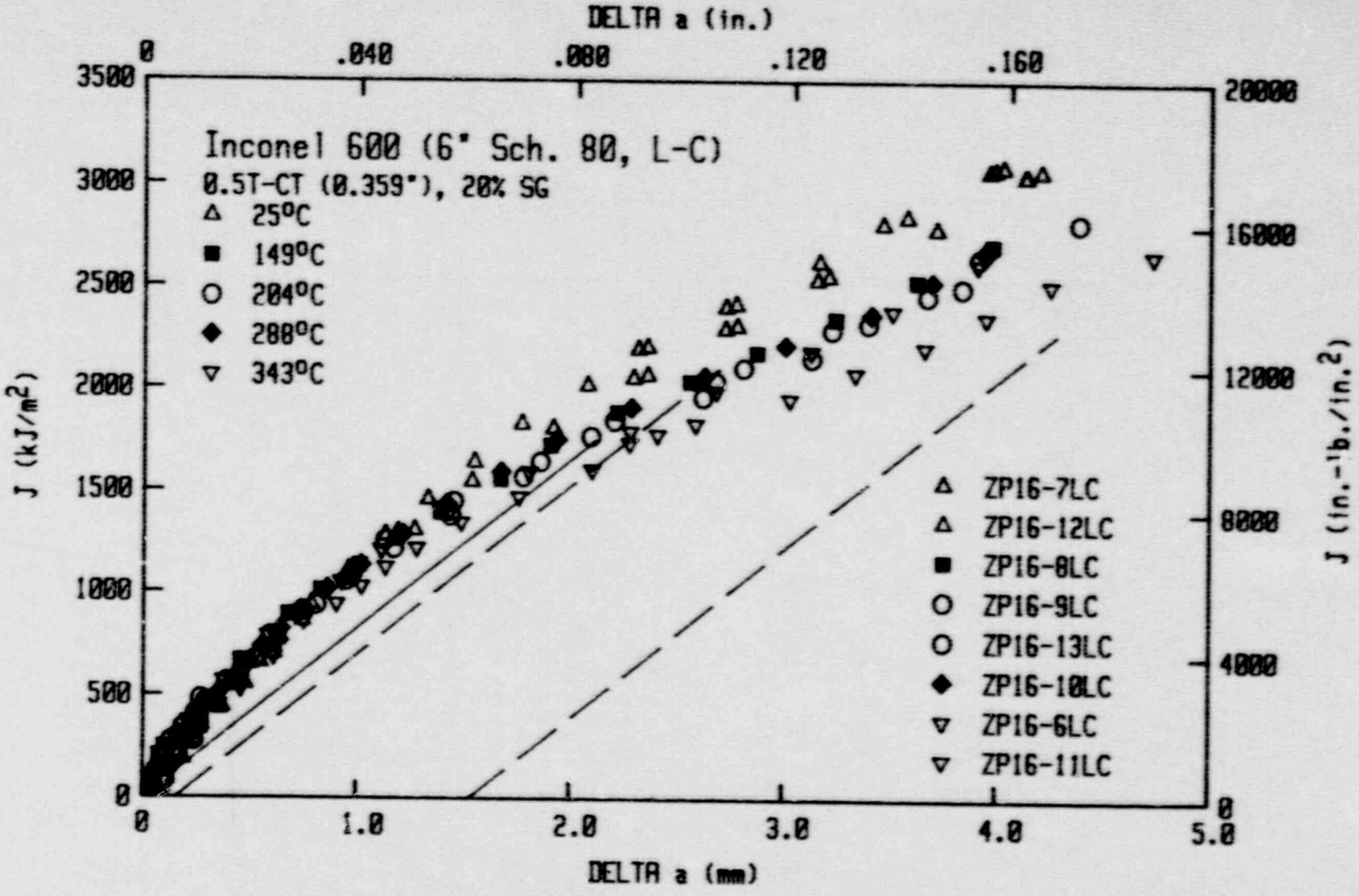

Fig. 5-2 J-R curves for the L-C orientation of Inconel 600 (Heat ZP16), using side-grooved specimens. These curves are almost invariant with temperature.

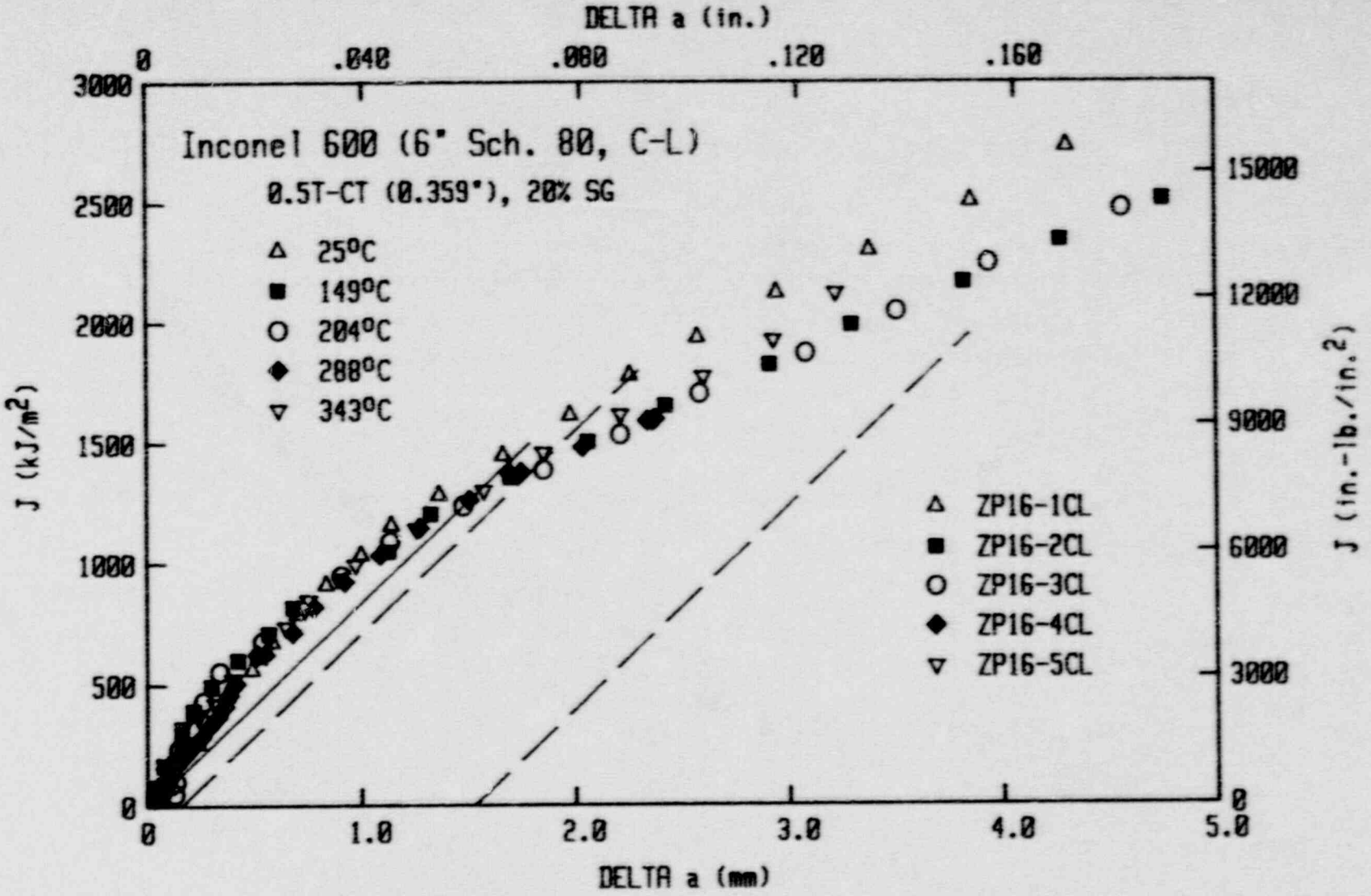

Fig. 5-3 J-R curves for the C-L orientation of Inconel 600 (Heat ZP16), using side-grooved specimens. These curves are almost invariant with temperature.

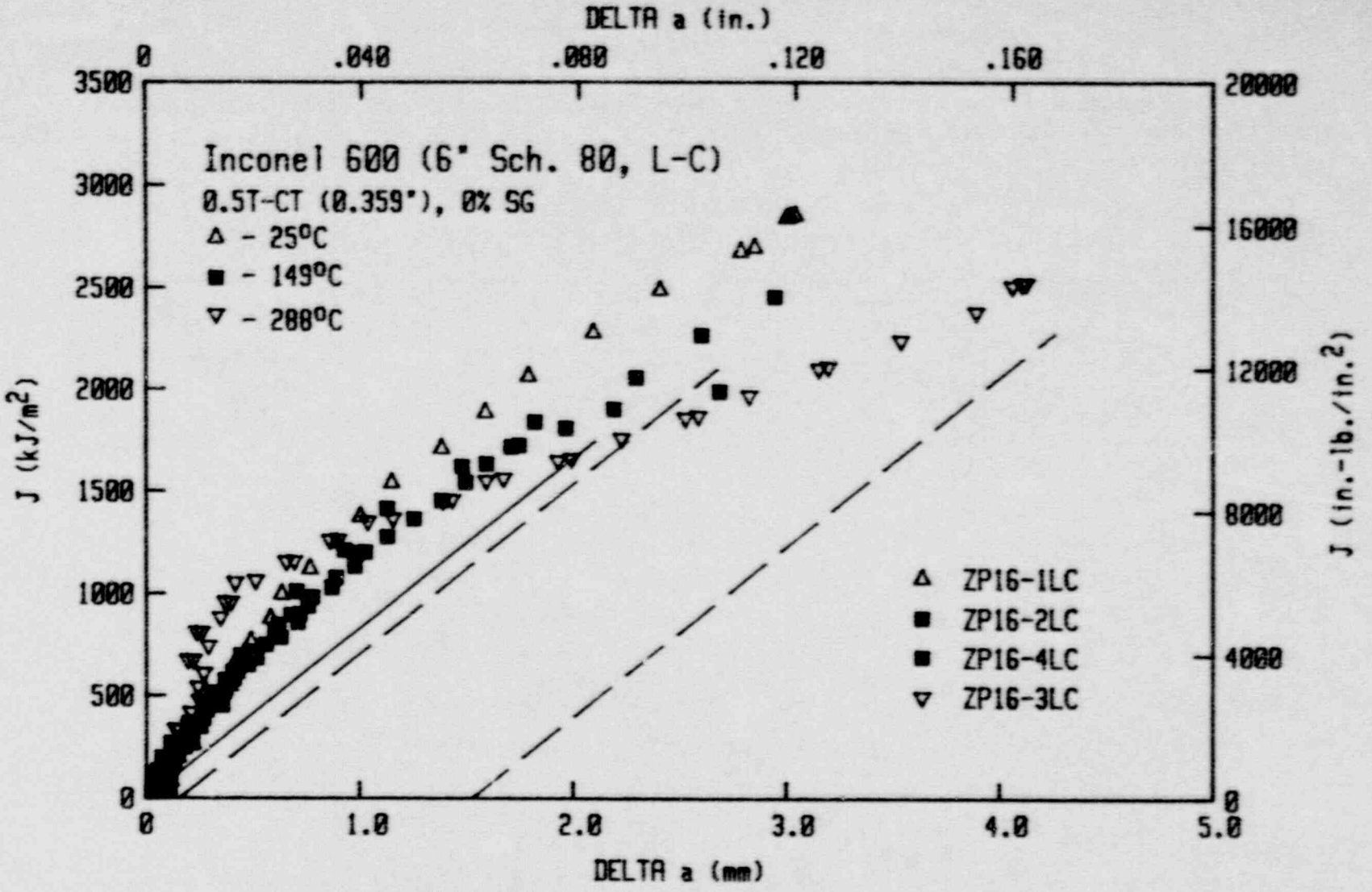

Fig. 5-4 J-R curves for the L-C orientation of Inconel 600 (Heat ZP16), using plane-sided specimens. These curves demonstrate a mild sensitivity to temperature.

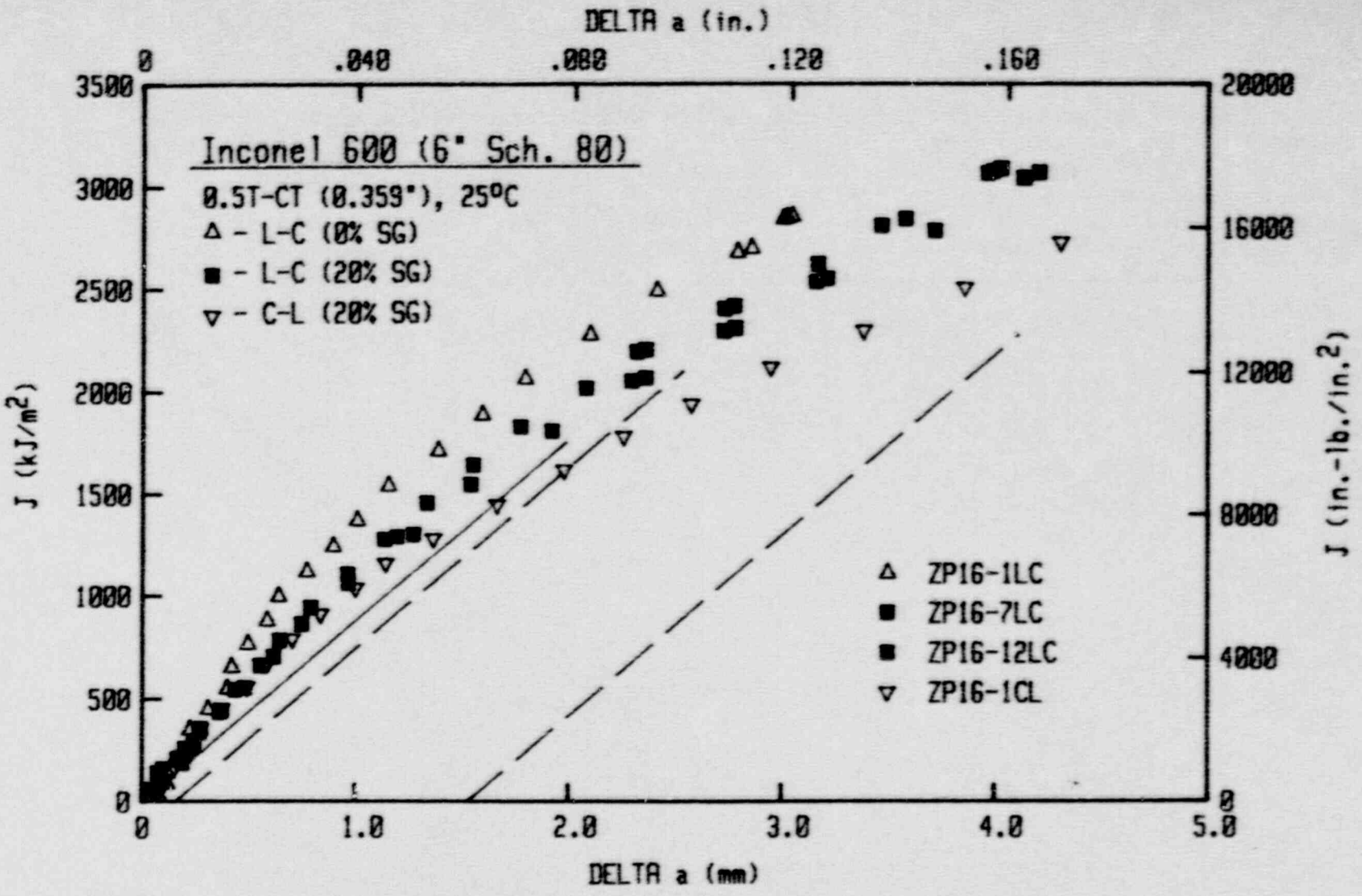

Fig. 5-5 J-R curves for Inconel 600 (Heat ZP16) at 25°C. There is a slight effect of side-grooving and the C-L orientation gives slightly lower J-R curves than the L-C orientation.

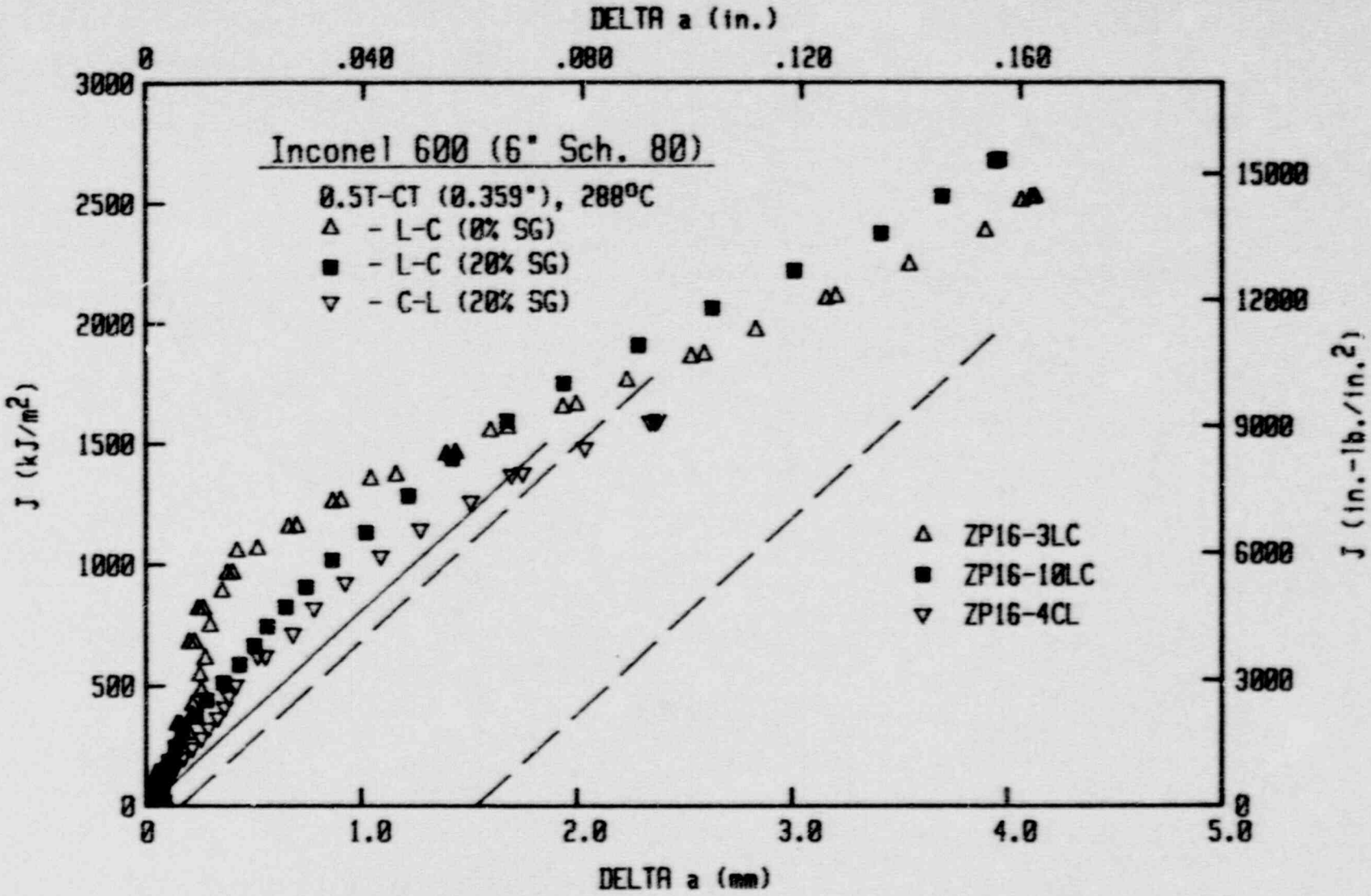

Fig. 5-6 J-R curves for Inconel 600 (Heat ZP16) at 288°C. There is no significant effect of side-grooving and the C-L orientation gives slightly lower J-R curves than the L-C orientation.

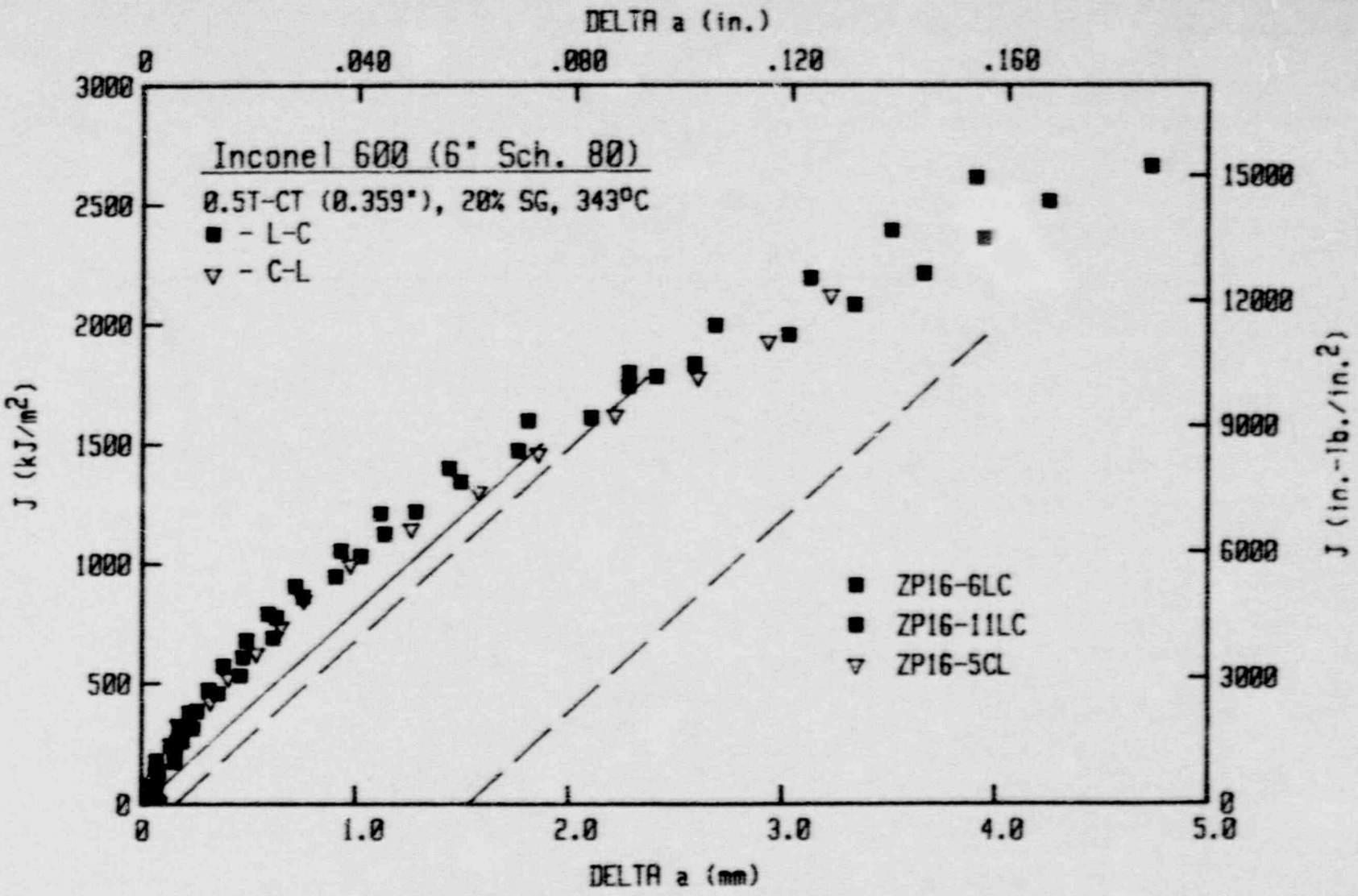

Fig. 5-7 J-R curves for Inconel 600 (Heat ZP16) at 343°C. The C-L and the L-C orientations give similar J-R curves.

6. EFFECT OF FLATTENING SPECIMEN BLANKS

6.1 Background

With the small diameter and/or thin wall typical of the piping in many nuclear power plant applications, the largest specimens which can be removed from the pipe restrict the J-R curve validity range to extremely small crack growth ranges, frequently preventing sufficient crack growth for any reasonable structural integrity assessment. One method for obtaining sufficiently large crack growth is to flatten sections of the pipe to make specimen blanks, thereby increasing the effective planar dimensions of the specimens. This method would increase the amount of crack growth possible for the material, while allowing for the specimen size to be maintained to almost the full pipe thickness.

This small study was undertaken to determine the effect of flattening on the resultant J-R curve, and also to determine if a stress relief heat treatment could negate the strain history of the material and restore the virgin toughness.

6.2 Materials and Test Conditions

The two materials used in this study were a carbon steel (A 106 Grade B, Heat ZP1) and a stainless steel (SA 376 Type 304, Heat ZP2). Each pipe was a 6 in. nominal diameter, Schedule 80 (168.3 mm O.D. x 11 mm wall, or 6.625 in. O.D. x 0.432 in. wall). For this pipe size, full thickness 0.394T-CT specimens (Fig. 6-1) could be used to assess as-received toughness. In addition, 1T- and 2T-CT plan-form specimens (Fig. 6-2 and 6-3) were machined from flattened blanks; the strain induced by the flattening process was calculated at +7%. The thickness of these plan-form specimens was identical to that of the full thickness 0.394T-CT specimens at 10 mm (0.394 in.). One-half of the flattened blanks were also given a stress-relief heat treatment, with these specimens referred to as "FSR" for flattened and stress relief heat treated. For the carbon steel, the heat treatment was a 2 h soak at 593°C (1100°F), with a furnace cool. For the stainless steel, the heat treatment was a 2 h soak at 427°C (800°F) with a furnace cool.

All of these specimens were side-grooved by 20% (10% per side) to induce straight crack growth. The crack growth orientation was the C-L direction per ASTM E 399. Testing was at ambient temperature, although the 2T-CT plan-form tests of the carbon steel were made at 57°C (135°F) to preclude brittle fracture of these specimens.

For analysis of the test data, tensile properties from mill tests were used. For the carbon steel, the mill tests indicated a yield strength of 330 MPa (47.8 ksi) and an ultimate strength of 504 MPa (73.1 ksi), for a flow strength of 417 MPa (60.45 ksi). For the stainless steel, the yield strength from the mill report was 358 MPa (51.9 ksi) and the flow strength was 486 MPa (70.5 ksi).

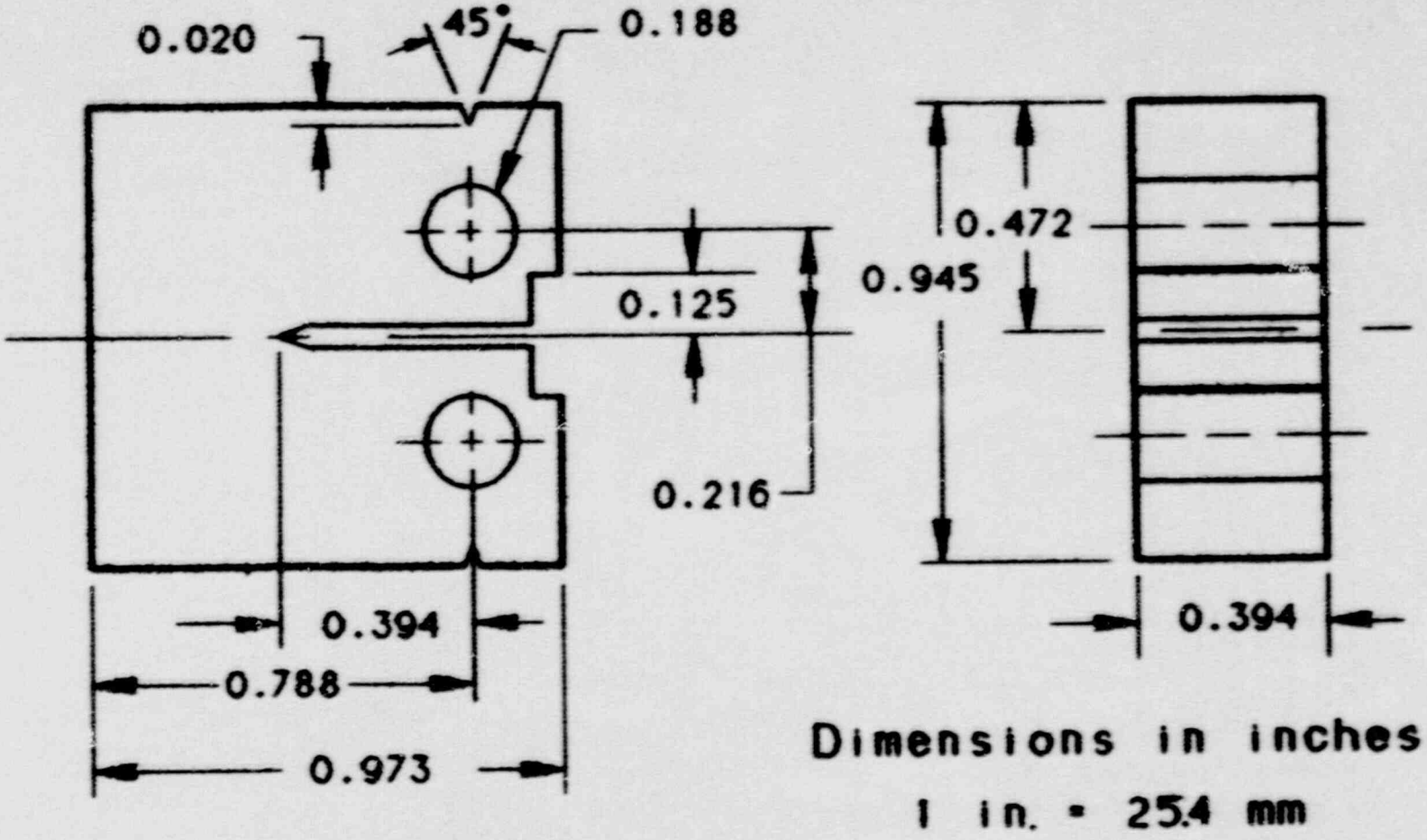

Fig. 6-1 The flattening study used this 0.394T-CT specimen design with a thickness of 10 mm (0.394 in.).

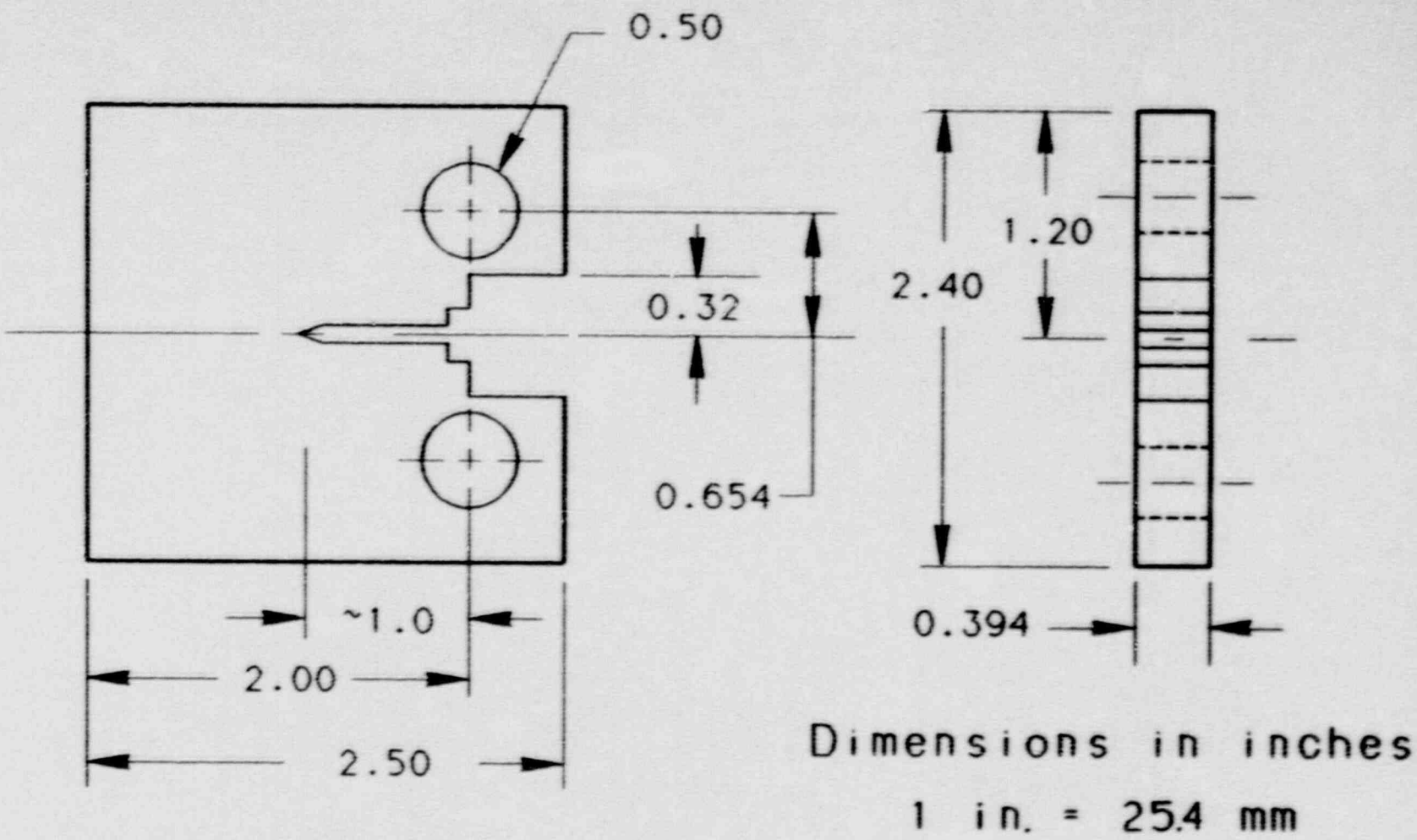

Fig. 6-2 The flattening study used this 1T-CT specimen design with a thickness of 10 mm (0.394 in.).

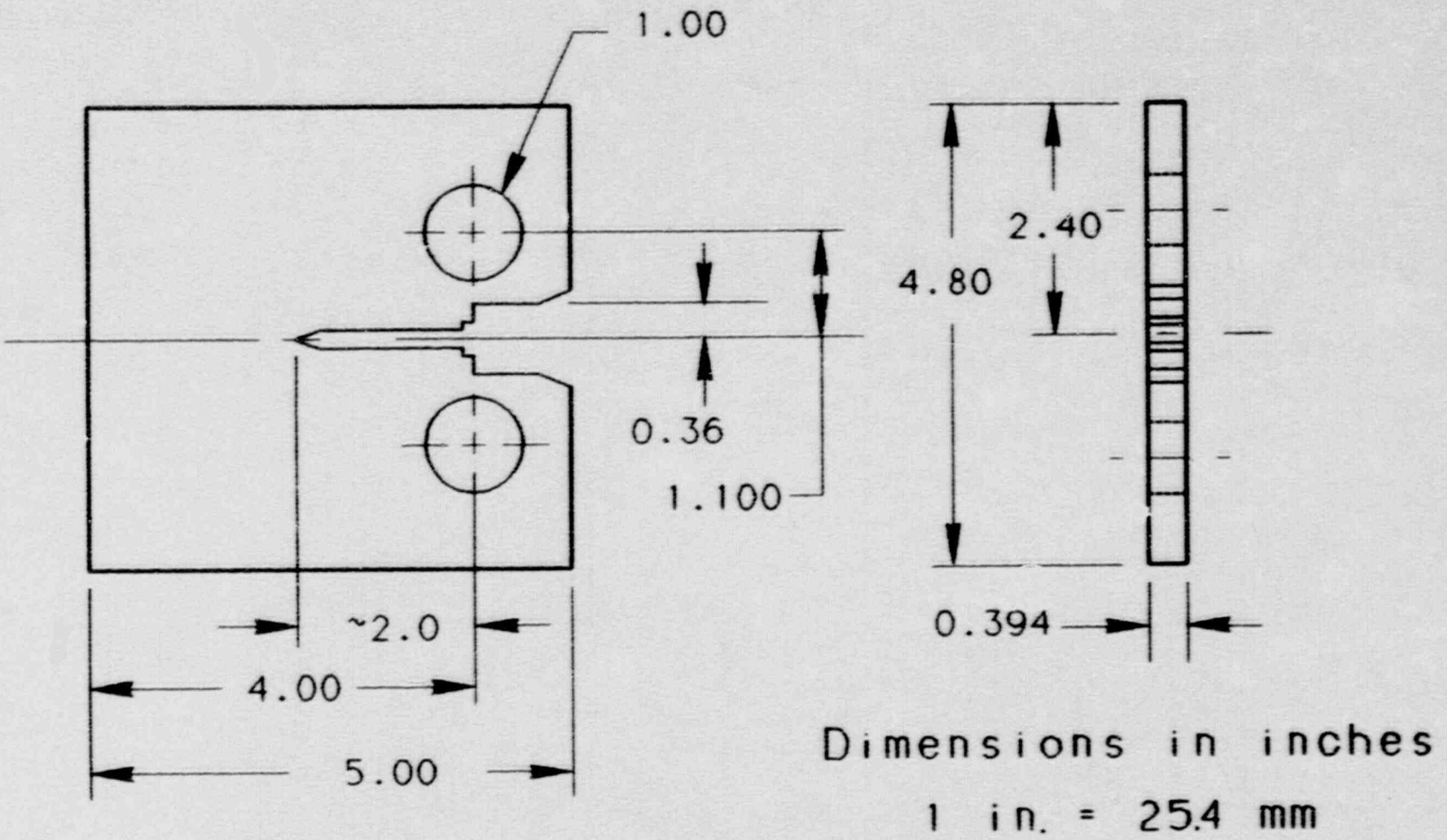

Fig. 6-3 The flattening study used this 2T-CT specimen design with a thickness of 10 mm (0.394 in.).

The effect of flattening followed by a stress relief at 593°C (1100°F) for 2 h was previously studied for another heat of A 106 Grade B pipe (Ref. 20). The latter was a 12 in. nominal diameter Schedule 160 pipe (324 mm OD x 33.3 mm wall, or 12.75 in. diameter x 1.31 in. wall). In this case the strain induced by the flattening process was ±11.5%, slightly greater than the ±7% for the fracture toughness tests. For the tensile tests, the yield strength was found to increase significantly after the flattening and stress relief treatment, but the ultimate strength did not change noticeably (Table 6-1). The properties for the as-received or the "unflattened" condition were determined for the nominal mid-plane of the pipe, whereas the FSR condition was sampled at the nominal OD and ID locations. Averaging together the results for the two locations for the flattened and heat-treated condition, the yield strength is found to increase by 24% at 23°C (75°F) and by 28.5% at 288°C (550°F). In contrast, the ultimate strength increased by only 1.1% and 0.6% at the two test temperatures. The flow strength increased by 9-10% at each test temperature. These specimens were oriented in the circumferential orientation, which is pertinent to the C-L orientation for fracture toughness tests. Therefore, for this orientation the effect of flattening is not mitigated by a stress relief heat treatment, and the apparent yield (and the flow) strength is increased for the flattened material.

6.3 Results

The J-R curve results are summarized in Tables 6-2 and 6-3 for the carbon steel and the stainless steel, respectively. Comparisons will be made using plots of the actual J-R curve data, along with the J_{Ic} and T_{avg} values. For both materials, tests of unflattened material were concentrated at ambient temperature (23°C or 75°F), with a single test at 52°C (125°F) to give an indication of the temperature sensitivity of these materials.

For the A 106 Grade B material, data for the unflattened condition are illustrated in Fig. 6-4, as the higher test temperature (52°C or 125°F) demonstrates similar J levels to those for the ambient temperature tests. Since the 2T-CT plan-form specimens were tested at a higher temperature (57°C or 135°F) due to brittle (cleavage) fracture of two of the 1T-CT plan-form specimens, the measured J levels for the 2T-CT specimens should be comparable to those for all of the tests at ambient temperature, as the effect of test temperature should be similar for all specimen sizes and was found to be insignificant for this material.

In contrast to data for the as-received condition, the flattened and the FSR conditions exhibit reduced toughness, as evidenced by lower J_{Ic} values and overall lower J levels using modified J, J_M in (Fig. 6-5). In contrast, the use of J_D (Fig. 6-6) indicates similar toughness for the three conditions. As mentioned previously, the tests of 1T-CT plan-form specimens resulted in two brittle fractures. In Δa space, the flattened only specimen exhibited only ~ 0.25 mm (0.010 in.) of stable crack growth prior to fracture, and the FSR condition specimen failed after only 0.8 mm (0.031 in.) of

Table 6-1 Tensile Properties of A 106 Grade B Before and After Flattening and Stress Relief Anneal

Specimen ID	Thickness Location	Test Temp. (°C)	0.2% Offset Yield Strength (MPa)	(ksi)	Ultimate Strength (MPa)	(ksi)	Elongation in 25.4 mm (%)	Reduction In Area (%)
As-Received (Unflattened)								
ZP4-R1-13	MID	23	300	43.6	553	80.2	30.8	43.5
ZP4-R1-15	MID	23	294	42.6	550	79.8	29.9	41.8
ZP4-R1-17	MID	23	295	42.8	543	78.7	29.2	43.5
Average		23	296	43.0	549	79.6	30.0	42.9
ZP4-R1-14	MID	288	269	39.0	532	77.2	25.7	42.2
ZP4-R1-16	MID	288	272	39.5	531	77.0	23.0	45.8
ZP4-R1-18	MID	288	251	36.4	534	77.4	24.6	43.4
Average		288	264	38.3	532	77.2	24.3	43.8
Flattened and Stress Relief Annealed								
ZP4-R1F-13	ID	23	386	56.0	573	83.2	22.2	42.4
ZP4-R1F-16	OD	23	363	52.7	535	77.7	30.1	44.7
ZP4-R1F-18	OD	23	365	52.9	534	77.5	27.6	42.9
ZP4-R1F-19	ID	23	358	51.9	576	83.5	24.8	44.0
Average		23	368	53.4	555	80.5	26.2	43.5
ZP4-R1F-14	OD	288	323	46.8	519	75.2	21.8	40.9
ZP4-R1F-15	ID	288	342	49.5	549	79.7	21.1	37.3
ZP4-R1F-17	ID	288	353	51.2	553	80.2	32.2	37.9
ZP4-R1F-19	OD	288	339	49.1	521	75.6	22.5	44.0
Average		288	339	49.2	536	77.7	24.4	40.0

Table 6-2 J-R Curve Results from the A106 Grade B Flattening Study

Specimen ID	Test Temp. (°C)	$(a/W)_o$	Δa_p (mm)	Δa_m (mm)	$(\Delta a_p - \Delta a_m)$ (mm)	J_M		J_D	
						J_{Ic}[a] (kJ/m^2)	T_{avg}[a]	J_{Ic}[a] (kJ/m^2)	T_{avg}[a]
0.394T-CT									
Unflattened									
EPCS-1	52	0.502	4.81	5.66	-0.85	116.1	98	114.2	71
EPCS-2	23	0.517	4.75	5.22	-0.47	103.3	128	102.0	99
EPCS-3	23	0.514	4.74	5.31	-0.57	105.0	119	104.5	90
EPCS-4	23	0.513	2.50	3.03	-0.53	92.5	106	91.6	82
1T-CT									
Flattened Only									
106BF1T-1	23	0.502	11.14	12.07	-0.93	75.5	71	75.2	65
106BF1T-2	23	0.540	---[b]	---[b]	---[b]	82.2	--[b]	81.6	--[b]
FSR Condition									
106BFST-1	23	0.515	---[b]	---[b]	---[b]	76.9	--[b]	76.5	--[b]
106BFST-2	23	0.513	11.86	12.75	-0.89	70.0	85	70.0	78
2T-CT									
Flattened									
106BF2T	57	0.504	26.77	28.04	-1.27	51.3	75	51.3	73
FSR Condition									
106BFS2T	57	0.503	26.34	26.28	+0.06	62.4	86	62.7	83

[a] From a power law analysis.

[b] Cleavage fracture precluded determination of this quantity.

Table 6-3 J-R Curve Results from the Type 304 Stainless Flattening Study

Specimen ID	Test Temp.	$(a/W)_o$	Δa_p	Δa_m	$(\Delta a_p - \Delta a_m)$	J_M		J_D	
						J_{Ic}[a]	T_{avg}[a]	J_{Ic}[a]	T_{avg}[a]
	(°C)		(mm)	(mm)	(mm)	(kJ/m^2)		(kJ/m^2)	
0.394T-CT									
Unflattened									
EPSS-1	25	0.558	4.56	5.15	-0.59	1274.2	365	1042.9	192
EPSS-2	23	0.526	1.35	1.46	-0.11	(1282.5)[b]	---	1006.5	---
EPSS-3	23	0.537	1.26	1.37	-0.11	(1287.1)[b]	---	958.2	---
EPSS-4	52	0.530	3.76	4.36	-0.60	849.5	271	756.5	143
1T-CT									
Flattened Only									
304F1T-1	24	0.517	10.88	11.22	-0.34	827.8	346	775.7	313
304F1T-2	23	0.512	4.70	4.80	-0.10	818.6	231	771.1	196
FSR Condition									
304FST-1	23	0.511	11.59	12.02	-0.43	830.3	273	793.7	229
304FST-2	24	0.514	11.47	11.85	-0.38	821.9	285	788.4	236
2T-CT									
Flattened Only									
304F2T	26	0.510	13.08	13.03	+0.05	457.7	319	450.1	302
Flattened and SR									
304FS2T	23	0.510	15.01	15.24	-0.23	345.1	439	380.2	411

[a] From a power law analysis.

[b] An extrapolated value (data do not cross the 0.15 mm exclusion line).

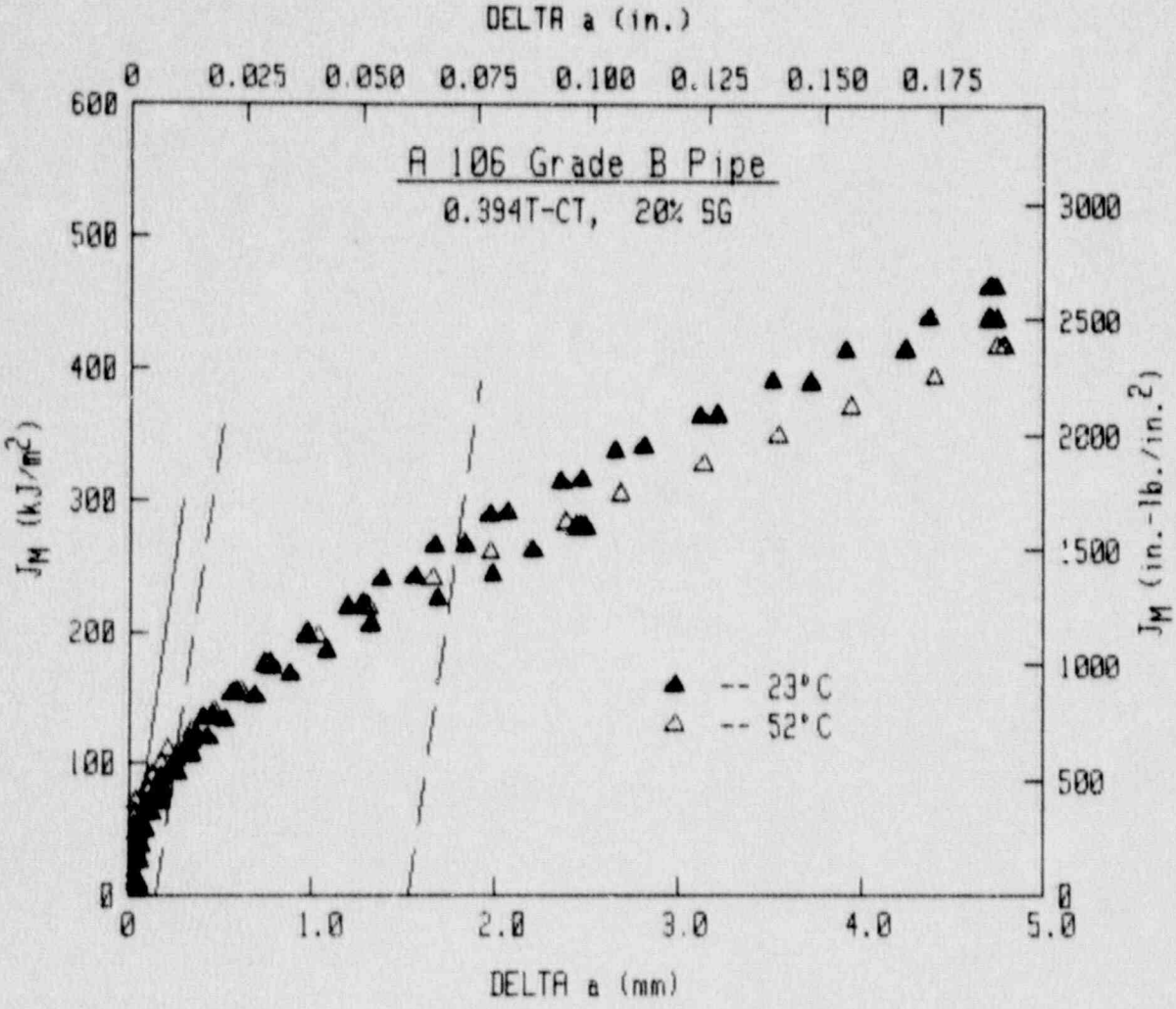

Fig. 6-4 J-R curves for A 106 Gr. B in the unflattened condition indicate similar J levels at 23°C and 52°C.

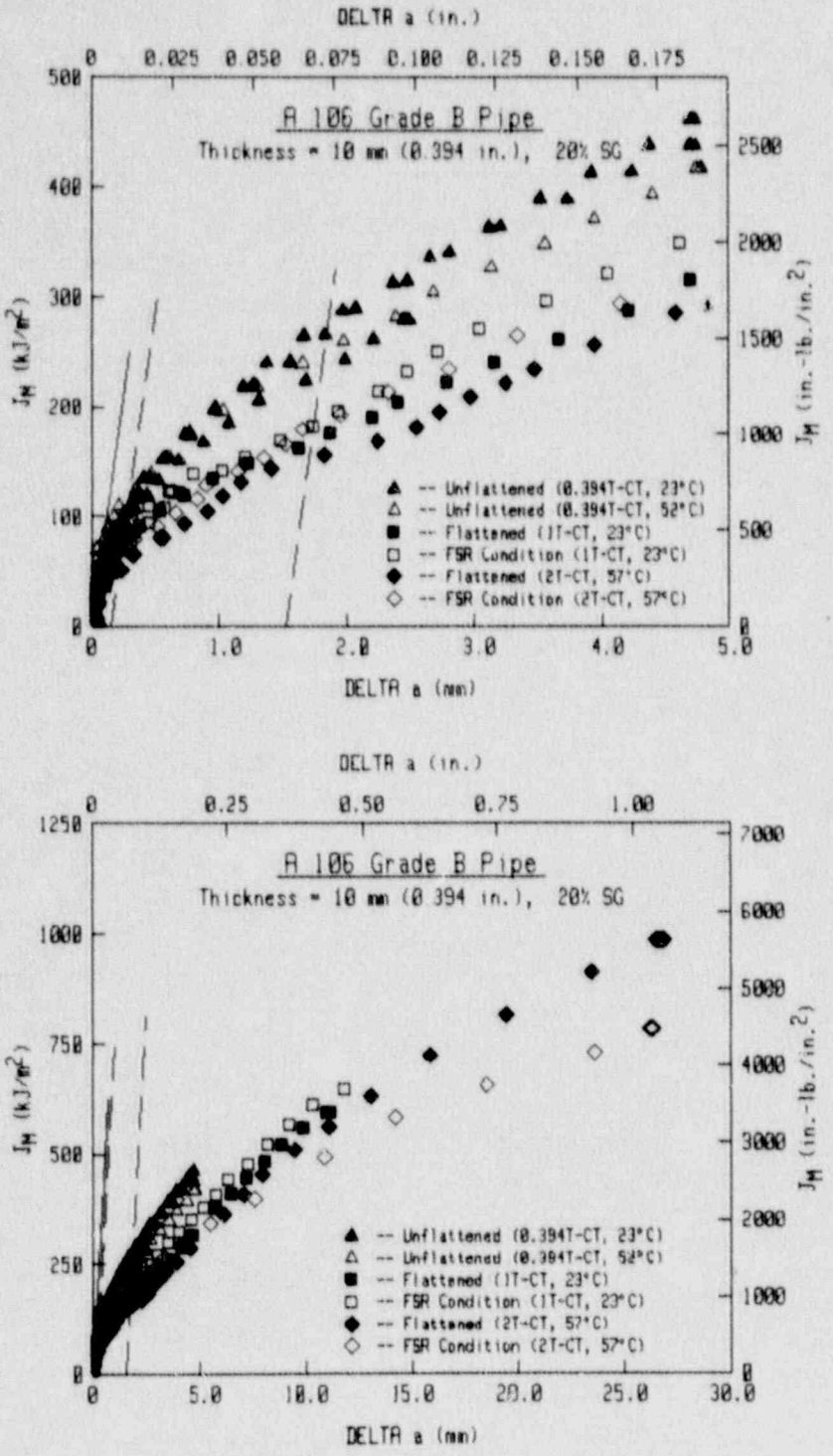

Fig. 6-5 J_M-R curves for A 106 Gr. B in the unflattened, flattened and FSR conditions indicate large reductions in toughness due to the stress history of the specimens, as compared to the as-received condition.

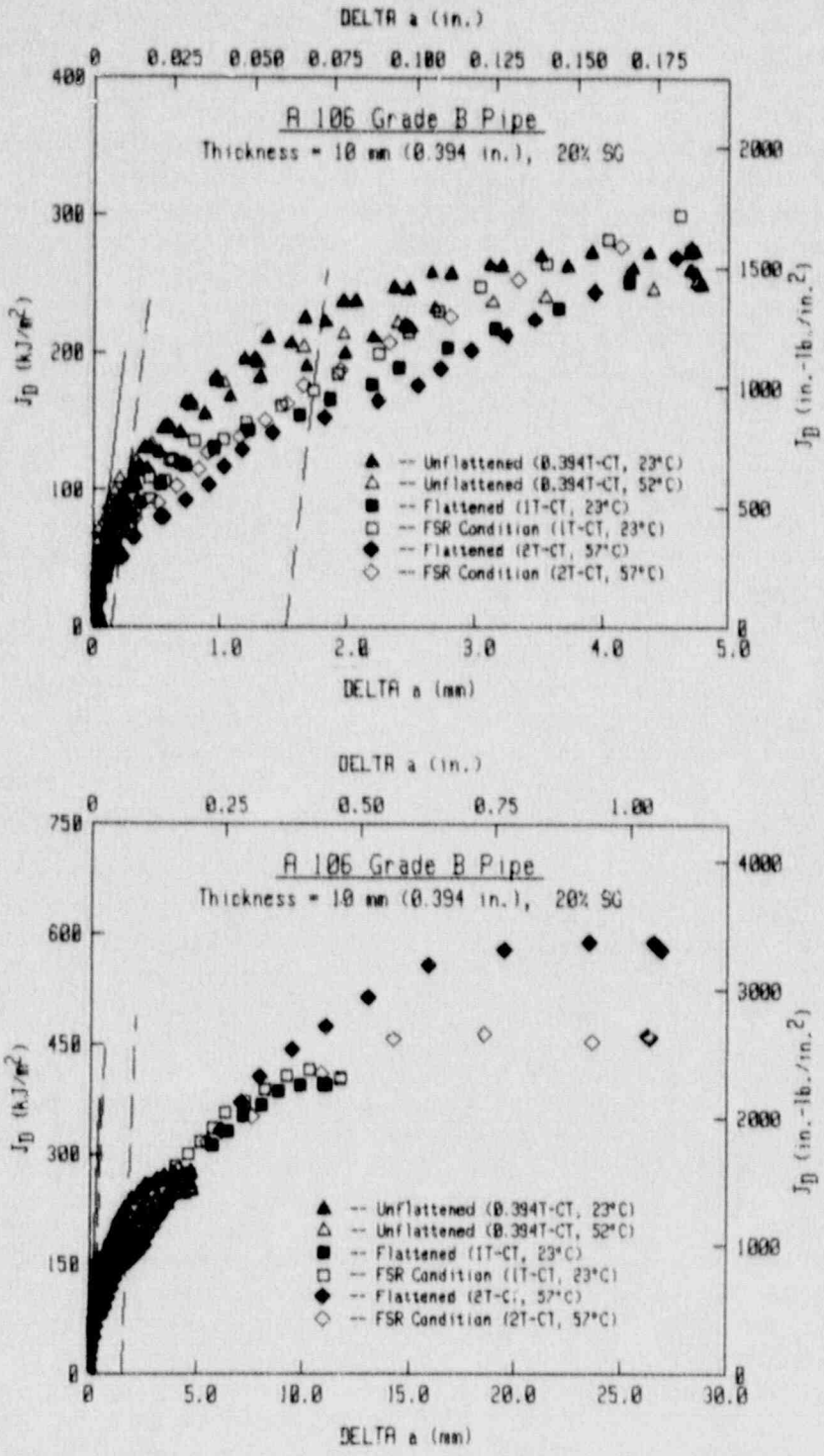

Fig. 6-6 J_D-R curves for A 106 Gr. B in the unflattened, flattened and FSR conditions indicate no significant changes in toughness due to the stress history of the specimens, as compared to the as-received condition.

stable crack growth. In contrast, the other 1T-CT plan-form specimens exhibited fully ductile fracture until the crack growth exceeded 50% of the initial unbroken ligament (~ 12.7 mm or 0.5 in.) and the test was terminated. The stress relief anneal did result in slight recovery of the toughness lost in the flattening process, principally as evidenced by the increase in the T_{avg} levels for those specimens. From the fracture surfaces for these specimens (Fig. 6-7), the unflattened specimens exhibit straight crack growth, but the flattened specimens exhibit significant irregular crack growth, with presumeably the ID side exhibiting more crack growth than the OD side due to the presence of tensile residual strain on the ID side and residual compressive strain on the OD side. In contrast, the FSR condition specimens exhibit straight crack growth for the 2T-CT plan-form specimen but irregular crack growth for the 1T-CT specimen, with the slope of the crack front in the latter case similar to that for the flattened condition.

Similar results can be found for the stainless steel as well. As illustrated in Fig. 6-8, the data for the unflattened condition exhibit some differences, as the curve for the test at 52°C (125°F) lies much lower than the other three curves. In this case, two of the specimens were tested to only 1.26 mm (0.05 in.) and 1.37 mm (0.54 in.) of crack growth, due to equipment limitations. The other two specimens were tested to greater crack growth amounts of 3.76 mm (0.148 in.) and 4.57 mm (0.18 in.). Although the effect of test temperature is not tremendously large for this stainless steel, the difference with the carbon steel, where no effect was found, is noteworthy.

As with the carbon steel, the flattened and FSR conditions of the stainless steel exhibit a significant reduction in toughness, principally in terms of J levels, including J_{Ic} and T_{avg}, using J_M but not using J_D (Fig. 6-9 and 6-10). One noteworthy observation from the evaluations using J_M (Fig. 6-9) is that the as-received condition test at 52°C (125°F) yields similar J_M levels to the flattened and the FSR conditions. The stress relief heat treatment does not provide any significant recovery in toughness for either the 1T- or the 2T-CT plan-form specimens. In addition, some effect of specimen size is apparent, as the data from the 1T-CT plan-form specimens are consistently higher than that for the 2T-CT specimens. This possible size effect may be due to the small number of specimens or could indicate a systematic size dependence. In contrast, using J_D indicates no significant differences in the overall J levels for the flattened and the FSR conditions. Therefore, the effect of flattening is not easily discerned due to the different specimen sizes and the different J equations used. The differences between J_M and J_D are due to the unbroken ligament differences in the different specimen sizes. Since one would expect to see some differences in the J-R curves due to flattening, then one could say that J_M does a better job in this case.

The fracture surfaces of the stainless steel specimens (Fig. 6-11) exhibit nominally straight crack growth for the as-received (unflattened) condition tests and some non-uniformity for both the 1T- and the 2T-CT plan-form specimens.

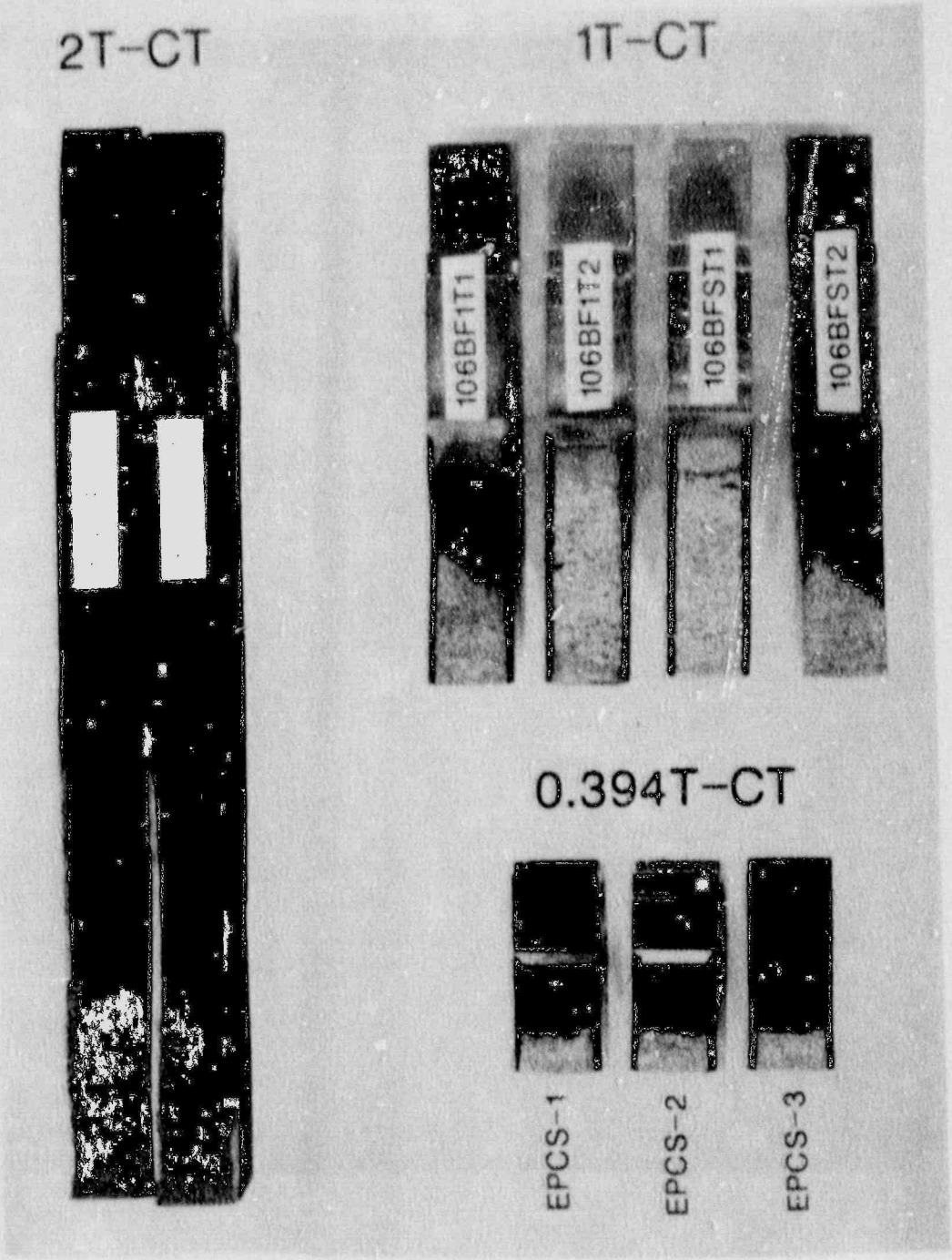

Fig. 6-7 Fracture surface photographs for the A 106 Gr. B specimens indicate straight (uniform) crack growth for the as-received condition and generally non-uniform crack growth for the flattened and the FSR conditions.

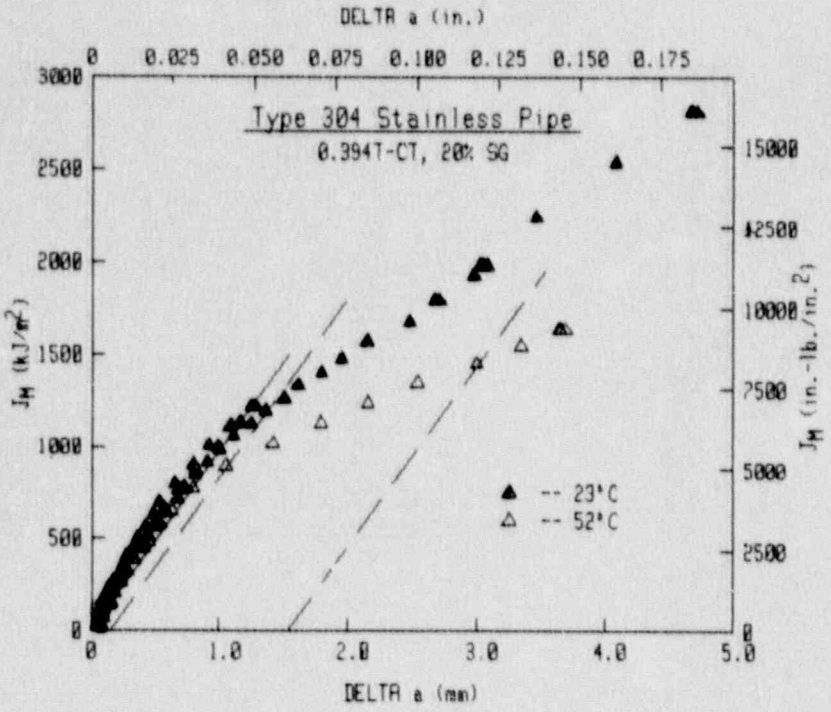

Fig. 6-8 J-R curves for Type 304 stainless steel in the unflattened condition indicate noticeable differences in J levels at 23°C and 52°C.

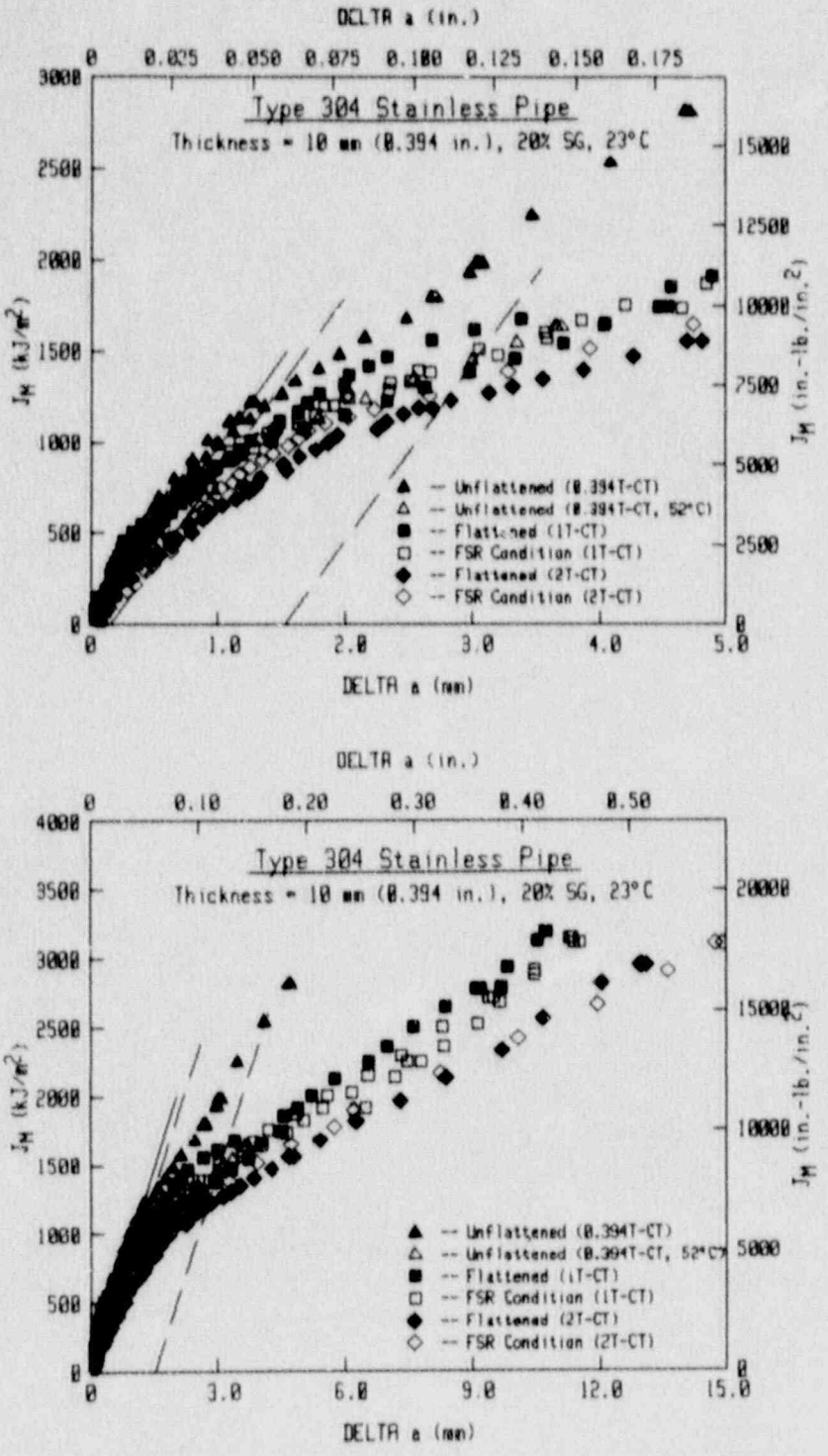

Fig. 6-9 J_M-R curves for Type 304 stainless steel in the unflattened, flattened and FSR conditions indicate large reductions in toughness due to the stress history of the specimens, as compared to the as-received condition.

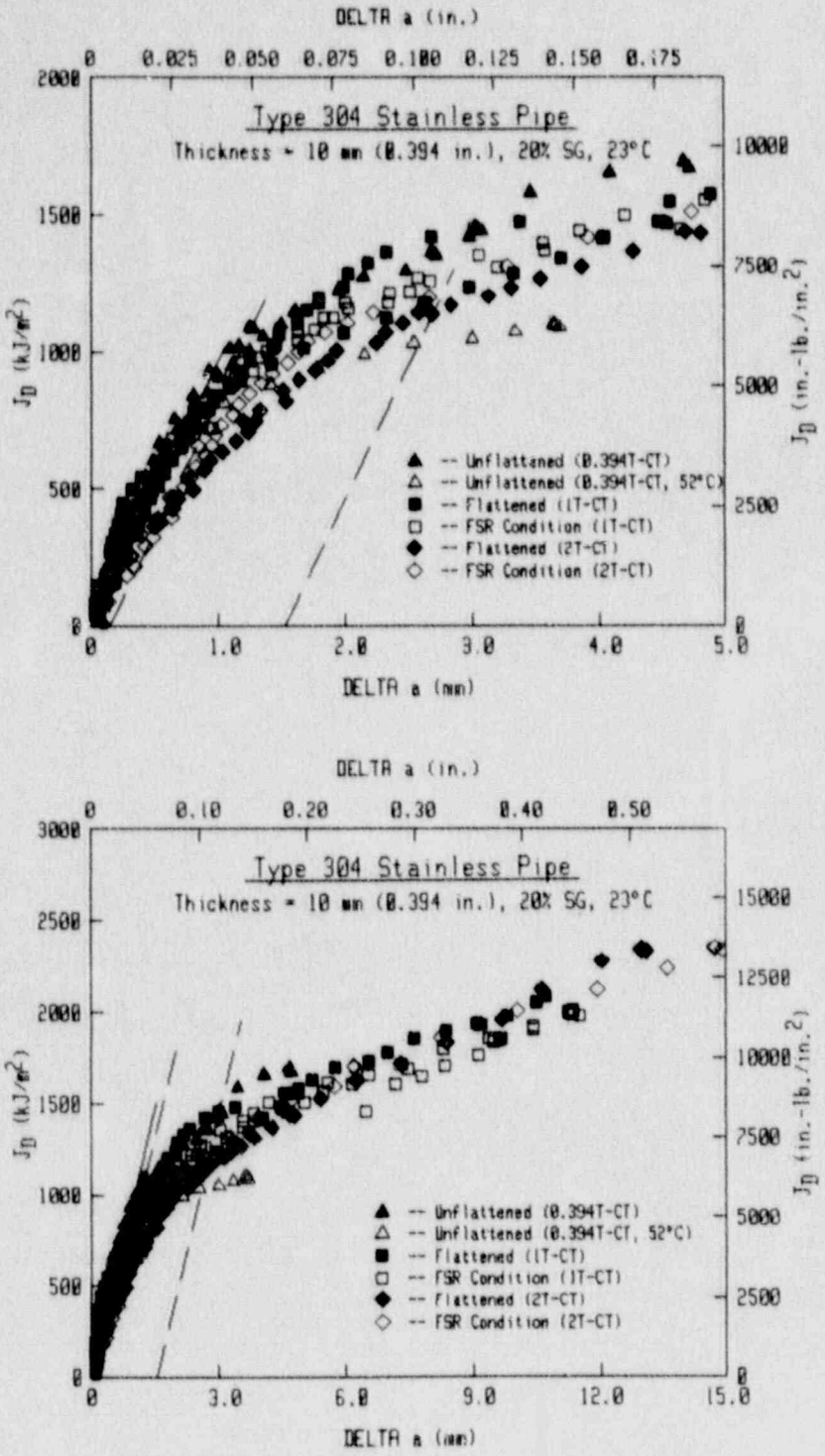

Fig. 6-10 J_D-R curves for Type 304 stainless steel in the unflattened, flattened and FSR conditions indicate no significant change in toughness due to the stress history of the specimens, as compared to the as-received condition.

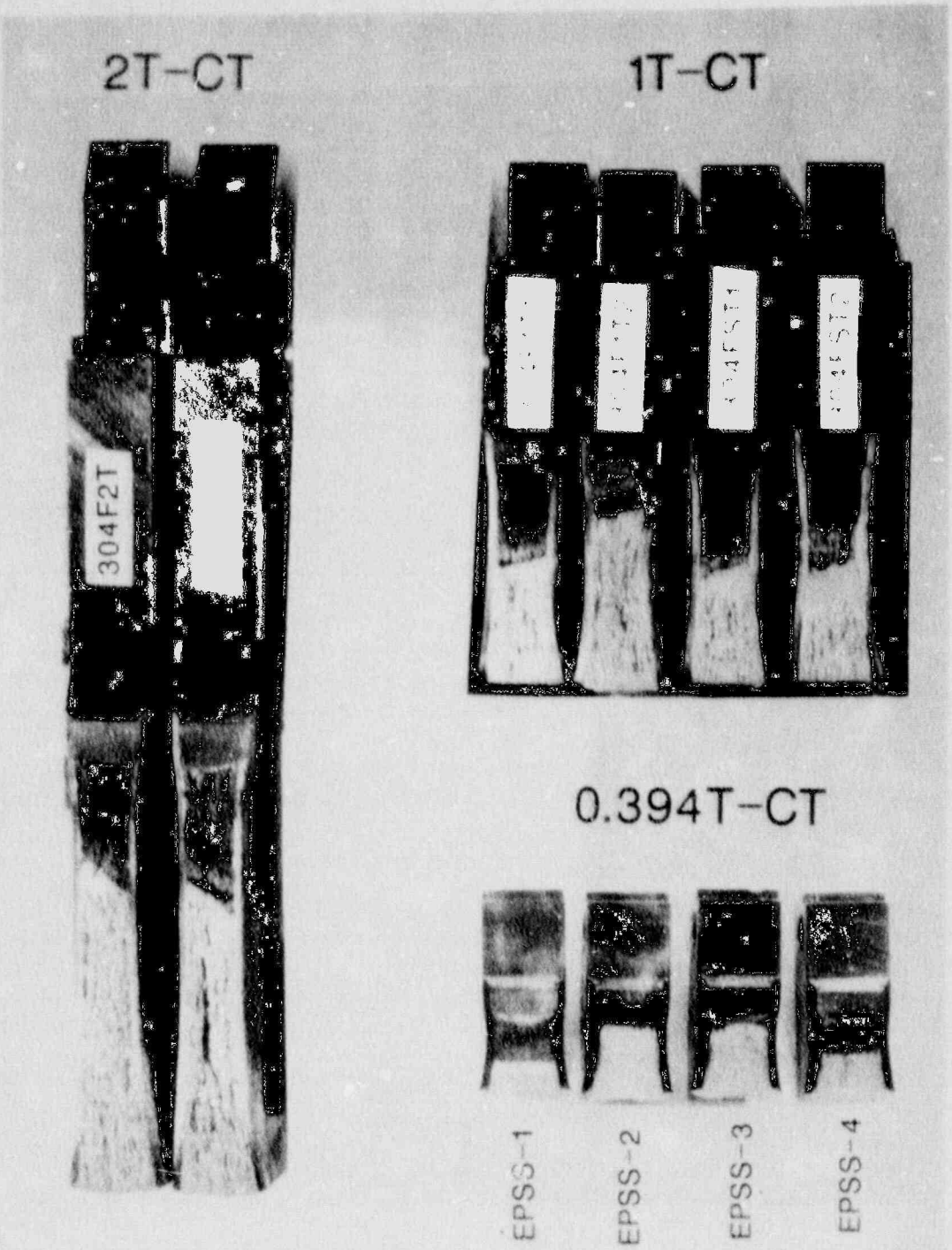

Fig. 6-11 Fracture surface photographs for the Type 304 stainless steel specimens indicate straight (uniform) crack growth for the as-received condition and generally non-uniform crack growth for the flattened and the FSR conditions.

7. SPECIMEN SIZE EFFECTS ON STRESS-STRAIN BEHAVIOR

7.1 Background

The stress-strain curve is an important input to structural integrity evaluations, principally for the case of extensive plastic deformation where improper evaluation of strain could lead to non-conservative calculation of applied J levels for the structure. Since the tensile specimens used in the characterization work reported in this report are generally small specimens with a gage diameter below ~ 6 mm, an evaluation of the effect of using such small specimens on the measured stress-strain curves was sought for a stainless steel and a ferritic steel.

The stainless steel used in this evaluation was the SA 182 Type 304 material (code ZP6) described in Section 4; the ferritic steel was the A 106 Grade C steel described in Section 3. Duplicate specimens through the pipe thickness were used, with all testing at 288°C (550°F). The larger specimen had a gage diameter of 12.83 mm (0.505 in.) and a gage length of ~ 51 mm (2.0 in.). The smaller specimen had a gage diameter of ~ 5.74 mm (0.226 in.) and a gage length of ~23 mm (0.9 in.). For the stainless steel, specimens were located at the nominal ID and OD and the midthickness. The same thickness locations were used for the ferritic steel, with the 1/4T and 3/4T locations also used for the smaller specimens.

In all other respects, the test and data analysis procedures were identical to those used for the tests reported in Sections 3 and 4.

7.2 Results

Results from these tests are given in Table 7-1, with a summary of the average results for each pipe given in Table 7-2. The tabulated Ramberg-Osgood values are determined from regression analysis to the stress-strain data and are generally applicable from just past the yield strain to strain of ~ 0.1.

As illustrated in Figs. 7-1 and 7-2, the two specimen sizes give nearly identical strength levels for each steel, as the yield strengths are always within 10% and the ultimate strengths are always within 3.5% at each location through the pipe thickness. The stainless steel did not exhibit any significant variation through the pipe thickness, although the OD tends to have the lowest strength levels and the ID tends to have the highest strength levels for the smaller specimen size, with the average strengths within 15% for all locations. In contrast the ferritic steel exhibited a moderate through-thickness variation, whereby the pipe surfaces exhibited higher strength levels than the internal locations, with the pipe midthickness exhibiting the lowest overall strength levels. For the smaller specimen size, the maximum difference in strength between the midthickness and the surfaces is 36% for yield strength and 8% for ultimate strength, with the larger specimen size exhibiting differences of 23% and 5%, respectively. Therefore, one effect of the larger specimen size is a moderating effect on the through-thickness

Table 7-1 Tensile Results for Specimen Size Effect Study at 288°C

Specimen ID	Specimen Size[a]	Location	0.2% Offset Yield Strength		Ultimate Strength		Elong.	Reduction In Area	Ramberg-Osgood Parameters				
									n	α	σ_o		ϵ_o
			(MPa)	(ksi)	(MPa)	(ksi)	(%)	(%)			(MPa)	(ksi)	
Type 304 Stainless Steel													
1E1-1	0.505	OD	126.7	18.38	391.4	56.77	62.6	75.7	2.478	3.504	127.1	18.43	0.00301
1E1-2	0.505	OD	130.9	18.99	392.0	56.86	65.7	78.3	2.380	4.299	131.3	19.04	0.00286
1E1-3	0.505	MID	133.8	19.41	395.1	57.30	65.3	77.4	2.714	3.500	134.2	19.46	0.00274
1E1-4	0.505	MID	127.3	18.47	390.7	56.66	63.2	77.4	2.519	3.821	127.8	18.53	0.00288
1E1-5	0.505	ID	123.0	17.84	389.8	56.53	64.7	76.0	2.427	4.191	123.3	17.89	0.00268
1E1-6	0.505	ID	131.7	19.10	389.2	56.45	63.0	76.0	2.492	4.162	132.1	19.16	0.00273
1E1-7	0.226	OD	116.7	16.93	393.5	57.07	64.2	77.6	2.047	4.663	117.1	16.98	0.00295
1E1-8	0.226	OD	124.3	18.03	394.6	57.23	59.6	78.8	2.565	3.230	124.7	18.08	0.00288
1E1-9	0.226	MID	132.2	19.18	396.0	57.43	62.6	75.2	2.718	3.301	132.7	19.24	0.00284
1E1-10	0.226	MID	138.6	20.10	398.8	57.84	65.0	78.8	2.547	4.324	139.0	20.16	0.00276
1E1-11	0.226	ID	133.8	19.40	396.8	57.55	65.8	77.2	2.508	4.226	134.1	19.45	0.00276
1E1-12	0.226	ID	143.3	20.78	401.9	58.29	64.0	77.4	2.755	3.620	143.7	20.84	0.00294
A 106 Grade C													
1E2-1	0.505	OD	331.8	48.12	630.9	91.50	[b]	64.7	4.672	0.7945	333.1	48.31	0.00392
1E2-2	0.505	OD	341.8	49.58	639.9	92.82	47.5	68.3	4.892	0.8056	343.1	49.76	0.00377
1E2-3	0.505	MID	289.5	41.99	609.8	88.44	42.3	57.3	4.703	0.5107	290.6	42.15	0.00389
1E2-4	0.505	MID	286.2	41.51	607.7	88.14	46.6	59.8	4.757	0.5623	287.2	41.65	0.00336
1E2-5	0.505	ID	368.2	53.40	646.7	93.80	48.9	67.4	5.474	0.7289	369.6	53.61	0.00391
1E2-6	0.505	ID	339.6	49.25	633.0	91.81	47.6	66.5	4.716	0.8521	340.9	49.44	0.00395
1E2-7	0.226	OD	338.1	49.04	632.9	91.79	49.4	70.9	5.054	0.6705	339.5	49.24	0.00420
1E2-8	0.226	OD	395.4	57.35	665.4	96.51	47.6	72.7	5.776	0.6734	397.1	57.60	0.00435
1E2-9	0.226	0.25	293.6	42.59	615.5	89.27	45.6	62.4	4.895	0.5156	294.8	42.75	0.00355
1E2-10	0.226	0.25	302.1	43.81	626.2	90.82	44.8	64.5	4.732	0.5815	306.3	44.43	0.00373
1E2-11	0.226	MID	279.9	40.60	608.0	88.18	45.4	61.6	4.520	0.5473	281.0	40.75	0.00370
1E2-12	0.226	MID	286.8	41.59	613.8	89.03	43.6	62.4	4.774	0.4959	287.8	41.74	0.00355
1E2-13	0.226	0.75	317.9	46.11	636.0	92.24	47.6	63.8	4.876	0.5866	318.3	46.16	0.00396
1E2-14	0.226	0.75	312.7	45.36	630.8	91.49	46.0	64.0	4.560	0.7842	313.8	45.52	0.00346
1E2-15	0.226	ID	383.2	55.58	661.0	95.87	49.4	70.5	5.842	0.5964	384.9	55.82	0.00424
1E2-16	0.226	ID	387.2	56.16	662.7	96.11	47.2	68.9	5.704	0.6971	388.8	56.39	0.00403

[a] 0.505 is gage diameter of 12.83 mm (0.505 in.).
0.226 is gage diameter of 5.74 mm (0.226 in.).
[b] Broke on gage mark.

Table 7-2 Summary of Tensile Results for Specimen Size Effect Study at 288°C

Location	0.2% Offset Yield Strength		Ultimate Strength		Ramberg-Osgood Parameters							
					n		α		σ_o		ε_o	
	0.505[a] (ksi)	0.226[a] (ksi)	0.505 (ksi)	0.226 (ksi)	0.505	0.226	0.505	0.226	0.505 (ksi)	0.226 (ksi)	0.505	0.226
Type 304 Stainless Steel												
OD	18.69	17.48	56.82	57.15	2.429	2.306	3.902	3.947	18.73	17.53	0.00293	0.00292
MID	18.94	19.64	56.98	57.64	2.616	2.633	3.660	3.813	19.00	19.70	0.00281	0.00280
ID	18.47	20.09	56.49	57.92	2.270	2.632	4.413	3.923	18.53	20.15	0.00271	0.00285
Average	18.70	19.07	56.76	57.57	2.438	2.524	3.992	3.894	18.75	19.13	0.00282	0.00286
A 106 Grade C												
OD	48.85	53.20	92.16	94.15	4.782	5.415	0.8001	0.6720	49.04	53.42	0.00385	0.00428
0.25	-----	43.20	-----	90.05	-----	4.809	------	0.5486	-----	43.59	-------	0.00364
MID	41.75	41.10	88.29	88.60	4.730	4.647	0.5365	0.5216	41.90	41.25	0.00363	0.00363
0.75	-----	45.74	-----	91.87	-----	4.718	------	0.6854	-----	45.84	-------	0.00371
ID	51.33	55.87	92.81	95.99	5.095	5.773	0.7905	0.6468	51.53	56.10	0.00393	0.00414
Average	47.31	47.82	91.09	92.13	4.869	5.072	0.7090	0.6149	47.49	48.04	0.00380	0.00388

[a] 0.505 is gage diameter of 12.83 mm (0.505 in.).
0.226 is gage diameter of 5.74 mm (0.226 in.).

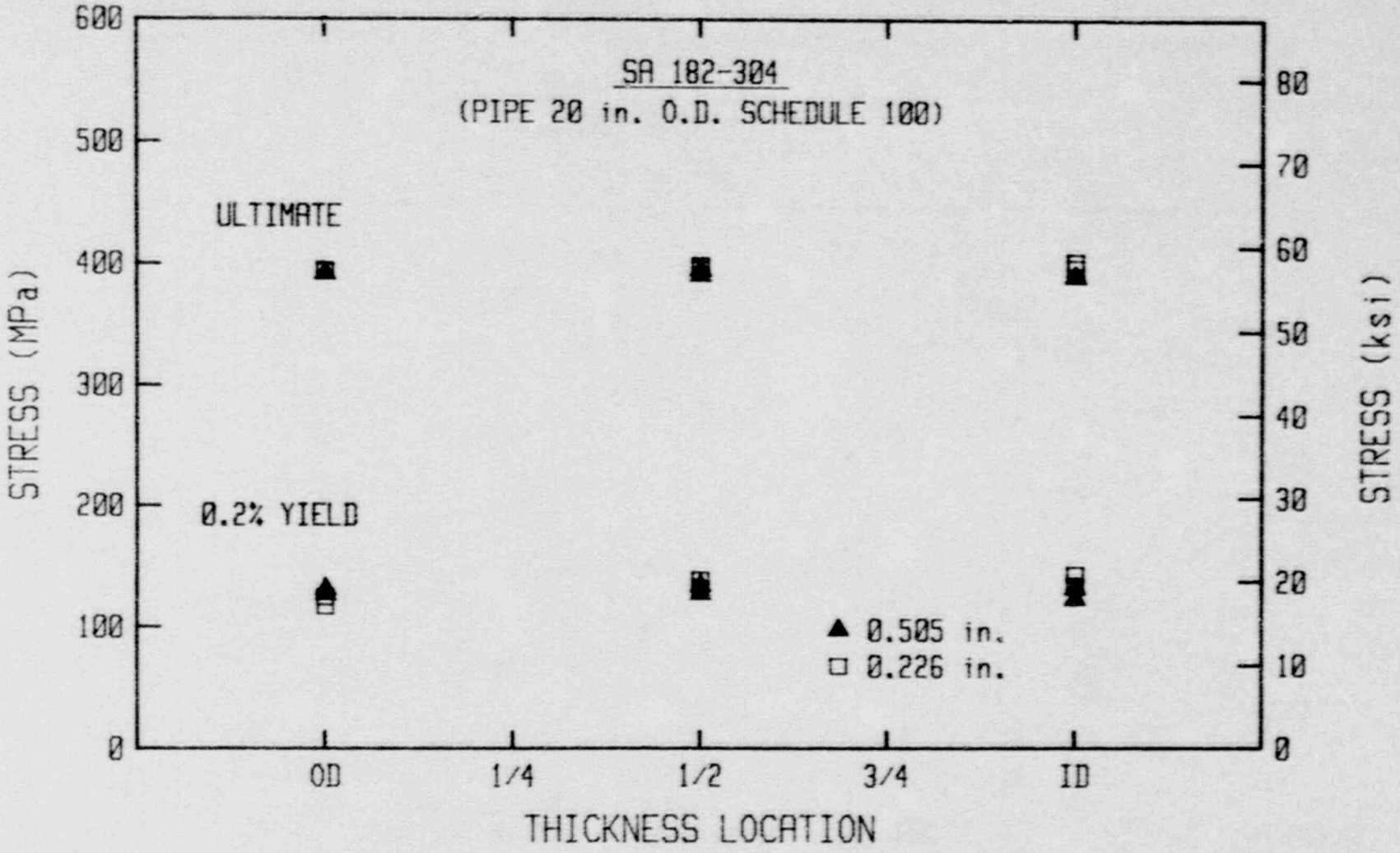

Fig. 7-1 Tensile strength data for the SA 182 Type 304 stainless steel used in the specimen size effect study.

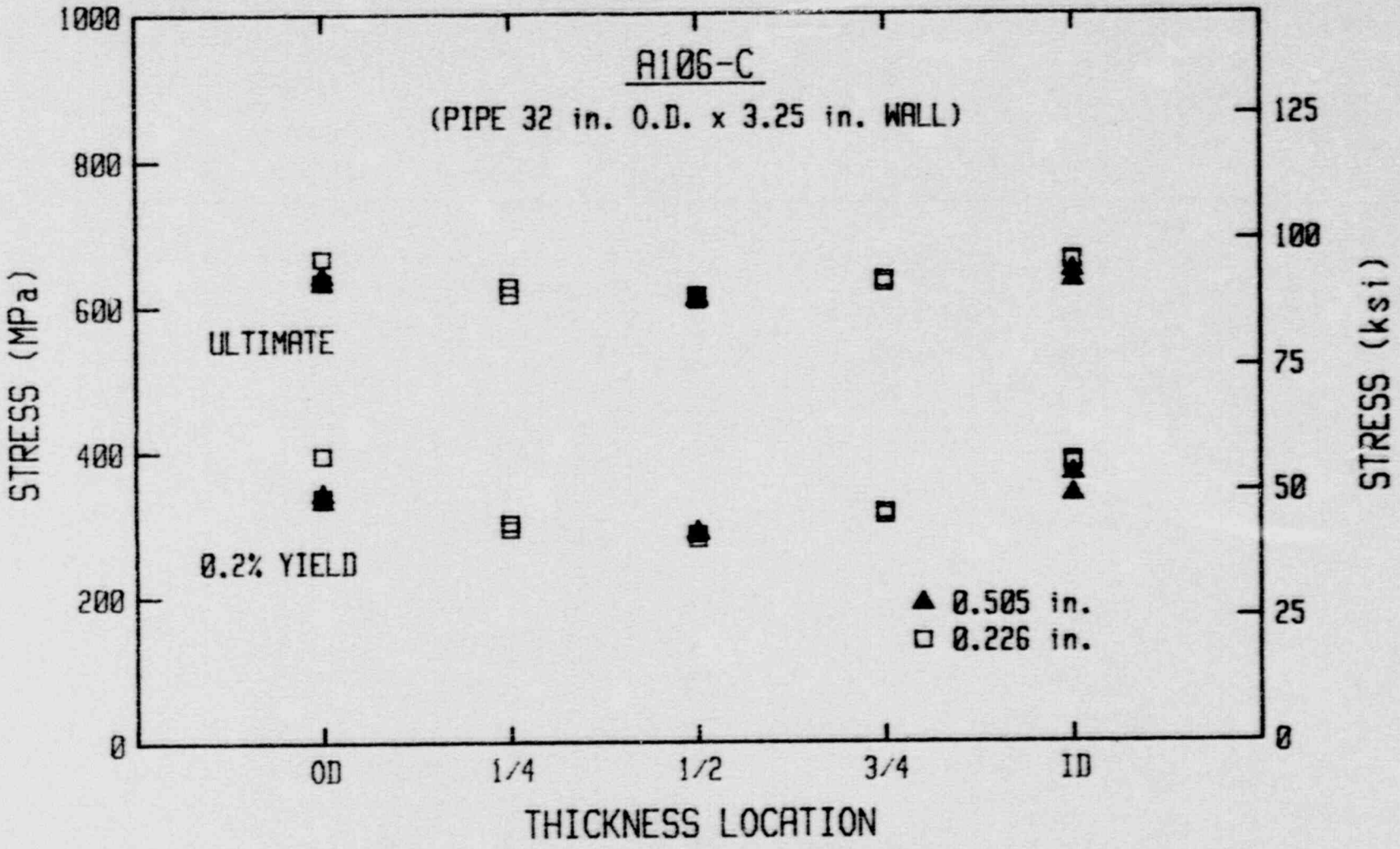

Fig. 7-2 Tensile strength data for the A 106 Gr. C steel used in the specimen size effect study.

variation in strength measured at the pipe surfaces. For the ferritic steel the ratio of yield to ultimate is ~ 2:1, whereas for the stainless steel the ratio of yield to ultimate is ~ 3:1.

Comparisons of the stress-strain behavior will be made using the engineering stress-strain curves, although a few comparisons of the true stress-strain curves will also be made. For all of the stress-strain comparisons, two curves will be shown, with one at the small strain region (i.e., $\epsilon < 0.01$) and the other illustrating the overall curves in each case. For the true stress-strain curves, the final data point (at fracture) is illustrated by an "X" in each case. As described in Section 2.2, the true stress-strain data can be determined using Eqs. 2-5 and 2-6 only up to maximum load, with Eqs. 2-7 and 2-8 used to determine true stress-strain values at the fracture point. To approximate the curve between these points (i.e., the fracture point and maximum load), a linear interpolation is used. Therefore, the true stress-strain comparisons covering the entire curves will exhibit a lengthy linear portion which is purely an artifact of the plotting method used, and which permits matching of the appropriate stress-strain curve with the fracture point for that curve.

Starting with the stainless steel, the true stress-strain curves for the large specimens (Fig. 7-3) indicate much less variability in terms of stress at a constant strain than do the curves for the small specimens (Fig. 7-4). For both specimen sizes, the maximum load occurs at ϵ_T of ~ 0.25, as an obvious change in curvature occurs where the linear interpolation of the stress-strain curve starts. In contrast, the engineering stress-strain curves are in much better agreement for the case of the overall curves (Figs. 7-5 and 7-6).

Comparisons of the engineering stress-strain curves at the three thickness locations (Figs. 7-7 to 7-9) indicate that the larger specimens tend to give (somewhat) lower stress-strain curves at the MID and the ID, but slightly higher curves at the OD location of this pipe.

For the ferritic steel, a clearer separation of the stress-strain curves for the different thickness locations occurs (Figs. 7-10 to 7-15). For the large specimens, the OD and the ID exhibit rounded stress-strain curves, in comparison to the distinct plateau behavior of the MID, which also has by far the lowest stress-strain curves. For the small specimens, curves for the MID location are plotted on both sets of graphs to use as a reference. For the small specimens, the ID and the OD specimens exhibit the rounded stress-strain curves described above, with specimens from intermediate locations exhibiting a plateau behavior. In each case, the stress-strain curves for the OD and the ID locations tend to be much higher than those for the other locations.

Comparisons of the engineering stress-strain curves at the three thickness locations (Figs. 7-16 to 7-18) indicate excellent agreement in the curves at the MID, with the small specimens tending to give somewhat higher stress-strain curves at the OD and the ID. One good

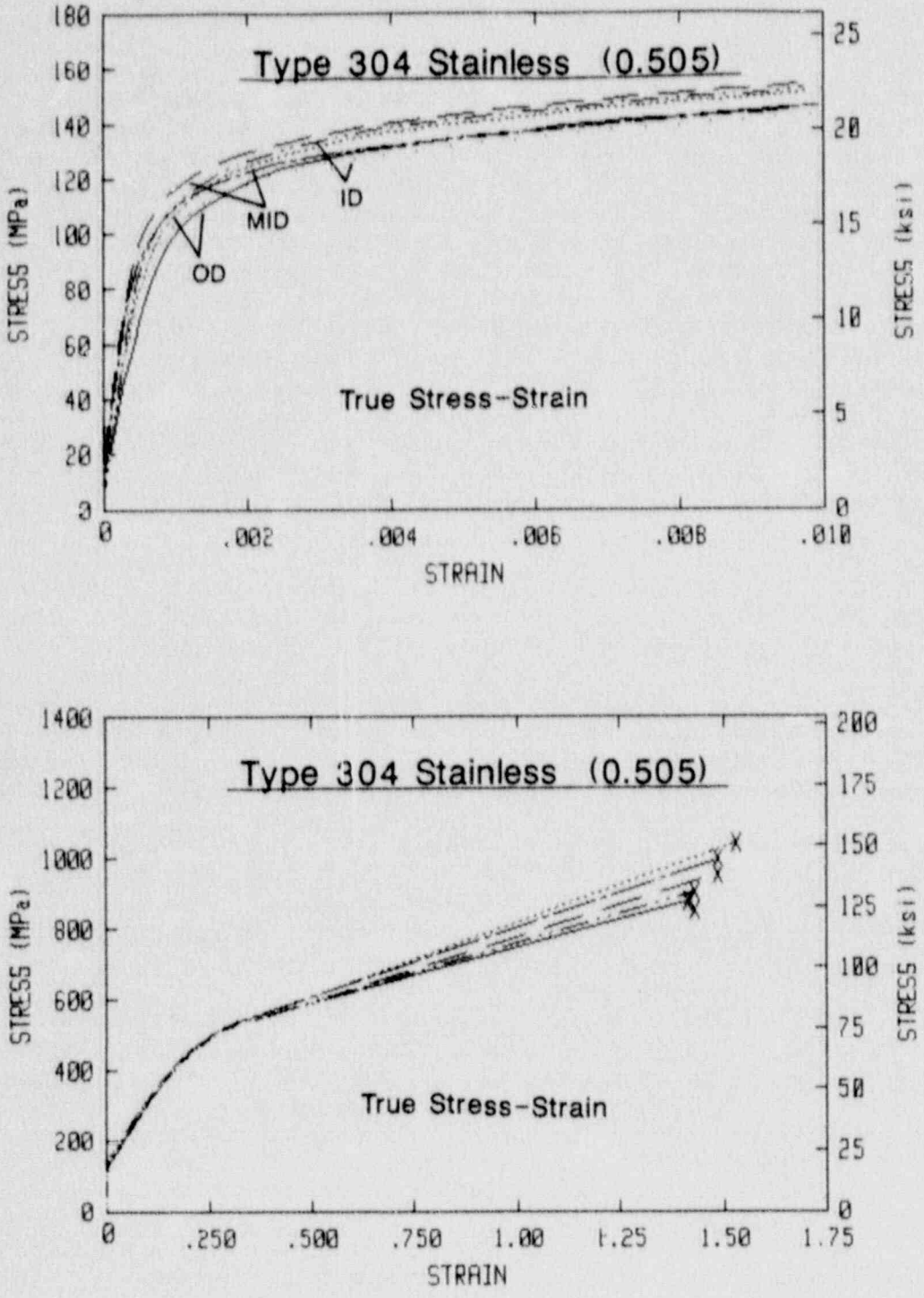

Fig. 7-3 True stress-strain curves for the large specimens of the SA 182 Type 304 stainless steel.

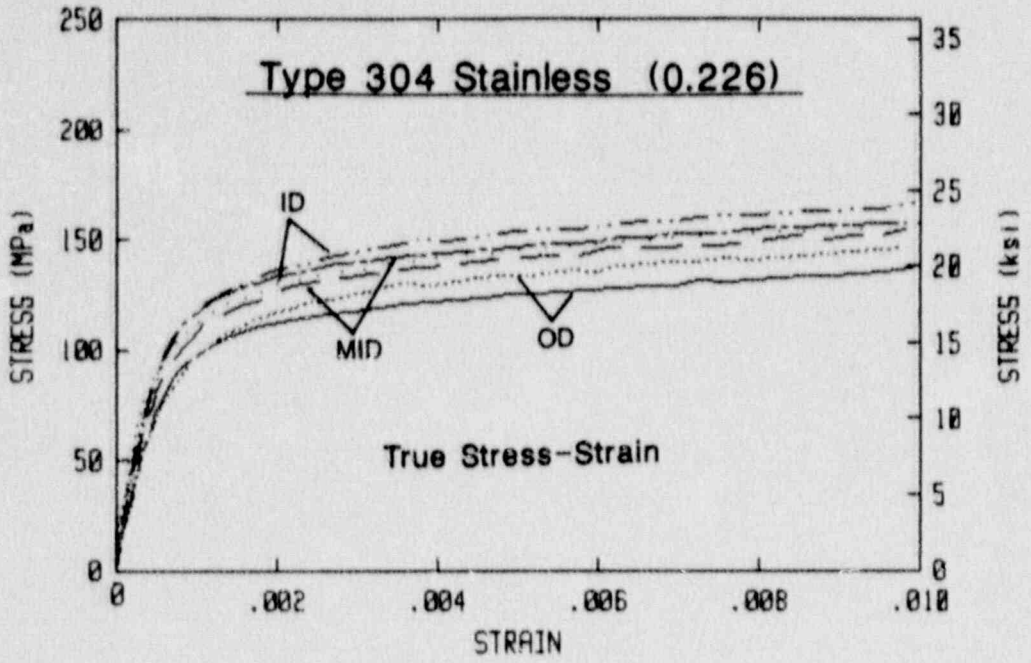

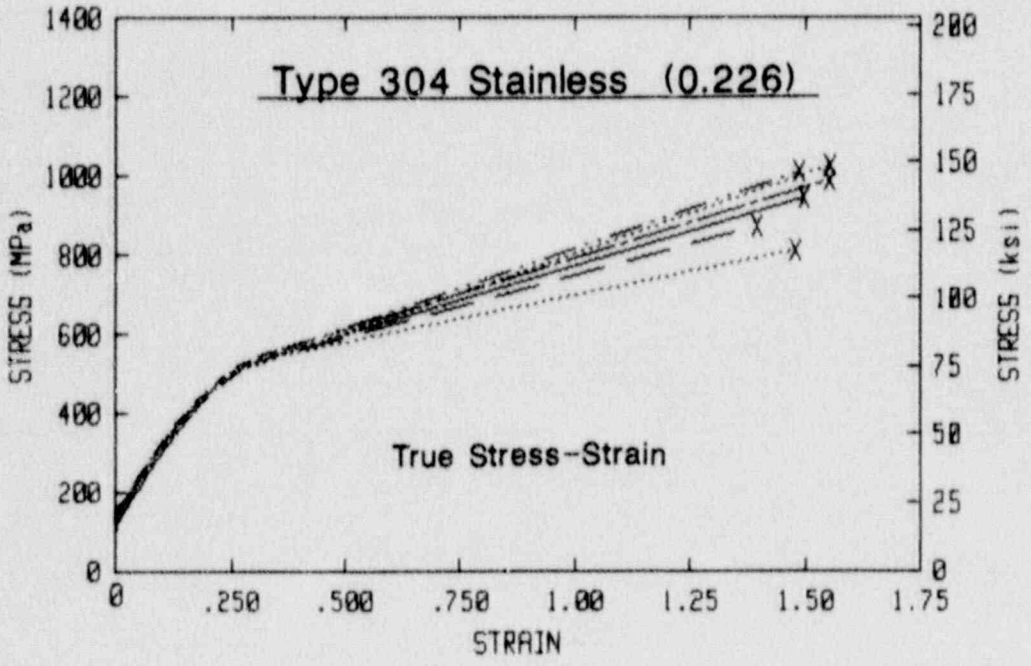

Fig. 7-4 True stress-strain curves for the small specimens of the SA 182 Type 304 stainless steel.

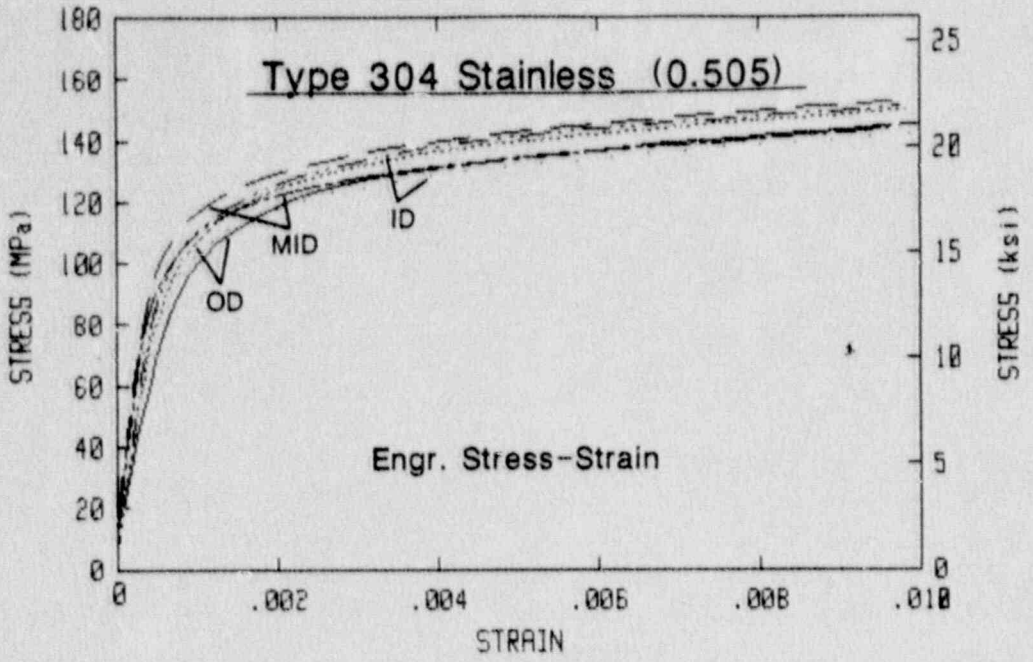

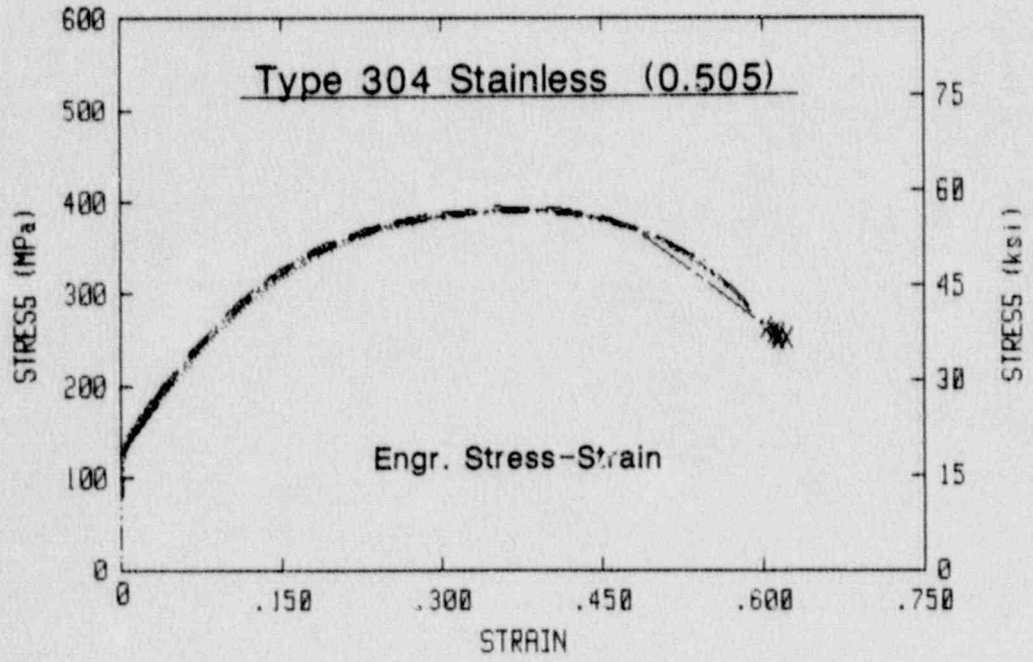

Fig. 7-5 Engineering stress-strain curves for the large specimens of the SA 182 Type 304 stainless steel.

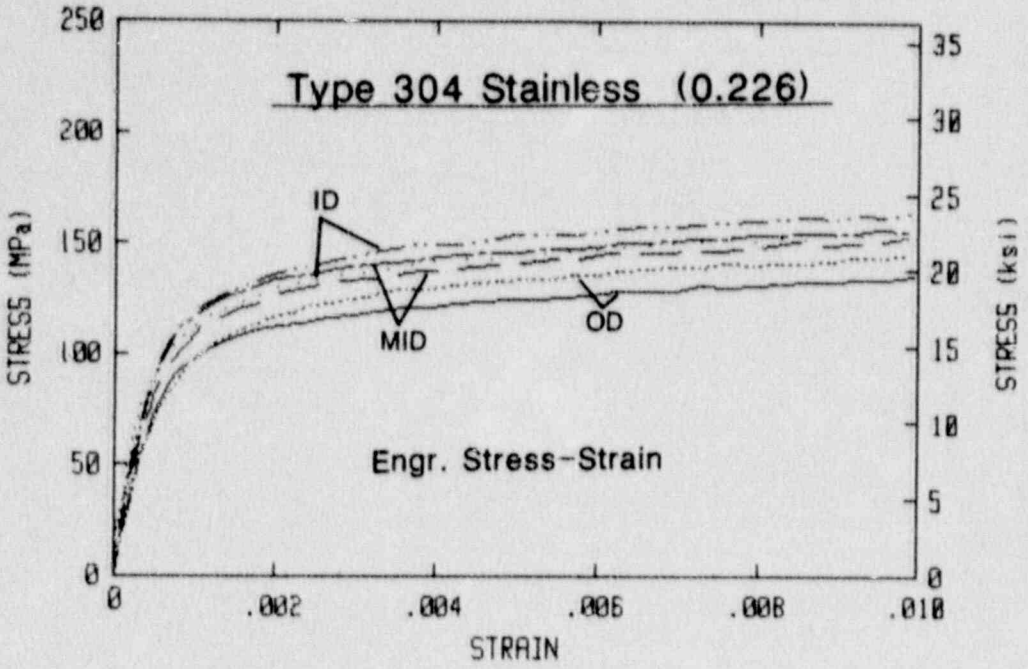

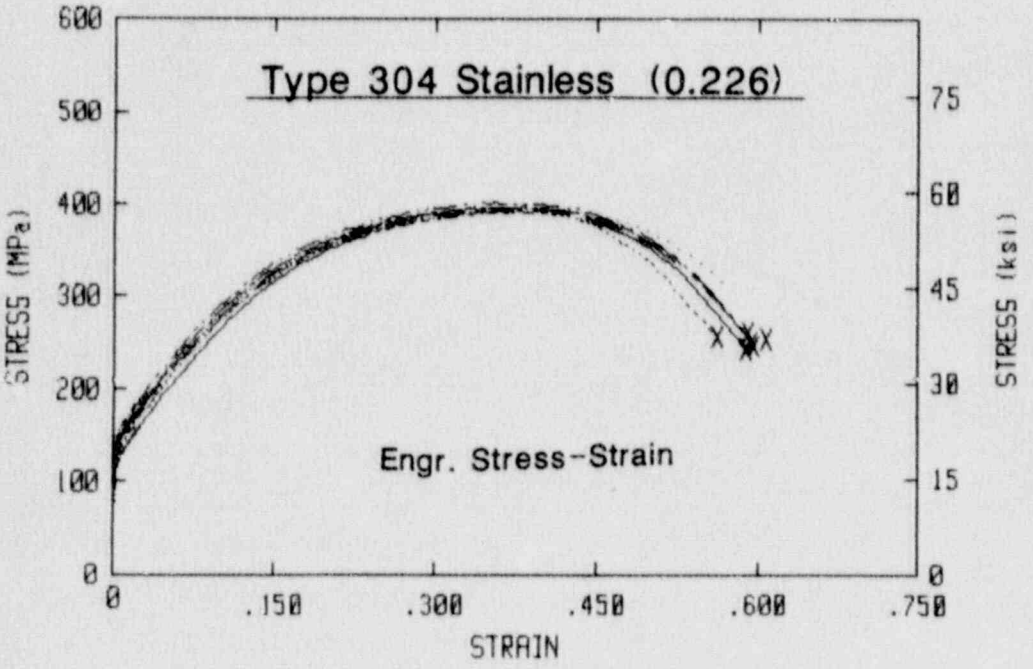

Fig. 7-6 Engineering stress-strain curves for the large specimens of the SA 182 Type 304 stainless steel.

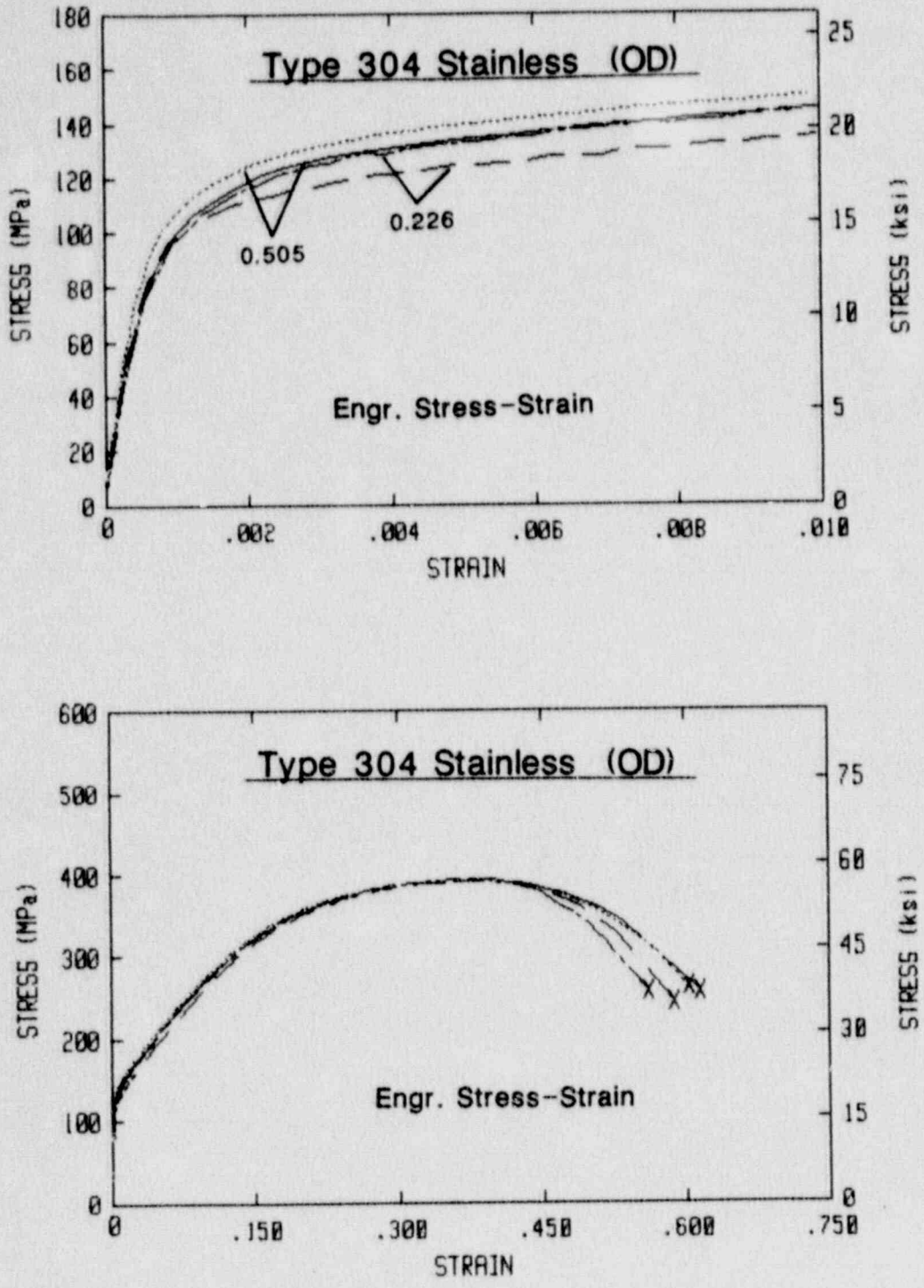

Fig. 7-7 For the OD, comparison of the engineering stress-strain curves for the SA 182 Type 304 stainless steel.

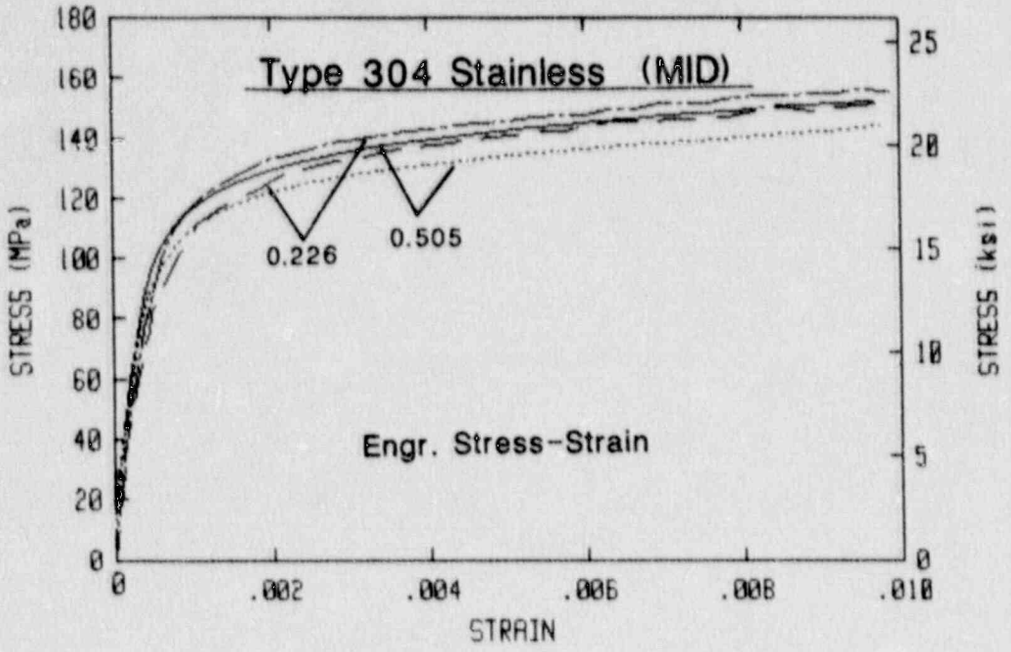

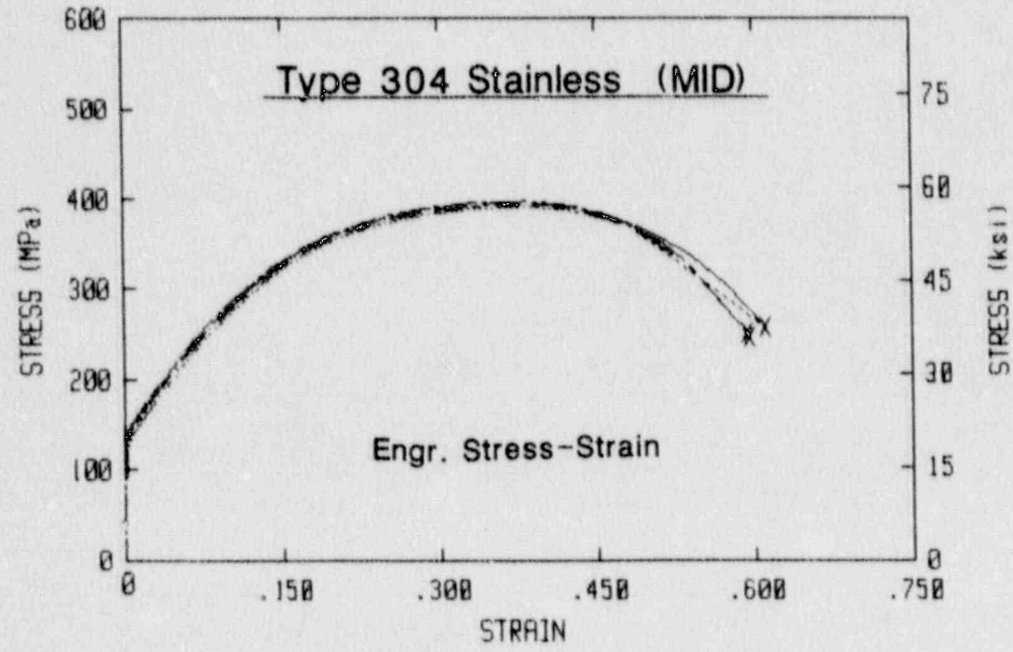

Fig. 7-8 For the MID, comparison of the engineering stress-strain curves for the SA 182 Type 304 stainless steel.

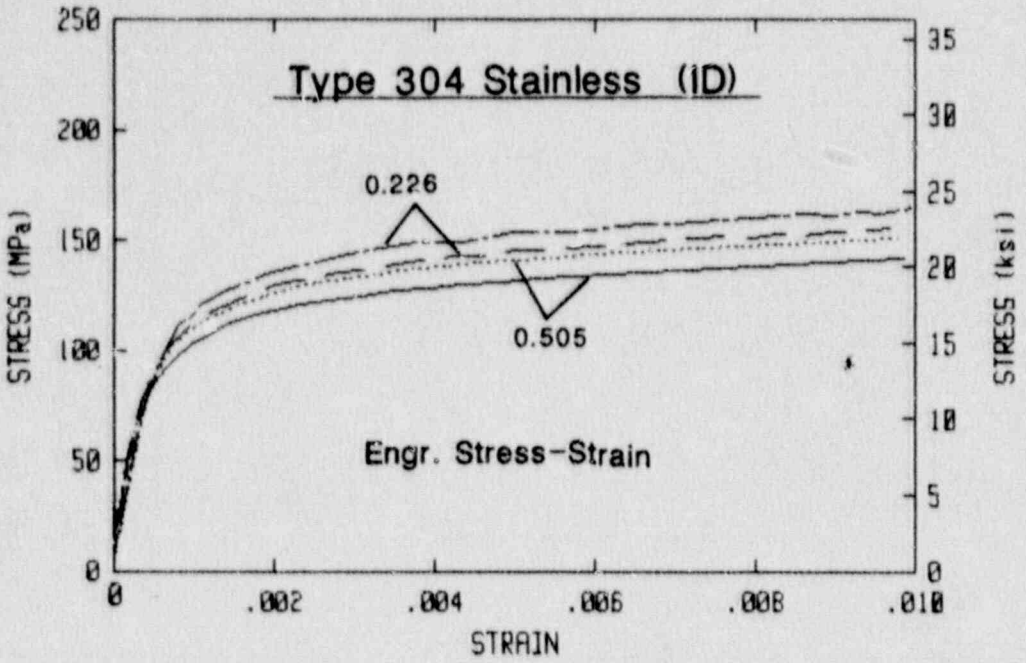

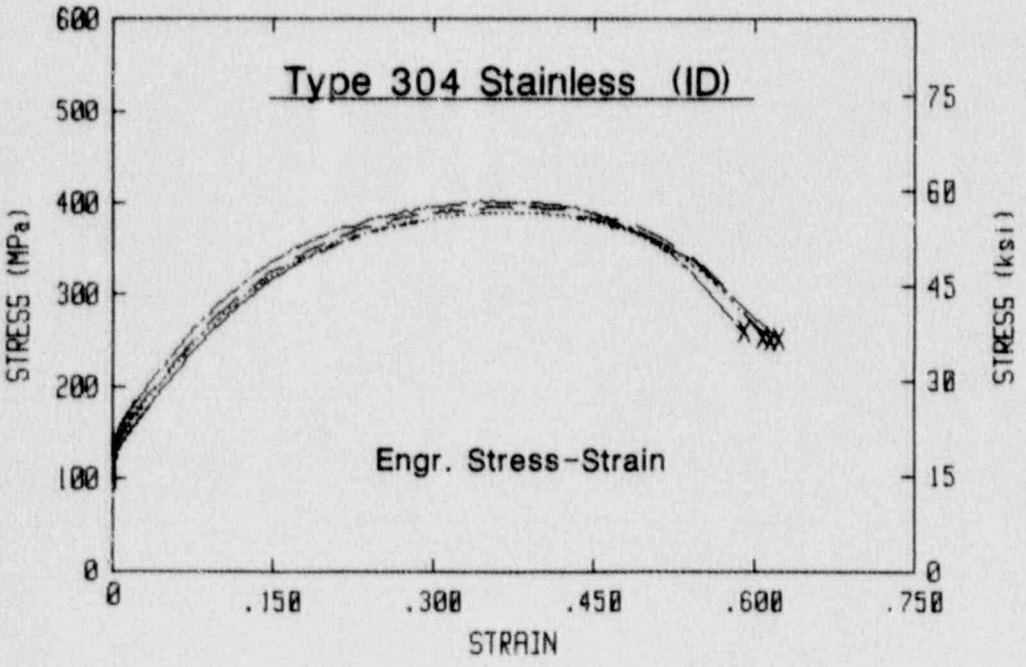

Fig. 7-9 For the ID, comparison of the engineering stress-strain curves for the SA 182 Type 304 stainless steel.

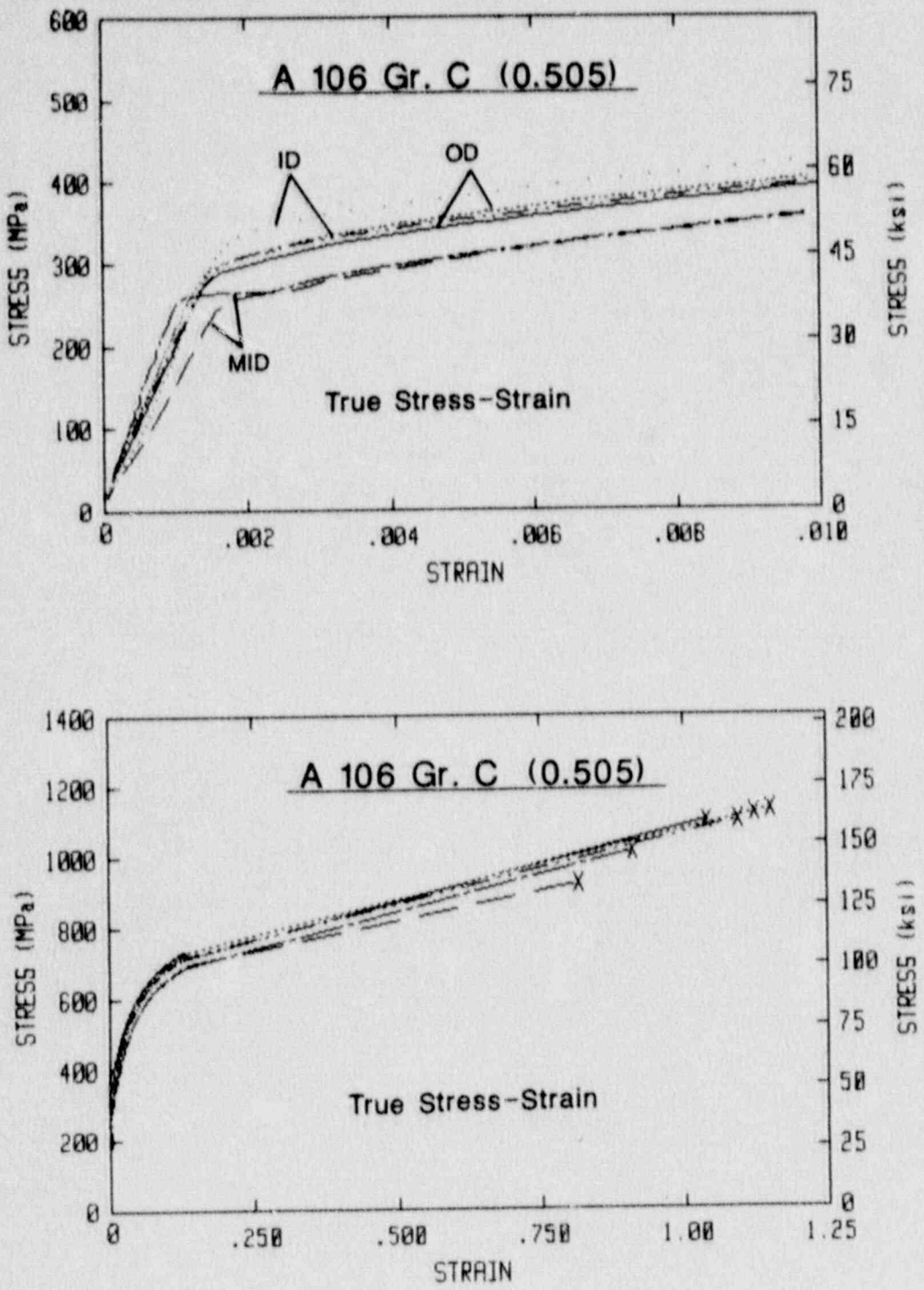

Fig. 7-10 True stress-strain curves for the large specimens of the A 106 Gr. C steel.

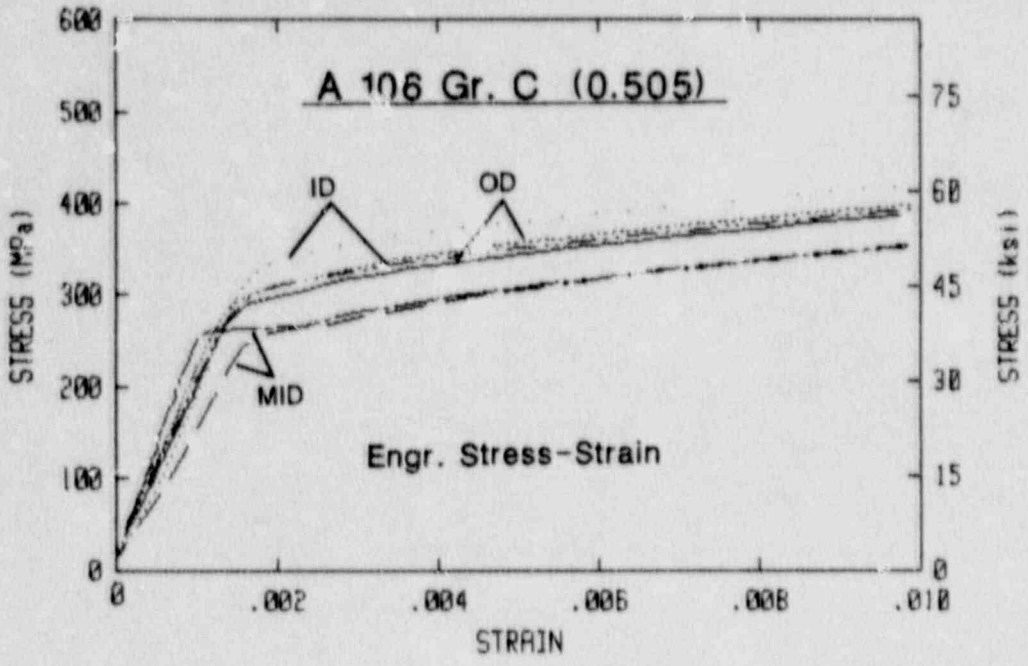

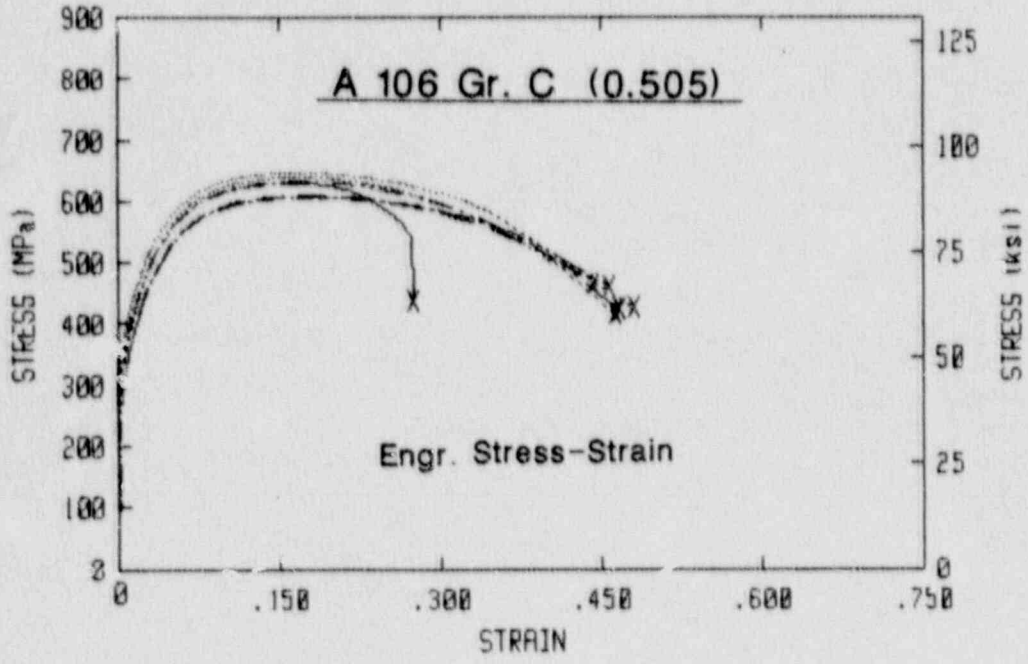

Fig. 7-11 Engineering stress-strain curves for the large specimens of the A 106 Gr. C steel.

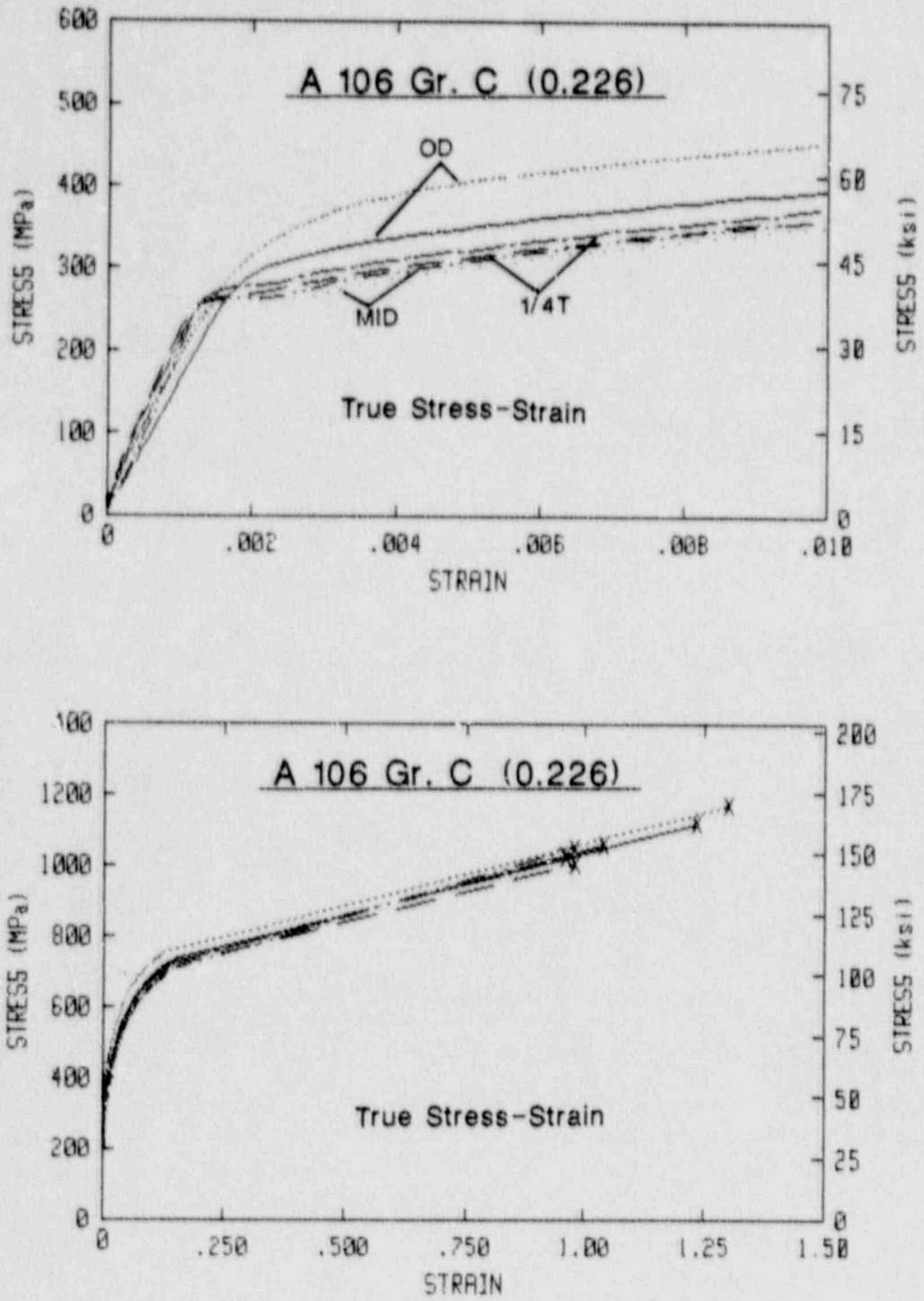

Fig. 7-12 True stress-strain curves for the small specimens from the OD, 1/4T and MID of the A 106 Gr. C steel.

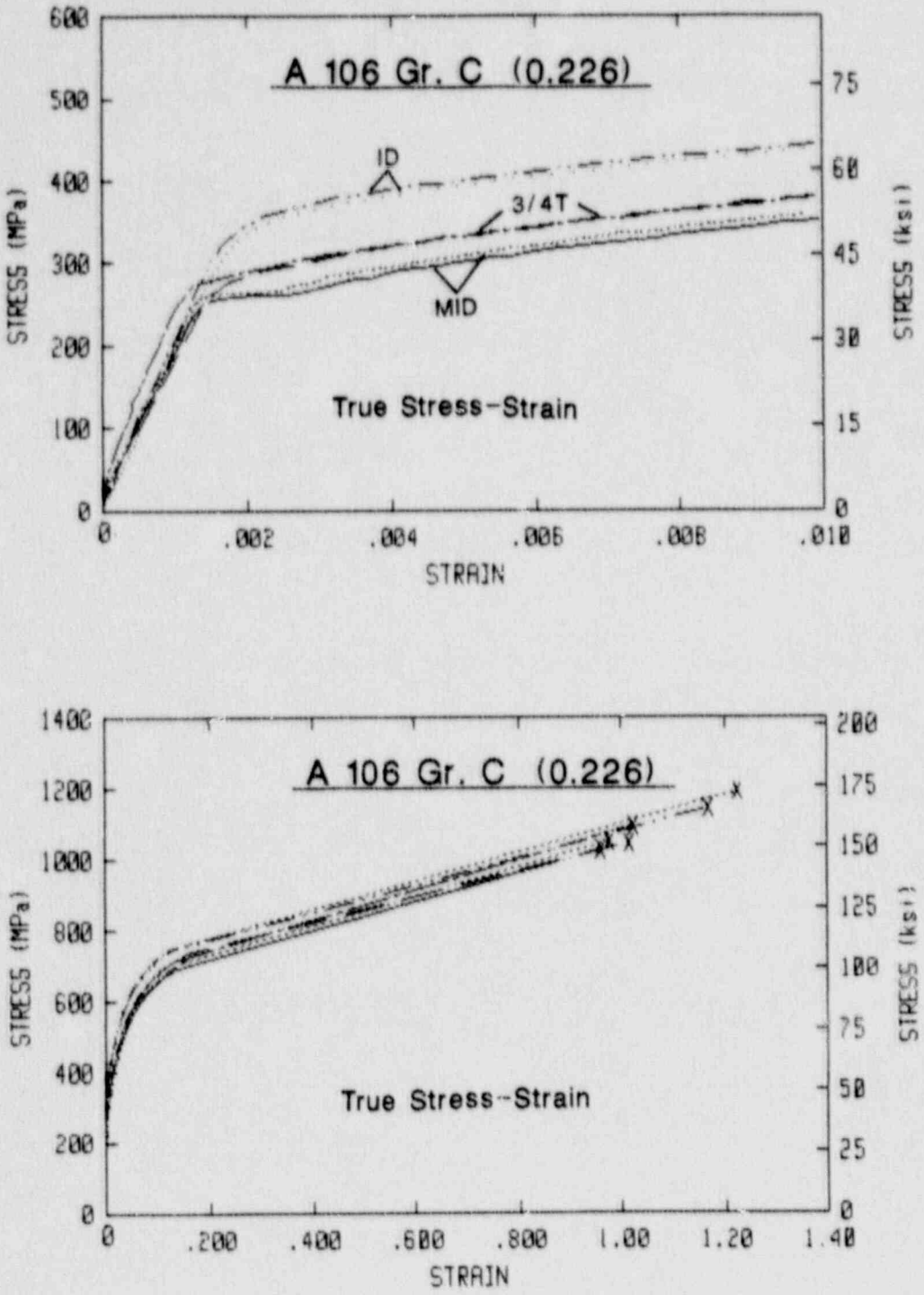

Fig. 7-13 True stress-strain curves for the small specimens from the MID, 3/4T and ID of the A 106 Gr. C steel.

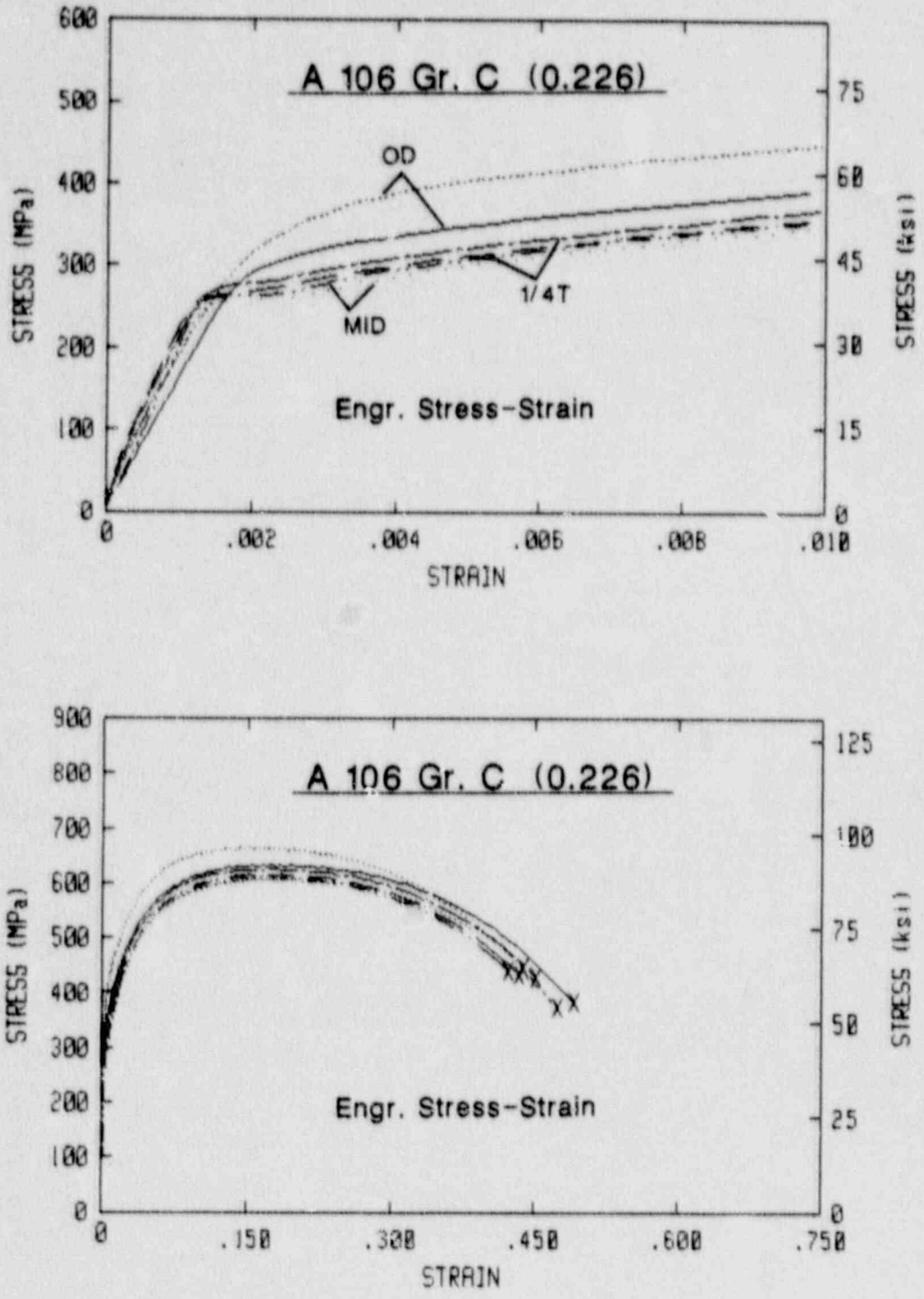

Fig. 7-14 Engineering stress-strain curves for the small specimens from the OD, 1/4T and MID of the A 106 Gr. C steel.

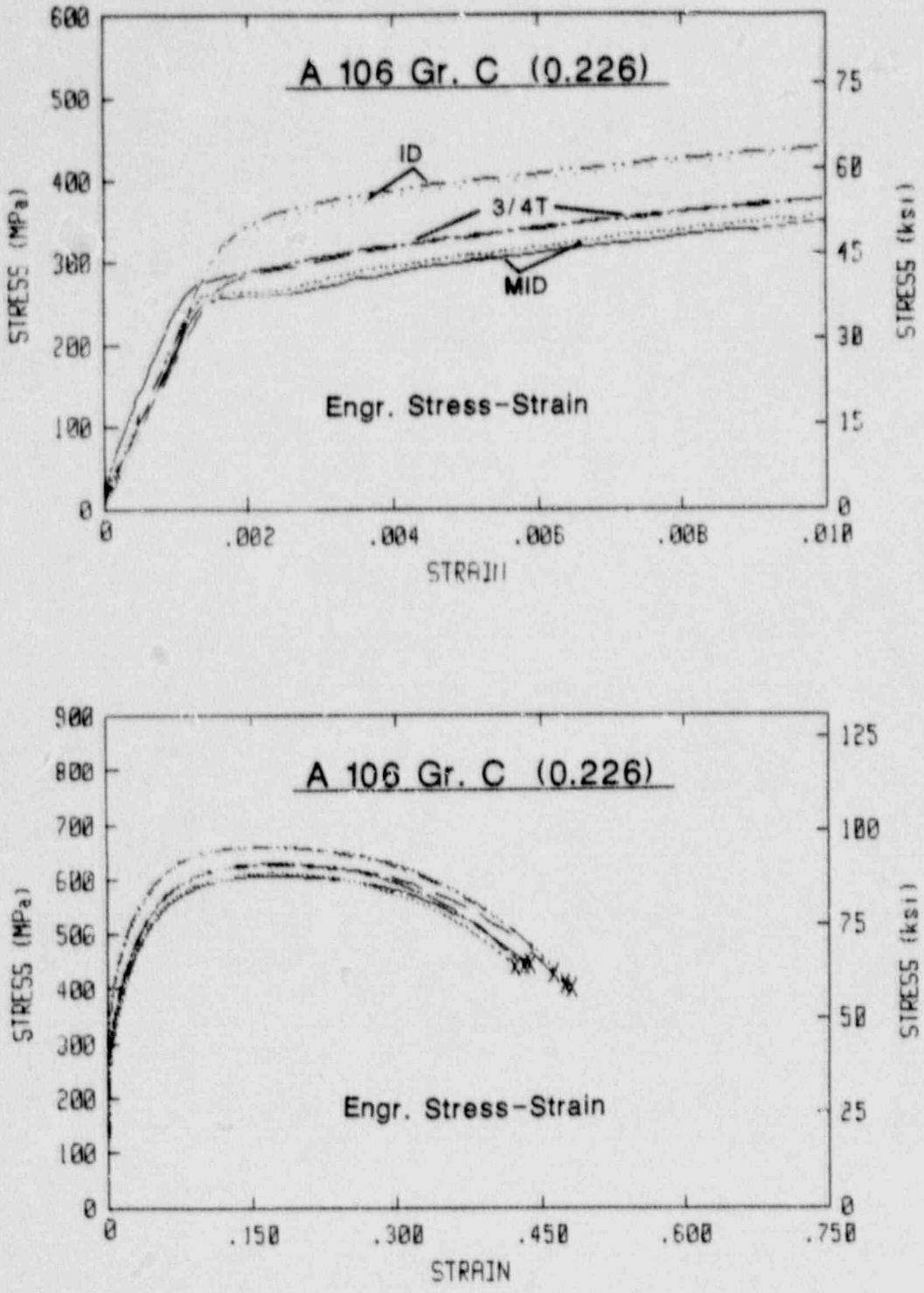

Fig. 7-15 Engineering stress-strain curves for the small specimens from the MID, 3/4T and ID of the A 106 Gr. C steel.

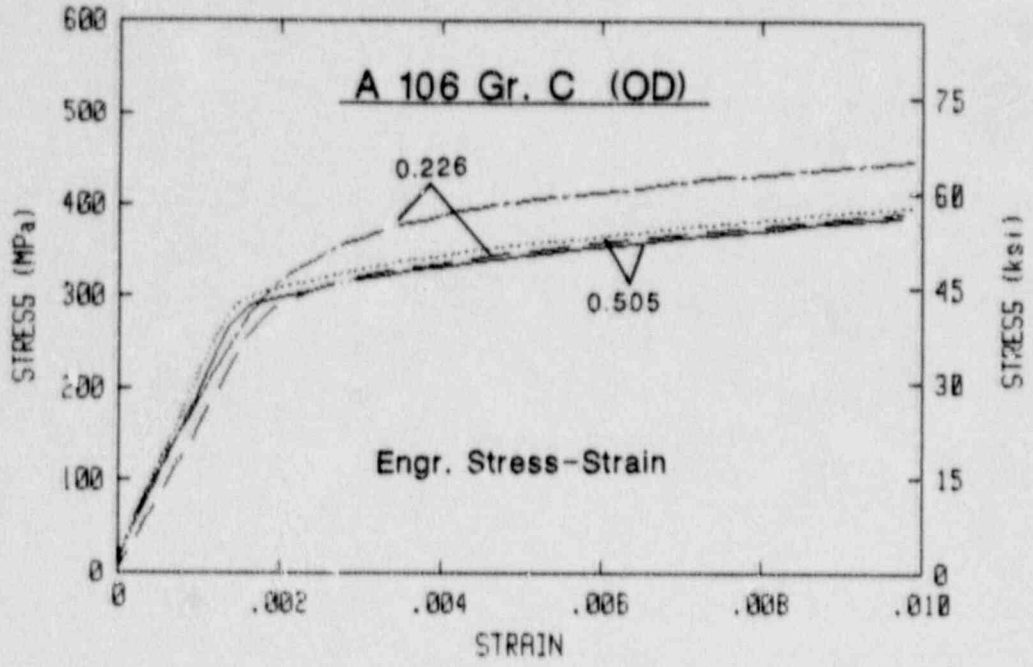

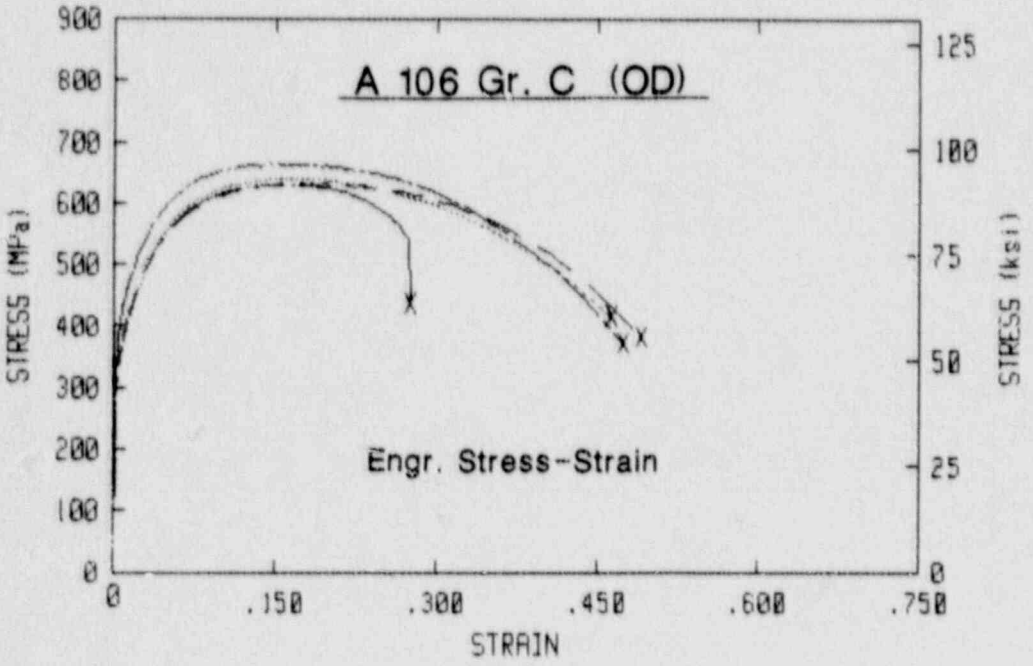

Fig. 7-16 For the OD, comparison of the engineering stress-strain curves for the A 106 Gr. C steel.

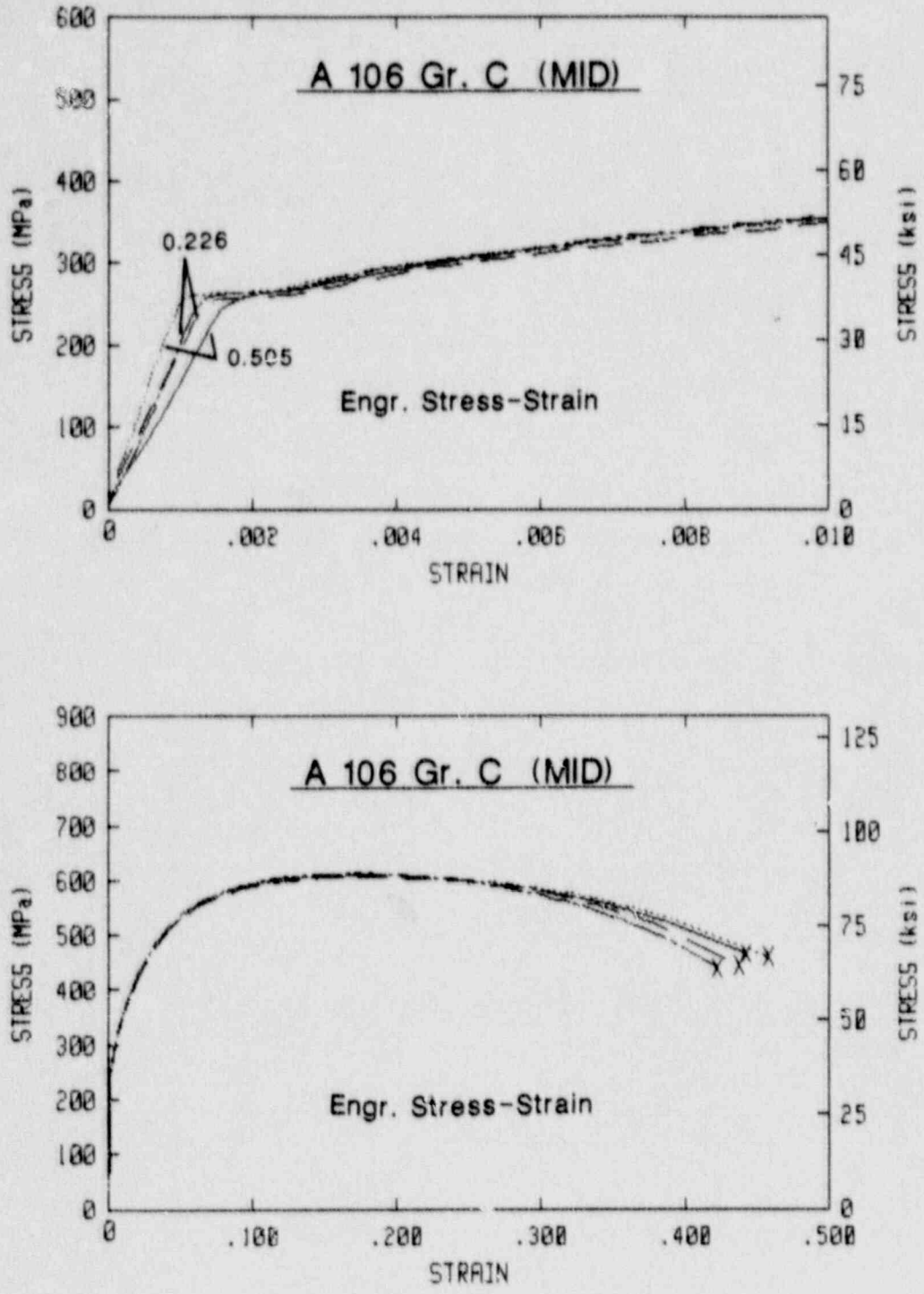

Fig. 7-17 For the MID, comparison of the engineering stress-strain curves for the A 106 Gr. C steel.

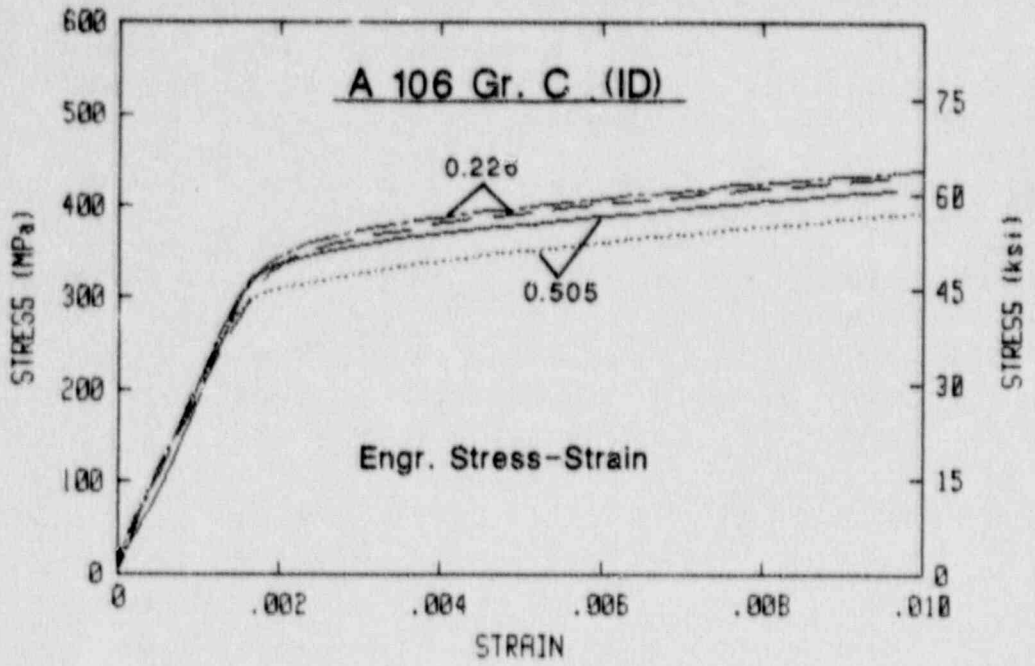

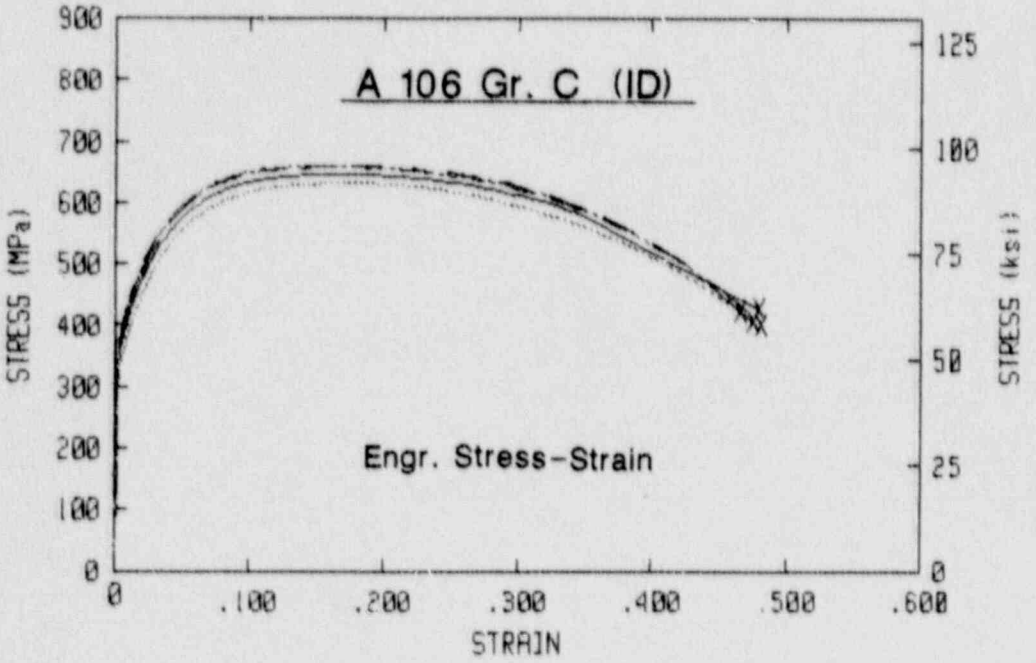

Fig. 7-18 For the ID, comparison of the engineering stress-strain curves for the A 106 Gr. C steel.

sign is that the general shape of the stress-strain curves is consistent with the two specimen sizes for the ID and the MID, with only the level of the curves deviating.

For the ferritic steel, the overall trends are consistent with expectations, as the small specimens are more sensitive to local strength variations near the wall surfaces. Where the two specimen sizes are nominally the same material, i.e., at the MID, the two specimen sizes give nearly identical stress-strain curves as well as strength levels.

8. CONCLUSIONS

General conclusions from this work include:

- As with other structural materials, side grooving reduces fracture toughness (J levels) from CT specimens.

- Characteristics of dynamic strain aging (DSA), including load drops and serrated tearing, have been found with A 106 Gr. B and C in the temperature range of 149°C to 204°C (300°F to 400°F). A possible additional characteristic found with many of the ferritic steels is an extremely sharp increase in C_v energy at 288°C (550°F).

- Except for forged Heat ZP6, a strong orientation dependence was found, with the L-C orientation giving much higher toughness than the C-L orientation.

- Within a given crack plane (such as those with the L or the C orientation as a perpendicular), the through-thickness and lengthwise crack growth directions exhibit similar fracture toughness trends.

- Significant through-thickness variability has been found with heavy wall (i.e., > 25 mm or 1 in.) carbon and stainless steel, in terms of stress-strain and strength properties, and also in terms of notch ductility (C_v) impact toughness. Similar variability can be expected with fracture toughness.

- J-R curves for the highly ductile stainless steels generally exceed the specimen size requirements.

- A 4 σ_f blunting line is a better approximation to the blunting trends of the stainless steels than is the standard 2 σ_f blunting line.

- Flattening of specimen blanks results in lower J_M-R curves than for the as-received condition. A stress-relief heat treatment does not recover the toughness loss to a significant degree. In contrast, J_D tends to minimize the toughness differences.

- Large and small tensile specimens are found to give similar stress-strain curves for cases in which the two specimen sizes are sampling similar material, as in the mid-thickness or MID. Small specimens are much more sensitive to local variability, principally in terms of the strength properties.

REFERENCES

1. A. L. Hiser, "Tensile and J-R Curve Characterization of Thermally-Aged Cast Stainless Steels," USNRC Report NUREG/CR-5024, Sept. 1988.

2. A. L. Hiser and G. M. Callahan, "A User's Guide to the NRC's Piping Fracture Mechanics Data Base (PIFRAC)," USNRC Report NUREG/CR-4894, May 1987.

3. A. L. Hiser, "Piping Fracture Mechanics Data Base," in Proceedings of the U. S. Nuclear Regulatory Commission Thirteenth Water Reactor Safety Research Information Meeting, USNRC Conference Proceedings NUREG/CP-0072, Vol. 2, Feb. 1986, pp. 321-336.

4. G. M. Wilkowski, et al., "Degraded Piping Program - Phase II," Sixth Program Report October 1986 -- September 1987, NUREG/CR-4082, Vol. 6, April 1988.

5. G. E. Dieter, Mechanical Metallurgy, McGraw-Hill Book Company, New York, 1976.

6. P. W. Bridgman, Trans. Am. Soc. Met., Vol. 32, 1944, p. 553.

7. A. Saxena and S. J. Hudak, Jr., "Review and Extension of Compliance Information for Common Crack Growth Specimens," International Journal of Fracture, Vol. 14(5), Oct. 1978, pp. 453-468.

8. F. J. Loss, B. H. Menke, and R. A. Gray, Jr., "Development of J-R Curve Procedures," NRL-EPRI Research Program (RP 886-2), Evaluation and Prediction of Neutron Embrittlement in Reactor Pressure Vessel Materials Annual Progress Report for CY 1978, J. R. Hawthorne, Ed., NRL Report 8327, Naval Research Laboratory, Washington, DC, Aug. 1979.

9. H. A. Ernst and P. C. Paris, "Techniques of Analysis of Load-Displacement Records by J-Integral Methods," USNRC Report NUREG/CR-1222, Jan. 1980.

10. A. L. Hiser, F. J. Loss, and B. H. Menke, "J-R Curve Characterization of Irradiated Low Upper Shelf Welds," USNRC Report NUREG/CR-3506, Apr. 1984.

11. H. A. Ernst, "Materials Resistance and Instability Beyond J-Controlled Crack Growth," Elastic-Plastic Fracture, (C. F. Shih and J. P. Gudas, Eds.), ASTM STP 803, Vol. 1, American Society for Testing and Materials, Phila., Pa, pp. 191-213.

12. F. J. Loss, Ed., "Structural Integrity of Water Reactor Pressure Boundary Components, Annual Report for 1983," USNRC Report NUREG/CR-3228, Vol. 2, Sep. 1984.

13. J. W. Hutchinson and P. C. Paris, "The Theory of Stability Analysis of J-Controlled Crack Growth," Elastic-Plastic Fracture, ASTM STP 668, American Society for Testing and Materials, Phila., PA, Mar. 1979, pp. 37-64.

14. C. F. Shih, "An Engineering Approach for Examining Crack Growth and Stability in Flawed Structures," Proceedings of CSNI Specialists Meeting in Plastic Tearing Instability, USNRC Conference Proceeding NUREG/CP-0010, Jan. 1980.

15. W. H. Cullen, "Fatigue Crack Growth Rates of Low-Carbon and Stainless Piping Steels in PWR Environment," USNRC Report NUREG/CR-3945, Feb. 1985.

16. M. T. Miglin, et. al, "Effects of Strain Aging in the Unloading Compliance J Test," Elastic Plastic Fracture Test Methods, The User's Experience, ASTM STP 856, American Society for Testing and Materials, Phila., PA, Apr. 1985, pp. 150-165.

17. H. E. Hanninen and W. H. Cullen, "Slow Strain Rate Testing of a Cyclically Stabilized A 516 Gr. 70 Piping Steel In PWR Environment," USNRC Report NUREG/CR-5327, Nov. 1989.

18. W. J. Mills, "On the Relationship Between Stretch Zone Formation and the J Integral for High Stain-Hardening Materials," Journal of Testing and Evaluation, JTEVA, Vol. 9, No. 1, Jan. 1981, pp. 56-62.

19. J. D. Landes and D. E. McCabe, "Toughness of Austenitic Stainless Steel Pipe Welds," EPRI NP-4768, Electric Power Research Institute, Oct. 1986.

20. F. J. Loss, Ed., "Structural Integrity of Water Reactor Pressure Boundary Components, Annual Report for 1984," USNRC Report NUREG/CR-3228, Vol. 3, May 1985.

NRC FORM 335 (2-89) NRCM 1102, 3201, 3202

U.S. NUCLEAR REGULATORY COMMISSION

BIBLIOGRAPHIC DATA SHEET

(See instructions on the reverse)

1. REPORT NUMBER (Assigned by NRC. Add Vol., Supp., Rev., and Addendum Numbers, if any.)

NUREG/CR-5188
MEA-2325

2. TITLE AND SUBTITLE

Fracture Toughness Characteristics of Nuclear Piping Steels

3. DATE REPORT PUBLISHED

MONTH: November
YEAR: 1989

4. FIN OR GRANT NUMBER

B8900

5. AUTHOR(S)

A. L. Hiser

6. TYPE OF REPORT

Technical

7. PERIOD COVERED *(Inclusive Dates)*

8. PERFORMING ORGANIZATION – NAME AND ADDRESS *(If NRC, provide Division, Office or Region, U.S. Nuclear Regulatory Commission, and mailing address. If contractor, provide name and mailing address.)*

Materials Engineering Associates, Inc.
9700-B Martin Luther King, Jr. Highway
Lanham, MD 20706-1837

9. SPONSORING ORGANIZATION – NAME AND ADDRESS *(If NRC, type "Same as above"; if contractor, provide NRC Division, Office or Region, U.S. Nuclear Regulatory Commission, and mailing address.)*

Division of Engineering
Office of Nuclear Regulatory Research
U.S. Nuclear Regulatory Commission
Washington, DC 20555

10. SUPPLEMENTARY NOTES

11. ABSTRACT *(200 words or less)*

To assess the integrity of piping systems in nuclear power plants, materials' property information such as fracture toughness and stress-strain data are required. This report summarizes findings from testing of heats of piping steel representing a cross-section of those included in nuclear plants. Included are ferritic steels, austenitic stainless steels, and one heat of an Inconel alloy.

Besides the characterization of piping steels, additional studies examined the effect on J-R curves of flattening specimen blanks, and assessed size effects and through-thickness variability on stress-strain curves.

12. KEY WORDS/DESCRIPTORS *(List words or phrases that will assist researchers in locating the report.)*

Nuclear piping steels, stainless steel, J-R curve, Inconel 600, Dynamic strain aging, Weld

13. AVAILABILITY STATEMENT

Unlimited

14. SECURITY CLASSIFICATION

(This Page)
Unclassified
(This Report)
Unclassified

15. NUMBER OF PAGES

16. PRICE

UNITED STATES
NUCLEAR REGULATORY COMMISSION
WASHINGTON, D.C. 20555